Dissertation
submitted to the
Combined Faculties for the Natural Sciences and for Mathematics
of the Ruperto-Carola University of Heidelberg, Germany
for the degree of
Doctor of Natural Sciences

presented by

Diplom- Upendo Lupanga
born in: Morogoro
Oral-examination: 14th March 2017

A tale of two routes:

The role of subunit a in targeting and regulation of the V-ATPase in *Arabidopsis thaliana*

Referees : Prof. Dr. Karin Schumacher
Prof. Dr. Jan Lohman
Prof. Dr. Irmgard Sinning

In Memoriam

Ildefons Joseph Lupanga

1945-2005

Table of Contents

Summary

One outcome of compartmentalization in eukaryotic cells is that each organelle has the ability to establish a unique pH environment. Homeostasis of the luminal pH within these organelles is essential for survival of the cell because important processes such as secondary active transport and enzymatic reactions depend on optimal pH conditions. Luminal pH is a product of the cooperative effort between H^+ pumps and ion transporters located on the limiting membrane of the organelle. The vacuolar H^+-ATPases (V-ATPases) are one class of proton pumps that are well conserved within eukaryotic cells. V-ATPases are multisubunit complexes that hydrolyze ATP and transport protons into the lumen of organelles. In plant cells, the V-ATPase is important for pH homeostasis at the vacuole and early endosome but most of the information available about the eukaryotic V-ATPase complex comes from studies in yeast and mammals. In plants, nothing is known about the mechanism of targeting in the cell, the regulation of its activity and whether the pump has secondary functions aside from pH homeostasis. Our research focus was on subunit a (VHA-a) of the V_O subcomplex of plants. The localization of the V-ATPase in the cell is determined by the isoforms of VHA-a. The sorting signal of any VHA-a subunit was not known. In the first chapter, we report the discovery of an acidic cluster and a critical leucine (L159) residue in the N-terminus of VHA-a1 that serves as both an ER export signal and as a TGN retention motif. This motif is reminiscent of mammalian endosomal targeting acidic clusters but the specific sequence of amino acids is unique to the plant kingdom and the motif originates in the gymnosperm sequences. In the second chapter we investigated whether the TGN localized V-ATPase not only fulfils its primary function of acidification, but whether it is also a component of the molecular machinery that senses the level of luminal acidification and its recruits cytosolic proteins involved in vesicle trafficking to the membrane. In the third chapter, we explore a new form of modification of the tonoplast localized isoform (VHA-a3). We show that S-acylation is not involved in targeting of VHA-a3 to the tonoplast and that V-ATPase activity is not compromised by a lack of S-acylation in the presence of high concentrations of zinc.

Zusammenfassung

Eukaryotische Zellen zeichnen sich durch ihre Organisation in individuelle Reaktionskompartimente aus, welche sich in ihren biochemischen Eigenschaften voneinander unterscheiden. Aufgrund der funktionellen Spezialisierung weisen unterschiedliche Kompartimente individuelle pH-Bedingungen auf. Die Aufrechterhaltung eines bestimmten pH-Wertes innerhalb eines Kompartiments hängt von der Funktion der membranständigen H^+-Pumpen und Ionen-Transportern ab. Hierbei sind die vakuolären H^+-ATPasen (V-ATPasen) für die intraluminale Ansäuerung von Bedeutung. V-ATPasen sind in allen Eukaryoten konserviert und lassen sich strukturell in zwei Komplexe unterteilen: Der zytosolische V_1-Komplex, verantwortlich für die ATP-Hydrolyse, und der membranständige V_O-Komplex welcher für die Protonentranslokation ins Innere des Kompartiments zuständig ist. Im Gegensatz zur weit fortgeschrittenen Charakterisierung in Hefe, ist über pflanzliche V-ATPasen nur wenig bekannt. Bis *dato* sind die Mechanismen für die differentielle Lokalsierung, sowie die Regulierung der Enzymaktivität nicht geklärt. Darüber hinaus ist unklar ob die V-ATPasen neben ihrer primären Funktion als Protonenpumpe noch sekundäre Funktionen für die Zelle ausüben. Der Fokus der vorliegenden Arbeit richtet sich auf die Untersuchung der drei Isoformen der Untereinheit ‚a' (VHA-a1, -a2, -a3) welche einen strukturellen Bestandteil des membranintegralen V_O-Komplexes darstellen. Die VHA-a Untereinheit ist für die differentielle Lokalisierung des V-ATPase-Komplexes innerhalb der Zelle verantwortlich. Einbau der VHA-a1-Untereinheit lokalisiert den Komplex in die Membran des *trans*-Golgi Netzwerks/*Early endosomes* (TGNs/EEs). Einbau der VHA-a2- oder VHA-a3-Untereinheit führt zur Lokalisierung des Komplexes in die Membran der Vakuole. Keines der Sortierung-Signale der VHA-a-Untereinheiten war bislang bekannt. Im ersten Abschnitt der Arbeit, berichten wir über die Identifizierung einer Gruppe von sauren Aminosäuren und einem Leucin-Rest (L159) innerhalb des N-Terminus der VHA-a1-Untereinheit. Dieses Motiv ist sowohl für den ER-Export als auch für die Zurückhaltung des Komplexes im TGN verantwortlich. Das Motiv ähnelt zwar dem endosomalen Sortier-Signal aus Säugern, weist jedoch eine Abfolge von Aminosäuren auf, die sich für das Pflanzenreich unabhängig

entwickelt hat. Im Pflanzenreich tritt die Sequenz erstmalig innerhalb der Gymnospermen auf. Im zweiten Abschnitt wurde untersucht ob die TGN-lokalisierte V-ATPase neben ihrer primären Funktion als Protonenpumpe, Teil eines molekularen Apparates ist, welcher für die pH-abhängige Rekrutierung von zytosolischen Komponenten des vesikulären Membrantransports zuständig ist. Gegenstand des dritten Abschnitts, ist die Untersuchung einer Proteinmodifikation der tonoplast-lokalisierten V-ATPase-Untereinheit VHA-a3. Wir zeigen, dass die S-Acylierung von VHA-a3 nicht notwendig ist für die Lokalisierung der V-ATPasen zum Tonoplasten und dass das Vorhandensein der S-Acylierung keinen Einfluss auf die Aktivität der V-ATPase hat, weder unter Standard-Bedingungen noch unter Zink-Stres

Contribution to the manuscript

The author of this thesis wrote all the manuscripts presented in the current work. Apart from the author and the supervisor, persons listed below contributed to this work as indicated.

Targeting of the V-ATPase to the TGN in *Arabidopsis thaliana*

Construct design and cloning	Phillip Bellon
In vitro V-ATPase activity assays	M. Görkem Patir Nebioglu
Technical assistance plant work	Beate Schöfer

The C-terminus of VHA-a1 as a potential pH sensor

Construct design and cloning	Phillip Bellon
Mass spectrometry	Core facility for mass spectrometry & proteomics (CFMP) at the ZMBH

Regulation of the plant V-ATPase by S-acylation

In vitro V-ATPase activity assays	M. Görkem Patir Nebioglu
Biotin switch assays and acyl-RAC	Fabian Fink
Technical assistance plant work	Beate Schöfer

Chapter 1

Targeting of the V-ATPase to the TGN in *Arabidopsis thaliana*

Scientific aim

The molecular mechanisms responsible for differential V-ATPase trafficking have not been determined and this chapter thus aimed:

1. To determine the sorting signal in VHA-a1 that targets it to the TGN/EE in *A. thaliana*

Abstract

The vacuolar H^+-ATPases (V-ATPases) are multisubunit complexes that are indispensable for pH homeostasis of various cellular compartments in all eukaryotic cells. The localization of this multifaceted enzyme is determined by the isoforms of the membrane integral subunit, VHA-a. The incorporation of VHA-a1 targets the V-ATPase to the trans-Golgi network/early endosome (TGN/EE) whilst the incorporation of VHA-a2 and VHA-a3 targets the V-ATPase to the tonoplast. The nature and location of the sorting signal in either VHA-a subunit was not known. We employed chimeric proteins, site directed mutagenesis and multiple sequence alignment techniques and discovered that an acidic cluster and a critical leucine (L159) residue in the N-terminus of VHA-a1 serves as both an ER export signal and as a TGN retention motif. This motif is reminiscent of mammalian endosomal targeting acidic clusters but the specific sequence of amino acids is unique to the plant kingdom and the motif originates in the gymnosperm sequences. VHA-a1 harbouring various mutations in the acidic cluster is partially mislocalized to the tonoplast to various degrees. Furthermore, these mislocalized mutated forms of VHA-a1 are able to complement the *vha-a2 vha-a3* double mutant which lacks V-ATPases at the tonoplast also to various degrees. For the very first time, the enzyme kinetics of VHA-a3 and VHA-a1 containing complexes were compared on the same membrane and we find that VHA-a1 containing complexes are less effective in acidifying vacuoles than VHA-a3 containing complexes in vivo.

Introduction

Cells need to maintain pH gradients across all compartments to ensure proper functioning of cell processes. The vacuolar H^+-ATPases (V-ATPases) are multisubunit complexes that are responsible for the acidification of various cellular compartments in all eukaryotic cells. The complex has been found on the membranes of the plasma membrane, Golgi, endosomes, lysosomes or vacuoles and secretory vesicles in all eukaryotic cells (Nishi and Forgac, 2002; Stevens and Forgac, 1997). Acidification of these organelles by the V-ATPase is important for a variety of functions which include receptor mediated endocytosis, intracellular membrane traffic, degradation and processing of proteins and active transport of small molecules (Qi and Forgac, 2007).

Structurally, the V-ATPases share a significant resemblance to the F_1F_O ATP synthases (F-ATPases) (Fillingame et al., 2000). But one significant difference is that F-ATPases synthesize ATP while V-ATPases hydrolyze ATP. The hydrolysis of ATP is carried out by the hydrophilic V_1 subcomplex. The energy generated by the hydrolysis of ATP is used to translocate protons through the membrane integral V_O subcomplex (Stevens and Forgac, 1997). The V-ATPases and F-ATPases share a common ancestor, the bacterial or archaeal ATPases (A-ATPases) (Forgac, 2007). V-ATPases bear an even closer structural and evolutionary relationship to the A-ATPases than to F-ATPases. Comparative to the V-ATPase, the A-ATPase has a similar overall structure, but is smaller and simpler and functions in vivo as an ATP synthase (Schep et al., 2016).

Synthesis and assembly of the V-ATPase subunits

The V-ATPase complex is a multimeric protein complex. The V_1 complex is composed of eight different subunits (A, B, C, D, E, F, G, H) and the V_O subcomplex consists of 6 subunits, a, d, e, c, c' and c" in *A. thaliana* **(Figure 1)**. A total of 27 *VHA* genes in the *Arabidopsis* genome encode for the different V-ATPase subunits and their corresponding isoforms (Sze et al., 2002). All the

subunits have to be synthesised and assembled into the complex and this occurs according to the paradigms of protein synthesis in the cell.

Protein synthesis in the cell occurs with the aid of ribosomes located in the cytosol and at the Endoplasmic Reticulum (ER) (Reid and Nicchitta, 2015). Proteins that are destined to enter the secretory pathway are inserted into the ER as unfolded polypeptide chains (Ron and Walter, 2007). Once inside the ER, they undergo folding with the aid of helper proteins called chaperones (Kostova and Wolf, 2003; Liu et al., 2015). Posttranslational modifications such as ER signal sequence cleavage, disulfide bond formation, N-glycosylation and GPI anchor addition may assist proteins to fold (Römisch, 2005). Many proteins need to be assembled into complexes in order to function. These complexes can be either homomers or heteromers (Perica et al., 2012). Assembly into complexes also occurs at the ER and it has recently been demonstrated that it is a multistep process that occurs via ordered assembly pathways (Marsh et al., 2013).

A quality control system exists in the ER (ERQC) that monitors, retains and targets misfolded proteins and proteins that fail to assemble for degradation via the ubiquitin-proteasome degradation system (Trombetta and Parodi, 2003). But those proteins that are able to fold and assemble properly are packaged for export out of the ER (Kostova and Wolf, 2003).

Most of the information available about the synthesis and assembly of the V-ATPase complex comes from studies of the V-ATPase of *Saccharomyces cerevisiae*. In yeast, assembly of the V_1 and V_O can occur independently or in a coordinated manner (Kane et al., 1999). Assembly of the yeast V_O subcomplex occurs at the endoplasmic reticulum (ER) with the aid of assembly factors (Graham et al., 1998). Yeast has five ER localized assembly factors, Vma12p, Vma21p, Vma22p, Voa1p and Pkr1p (Nishi and Forgac, 2002; Margret Ryan, Laurie A. Graham, 2008; Davis-Kaplan et al., 2006). Homologues of yeast assembly factors have also been identified in *Arabidopsis thaliana.* The two isoforms AtVMA21a and AtVMA21b are orthologues to Vma21p and are located

at the ER. They assist in the assembly of the V-ATPase complex (Neubert et al., 2008).

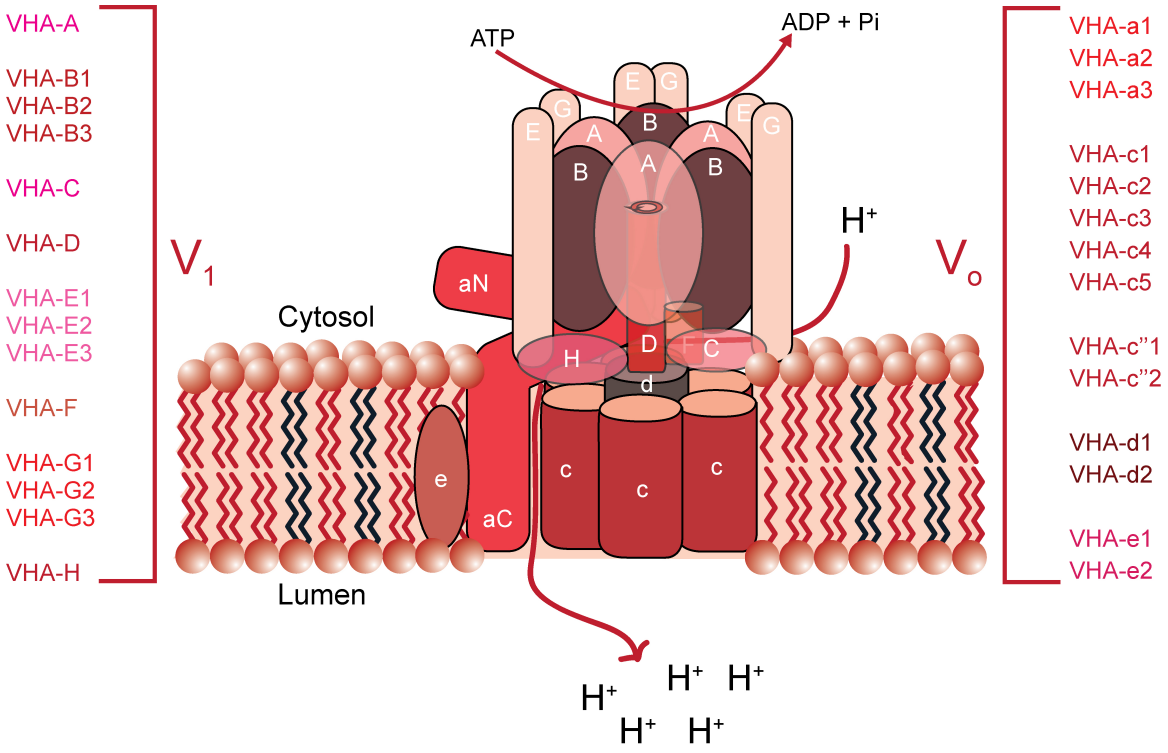

Figure 1. The V-ATPase is a rotary pump consisting of 14 subunits divided into two subcomplexes. The membrane peripheral V_1 subcomplex is composed of subunits A, B, C, D, E, F, G and H and the membrane integral V_O subcomplex is composed of subunits a, d, e, c, c' and c".

Export of the V-ATPase out of the ER

Once assembled, the V-ATPase complex has to be exported out of the ER and transported to specific organelles in the cell where it can perform its function. In yeast, it has been shown that this export occurs with the aid of COPII (coat protein complex II) carrier vesicles (Malkus et. al., 2004).

These carrier vesicles also exist in plant cells, in fact there are two types of carrier vesicles that exist at the ER/Golgi interphase. These are COPI and COPII

vesicles. These vesicles can be distinguished based on the proteins coating their surface. The coat proteins or coatomer aid in vesicle formation by initiating and promoting membrane curvature through protein interactions and they may also be involved in cargo selection (Kirchhausen, 2000). COPI carrier vesicles are vesicles that are coated with the coatomer protein complex, COPI. The COPI coat is a heptameric protein complex consisting of the following subunits, α,β,β',ε,γ,δ and ζ (Jackson, 2014). COPI vesicles are responsible for retrograde transport of proteins from the Golgi to the ER and between Golgi cisternae (Paul and Frigerio, 2007; Jackson, 2014).

COPII carrier vesicles are vesicles that are coated with the coatomer protein complex, COPII. The COPII coat is a pentameric protein complex consisting of the following subunits, Sec23, Sec24, Sec13, Sec31 and the small GTPase Sar1(secretion-associated, Ras related protein 1)(Marti et al., 2010). COPII vesicles are involved in anterograde transport of proteins from the ER to the Golgi (Phillipson et al., 2001; Kirchhausen, 2000).

The majority of information that is available for COP coated carrier vesicles comes from studies in yeast and mammals (Marti et al., 2010). It is believed that the mechanism of COP vesicle transport is conserved amongst all eukaryotes although higher organisms have multiple paralogs of COPI and COPII components due to gene duplication events (Chung et al., 2016; Ahn et al., 2015). *Arabidopsis* encodes five Sar1, two Sec13, two Sec31, seven Sec23, and three Sec24 isoforms in its genome (Marti et al., 2010). Some of these isoforms, AtSar1a and AtSec23a, have been shown to preferentially pair to create a plant-unique COPII coat (Zeng et al., 2015).

The prevailing understanding of COPII vesicle transport is as follows. COPII vesicle assembly is initiated by Sec12, an ER membrane associated guanine nucleotide exchange factor (GEF). Sec12 recruits and activates the cytosolic GTPase Sar1 at ER exit sites (ERES) (Barlowe and Schekman, 1993). This is followed by the recruitment of the Sec23-24 heterodimer complex. Sec24 acts as

a cargo receptor that selects cargo to be incorporated into the vesicle (Pagant et al., 2015).

The GTP-bound form of Sar1 also activates Sec23 to bind tethering and v-SNARE (soluble N-ethylmaleimide-sensitive factor attachment protein receptor) proteins that assist in targeting and fusion of the COPII vesicles to the cis-Golgi membrane (Springer and Schekman, 1998). COPII coat formation is completed by binding of the heterodimer Sec13-31 complex. The Sec13-31 complex aids in the deformation of the ER membrane (Gürkan et al., 2006). The final stages of COPII vesicle formation constituting the deformation and fission of the vesicle from the ER membrane have been shown to be promoted by the N-terminal tail of Sar1 as well as its hydrolysis of GTP (Lee et al., 2005; Bielli et al., 2005). Throughout the COPII vesicle formation process, Sar1 undergoes repeated cycles of GTP hydrolysis. A component of the coat, Sec23, is also the GAP (GTPase-activating protein) for Sar1, meaning that coat polymerization triggers disassembly (Sato and Nakano, 2007). The stability of the coat is maintained by Sec12 acting as a GEF, which continuously charges Sar1 with GTP (Futai et al., 2004). Coat stability is also prolonged by the presence of cargo on the vesicle which maintains the assembly of the Sec23-24 complex even in the presence of Sar1 GTP hydrolysis (Sato and Nakano, 2007).

The COPII dependent ER exit of proteins can be disrupted at two stages. First, by over expressing Sec12, the exchange factor of the small GTPase Sar1, resulting in depletion of Sar1 from the cytosol, disruption of COPII coat formation, and disruption of ER export sites (Phillipson et al., 2001). Second, by expressing a mutant form of Sar1 (Sar1 H74L) that is trapped in the GTP-bound form. This would prevent vesicle uncoating and fusion with the target membrane (Phillipson et al., 2001).

The COPII coat has to be shed in order to allow the vesicle to fuse with the target cis-Golgi membrane. COPII vesicle uncoating is triggered by the hydrolysis of GTP by Sar1(Kirchhausen, 2000). It is thought that, after GTP hydrolysis, Sar1–GDP is released (Gillon et al., 2012). Membrane fusion of the vesicles and target

membrane is mediated by the interaction of a monomeric v-SNARE on the vesicle and oligomeric t-SNARE on the target membrane, forming a stable four-helix bundle that promotes membrane fusion (Bonifacino and Glick, 2004).
Although it has been established that the V-ATPase leaves the ER via COPII vesicles in yeast (Malkus et al., 2004), nothing has been reported concerning the specific amino acid sequences on the V-ATPase subunits that are required for entry into COPII vesicles. The entry into COPII vesicles is dependent on specific amino acid signals recognized by Sec24 and have so far been classified as di-acidic (D/E-X-D/E) and di-hydrophobic or di-aromatic (FF, YY, LL or FY) sequences (Pedrazzini et al., 2013). Neither of these signals have been identified in yeast. In plants, the export of the *trans*-Golgi network/early endosome (TGN/EE) targeted V-ATPase has been suggested to be dependent on COPII vesicles (Viotti et al., 2013). However a direct interaction of V-ATPase subunits with COPII vesicles components has not been shown and amino acid sequences required for COPII vesicle entry have also not been identified.

Trafficking of the V-ATPase complex through the cell

The V-ATPase has two important localizations in the plant cell, the limiting membrane of the vacuole (tonoplast) and the TGN/EE. It has long since been established from studies in yeast that the N-terminal domain of subunit a of the V_O subcomplex is responsible for targeting of the entire V-ATPase complex to different organelles in the yeast cell. Yeast has two isoforms of subunit a, Vph1p and Stv1p. Vph1p targets the V-ATPase to the vacuole and Stv1p targets the V-ATPase to the Golgi/endosomal network (Kawasaki-Nishi et al., 2001). Similarly to yeast, all other eukaryotes studied so far also possess several isoforms of subunit a. Three isoforms of subunit a exist in *A. thaliana*, VHA-a1, VHA-a2 and VHA-a3. VHA-a1 and VHA-a3 have a sequence identity of 69%. The localization of the V-ATPase in *A. thaliana* is also determined by the isoform of VHA-a that is assembled into the multi-subunit enzyme complex at the ER (Dettmer et al., 2006). The incorporation of VHA-a1 targets the V-ATPase to the TGN/EE whilst the incorporation of VHA-a2 or VHA-a3 targets the V-ATPase to the tonoplast

(Dettmer et al., 2006). The molecular mechanisms such as how V-ATPases with the different VHA-a isoforms are sorted at the ER and how each of the complexes are targeted to their final destinations in the cell remain to be determined.

The export of proteins out of the ER may occur independently of COPII vesicles. One protein for which this has been demonstrated is VHA-a3. It has been discovered that VHA-a1 and VHA-a3 containing complexes leave the ER by using different routes (Viotti et al., 2013). VHA-a1 containing complexes which are destined for the TGN are dependent on passage through the Golgi to reach their destination. For VHA-a3 containing complexes however, it was shown that in the meristematic cells of the *Arabidopsis* root tip; VHA-a3 containing complexes are delivered to the tonoplast in a Golgi-independent manner (Viotti et al., 2013). This conclusion comes from observations that inhibition of post-Golgi trafficking by the V-ATPase inhibitor Concanamycin A (ConcA) did not affect the transport of VHA-a3 to the tonoplast. Furthermore, ultrastructure and immunogold electron microscopy showed that VHA-a3 containing complexes are delivered directly from the ER to the tonoplast via membranous structures known as provacuoles (Viotti et al., 2013) **(Figure 2)**.

This unique form of trafficking to the tonoplast is not restricted to VHA-a3. Other tonoplast proteins have also been found to use different ways to reach the tonoplast. Soluble proteins that are destined for the vacuole have been shown to use a single route to reach their destination (ER to Golgi and TGN to vacuole) (Bottanelli et al., 2011) **(Figure 2)**. Transmembrane proteins however, have been shown to use many ways to reach the vacuole (Pedrazzini et al., 2013). These trafficking routes are protein specific and can be classified as Golgi dependent or Golgi independent (Pedrazzini et al., 2013).

The trafficking of proteins that follow the Golgi dependent route is also sensitive to Brefeldin A (BFA). The fungal toxin BFA has been used extensively to study vesicle trafficking. The effects of BFA in a cell depend on the type of plant cell and most importantly the Arf-GEFs (ADP-ribosylation factor GTPases) which are

present at the Golgi and TGN (Richter et al., 2007). These ARF-GEFs can be either BFA sensitive or BFA resistant.

BFA can cause redistribution of Golgi cisternae into the ER if a BFA sensitive Arf-GEF is present at the Golgi stacks such as in tobacco BY-2 cells (Ritzenthaler and Robinson, 2002). This will inhibit coat protein complex I (COPI) vesicle formation and thus effectively block ER to Golgi transport (Viotti et al., 2013). Or BFA can cause Golgi stacks and TGNs to aggregate forming BFA compartments. This occurs when a BFA insensitive Arf-GEF is present at the Golgi stacks like in *A. thaliana* wild type root cells (Langhans et al., 2011). On the whole, regardless of the specific effects of BFA on the different cell types, the global effect is that trafficking through the Golgi is inhibited. It therefore follows that, the sensitivity of a protein's trafficking to BFA is an indicator of passage through the Golgi (Pedrazzini et al., 2013). And insensitivity to BFA is an indicator of bypassing the Golgi to reach the vacuole.

GNOM-like-1 (GNL1) is a GEF for the GTPase Arf1 that is involved in COPI retrograde transport form the Golgi to the ER (Richter et al., 2007) and it is naturally resistant to BFA (Anders and Jürgens, 2008). GNL1 was artificially rendered to be BFA sensitive by mutation and was expressed together with VHA-a1 and VHA-a3 in a GNOM-like-1 (GNL1) mutant background (Viotti et al., 2013). After the application of BFA, only the ER export of VHA-a1 but not VHA-a3 was inhibited thus again demonstrating that the trafficking of VHA-a3 to the tonoplast is independent of Golgi function.

The Golgi dependent route can further be subdivided into adapter protein complex 3 (AP3) dependent or independent routes. Adaptor protein (AP) complexes sort cargo into vesicles for transport from one membrane compartment of the cell to another (Boehm and Bonifacino, 2001). The AP3 dependent route bypasses the MVBs or late endosome (Zwiewka et al., 2011)(**Figure 2**). The sucrose transporter SUC4 is transported in an AP-3–dependent manner to the tonoplast (Wolfenstetter et al., 2012). The AP3

independent route involves passage through the TGN and MVBs to reach the vacuole.

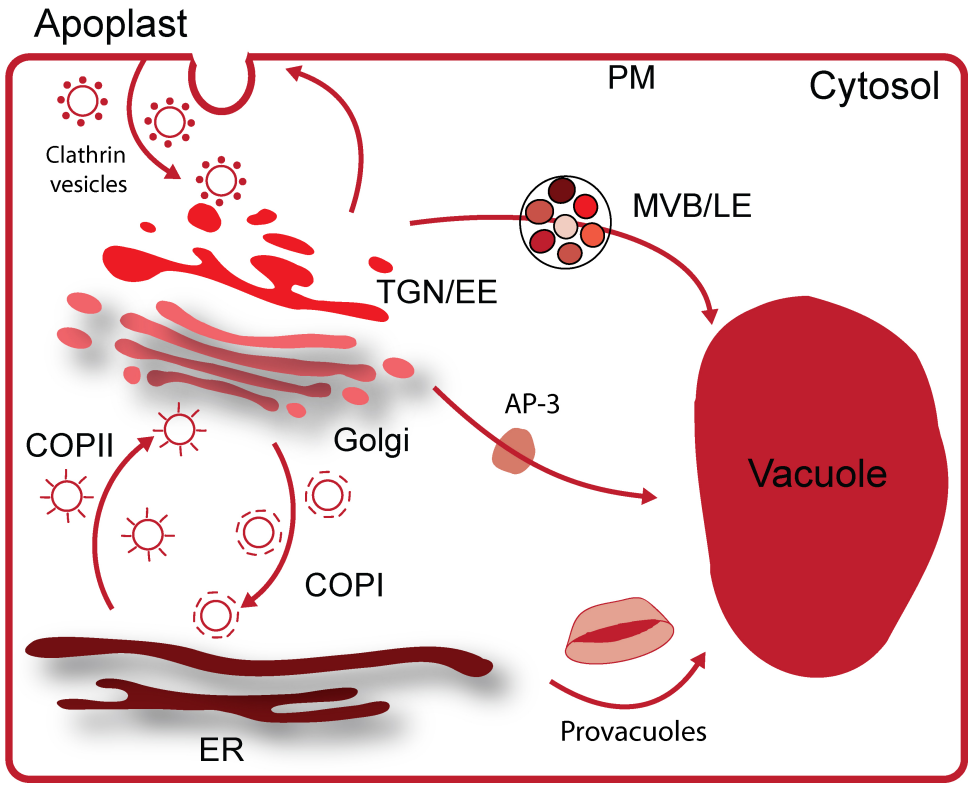

Figure 2. The secretory pathway in plants

Proteins synthesized at the Endoplasmic reticulum (ER) are transported via COPII vesicles to the Golgi. Side chain modifications can occur in the golgi cisternae before the proteins are passed to the trans-Golgi network. The TGN is the sorting center of the cell. Proteins are either directed to the plasma membrane (PM) or vacuole via multivesicular bodies/late endosome (MVB/LE). The TGN is also the early endosome in plants. Molecules internalized at the plasma membrane are recieved at the TGN before being recycled back to the plasma membrane or directed to the vacuole for degradation. Proteins can also be be delivered to the vacuole directly from the Golgi via Adapter Protein Complex 3 (AP-3) and Golgi derived vesicles. Some proteins can bypass the Golgi altogether to reach the vacuole by using provacuoles that are derived from the ER membrane.

TGN targeting motifs

After passage through the Golgi, proteins migrate further on to the sorting centre of the cell, the trans Golgi network (TGN). The plant TGN is a bustling port that receives cargo from the endocytic, recycling and secretory pathways (Viotti et al., 2010). It is a meeting point for newly synthesized proteins coming from the Golgi as well as recycled proteins coming from the plasma membrane. As a result of this latter function, the TGN also serves as the early endosome in plants (Viotti et al., 2010). The significance of this organelle in cellular trafficking cannot be understated as it performs vital functions that are needed for maintaining the integrity of the cell. By sorting receptors, transporters and other plasma membrane proteins either for recycling to the plasma membrane or for degradation at the lytic vacuoles, the TGN plays a key role in the way cells adapt to the prevailing environmental conditions (Reyes et al., 2011).

TGN resident proteins need to be retained in order to maintain the organelle identity and functionality such as the vacuolar H^+-ATPase (V-ATPase) which is needed for acidification of the TGN (Luo et al., 2015). Intuitively, this points to the existence of a localization signals, that aid in the retention or retrieval of TGN resident proteins. Information available for the localization of proteins to the TGN in *A. thaliana* is sparse compared to what is known about the mechanisms of retention and retrieval of ER resident proteins. However, there is some information available about motifs necessary for targeting and retrieval to the TGN from yeast and mammals.

Studies in yeast have revealed that retention at the Golgi involves transmembrane domains (TMD) whilst retention in the last Golgi sub-compartment (equivalent to the TGN) is dependent on signals in the cytoplasmic tails of proteins (Machamer, 1993). It has been demonstrated that several yeast proteins have aromatic-based amino acid motifs that are required for retrieval from the PVC (Pre-Vacuolar Compartment) to the TGN (Bowers and Stevens, 2005). These aromatic amino acid based motifs can be the canonical FXFXD motif) as is the case for Ste13p (Bryant and Stevens, 1997) and Vps10p

(Cereghino et al., 1995; Cooper and Stevens, 1996). Alternatively, a single critical tyrosine residue has been shown to be important for TGN localization such as is the case for the protease KEX2p (Wilcox et al., 1992). The targeting information in Stv1p that targets the V-ATPase to the Golgi/endosomal network was discovered to be a tri-peptide motif, WKY(aa 83-85) (Finnigan et al., 2012a). This tri-peptide motif is different from the canonical FXFXD motif that has been shown to be responsible for the TGN localization of proteins in yeast (Finnigan et al., 2012a). In addition this motif appears to be unique to the yeast V-ATPase subunit a and has not been found in plant or mammalian subunit a.

In mammals, three types of sorting motifs have been identified to be associated with TGN localization. Namely, tyrosine based motifs, dileucine based motifs and acidic clusters (Gu et al., 2001) **(Table1)**. Tyrosine based motifs, summarized as YXXØ (where X is any amino acid and Ø is an amino acid with a bulky hydrophobic side chain) have mainly been shown as retrieval signals for cycling proteins from the plasma membrane to the TGN (Gu et al., 2001). The YXXØ motif has been shown to interact directly with the μ subunits of all known adaptor complexes (Owen and Evans, 1998). Stretches of several acidic amino acids constitute an acidic cluster. Acidic clusters have been found to work in conjunction with dileucine and tyrosine-based motifs to achieve TGN localization as is the case with the protease Furin **(Table 1)**. It has also been shown that these acidic clusters need to be phosphorylated as a prerequisite for TGN localization (Jones et al., 1995). None of these mammalian endosomal targeting motifs have been reported for the plant VHA-a subunits.

Table1. TGN localization motifs that have been identified in mammalian proteins and viral proteins

Protein	Nature of signal	Sequence	Reference
Furin	Acidic cluster and Tyrosine based motif	1. CPSDSEEDEG$_{783}$ 2. YKGL$_{765}$	(Schäfer et al., 1995)
PC6B	Two acidic clusters (AC1 and AC2) and a Tyrosine based motif	1.AC1: VIEYRDRDYDEDDEDDIVYM$_{1844}$ AC2: YGLLDEAEDDELEYDDESYSYQ$_{1877}$ 2. YEKL$_{1805}$	(Xiang et al., 2000)
TGN38	Tyrosine based motif	YQRL$_{336}$	(Bos et al., 1993)
Glut4	Acidic cluster	TELEYLGP$_{505}$	(Shewan et al., 2003)
gPI	Acidic cluster and Tyrosine based motif	1. DDFEDSESTDTEEE$_{600}$ 2. YAGL5$_{84}$	(Alconada et al., 1996)

As the molecular mechanisms responsible for differential V-ATPase trafficking have yet not been determined in *A. thaliana*. We set about to determine the sorting signal in VHA-a1 that targets it to the TGN/EE in *A. thaliana* as well as the signal needed for its ER export.

Initial studies on subunit a sorting motifs utilized protein chimeras between VHA-a1 and VHA-a2 and found that the location of the targeting information within VHA-a1 resides within the first 228 amino acids (Dettmer et al., 2006). We made further chimeras between VHA-a1 and VHA-a3 that narrowed down the location of the targeting information further. Site directed mutagenesis of conserved residues was then performed to uncover the sorting signal of VHA-a1. We show that an acidic cluster and a critical leucine (L159) residue in the N-terminus of VHA-a1 serves as an ER export signal. Mutation of amino acids in this acidic cluster leads to partial mislocalization of VHA-a1 to the tonoplast. The mutated mislocalized forms of VHA-a1 are functional as they complement the *vha-a2 vha-a3* double mutant to varying degrees. We also interfered with COPII vesicle trafficking by expressing a dominant negative mutant of Sar1 GTPase (Sar1

H74L). By interfering directly with COPII vesicle transport, we show for the first time that the export of VHA-a1 out of the ER is dependent on COPII vesicles and that mutated VHA-a1 subunits reach the tonoplast via provacuoles.

The acidic cluster in VHA-a1 also serves as a TGN retention signal because VHA-a3 with these amino acids is partially targeted and retained at the TGN. Finally, we performed phylogenetic analysis to determine the evolution of the acidic cluster in the plant kingdom and we discovered that this sorting motif originates in the gymnosperm sequences and is unique to the plant kingdom. Homologous sequences from the animal kingdom also contain acidic clusters in the region corresponding to the location of the sorting motif of VHA-a1. It is yet to be determined if these clusters also serve as sorting motifs in the animal kingdom. This study presents the first sorting signal for a plant V-ATPase subunit a that is both necessary and sufficient for export out of the ER and retention at the TGN/EE.

Results

Yeast and *Arabidopsis thaliana* have different mechanisms of targeting the V-ATPase to the endosomes.

Yeast and *Arabidopsis* both possess V-ATPases that localize at vacuolar and endosomal membranes. Furthermore, what is additionally common to both yeast and *Arabidopsis* is that they make use of different isoforms of subunit a of the V_o sub complex to target the V-ATPase to the different cellular compartments. The targeting information of Stv1p, the isoform that targets the yeast V-ATPase to the Golgi/endosomes was found to be a tripeptide motif. This tripeptide motif, WKY(aa 83-85), is located in the N-terminus of Stv1p (Finnigan et al., 2012a). An alignment of Stv1p with the *Arabidopsis* subunit a isoforms showed that this tripeptide motif is absent in the VHA-a1 N-terminus (**Figure 1**). This implies that *Arabidopsis* must use a signal that is different from the yeast Stv1p signal to target the V-ATPase to the early endosome/TGN.

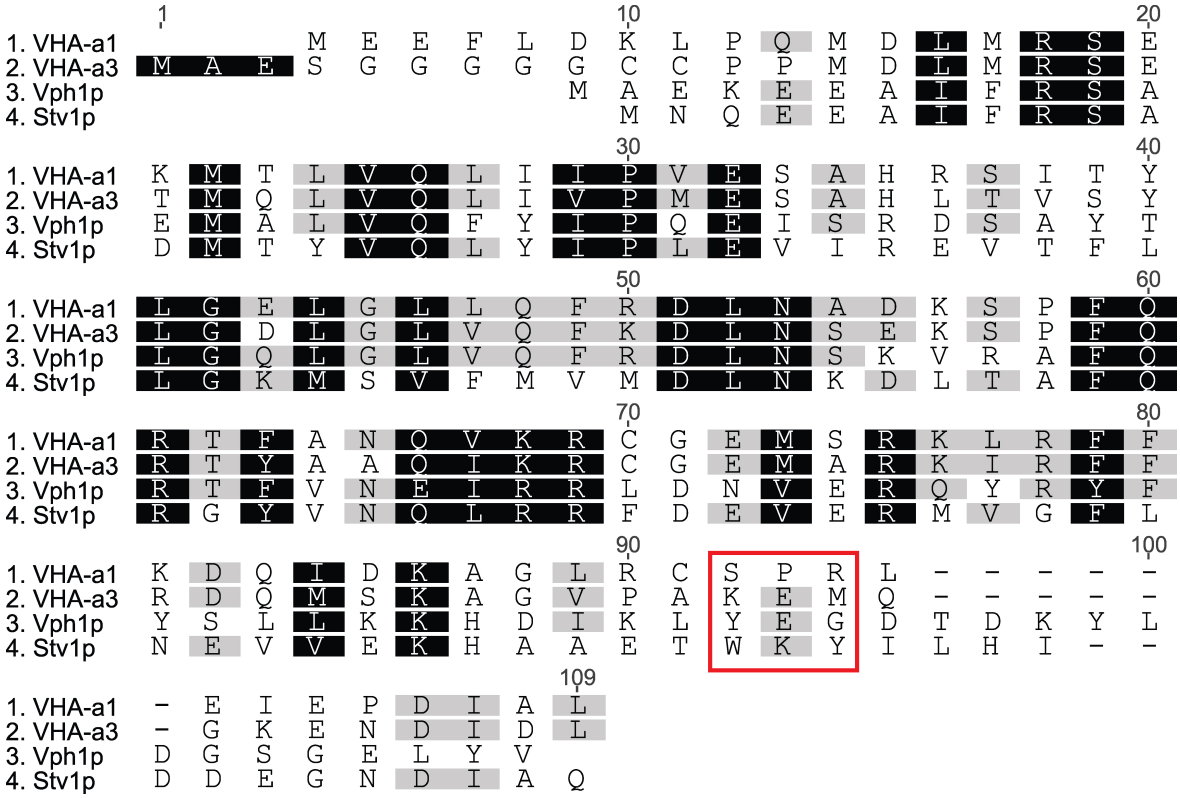

Figure 1. The tri-peptide motif that is responsible for the targeting of Stv1p is absent in VHA-a1

Amino acid sequence alignment of the yeast subunit a isoforms Vph1p and Stv1p with the *Arabidopsis* isoforms VHA-a1 and VHA-a3. Residues similar between all proteins at the same position are shown against a black background. Residues similar between only three of the proteins at the same position are shown against a grey background. Un-highlighted residues have no similarity in all four sequences at the same position. The position of the tri-peptide motif that is responsible for the targeting of Stv1p is indicated with a red box. Multiple sequence alignment was performed using Clustal Omega (Sievers et al., 2011).

The targeting information of VHA-a1 is located between L132 and E179

We then endeavoured to find out what this unique signal in VHA-a1 was. Earlier studies had shown that the targeting information for VHA-a1 was located within the first 228 aa (Dettmer et al., 2006) (amino acids). We decided to use two approaches to determine where and what the signal was in these 228 aa. The first approach involved constructing chimeric proteins consisting of various lengths of the VHA-a1 N-terminus and VHA-a3 C-terminus. The second approach involved attempting to identify differences in structure between the VHA-a1 and VHA-a3 N-termini using three dimensional (3D) models. The underlying idea was that one of the differences in the 3D structure might coincide with the location of the targeting signal in VHA-a1.

For the first approach, five chimeric proteins were made which consisted of increasing lengths of the VHAa1 N-terminus (37aa, 85aa, 131aa, 179 aa and 228 aa) fused to decreasing lengths of the C-terminal domain of VHA-a3 (**Figure 2 A and Supplemental figure S1**). When the chimeric proteins were expressed in *A. thaliana*, the first three chimeric proteins consisting of 37 aa, 85 aa and 131 aa of the VHA-a1 N-terminal domain all localized to the tonoplast. This indicates that the first 131 aa do not contain the targeting information.

The chimeric constructs consisting of 179 aa and 228 aa of the VHA-a1 N-terminal domain localized at the tonoplast and notably also at the TGN (**Figure 2 A and B**).The TGN localization was confirmed by co-localization with the endocytic dye FM4-64 (**Figure 2 B**). Treatment with the fungal drug Brefeldin A (BFA) causes the aggregation of endosomal compartments, including the TGN/EE, to from BFA compartments (Robinson et al., 2008). After 3 hours treatment with BFA, the core of BFA compartments were labelled with a1NT**179**a3-GFP and a1NT**228**a3-GFP (**Figure 2 C**). This further confirmed the TGN localization of the a1NT**179**a3-GFP and a1NT**228**a3-GFP chimeras. From these observations, it can be stated that the targeting information of VHA-a1 is

located in a region of 50aa between L132 and E179 and we called this region the VHA-a1 targeting domain (a1-TD).

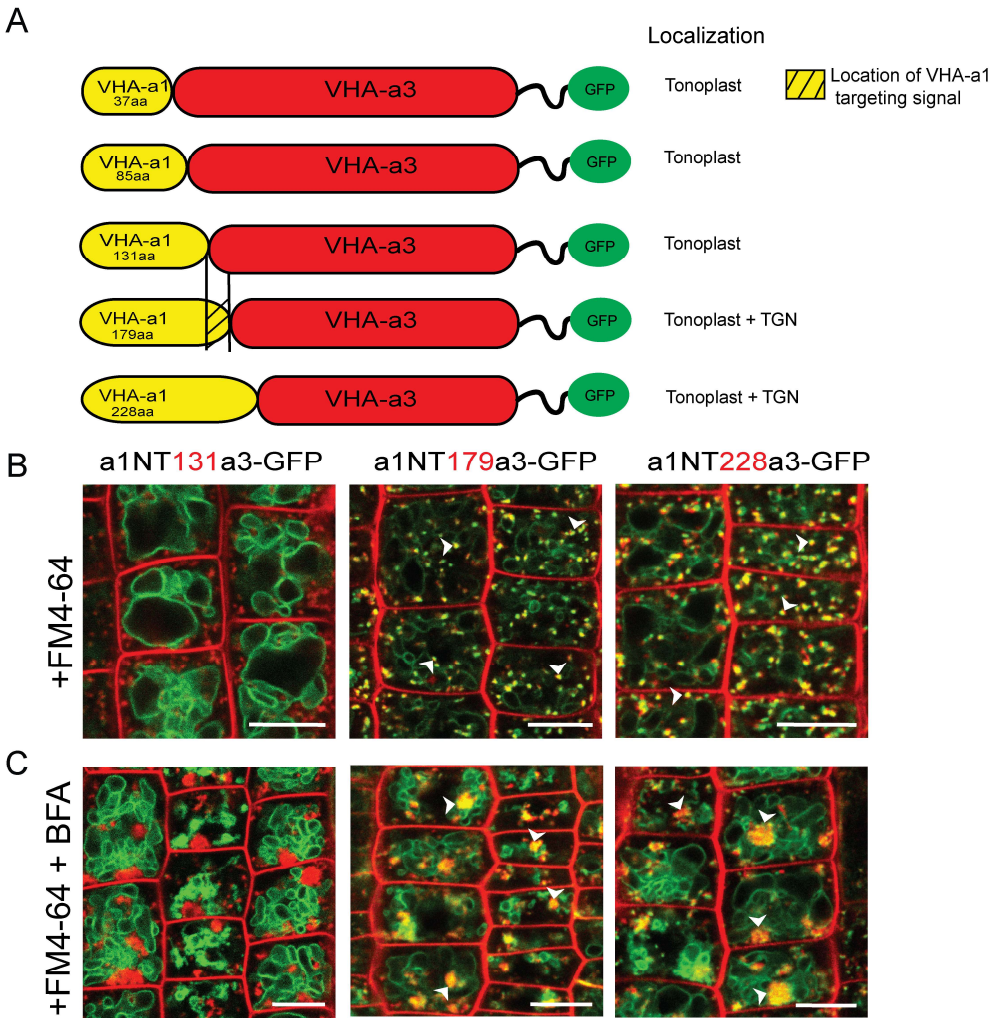

Figure 2. Chimeric proteins reveal that the targeting signal of VHA-a1 is located between L132 and E179.

(A) Chimeric proteins were made which consisted of increasing lengths of the VHA-a1 N-terminus (37aa, 85aa,131aa, 179 aa and 228 aa) fused to decreasing lengths of the C-terminal domain of VHA-a3. All constructs were fused to GFP. Root tips of 6 day old seedlings were analyzed by confocal laser scanning microscopy (CLSM). The chimeric constructs consisting of 179 aa and 228 aa of the VHA-a1 N-terminal domain show dual localization at the TGN and tonoplast. **(B)** The a1NT**179**a3-GFP and a1NT**228**a3-GFP signal colocalized with compartments labelled with FM4-64 after 30 minutes of staining. **(C)** When BFA treatment of 3 hours preceded the FM4-64 staining the core of BFA compartments were labelled with a1NT**179**a3-GFP and a1NT**228**a3-GFP. Arrows indicate colocalization of FM4-64 and GFP.

A difference in the 3D structure between the VHA-a1 and VHA-a3N-termini coincides with the location of the VHA-a1 targeting signal.

At present, the crystal structure of V-ATPase subunit a has not been determined. The only related crystal structure available is that of the N-terminus of subunit I of the A-ATPase from *M.ruber* (Srinivasan, et al., 2011) (PDB=3RRK). Although the sequence homology between *A. thaliana* subunit a isoforms and subunit I of the A-ATPase is low (identity of only 15%), homology modelling of VHA-a1 and VHA-a3 N-termini was performed using the crystal structure of the N-terminus of subunit I from *M.ruber* as a template to obtain 3D models (**Supplemental Figure S3 and S4**). 3D models for VHA-a1 and VHA-a3 were created by using the web based program I-TASSER (Roy et al., 2010).

A similar approach had already been undertaken to obtain 3D models of yeast subunits Stv1p and Vph1p N-termini (Finnigan et al., 2012a; Liberman et al., 2013). The model for Vph1p was validated by strategically introducing unique cysteine residues into a Cys-less form of Vph1p and testing their accessibility to modification (Liberman et al., 2013). It is appreciable that the 3D models obtained for Stv1p and Vph1p are highly similar in topology to the models obtained for VHA-a1 and VHA-a3 (**Supplemental Figure S4 and table S1**). In order to make any differences in the 3D models of the VHA-a1 and VHA-a3 N-termini more apparent, an alignment of the two models was performed (**Figure 3 A**). Three key differences could be observed in the alignment (**Figure 3 A**) and one of these differences corresponds to the location of the VHA-a1 targeting domain.

Three rotational states of the yeast V-ATPase have been identified using electron cryo-microscopy (Zhao et al., 2015). In order to determine the orientation of the VHA-a1 N-terminus within the V-ATPase complex, the VHA-a1 N-terminus model was aligned to a model of one of the rotational states of the V-ATPase (PDB = 3J9V). This alignment revealed that the VHA-a1 targeting domain is exposed and would be accessible for recognition (**Figure 3 B**).

A

Alignment of
VHA-a1 and VHA-a3 N-termini

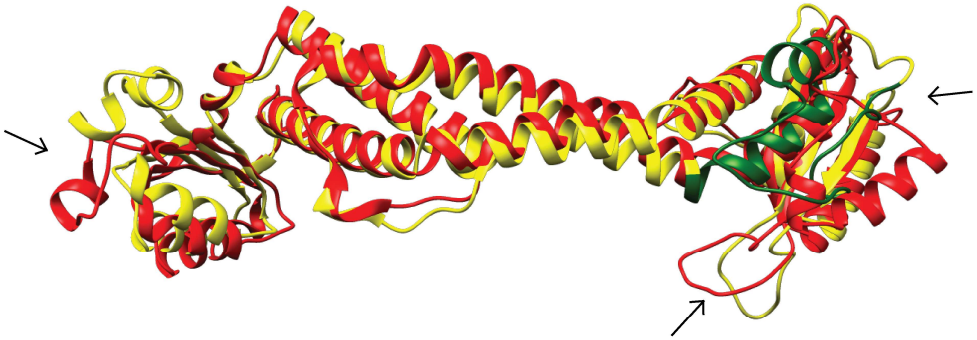

VHA-a3 N-terminus
VHA-a1 N-terminus
VHA-a1 targeting domain (a1TD)

B

Alignment of
VHA-a1 N-terminus with rotational state 1 (PDB = 3J9V) of the yeast V-ATPase

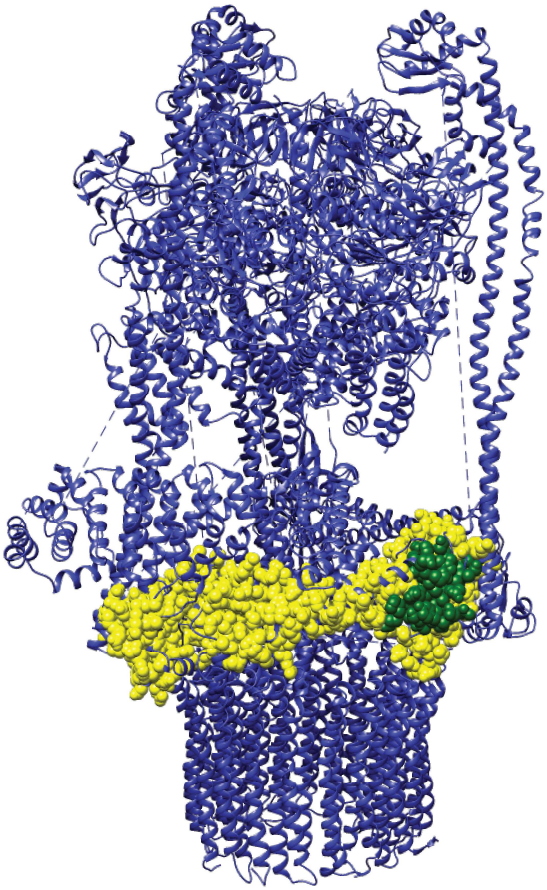

V-ATPase
VHA-a1 N-terminus
VHA-a1 targeting domain (a1TD)

Figure 3. Three-dimensional homology modelling of the VHA-a1 and VHA-a3 N termini reveals that one of the structural differences corresponds to the VHA-a1 targeting domain

(A) In order to make any structural differences between the of VHA-a1 and VHA-a3 N-termini models visible, an alignment of the two models was done. Three key differences (arrows) could be seen and one of these differences corresponds to the location of the identified VHA-a1 targeting domain (green). (**B)** An alignment of the VHA-a1 N-terminus model with a model of one of the rotational states of the V-ATPase (Zhao et al., 2015) revealed that the VHA-a1 targeting domain is exposed and would be accessible for recognition. Alignments were done using the TM align tool of I-TASSER (Roy et al., 2010).

Conserved amino acids in the VHA-a1 clade within the VHA-a1 targeting domain (a1-TD) are the sorting motif

At this juncture in our quest to uncover the targeting mechanism of VHA-a1, we had already established several milestones. We had narrowed down the targeting region in VHA-a1 to 50 aa and through homology modelling, we showed that this region is exposed for identification. We now wanted to determine the specific sequences in VHA-a1 between L132 and G179 that are responsible for targeting of VHA-a1 complexes to the TGN. In order to identify the targeting signal, we aligned all available plant VHA-a sequences. A total of 206 sequences were analyzed (**Supplemental table S2**). Selected sequences that represent the VHA-a1 and VHA-a3 clades are shown in **Figure 4**. The alignment of VHA-a sequences revealed that a number of amino acids are highly conserved in the region between L132 and E179 in all of the VHA-a1-related sequences but not in the VHA-a3 clade. These conserved amino acids include several acidic amino acids (**Figure 4**). Based on the VHA-a sequence alignment, conserved amino acids of *A. thaliana* VHA-a1 were exchanged by site directed mutagenesis to determine if they were responsible for the targeting of VHA-a1 complexes to the TGN. A collection of single, double and triple point mutations was introduced in this region. The mutations all involved exchanging an amino acid in VHA-a1 for the corresponding amino acid in VHA-a3. The mutations were introduced into the full length *VHA-a1* coding sequence.

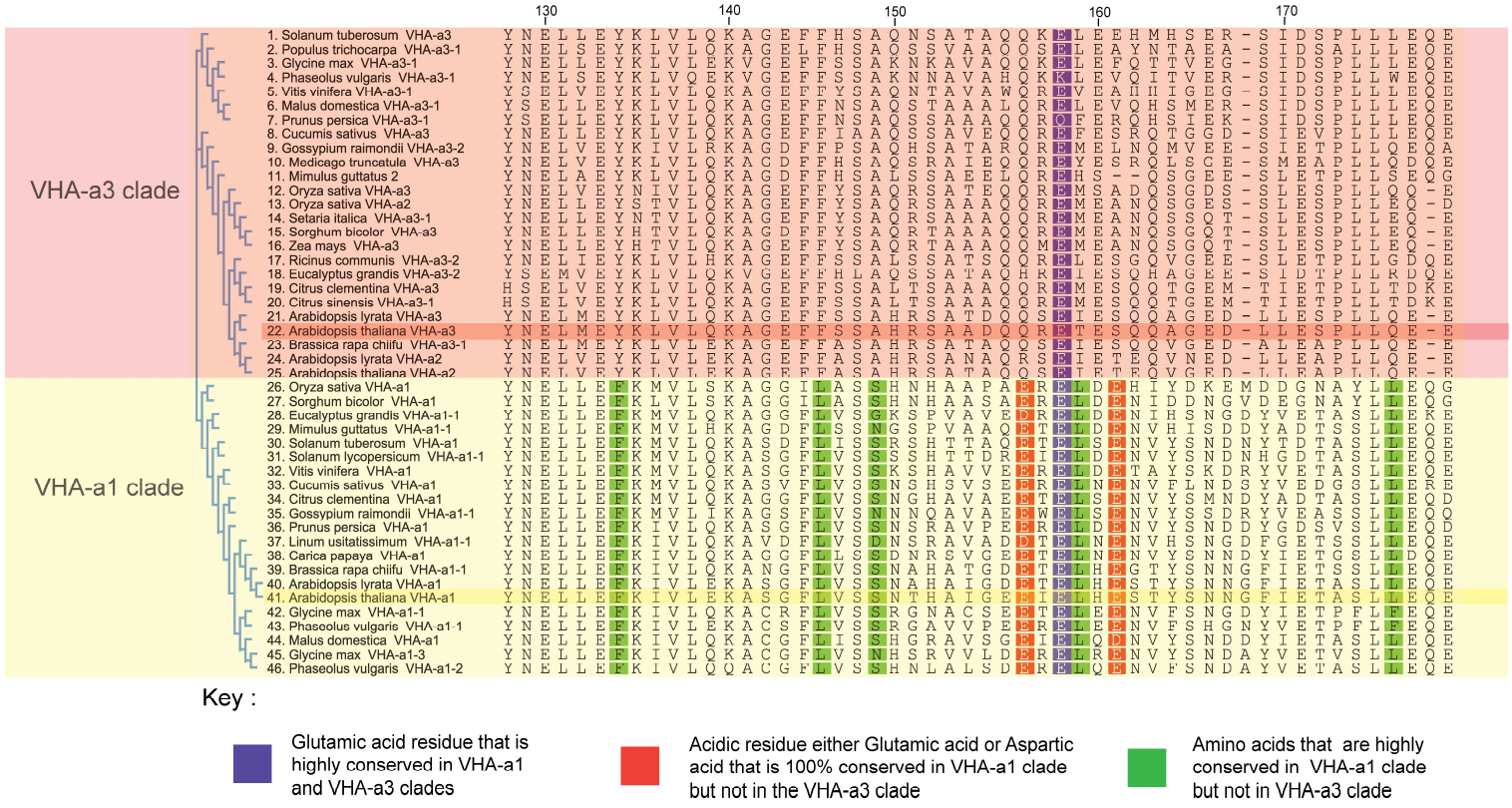

Figure 4. An alignment of selected sequences to represent the VHA-a1 and VHA-a3 clade reveals that there is an acidic cluster that is only present in the VHA-a1 clade.

Amino acid sequence alignment of representative sequences from the VHA-a1 and VHA-a3 clades. The sequence numbers are in reference to the *A. thaliana* VHA-a1 sequence. The VHA-a3 clade is highlighted in red and the VHA-a1 clade is highlighted in yellow.

The localization of the mutated VHA-a1-GFP proteins in *A. thaliana* roots was analyzed by CLSM. In the wild type background, the mutations in VHA-a1 produced punctate patterns that could be grouped into the following classes:

Class 1: Punctae that colocalized with VHA-a1-RFP, were therefore classified TGN signals (**Figure 5**)

Class 2: Punctae that colocalized with VHA-a1-RFP with additional tonoplast signal (**Figure 5**).

Class 3: Punctae that did not colocalize with VHA-a1-RFP signals (**Figure 5)**

A

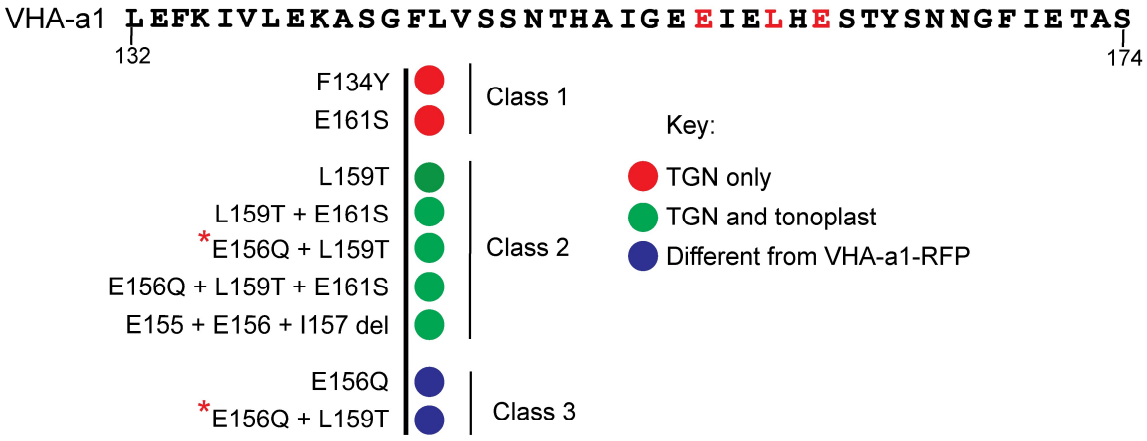

B

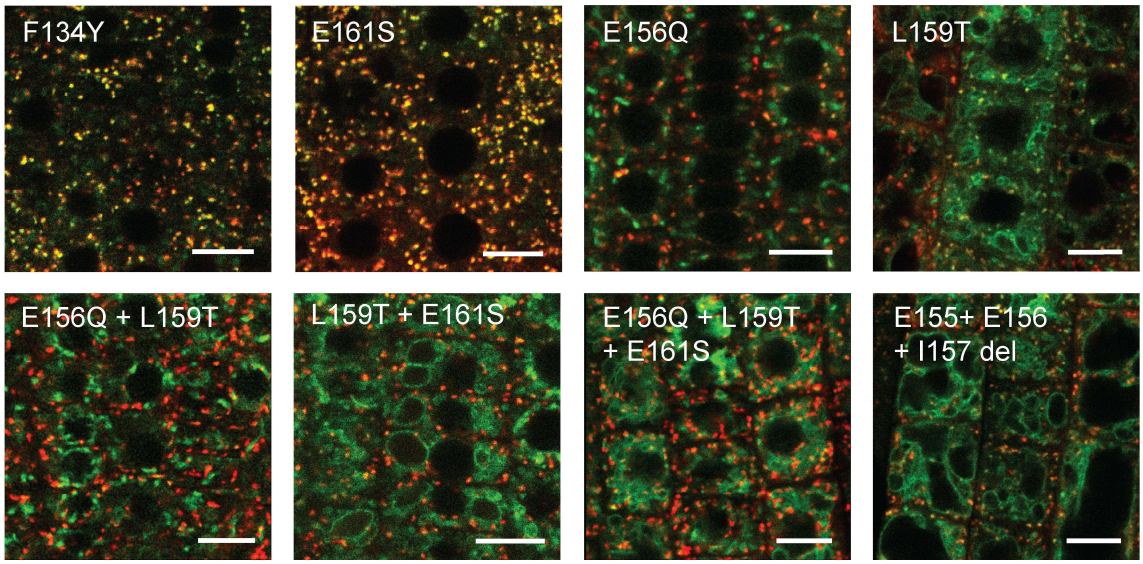

Figure 5. Site directed mutagenesis reveals the importance of E155, E156 and L159 in the targeting of VHA-a1 to the TGN.

Conserved amino acids were mutated individually and combinatorially and the effect on the localization of GFP tagged VHA-a1 was analyzed in the wild type background. **(A)** The mutations in VHA-a1 produced three classes of punctate patterns in the wild type background that could be classified as TGN only (**E161S** and **F134Y**), TGN and tonoplast (**L159T**, **E156Q + L159T, L159T + E161S, E156Q + L159T + E161S and E155 + E156 + I157 deletion)** and different from VHA-a1-RFP (**E156Q** and **E156Q + L159T**). The VHA-a1 targeting domain sequence (a1TD) is also depicted.***E156Q + L159T** resulted in a punctate pattern that was different form VHA-a1-RFP in meristematic cells and a tonoplast localization pattern in mature cells (see **Figure 8 B**). **(B)** Root tips of 6 day old seedlings were analyzed by CLSM. The overlay of GFP (mutated VHA-a1 proteins) and VHA-a1-RFP fluorescence is shown. Scale bars = 10 µm unless otherwise indicated .

There are two possibilities that could explain the presence of the tonoplast signal in the class 2 localization pattern. It is either:

1. The mutations affect a TGN retention signal and thus retention at the TGN is affected. Therefore, the mutated VHA-a1 proteins escape from the TGN to the vacuole (**Figure 6)**.

or

2. The mutations affect the COPII dependent ER exit of VHA-a1. Therefore, mutated VHA-a1 proteins are retained at the ER and the only way to leave the ER is via provacuoles to the tonoplast (**Figure 6)**. It is deduced that VHA-a3 has an intrinsic feature that steers it into provacuoles because the chimeric proteins between VHA-a1 and VHA-a3 are not directed to the TGN completely **(Figure 2 B)**. A portion of the chimeric proteins is still able to reach the tonoplast. This happens because of the presence of a provacuole entry signal in the remaining C-terminus of VHA-a3.

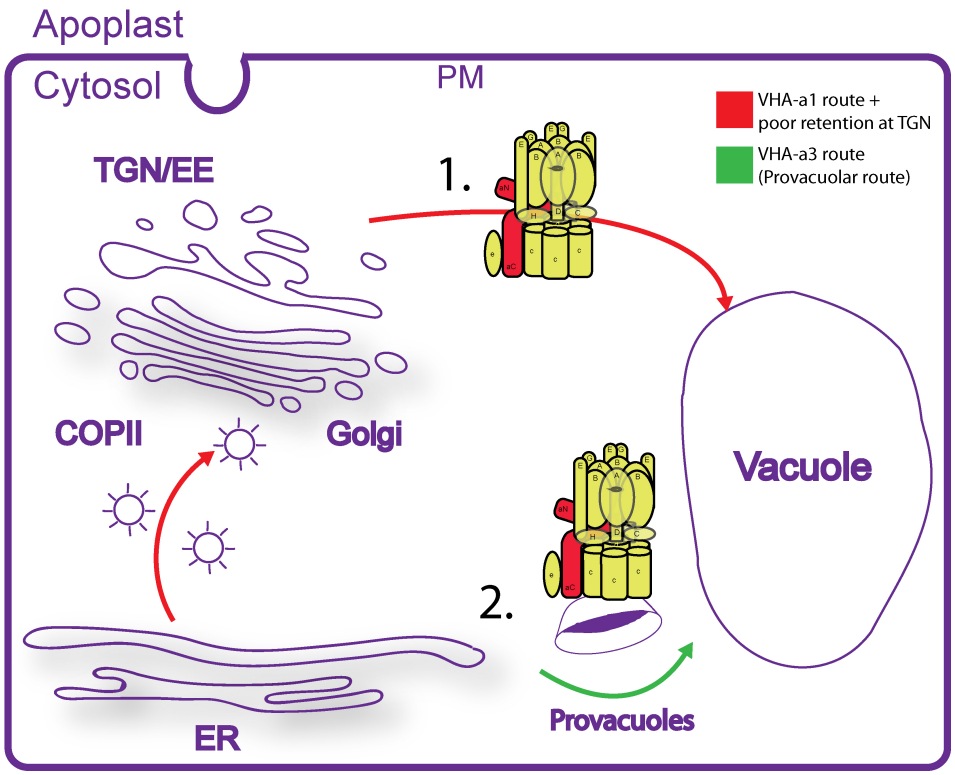

Figure 6. The two possible routes that V-ATPase complexes that incorporate mutated VHA-a1 proteins could be taking to the tonoplast

1.The mutations affect a TGN retention motif which leads to faulty retention at the TGN and escape of the complexes to the vacuole. 2. The mutations affect an ER exit motif and are transported to the tonoplast via provacuoles.

To find out which of these two routes the mutated VHA-a1 proteins were using to reach the tonoplast, we made use of the *vha-a2 vha-a3* double mutant (Krebs et al., 2010). Previous work with mutant forms of VHA-a3 has shown that a competition exists to enter provacuoles when complexes that incorporate mutated forms of VHA-a3 and complexes that incorporate non mutated isoforms are all present at the ER in *Arabidopsis* root tip cells (Neubert, 2011). VHA-a3 with a **R729N** mutation (VHA-a3-**R729N**) allows proper assembly of the V-ATPase complex but renders the complex inactive (Neubert, 2011). In the wild type background where both endogenous VHA-a2 and VHA-a3 are present, VHA-a3-**R729N** is predominately retained at the ER and only a few complexes that incorporate this mutated subunit reach the tonoplast. But in the *vha-a2 vha-*

a3 double mutant which lacks VHA-a2 and VHA-a3, complexes that incorporate VHA-a3-**R729N** are transported more efficiently to the tonoplast. This is because the competition created by VHA-a2 and VHA-a3 containing complexes to enter provacuoles is absent.

Therefore we developed the following hypothesis, that if we express mutated VHA-a1 proteins in an environment where competition to enter provacuoles is absent such as in the *vha-a2 vha-a3* double mutant, then the amount of complexes that incorporate mutated VHA-a1 proteins and that are able to enter the provacuolar route should increase. Consequentially, the intensity of the signal at the tonoplast should also increase.

Indeed, when the mutated VHA-a1 proteins were expressed in the *vha-a2 vha-a3* double mutant, the ratio of tonoplast-to-TGN fluorescence intensity decreased as compared to the wild type background (**Figure 7**). This signifies that the mutations affect an ER export motif and that the tonoplast signal in the class 2 localization pattern is due to the mutated VHA-a1 proteins being transported to the tonoplast via provacuoles and not as a result of poor retention at the TGN.

A

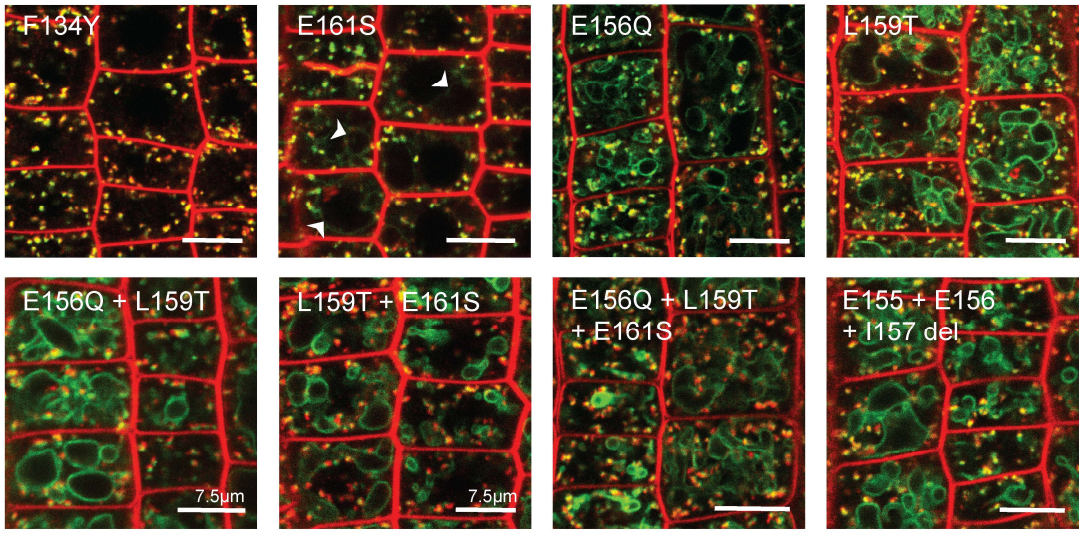
F134Y
E161S
E156Q
L159T
E156Q + L159T
L159T + E161S
E156Q + L159T
+ E161S
E155 + E156
+ I157 del
7.5µm
7.5µm

B

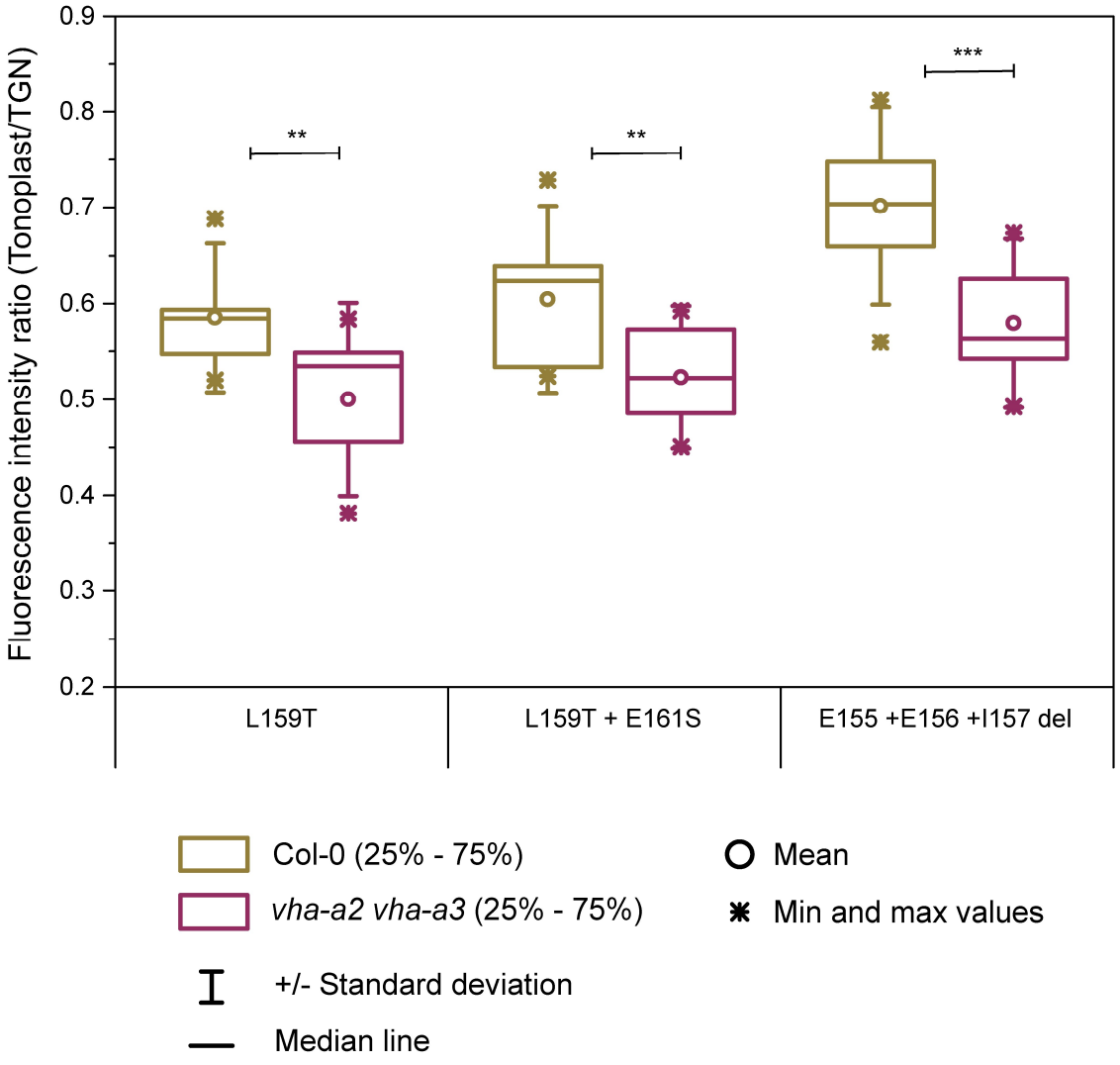
Fluorescence intensity ratio (Tonoplast/TGN)
0.9
0.8
0.7
0.6
0.5
0.4
0.3
0.2
**
**
***
L159T
L159T + E161S
E155 +E156 +I157 del
Col-0 (25% - 75%)
vha-a2 vha-a3 (25% - 75%)
+/- Standard deviation
Median line
Mean
Min and max values

Figure 7. Mutated VHA-a1 proteins are transported more efficiently to the tonoplast in the *vha-a2 vha-a3* double mutant indicating that the mutations affect an ER exit motif.

(A) The localization of mutated VHA-a1 proteins tagged to GFP were analyzed in the *vha-a2 vha-a3* double mutant background. Root tips of 6 day old seedlings were analyzed by CLSM after 20 minutes staining with FM4-64. In the *vha-a2 vha-3* double mutant, the competition to enter the provacuolar route is removed due to the absence of endogenous VHA-a2 and VHA-a3 containing complexes. As a result, complexes that incorporate the mutated VHA-a1 proteins are transported more efficiently to the tonoplast leading to a more intense tonoplast signal. The absence of competition to enter the provacuolar route in the *vha-a2 vha-3* double mutant is further accentuated by the observation that mutated VHA-a1 proteins that showed only a TGN localization (**E161S**) or a punctate pattern that is different from VHA-a1-RFP (**E156Q** and **E156Q+ L159T**) in the wild type background, also display a tonoplast signal in the *vha-a2 vha-3* double mutant. Scale bars= 10 µm unless otherwise indicated. **(B)** Tonoplast-to-TGN fluorescence intensity ratios were calculated for selected mutations in the wild type background and in the *vha-a2 vha-3* double mutant background. Box plots define the median values, 25% to 75% of values around the median and the range of values. The ratio of tonoplast-to-TGN fluorescence intensity decreased in the *vha-a2 vha-a3* double mutant indicating a more intense tonoplast signal in the mutant background. Tonoplast and TGN fluorescence intensity were measured from at least 11 independent cell images. Asterisks indicate statistically significant differences by the Students *t* test (*P < 0.05; **P < 0.005; ***P < 0.001).

We also wondered what the punctae in the class 3 localization pattern were? These punctae are different from VHA-a1-RFP therefore do not mark TGNs. This punctae were observed with the **E156Q** and **E156Q + L159T** mutations (**Figure 5 B, 8 A and B**). We hypothesised that these unidentified punctae could be specific domains in the ER or quiet possibly, COPII ER export sites. To investigate this further we first compared this localization pattern to that of a protein that is retained in the ER but not recruited to COPII ER exit sites. The protein selected was VHA-a3-**R729N** because it was established that is retained in the ER in wild type cells.

When the ER localization pattern of VHA-a3-**R729N**-GFP in wild type cells was compared to the class 3 localization pattern of the mutated VHA-a1 proteins**,** the localization patterns are distinct (**Figure 8**). The ER pattern produced by the

VHA-a3-GFP with a **R729N** mutation is more homogeneous (**Figure 8 D**). From this observation we speculated that mutated VHA-a1 proteins are recruited to specific domains in the ER for export but because the ER exit signal is mutated, the proteins cannot leave the ER and accumulate at these sites. Overall, this observation further suggested that the mutations in VHA-a1 affect an ER exit motif and beckoned the need to find a way to manipulate ER export and investigate how the export of VHA-a1 with the various mutations is affected.

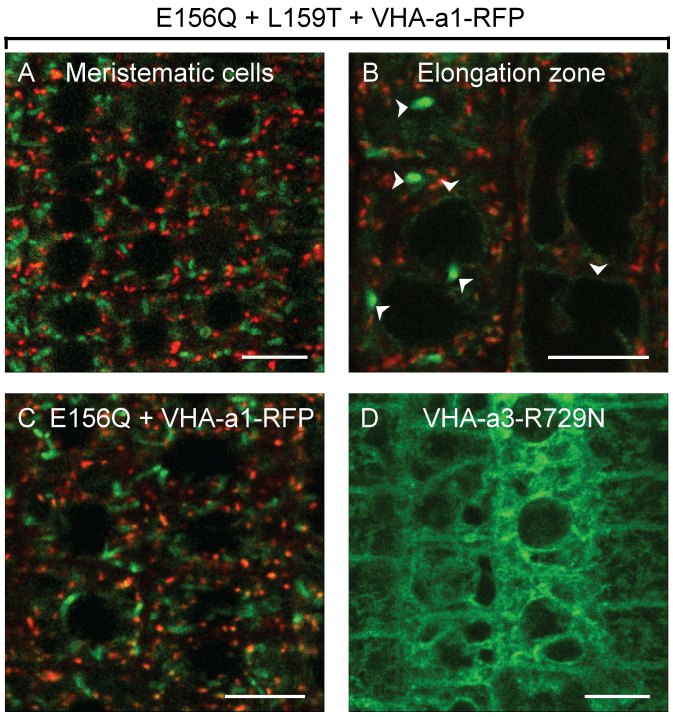

Figure 8. Mutated VHA-a1 proteins that cannot leave the ER because of a faulty ER exit motif are maybe retained in specific domains in the ER.

Root tips of 6 day old wild type seedlings were analyzed by CLSM. VHA-a1 with mutations involving E156 localizes in punctae that do not colocalize with VHA-a1-RFP. **(A) E156Q + L159T** results in a punctate localization pattern of VHA-a1 in meristematic cells. **(B)** VHA-a1 with the **E156Q + L159T** mutation is visible at the tonoplast in the elongation zone but still produces large punctae that do not colocalize with VHA-a1-RFP (white arrows). **(C)** VHA-a1 with the **E156Q** mutation alone produces punctae that do not colocalize with VHA-a1-RFP. This means that the **E156Q** mutation is dominant over the **L159T** mutation. **(D)** VHA-a3-**R729N**-GFP is retained in the ER in *Arabidopsis* wild type root tip cells but does not accumulate in punctae. Scale bars = 10.

To explore the arena of ER export, we decided to make use of a mutant of Secretion associated Ras-related GTPase (Sar1 GTPase). Sar1 GTPases are small GTPases that regulate COPII vesicle retrograde transport between the ER and Golgi membranes (Yorimitsu et al., 2014). It has been shown by transient expression in tobacco cells that AtSar1b is equally partitioned between the cytosol and ER (Hanton et al., 2008). AtSar1b with a dominant negative mutation (AtSar1b-H74L) hydrolyses GTP at a much slower rate (daSilva et al., 2004). In the presence of Sar1-H74L,vesicles are allowed to form but they accumulate to large quantities because of slow uncoating which is required for fusion with the Golgi (daSilva et al., 2004). AtSar1b-H74L has been shown to block ER export in tobacco cells and *Arabidopsis* protoplasts (Takeuchi et al., 2000; Phillipson et al., 2001; Hanton et al., 2008).

Localization studies in the *vha-a2 vha-a3* double mutant already asserted that the mutations are related to ER export. We wanted to make use of AtSar1b-H74L as a tool to directly interfere with ER exit to further confirm that the mutations in VHA-a1 affect an ER exit motif.

It was imperative to first establish that AtSar1b-H74L-CFP was able to block the ER exit of VHA-a1-GFP. The export of VHA-a1 out of the ER has been shown to be sensitive to BFA which blocks transport from the ER to the Golgi in general (Viotti et al., 2013). We expressed AtSar1b-H74L-CFP under a dexamethasone (DEX) inducible promoter (Moore et al., 1998) in an *Arabidopsis* transgenic line expressing VHA-a1-GFP. After DEX induced expression of AtSar1b-H74L-CFP, VHA-a1-GFP no longer had a punctate pattern **(Figure 9 A)** but had a characteristic ER pattern and also accumulated in dense punctae **(Figure 9 B)**. These punctae had a high degree of colocalization with AtSar1b-H74L-CFP punctae **(Figure 9 D-E)**.

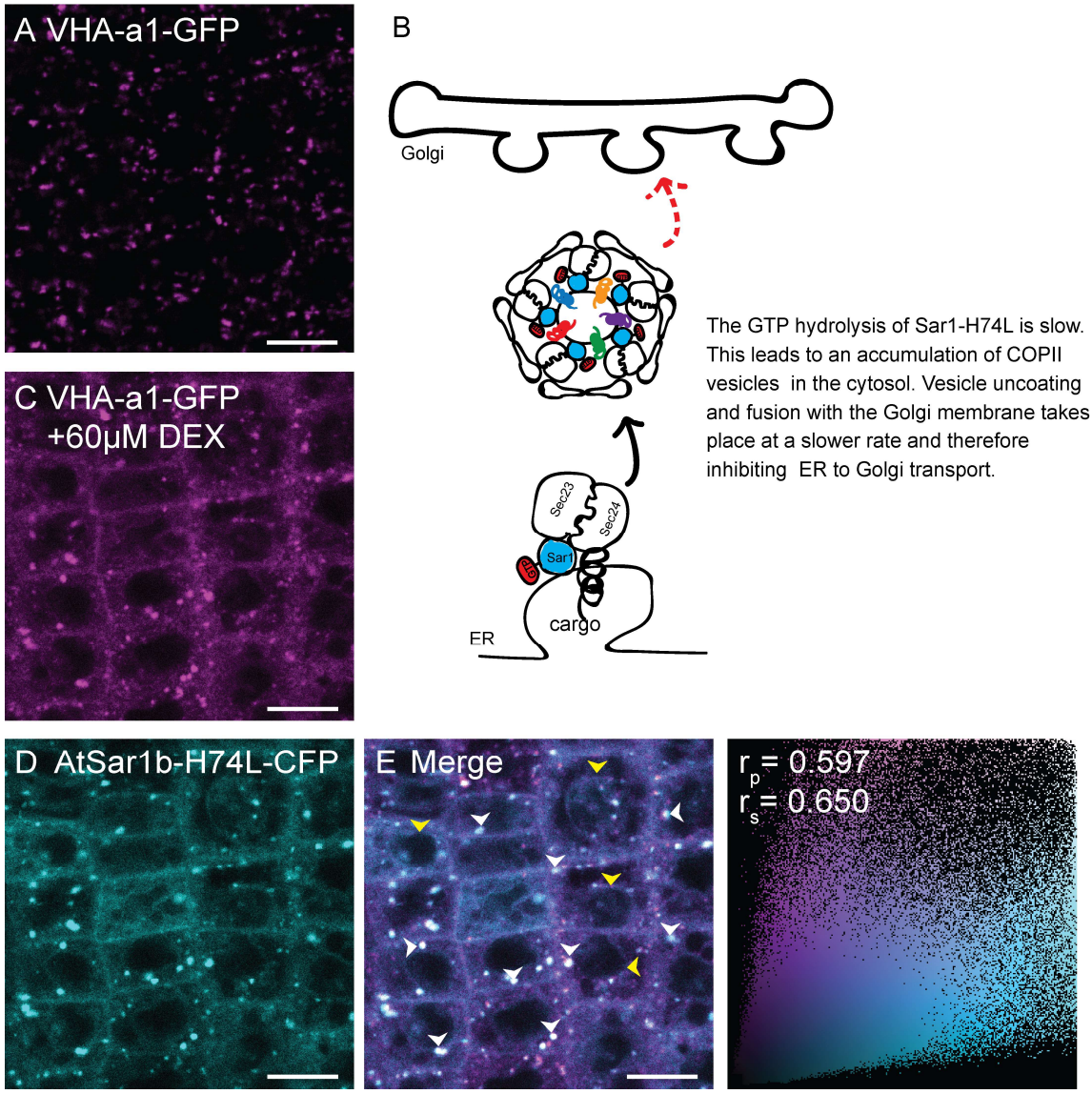

Figure 9. VHA-a1 is retained at the ER after AtSar1b-H74L-CFPexpression.

Root tips of 6 day old seedlings were analyzed by CLSM. **(A)**. VHA-a1-GFP has a punctate pattern before the expression of AtSar1b-H74L-CFP. **(B)** An illustration of the mechanism by which AtSar1b-H74L blocks COPII dependent ER to Golgi transport. **(C and D)** After 6 hours induction with 60 µM DEX, AtSar1b-H74L-CFP is expressed. VHA-a1-GFP is retained in the ER and also agglomerates to produce bright punctae. **(E)** VHA-a1-GFP and AtSar1b-H74L-CFP colocalize at the ER (yellow arrows mark perinuclear ER), cytosol and in bright punctae (white arrows). The scatter plot at the right-hand side was obtained after manual masking of individual punctae from at least 10 independent cell images. The associated Pearson or Spearman r values indicate the level of colocalization ranging from +1 for perfect colocalization to -1 for negative correlation. Scale Bars = 10 µm.

After establishing that AtSar1b-H74L-CFP is able to block ER exit via COPII vesicles (VHA-a1 route), we then investigated what happens to the trafficking of the mutated VHA-a1 proteins in the presence of AtSar1b-H74L-CFP. VHA-a3 and VHP1 (Vacuolar H^+ pyrophosphatase) (Kriegel et al., 2015) were used as controls because it has been shown that the trafficking of VHA-a3 to the tonoplast is resistant to BFA treatment and it follows the provacuolar route (Viotti et al., 2013).

As expected, the localization of VHA-a3-GFP to the tonoplast was unaffected (**Figure 10**) although the tonoplast fluorescence intensity decreased after AtSar1b-H74L-CFP expression (**Figure 11 B**). The same applies to VHP1-GFP. It can now be stated that the transport of VHP1 out of the ER to the tonoplast is also independent of COPII vesicles.

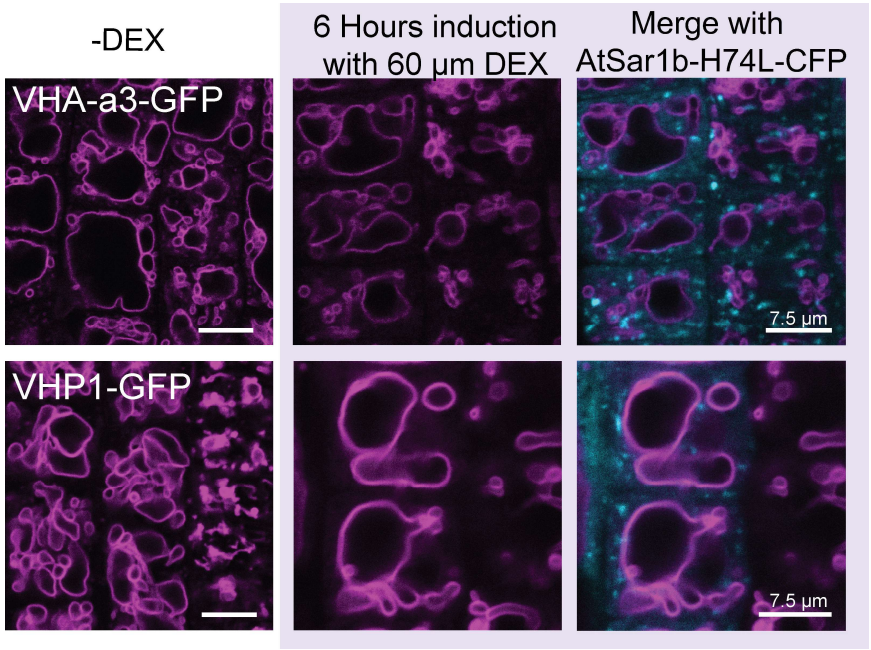

Figure 10. The trafficking of VHA-a3-GFP and VHP1-GFP to the tonoplast is independent of COPII vesicles.

Root tips of 6 day old seedlings were analyzed by confocal laser scanning microscopy (CLSM) after 6 hours induction with 60 µM DEX and in the absence of DEX. VHA-a3-GFP and VHP1-GFP still localized to the tonoplast when exit from the ER via COPII vesicles was blocked by expression of AtSar1b-H74L-CFP. Scale bars = 10 µm unless otherwise indicated.

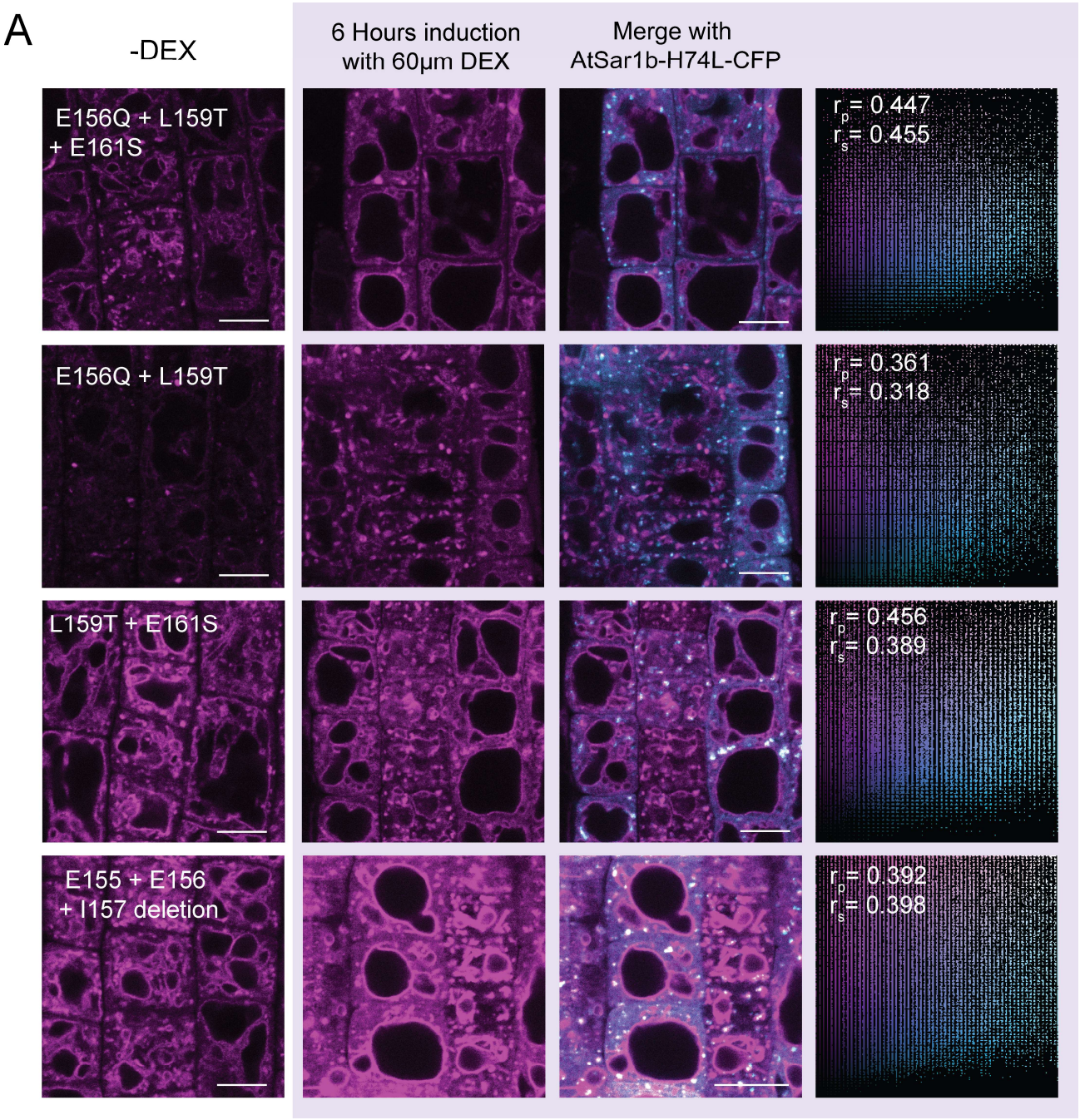
A
-DEX
6 Hours induction with 60µm DEX
Merge with AtSar1b-H74L-CFP
E156Q + L159T + E161S
r_p = 0.447
r_s = 0.455
E156Q + L159T
r_p = 0.361
r_s = 0.318
L159T + E161S
r_p = 0.456
r_s = 0.389
E155 + E156 + I157 deletion
r_p = 0.392
r_s = 0.398

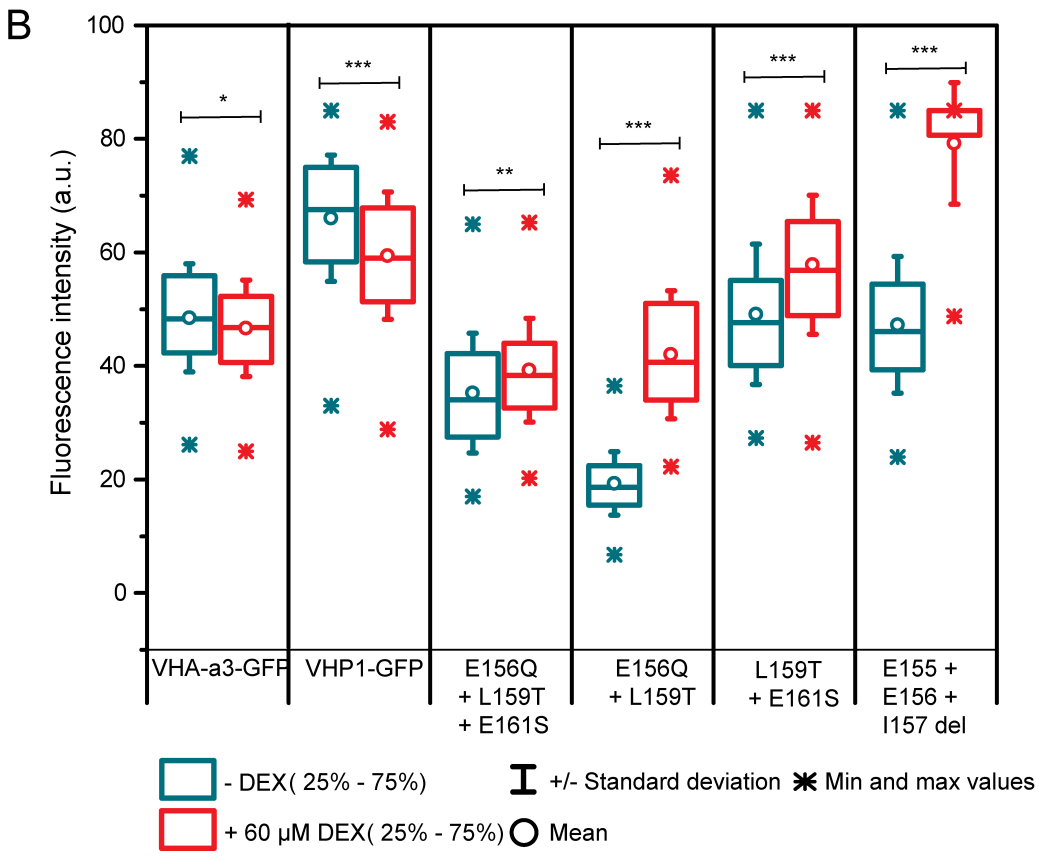

Figure 11. There is an increase in the tonoplast fluorescence intensity of mutated VHA-a1 proteins when exit from the ER via COPII vesicles is blocked by expression of AtSar1b-H74L-CFP

(A) Root tips of 6 day old seedlings were analyzed by confocal laser scanning microscopy (CLSM) after 6 hours induction with 60 µm DEX and in the absence of DEX. The mutated VHA-a1 proteins still localized at the tonoplast when exit from the ER via COPII vesicles was blocked by expression of AtSar1b-H74L-CFP. The mutated VHA-a1 proteins also localized in punctae that colocalized to a moderate degree with AtSar1b-H74L-CFP punctae meaning that the mutated proteins were still able to make contact with ER export machinery. The scatter plots at the right-hand side were obtained after manual masking of individual punctae from at least 10 independent cell images. The associated Pearson or Spearman r values indicate the level of colocalization ranging from +1 for perfect colocalization to -1 for negative correlation. **(B)** The tonoplast fluorescence intensity was measured in the presence and absence of DEX for all lines. Box plots define the median values, 25% to 75% of values around the median and the range of values. There is a significant increase in the GFP fluorescence intensity at the tonoplast of mutated VHA-a1 proteins when exit from the ER via COPII vesicles is blocked by expression of AtSar1b-H74L-CFP. Asterisks indicate statistically significant differences between the uninduced and induced conditions by the Students *t* test (*P < 0.05; **P < 0.005; ***P < 0.001). Scale bars= 10 µm.

With regard to the mutated VHA-a1 proteins, two key observations could be made when exit from the ER via COPII vesicles was blocked by expression of AtSar1b-H74L-CFP:

1. There was a significant increase in the GFP fluorescence intensity at the tonoplast for all the mutated VHA-a1 proteins (**Figure 11 A and B)**. This means that after blocking ER exit there is an increase in the trafficking of mutated VHA-a1 proteins to the tonoplast.

2. The mutated VHA-a1 proteins also localized in punctae that colocalized with AtSar1b-H74L-CFP punctae even though it was to a lesser degree than the unmutated VHA-a1 (**Figure 11 A)**. This implies that the mutated proteins are still able to make contact with ER export machinery.

These two observations reinforce the conclusions made from the observations in the *vha-a2 vha-a3* double mutant, they corroborate that the mutations are related to ER export and that the mutated VHA-a1 proteins follow the provacuolar route to reach the tonoplast.

The VHA-a1 targeting domain (a1-TD) is necessary and sufficient for targeting of VHA-a3 to the TGN

We then tested whether a1-TD was sufficient for targeting of VHA-a3 to the TGN by introducing it into the N-terminus of VHA-a3. The mutated VHA-a3 sequence was tagged to GFP and was expressed in a VHA-a1-RFP background. A portion of VHA-a3-GFP with the VHA-a1 targeting domain co-localized with VHA-a1-RFP (**Figure 12**).Therefore, the VHA-a1 targeting domain is necessary and sufficient for exit of VHA-a3 out of the ER and is also sufficient for the retention of VHA-a3 at the TGN. It is most probable that a1-TD contains overlapping ER and TGN retention motifs.

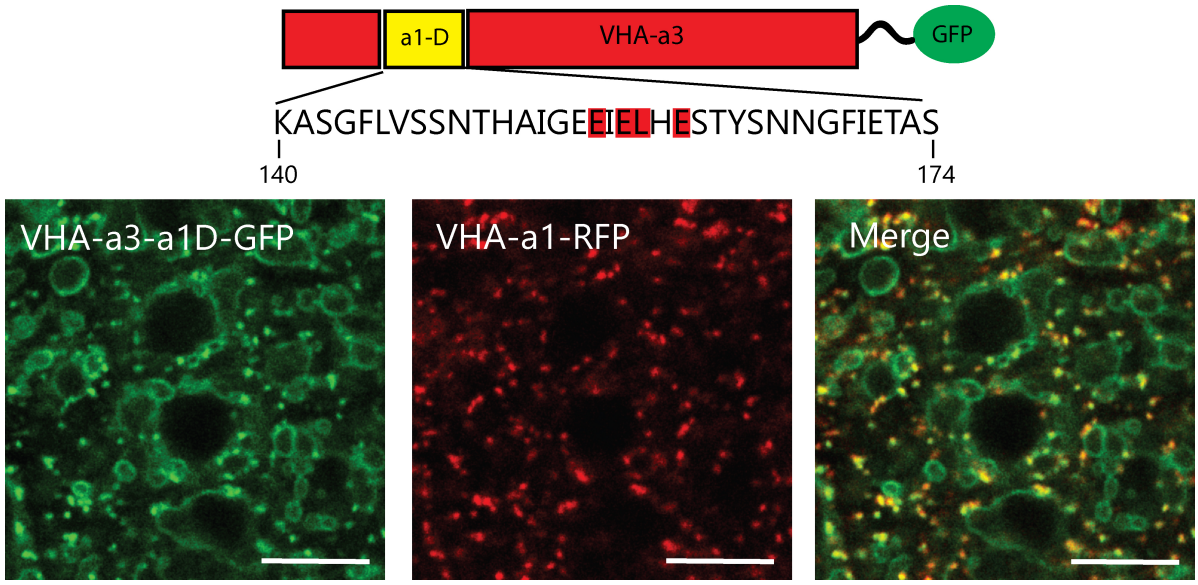

Figure 12. The a1-TD is sufficient for targeting of VHA-a3 to the TGN.

The VHA-a1 targeting domain (a1-TD) was introduced into the VHA-a3 sequence and tagged to GFP. The mutated VHA-a3 protein was expressed in a VHA-a1-RFP background. Root tips of 6 day old seedlings were analyzed by CLSM. A portion of VHA-a3-GFP with the VHA-a1 targeting domain colocalizes with VHA-a1-RFP. Scale bars= 10 µm.

V-ATPase complexes that incorporate mutated VHA-a1 subunits are functional

For the very first time, the mutations in VHA-a1 brought VHA-a1 containing V-ATPase complexes to the tonoplast. This offered a rare opportunity to compare the enzyme kinetics of VHA-a1 and VHA-a3 containing complexes on the same membrane in the cell. We were interested to know if V-ATPases that incorporate mutated VHA-a1 subunits are functional. And if they are functional, how does this activity compare to the activity of VHA-a3 containing complexes? It is known that amino acids that influence the activity of the V-ATPase are located in the C-terminus of the VHA-a subunit (Leng et al., 1998). None the less, we also wanted to investigate if the different mutations affect the activity of the enzyme.

We first assessed how each of the mutations in VHA-a1 can complement the dwarfed phenotype of the *vha-a2 vha-a3* double mutant (Krebs et al., 2010). The growth phenotype of the *vha-a2 vha-a3* double mutant is more severe in short day conditions (22˚C and 8-10 hours light)(Krebs et al., 2010). We performed phenotype assays in standard long day conditions (22˚C and 16 hours light) **(Supplemental figure S6)** as well as in short day conditions (22˚C and 10 hours light) **(Figure 13)**.

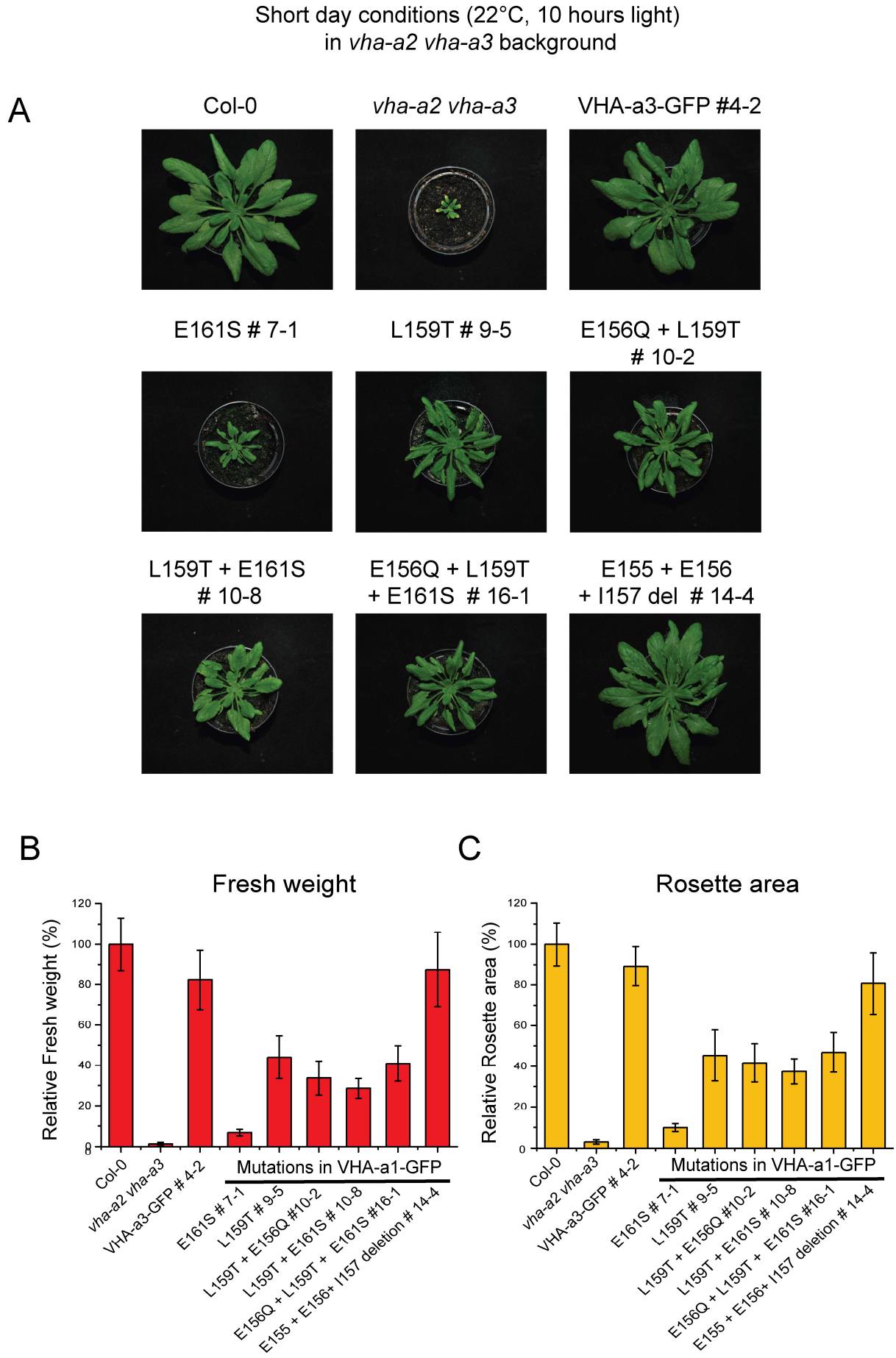
Short day conditions (22°C, 10 hours light)
in vha-a2 vha-a3 background
A
Col-0
vha-a2 vha-a3
VHA-a3-GFP #4-2
E161S # 7-1
L159T # 9-5
E156Q + L159T
10-2
L159T + E161S
10-8
E156Q + L159T
+ E161S # 16-1
E155 + E156
+ I157 del # 14-4
B
Fresh weight
Relative Fresh weight (%)
0
20
40
60
80
100
120
Col-0
vha-a2 vha-a3
VHA-a3-GFP # 4-2
Mutations in VHA-a1-GFP
E161S # 7-1
L159T # 9-5
L159T + E156Q #10-2
L159T + E161S # 10-8
L159T + L159T + E161S #16-1
E156Q + L159T + E161S #16-1
E155 + E156+ I157 deletion # 14-4
C
Rosette area
Relative Rosette area (%)
0
20
40
60
80
100
120
Col-0
vha-a2 vha-a3
VHA-a3-GFP # 4-2
Mutations in VHA-a1-GFP
E161S # 7-1
L159T # 9-5
L159T + E156Q #10-2
L159T + E161S # 10-8
L159T + L159T + E161S #16-1
E156Q + L159T + E161S #16-1
E155 + E156+ I157 deletion # 14-4

Figure 13. The mutated VHA-a1-GFP proteins complement the *vha-a2 vha-a3* double mutant to varying degrees.

(A) Plants were grown in short day conditions (22˚C and 10 hours light) for 6 weeks. All mutant variants of VHA-a1-GFP displayed bigger rosette size than the *vha-a2 vha-a3* double mutant. **E161S** which had a faint signal at the tonoplast in the *vha-a2 vha-a3* background (**Figure 7 A**) also partially complemented the dwarf phenotype of the *vha-a2 vha-a3* double mutant. **(B)** Rosette fresh weight of 6 week old plants grown under short day conditions (n=12). Wild type rosette size is set to 100%. VHA-a1 with **E155+ E156 + I157** deletion complements the *vha-a2 vha-a3* double mutant the best. **(C)** Rosette area of 6 week old plants (n=12). Wild type rosette size is set to 100%.

All the mutations in VHA-a1 complemented the *vha-a2 vha-a3* double mutant but to varying degrees which reflected the intensity of the proteins observed at the tonoplast **(Figure 7).** VHA-a1 with the **E155 + E156 + I157** deletion conferred the highest degree of rescue. The rosette area and diameter of plants expressing VHA-a1 with this triple deletion were comparable to that of *vha-a2 vha-a3* double mutant plants expressing VHA-a3-GFP (**Figure 13**). The differences in rosette size were more perceptible in short day conditions. The poorest complementation was observed with the **E161S** mutation. This is in agreement with the faint tonoplast signal which was observed with this mutation in the *vha-a2 vha-a3* double mutant.

We then wondered if the differences in rosette size reflected differences in V-ATPase activities. Three VHA-a1-GFP mutation lines which represented high, intermediate and low degrees of rescue were selected for further analysis. Tonoplast vesicles were prepared from 6 week old rosettes of short day grown plants and the ATP hydrolysis and proton translocation activities were measured (**Figure 14 A**). The first key observation made was that all V-ATPases that incorporate the mutated VHA-a1 subunits had some level of activity, they are functional. This was expected because all the selected mutations in VHA-a1 complemented the *vha-a2 vha-a3* double mutant. The pumps which incorporated mutated VHA-a1 subunits had comparable ATP hydrolysis activity to pumps that incorporated VHA-a3-GFP (**Figure 14 A**).

Proton translocation activities were estimated by loading the tonoplast vesicles with the fluorescence dye ACMA (9-Amino-6-Chloro-2-Methoxyacridine) and then measuring the ATP-dependent fluorescence quenching of the dye in the presence of 3 mM ATP (**Figure 14 A**). The fluorescence quenching experiments were performed in the presence of 1 mM Sodium Vanadate which is an inhibitor of P-type ATPases. VHA-a1 with the **L159T + E161S** exhibited the most efficient coupling of ATP hydrolysis to proton translocation (**Figure 14 C$^{\delta}$**).

In fully expanded cells, the cell sap pH is generally accepted to represent the vacuolar pH because in mature cells the vacuolar lumen accounts for 80-90 % of the whole cell volume (Kurkdjian and Guern, 1981), therefore cell sap pH measurements were performed to determine the vacuolar pH. Surprisingly, cell sap pH measurements showed that the VHA-a1-GFP mutation lines had more alkaline vacuoles (pH ~6.1) compared to wild type vacuoles (pH 5.89) under short day growth conditions at 22˚C (**Figure 14 B**). However the vacuoles of the VHA-a1-GFP mutation lines were not as alkaline as the *vha-a2 vha-a3* double mutant vacuoles (pH 6.49).

As a final assessment of the enzyme dynamics of VHA-a1 and VHA-a3 containing complexes, we analyzed a situation where increased coupling

efficiency may be advantageous. We investigated the process of cold acclimation where V-ATPases play a central role. Cold acclimation is a process whereby plants acquire increased freezing tolerance after being exposed to low non freezing temperatures for days or weeks depending on the species (Xin and Browse, 2000). The cold acclimation process is dependent on increased tonoplast proton pumping activity (Kriegel et al., 2015). Cell sap pH measurements were performed after cold acclimation at 4˚C for 4 days. The wild type cell sap pH underwent a slight cold induced drop from 5.89 to 5.80, consistent to what has been previously reported (Kriegel et al., 2015) (**Figure 14 B)**. After cold acclimation, the VHA-a1-GFP mutation lines still displayed more alkaline cell sap pH values than the wild type and VHA-a3-GFP line but they also exhibited a cold induced drop in pH (**Figure 14 B)**.VHA-a1 with the **E155 + E156 + I157** deletion exhibited the largest cold induced drop in cell sap pH (comparable to wild type pH drop) from 6.14 to 6.03.

The amount of V-ATPases in each line was determined via western blot. VHA-a1 with the **E155 + E156 + I157** deletion has the highest amount V-ATPases which may account for its good complementation of the *vha-a2 vha-a3* double mutant (**Figure 14 D**). But high protein levels cannot be solely responsible for the good complementation because other mutation lines (**L159T** and **E156Q +L159T**) also have high amounts of protein but do not complement the *vha-a2 vha-a3* double mutant to comparable degrees as VHA-a1 with the **E155 + E156 + I157** deletion.

Short day conditions
in *vha-a2 vha-a3* background

A

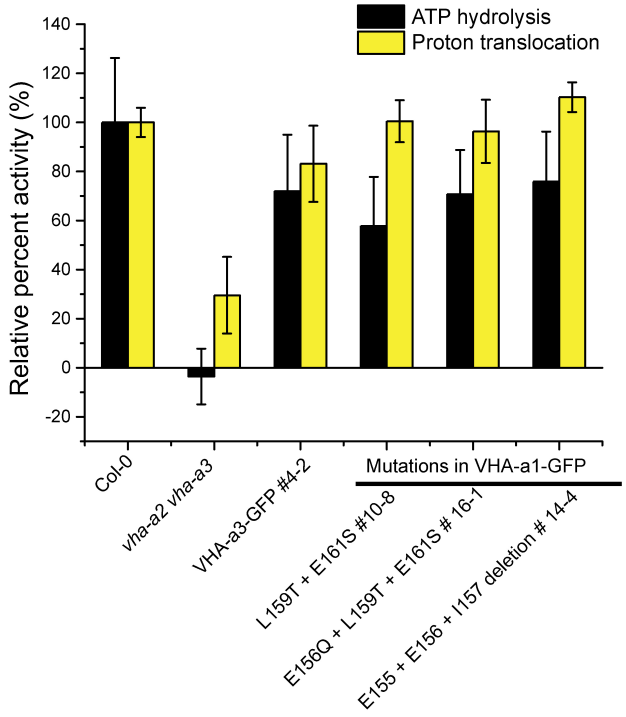

B

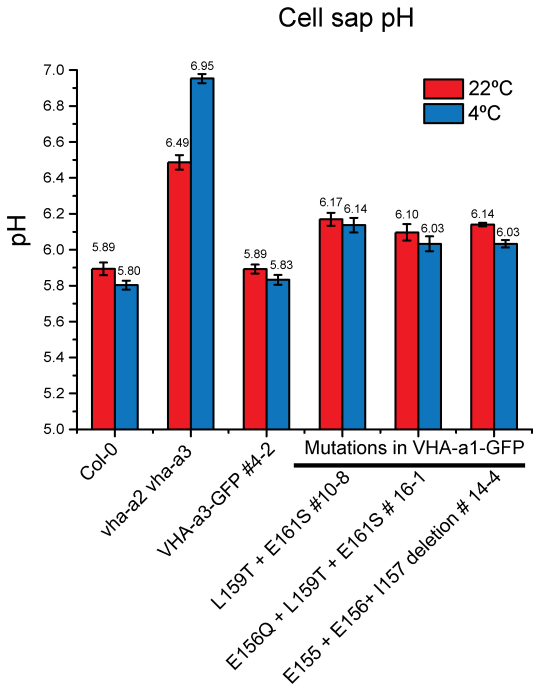

C

Kinetic analysis of V-ATPases containing mutated VHA-a1 subunits

	ATP hydrolysis[α]	Initial rate of[β] fluorescent quenching	Coupling[δ] ratio
	µmol ATP/min/mg	ΔF/s/mg	fluorescent quenching/ ATPase activity
Col-0	0.0917	2.284	24.9
VHA-a3-GFP #4-2	0.0660	1.899	28.8
L159T + E161S #10-8	0.0530	2.295	43.3
E156Q + L159T + E161S # 16-1	0.0649	2.201	33.9
E155 + E156 + I157 deletion # 14-4	0.0695	2.519	36.2

D

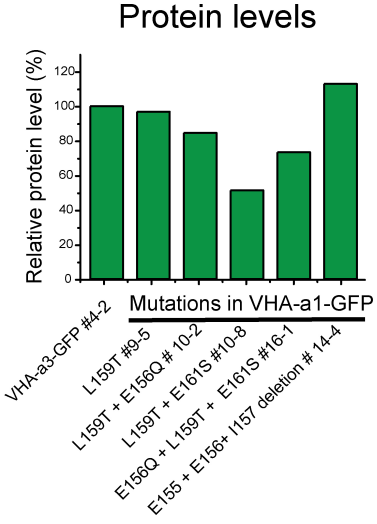

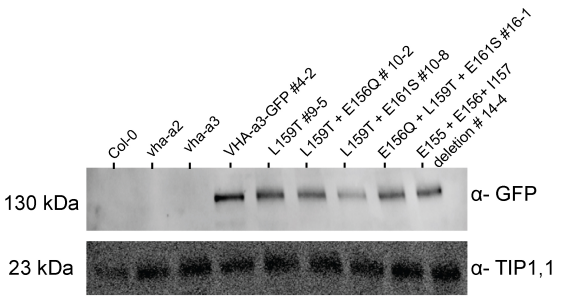

Figure 14. V-ATPases that incorporate mutated VHA-a1 subunits are functional.

(A) V-ATPases that incorporate the mutated VHA-a1 subunits have comparable V-ATPase activities as VHA-a3-GFP. Tonoplast membranes were isolated from 6 week old plants grown under short day conditions at 22°C. KNO_3-inhibited V-ATPase activity was measured. The ATP-dependent proton transport activities were estimated from the initial rate of ATP-dependent fluorescence quenching in the presence of 3 mM ATP using the fluorescence dye ACMA (9-Amino-6-Chloro-2-Methoxyacridine) in the presence of 1 mM Sodium Vanadate. Sodium Vanadate inhibits P-type ATPases. Approximately 25 µg of protein was used for these assays. The average of two individual experiments is shown (**B)** Mutated VHA-a1 containing V-ATPases have more alkaline cell sap pH values. All lines display a slight drop in cell sap pH after cold acclimation with the exception of the *vha-a2 vha-a3* double mutant. Plants for cell sap pH measurements were grown for 6 weeks under short-day conditions at 22°C. Cold acclimation was performed at 4˚C for 4 days. Cell sap pH measurements were performed at the same time for both temperature conditions. Error bars represent SD of *n = 4* technical replicates. **(C)** VHA-a1 with the double mutation **L159T+E161S** confers the most efficiency in coupling ATP hydrolysis to proton transport. $^{\alpha}$ KNO_3-inhibited V-ATPase activities in µmol ATP/min/mg. $^{\beta}$ Initial rate of ATP-dependent fluorescence quenching (ΔF/s/mg) . $^{\delta}$ The coupling ratio was calculated by dividing the initial rate of fluorescence quenching by the ATPase activity measured at the same ATP concentration (3 mM). **(D)** Abundance of the GFP tagged proteins was determined via western blot.Tonoplast membrane proteins from the same preparations used for the activity assays were separated by SDS-PAGE and subsequently immunoblotted with an anti-GFP antibody. Equal protein loading is indicated by TIP1;1 detection. Protein levels were measured using Fiji and normalized to TIP1;1. The VHA-a3-GFP #4-2 protein level is set to 100%. Bar charts represent quantification of one representative immunoblot.

The a1-TD is evolutionary conserved in the VHA-a1 clade and originates from the gymnosperms

The V-ATPase is an evolutionary conserved nano-engine found in all eukaryotes (Finnigan et al., 2012b). We were interested to trace the distribution of the a1-TD in the plant kingdom and to trace its evolutionary origin. In order to accomplish this, VHA-a related sequences from higher plants, lower plants and algae were collected from various online databases. The sequences collected included predicted protein sequences as wells as cDNA sequences.

The C-terminus of subunit a of the V-ATPase is more conserved in terms of amino acid sequence than the N-terminus (Kawasaki-Nishi et al., 2001). For this reason, and the fact that the a1-TD is found in the N-terminus of AtVHA-a1, phylogenetic analysis was performed on N-terminal sequences only. Phylogenetic analysis of the collected sequences showed that the hallmarks of the a1-TD (acidic residues and a critical leucine residue) are absent in the green algae sequences (chlorophytes) **(Figure 15 and 16).** The bryophytes: *P.patens*, *M. polymorpha*, *S. fallax* and the lycophyte: *S. moellendorfii* also do not contain the a1-TD sequence.

A noteworthy observation is that in the algae *K. flaccidum* (Division *Charophyta*, Order *Klebsormidiales*) all the amino acids thought to comprise the ER exit signal are conserved with the exception of E156 (sequence number based on AtVHA-a1) (**Figure 15)**. Charophytes are considered to be the closest relative to the ancestor of land plants (Hori et al., 2014).

The acidic residues and the critical leucine residue in the a1-TD are conserved throughout the angiosperms (**Figure 16**). Some angiosperm species have an occasional substitution of a glutamic acid residue with an aspartic acid residue (the grasses: *B. distachyon*, *B. stacei* and *T. aestivum*). The critical leucine residue is hundred percent conserved within the charophyte, gymnosperm and angiosperm sequences with only one exception, the sea grass: *S.polyrhiza* (**Figure 16**).

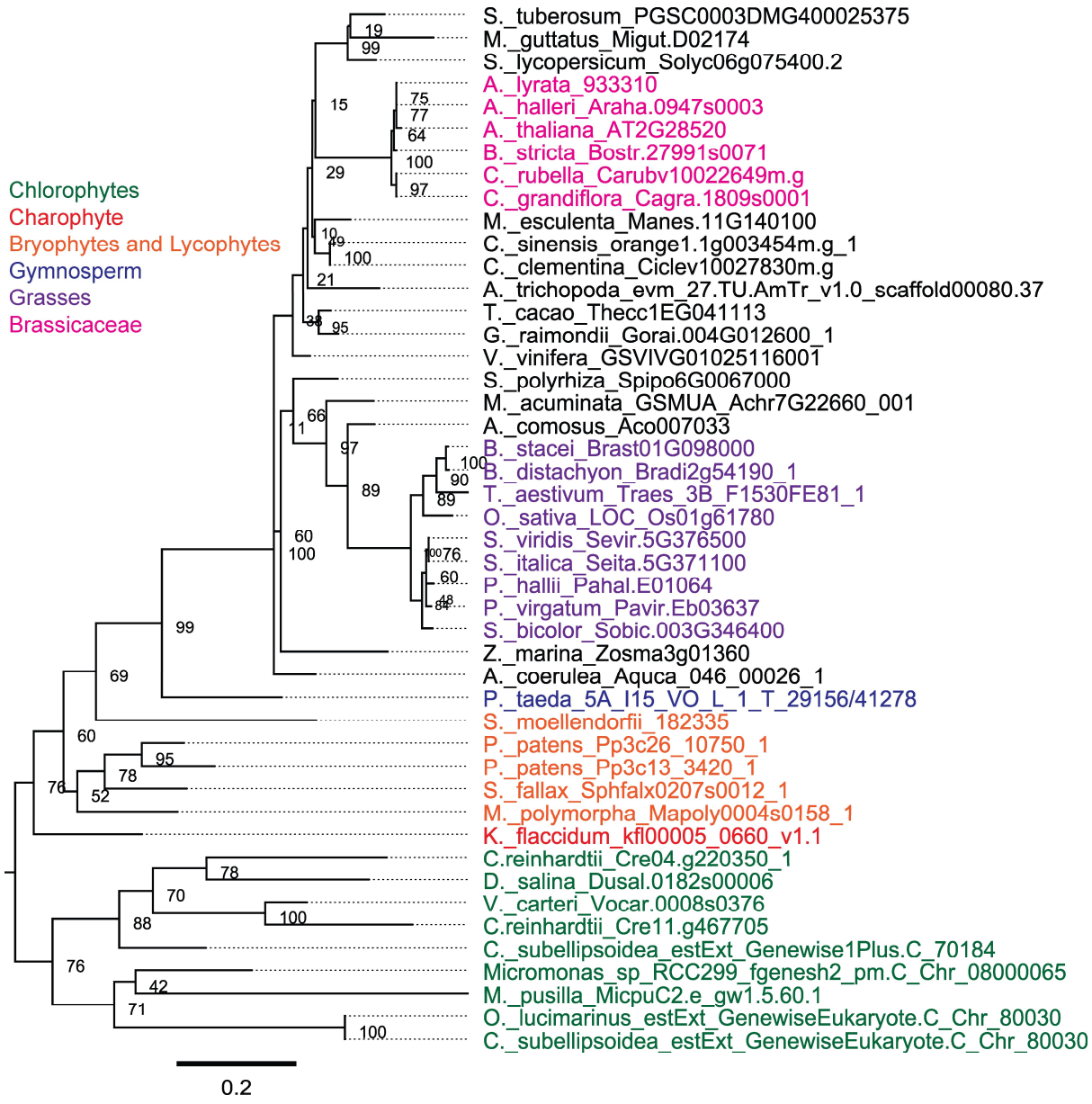

Figure 15. Phylogenetic analysis of the N-terminal sequences of VHA-a1 related proteins.

For each species a selected VHA-a1 related protein sequences is shown. Branch support is calculated on the basis of 500 bootstraps. The protein sequences from which the tree was generated are reported in **Supplemental table S2**. A larger version of this tree encompassing more species is shown in **Supplemental Figure S9**. Tree was constructed with Maximum likelihood (PHYML) (Guindon et al., 2010).

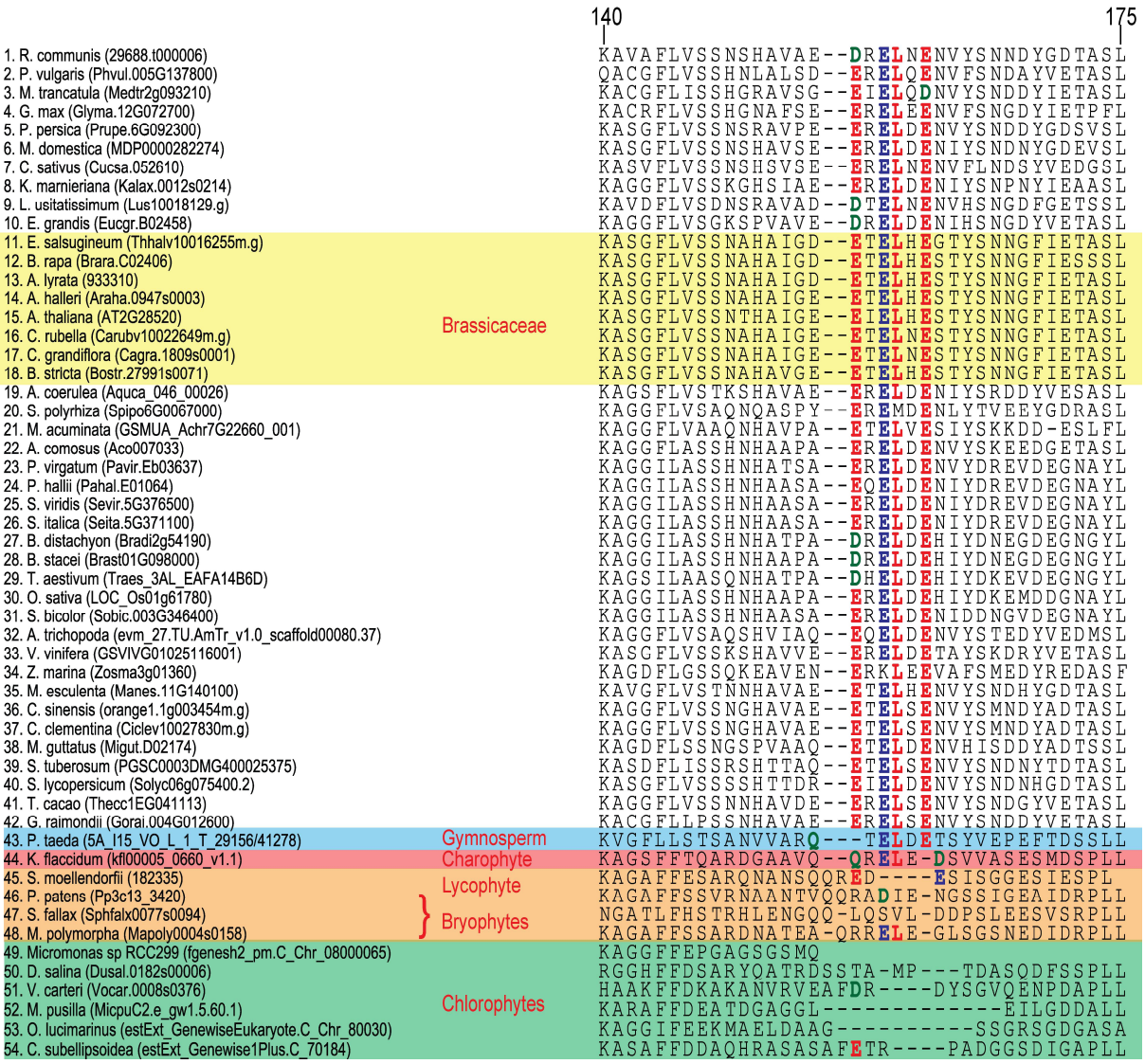

Figure 16. The a1-TD sequence originates in the gymnosperms.

Hallmarks of the a1-TD (acidic residues and a critical leucine residue) are absent from the chlorophytes, bryophytes and lycophytes. The sequence of the gymnosperm, *P. taeda* and that of the charophyte, *K.flaccidum* contain all the amino acids thought to comprise the ER exit signal with the exception of E156 (sequence number based on AtVHA-a1). Amino acids in red are the acidic residues and the critical leucine whose solitary mutation has been shown to partially change the localisation of AtVHA-a1 from the TGN to the tonoplast. The glutamic acid residue in blue is conserved in the VHA-a1 and VHA-a3 clade. Amino acids in green are ones that deviate from the conserved ones but share similar properties. The sequence numbers are in reference to the *A. thaliana* VHA-a1 sequence. Multiple sequence alignments were performed using Clustal Omega (Sievers et al., 2011).

Acidic clusters are also found in VHA-a1 homologues from other kingdoms

After tracing the origin of the VHA-a1 targeting sequence in the plant kingdom, we were interested to know if the VHA-a1 targeting sequence exists in other non plant organisms. We collected sequences with the highest homology to VHA-a1 from *M. musculus* (a2 isoform), *C. elegans* (UNC-32 isoform c), *D. melanogaster* (VHA100-2_PB), *D. rerio* (ATP6VOa1b) and yeast (Stv1p) (**Table 1**). An alignment of amino acids corresponding to the first 412 amino acids of VHA-a1 (the N-terminus) was performed. At first glance, the alignment showed that the specific sequence of amino acids of the a1-TD is absent from the mouse, yeast, fly, worm, and zebra fish homologous sequences (**Figure17 A**). Furthermore, the Stv1p targeting motif is absent in all the other organisms from the other kingdoms. It appears this sequence is unique to yeast.

Table 1. Localization of V-ATPases with different homologues of VHA-a1 from other species

Organism	Subunit	Localization	Reference
M. musculus (Mouse)	a2	Endosome (kidney proximal tubule cells)	(Marshansky and Futai, 2008)
C. elegans (Worm)	UNC-32 isoform c	Neuronal cells (compartment not mentioned)	(Lee et al., 2010)
*D.melanogaster (*Fly)	Vha100-2_PB	Plasma membrane	(Allan et al., 2005)
D. rerio (Zebra fish)	ATP6VOa1b	Lysosome	(Peri and Nüsslein-Volhard, 2008)
S. cerevisiae (Yeast)	Stv1p	Golgi/endosmal network	(Kawasaki-Nishi et al., 2001)

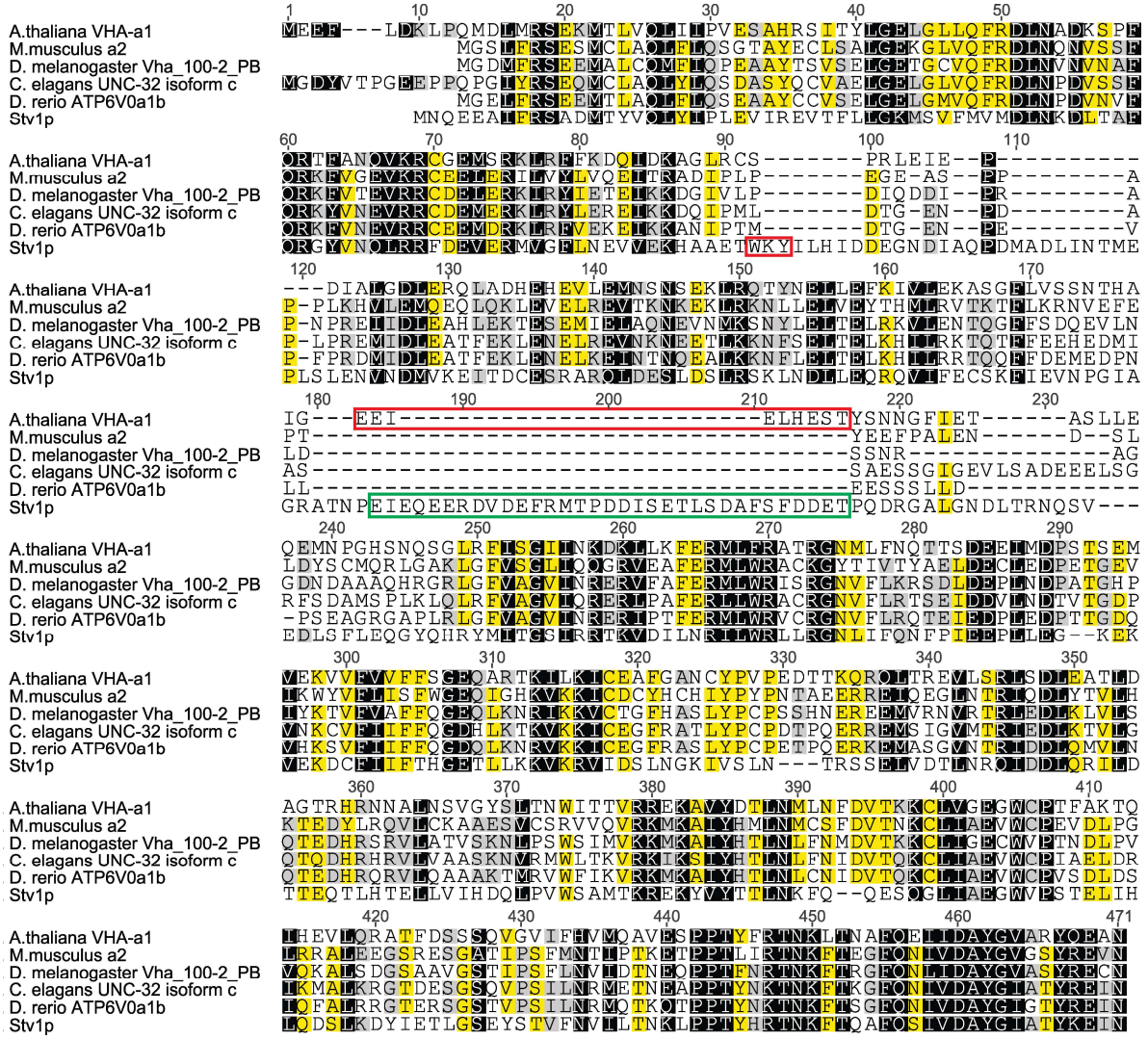

Figure 17. The specific sequence of acidic amino acids of the a1-TD is unique to the plant kingdom.

An alignment of amino acid sequences corresponding to the first 412 amino acids of VHA-a1 (the N-terminus) from *M. musculus* (a2 isoform), *C. elegans* (UNC-32 isoform c), *D. melanogaster* (Vha100-2_PB), *D. rerio* (ATP6VOa1b) and *S. cerevisiae* (Stv1p). Residues similar between all proteins at the same position are shown against a black background. Residues similar between only four of the proteins at the same position are shown against a yellow background. Residues similar between only three of the proteins at the same position are shown against a grey background. Un highlighted residues are variable in all five sequences at the same position. The position of the tri-peptide motif that is responsible for the targeting of Stv1p and the acidic cluster of the a1-TD are indicated with red boxes. An acidic cluster in Stv1p is indicated with a green box. An alignment excluding the Stv1p sequence was performed for better visualization of the a1-TD. The full alignment is reported in **Supplemental Figure S10**. Multiple sequence alignments were performed using Clustal Omega (Sievers et al., 2011).

Since it has been established that the acidic cluster in VHA-a1 serves as an ER exit motif. We investigated whether VHA-a1 homologous sequences from other kingdoms also contain acidic clusters in the region corresponding to the location of the a1-TD in VHA-a1. Indeed when the multiple sequence alignments were analysed further, we identified some acidic clusters in the mouse, yeast and worm sequences (**Figure 17 and 18**). This acidic clusters are not restricted to endosomal targeting isoforms. But since the acidic cluster is an ER exit motif, all isoforms in these organisms might possess them. Further investigations in these organisms is warranted.

S. cerevisiae

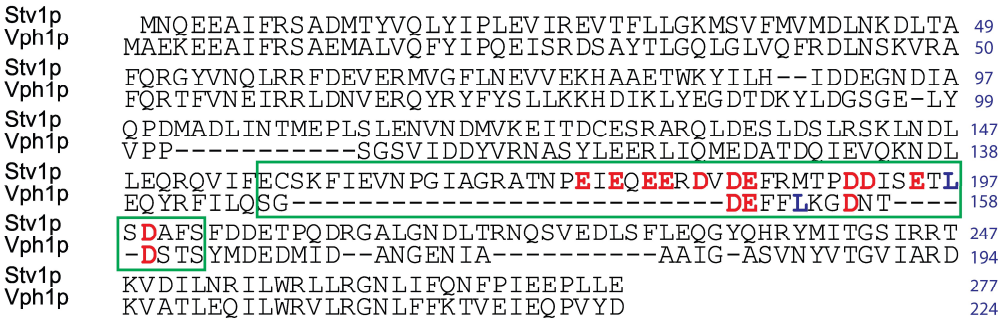

M. musculus

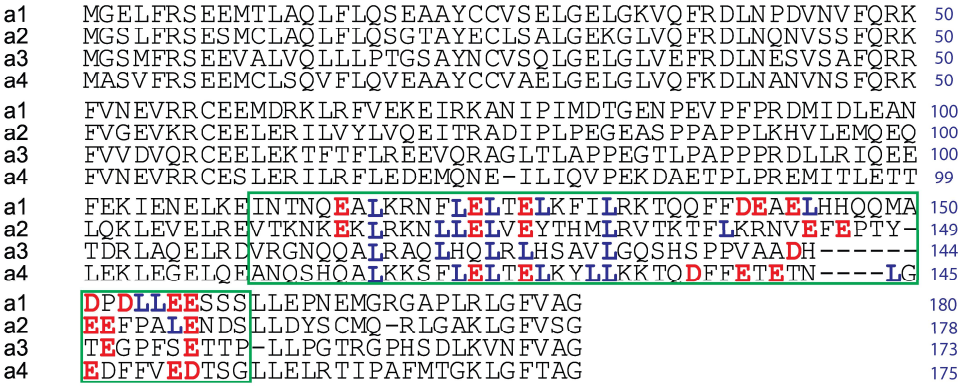

C. elegans

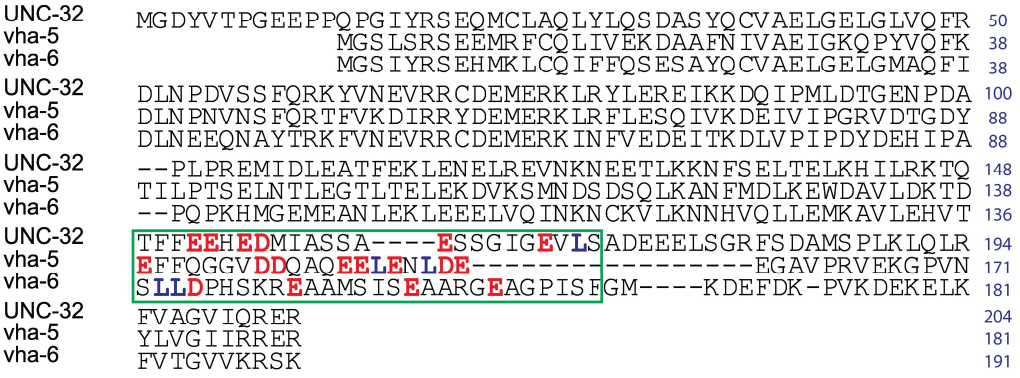

Figure 18. Sequences homologous to VHA-a1 from other kingdoms also contain acidic clusters.

An alignment of VHA-a1 homologous sequences from *S. cerevisiae* , *M. musculus* and *C. elegans*. Green boxes indicate regions corresponding to the position of the a1-TD in VHA-a1. Glutamic and aspartic acid residues are depicted in red and leucines in blue. Acidic clusters are not restricted to endosomal targeting isoforms in all organisms. The function of these acidic clusters in these organisms is yet to be determined. Multiple sequence alignments were performed using Clustal Omega (Sievers et al., 2011)

Discussion

VHA-a1 possesses an acidic motif that is both an ER exit and TGN retention signal

The V-ATPase is a multifaceted enzyme which has two important localizations in the plant cell: the TGN/early endosome and the tonoplast. These localizations are achieved by the subunit a isoforms VHA-a1,VHA-a2 and VHA-a3. It has been reported that in the meristematic cells of the *Arabidopsis* root tip, VHA-a1 and not VHA-a3 is transported to its destination in the cell in a Golgi dependent manner (Viotti et al., 2013). This implies that V-ATPase pumps that incorporate the different VHA-a subunits are sorted already at the ER. With this information in mind, interesting questions arose. Such as how are VHA-a1 containing complexes sorted at the ER? And once they enter the secretory pathway, how are VHA-a1 containing complexes retained at the TGN? Does VHA-a1 posses a specific signal?

In this study we have identified a region in VHA-a1 that is necessary and sufficient for the ER export and TGN retention of VHA-a1. We called this region the VHA-a1 targeting domain (a1-TD) and it consists of 34 amino acids (K140-S174). This region contains an acidic cluster and a critical leucine residue that are important for proper localization of VHA-a1. A site directed mutagenesis approach was taken to uncover the contribution of each of the conserved amino acids to the targeting of VHA-a1 and we show that this region contains an overlapping ER exit and TGN retention motif. VHA-a3 with the a1-TD localized at the tonoplast and TGN and does not end up at the apoplast which is the default destination for all proteins in the secretory pathway with no targeting signals (Rojo and Denecke, 2008).

We show that mutated VHA-a1-GFP proteins leave the ER via the provacuolar route (ER to tonoplast) because when competition to enter this route is removed such as in the *vha-a2 vha-a3* double mutant and when ER exit via COPII vesicles

is blocked via expression of AtSar1H74L-CFP, the mutated VHA-a1-GFP proteins localize more efficiently to the tonoplast. The ability of the mutated VHA-a1-GFP proteins to rescue the dwarfed phenotype of the *vha-a2 vha-a3* double mutant to varying degrees provides evidence for the existence of the provacuolar route in other developmental growth stages of the plant and not just meristematic cells of the root tip as was previously reported.

The location of the a1-TD in the N-terminus of VHA-a1 is consistent with what has been reported about the location of the targeting information in the yeast subunit a homologues (Kawasaki-Nishi et al., 2001). The targeting information of Stv1p is located in its N-terminus and it was found to be a tripeptide motif WKY(aa 83-85) (Finnigan et al., 2012a). Surprisingly, the WKY motif is absent in the VHA-a1 sequence which implies that the targeting motifs for plant and yeast evolved independently.

A crucial observation is that the TGN signal is not lost with all the mutations that cause a tonoplast localization of VHA-a1-GFP. One interpretation of this observation would be that the mutations each affect the targeting signal of VHA-a1 partially and so some of the protein is still able to localize properly at the TGN. The degree of change in the GFP fluorescence at the tonoplast after AtSar1H74L-CFP expression can be an indicator of how each of the mutations affects the targeting motif of VHA-a1. Simultaneously, the degree of the change in GFP fluorescence at the tonoplast after AtSar1H74L-CFP expression can also be an indicator of how VHA-a3- like the proteins become. A complete tonoplast localization pattern for VHA-a1 may not be achievable through further mutagenesis of the a1-TD because further point mutations might lead to mis-folding and subsequent degradation of the protein. However, we have identified residues that are very important in the a1-TD. E156 is absolutely essential for ER exit. Its mutation to glutamine (E156Q) results in a punctate localization pattern that is different from VHA-a1-RFP. In addition, the sole mutation of L159 to threonine (L159T) resulted in a dual localization of the mutated VHA-a1 protein at the TGN and tonoplast

We were unable to determine the cellular localization of VHA-a1-GFP with some mutations. For some of the mutations, we observed localization patterns that were different from the VHA-a1-RFP localization pattern but also not consistent with a general ER localization pattern. We postulate that the punctae observed could be ER export sites or they could also be autophagosomes which would concur with the weak fluorescence of VHA-a1-GFP observed with these mutations. Ultrastructure and immunogold electron microscopy analysis will be able to identify the true nature of these punctae.

The 3D models obtained in this study may be useful in studying other aspects related to subunit a function. They may also be used in computational docking experiments with Sec24, which is responsible for cargo selection for the COPII coat (Miller et al., 2003). Docking experiments may help to determine if a1-TD can interact with any of the cargo binding sites in Sec24.

The VHA-a1 and VHA-a3 containing V-ATPases may be differentially regulated by luminal pH

Mutated VHA-a1 subunits were able to complement the dwarf phenotype of the *vha-a2 vha-a3* double mutant to varying degrees. This implied that complexes that incorporated the mutated VHA-a1 subunits were functional. To gain some insight into the kinetics of these pumps, we estimated their ATP hydrolysis activities and proton translocation activities on isolated tonoplast vesicles. We discovered that these pumps achieve comparable levels of ATP hydrolysis and proton translocation activities to each other and to VHA-a3-GFP containing V-ATPases in vitro.

Surprisingly however, the VHA-a1-GFP mutation lines do not have similar cell sap pH values as the VHA-a3 GFP line and wild type. The VHA-a1-GFP mutation lines have more alkaline vacuoles. After cold acclimation, the VHA-a1-GFP mutation lines exhibited a cold induced drop in cell sap pH but still displayed more alkaline cell sap pH values than the wild type and VHA-a3-GFP line.

One possibility that could account for these observations could be the inherent property of the V-ATPase complex. The V-ATPase complex differs from other ATPases because it can adjust its coupling of ATP hydrolysis to proton translocation depending on the electrical gradient across the membrane (Rienmüller et al., 2012). The pump is most active when the gradient is low and slows down when the luminal pH becomes more acidic (Rienmüller et al., 2012).

The in vitro assays suggest that there is no difference between VHA-a1 and VHA-a3 containing complexes. This may be due to the fact that the V-ATPase activities are determined on vesicles which are of the same size with the same luminal pH values. In vivo, VHA-a1 containing complexes localize to a different membrane (TGN membrane) which has a different electrical gradient to the tonoplast membrane. The steady state luminal pH values of the TGN and vacuole are different. These compartments have pH values of 5.66 and 5.91 respectively (Luo et al., 2015). It is possible that the V-ATPases that incorporate the mutated VHA-a1 subunits are only able to acidify to certain pH limits in vivo. This alludes that VHA-a1 and VHA-a3 confer different regulation properties to the V-ATPase complex. To further compare the kinetic properties of V-ATPase complexes containing VHA-a1 and VHA-a3, ATPase activities could be measured over a range of ATP concentrations to determine Vmax and Km values. Electrophysiology experiments should also be conducted to investigate the enzyme kinetics even further.

Over all, the results imply that the rosette size of the plants expressing VHA-a1-GFP with various mutations is contributed by, but not limited to, good protein expression. Because some mutation lines have high amounts of protein but do not complement the *vha-a2 vha-a3* double mutant to a comparable degree as VHA-a3-GFP. There must be another underlying factor.

The a1-TD is conserved in the plant kingdom

V-ATPases in various endomembranes are ancient proton pumps that appeared before the separation of green plants from fungi and animals (Li, Yanbang, Provenzano et al., 2016). Multiple sequence alignments of sequences related to VHA-a1 from various plant species revealed that the acidic cluster is not unique to *A. thaliana*. It has yet to be shown whether the motif is operational in the other plant species.

Here we present evidence that the targeting motif of the TGN localized isoform arose even before the appearance of gymnosperms and is now conserved amongst higher plants (**Figure 19**). The alga *K. flaccidum*, a charophyte who are considered to be the closest relative to the ancestor of modern day plants (Hori et al., 2014), contains the acidic cluster minus the first glutamic acid residue. The acidic cluster in the *K. flaccidum* sequence is similar to the one in the gymnosperm sequence of *P. taeda*.

None of the sequences obtained for the basal land plants, bryophytes and lycophytes, contain the acidic cluster. Studies in the liverwort *M. polymorpha* and the moss *P. patens* that focused on machinery components of membrane trafficking pathways such as Soluble N-ethylmaleimide-sensitive factor attachment proteins (SNAREs) have shown that these basal plants have an endomembrane system like in higher plants (Kanazawa et al., 2016; Furt et al., 2012). Therefore, theoretically it is possible for these plants to possess differently localizing V-ATPases. These basal plants already have multiple VHA-a1 homologous sequences, it is yet to be determined if all these homologues are different isoforms and if they localize the V-ATPase differently. The best approach to answer these questions would be to express these *M. polymorpha* and *P. patens* sequences in *A. thaliana* and see where they localize.

The absence of the Stv1p sorting signal in VHA-a1 argues that the Golgi/TGN-localized subunit a isoforms in fungi and plants evolved independently and that

the vacuolar isoforms are the ancestral isoforms. A recent study in yeast proposes that the two subunit a isoforms evolved from a duplication event (Finnigan et al., 2011). In the latter study, an ancestral subunit a was constructed by calculating the maximum likelihood sequence from a large set of subunit a isoforms from modern yeast species. Subsequent localization studies in *S. cerevisiae* revealed that this ancestral subunit a caused a dual localization of the V-ATPase to the vacuolar membrane and Golgi/endosomal network. Most significantly, this ancestral isoform does not contain the Golgi/endosome retention motif of Stv1p and retention at the Golgi is achieved by slow anterograde trafficking towards the vacuole. Therefore the specialization of the two yeast isoforms came later in evolution. Thus, we can also speculate that the absence of the VHA-a1 targeting motif in the basal plant sequences might indicate that they possesses a dual localizing V-ATPase and that the specialization of the different isoforms in higher plants came later during evolution.

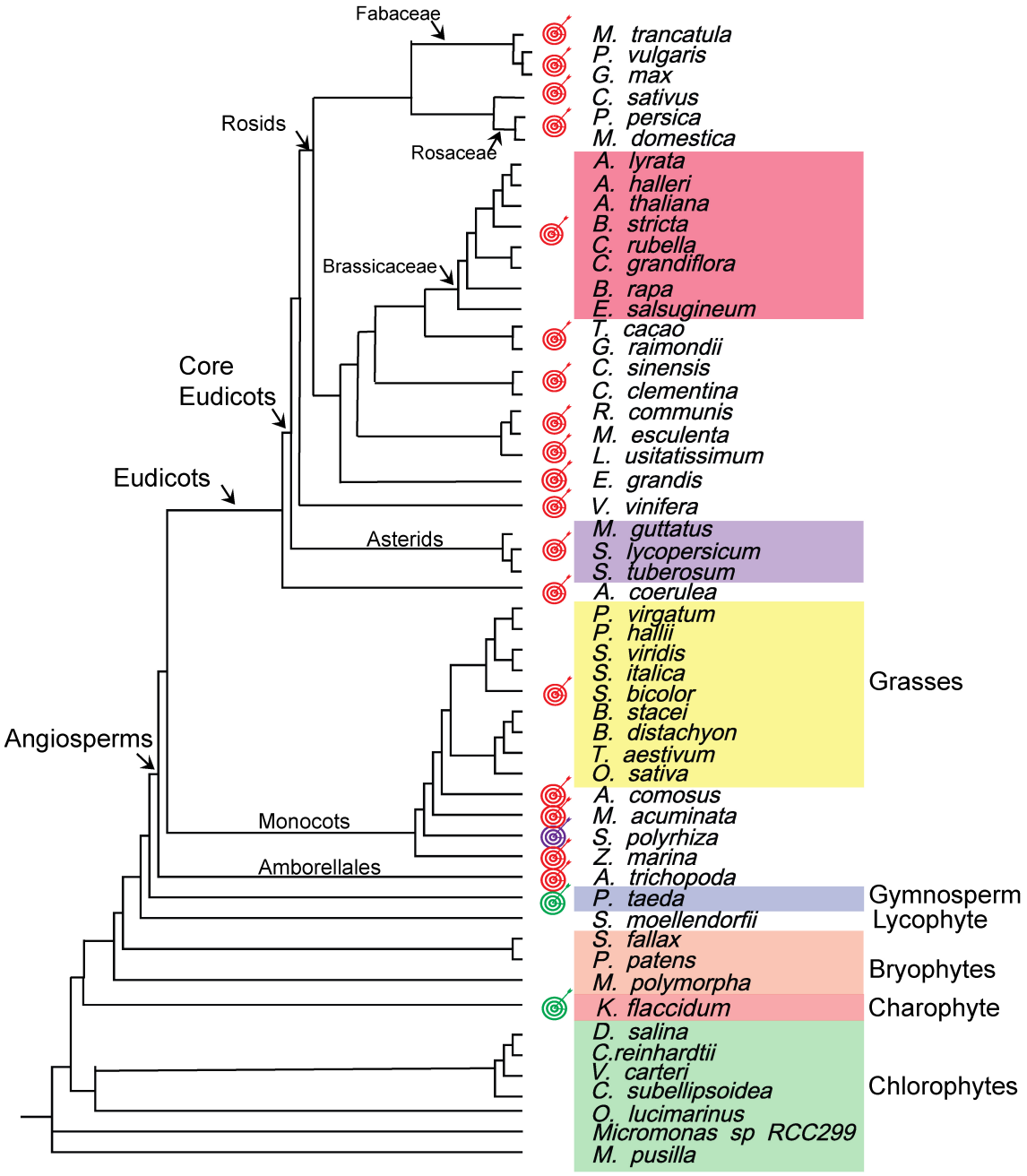

Figure 19. The distribution of the a1-TD in the plant kingdom.

The presence of the complete acidic cluster and leucine is indicated by a red dart board. A purple dartboard indicates the absence of the critical leucine. A green dartboard indicates that one of the acidic amino acids of the acidic cluster is missing, such as is the case for *P. taeda* and *K. flaccidum*.

Acidic clusters as potential COPII ER exit motifs in the animal kingdom

The unique sequence of amino acids of the acidic cluster of the a1-TD is unique to the plant kingdom. Analysis of VHA-a1 homologous sequences form *C. elegans*, *D. rerio* and *D. melanogaster* showed that the acidic cluster is clearly absent in these sequences. However, closer analysis of these sequences in the region corresponding to the location of the a1-TD in VHA-a1 revealed that there are multiple acidic residues in all the animal sequences. These acidic residues are present in all isoforms from these organisms. It is worth mentioning that the vacuoles or lysosomes in animal cells are not as large and prominent as in plant cells. The provacuolar route in plant cells is believed to exist because of the need to deliver large quantities of membranes to build the large vacuole of plant cells. If in animal cells, the only way out of the ER is via COPII vesicles, than all subunit a isoforms should contain an ER exit motif. Therefore it is worth investigating if these acidic amino acids identified in this study are the ER exit motif in the animal proteins.

Yeast Stv1p and Vph1p both contain acidic clusters that are different from the a1-TD. Since Vph1 containing V_O subcomplexes were shown to be packaged into COPII vesicles (Per Malkus, Laurie A. Graham, Tom H. Stevens, 2004), it follows that a signal is required to enter this pathway. Therefore it would be interesting to determine if the identified acidic clusters in Stv1p and Vph1p are important for COPII entry.

Supplementary material

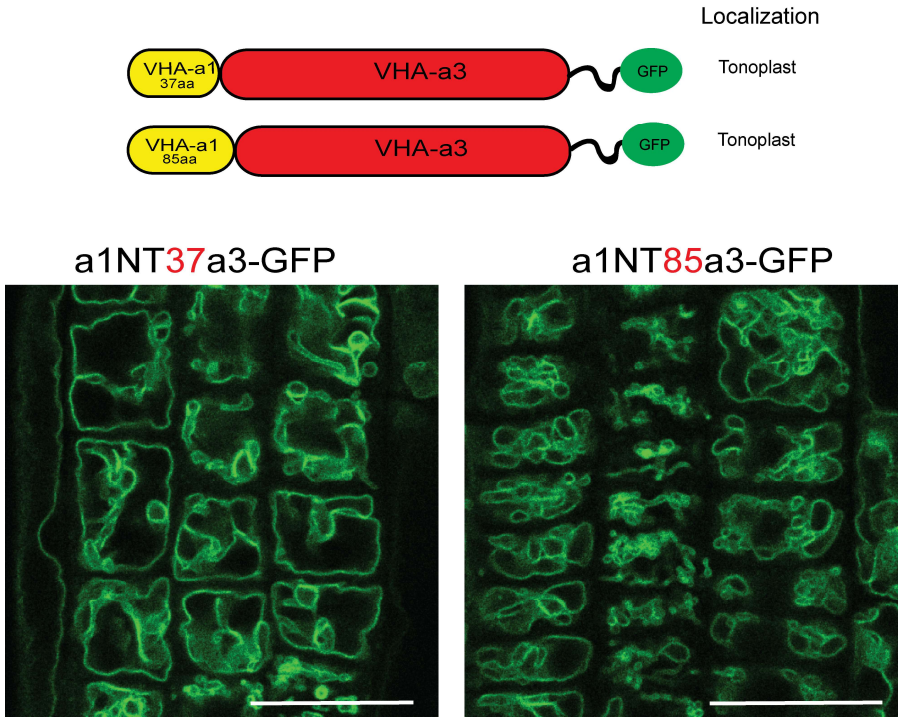

Figure S1. The targeting signal of VHA-a1 is not located in the first 85 amino acids.

Chimeric proteins were made which consisted of increasing lengths of the VHA-a1 N-terminus fused to decreasing lengths of the C-terminal domain of VHA-a3. All constructs were fused to GFP. Root tips of 6 day old seedlings were analyzed by confocal laser scanning microscopy (CLSM). The first two chimeric constructs consisting of 37 aa and 85 aa of the VHA-a1 N-terminal domain localized at the tonoplast. Scale bars = 25 µM.

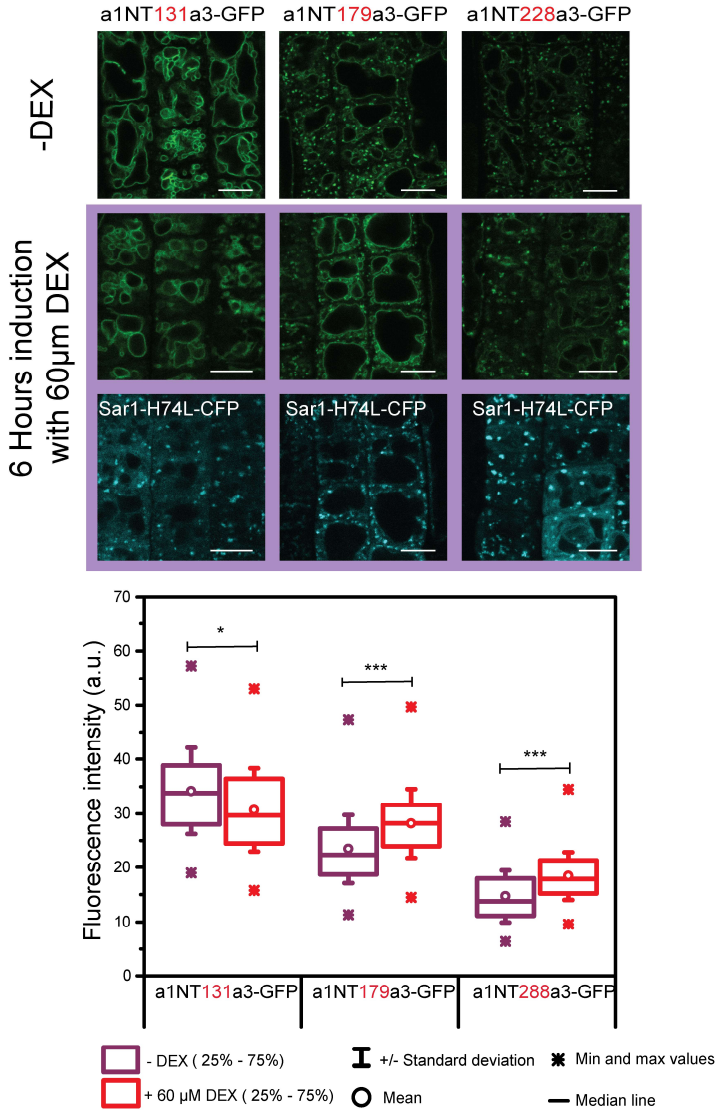

Figure S2. There is an increase in the tonoplast fluorescence intensity of the chimeric proteins that show dual TGN and tonoplast localization when exit from the ER via COPII vesicles is blocked by expression of Sar1H74L-CFP.

Sar1-H74L-CFP was expressed under the dexamethasone (DEX) inducible promoter system in the transgenic lines expressing the chimeric constructs. Root tips of 6 day old seedlings were analyzed by confocal laser scanning microscopy (CLSM) after 6 hours induction with 60 µm DEX and in the absence of DEX. There is a significant increase in the GFP fluorescence intensity at the tonoplast of a1NT**179**a3-GFP and a1NT**228**a3-GFP when exit from the ER via COPII vesicles is blocked by expression of Sar1H74L-CFP. Box plots define the median values, 25% to 75% of values around the median and the range of values. Asterisks indicate statistically significant differences between the uninduced and induced conditions for each chimeric construct by the Students *t* test (*P < 0.05; **P < 0.005; ***P < 0.001). Scale bars = 10 µm.

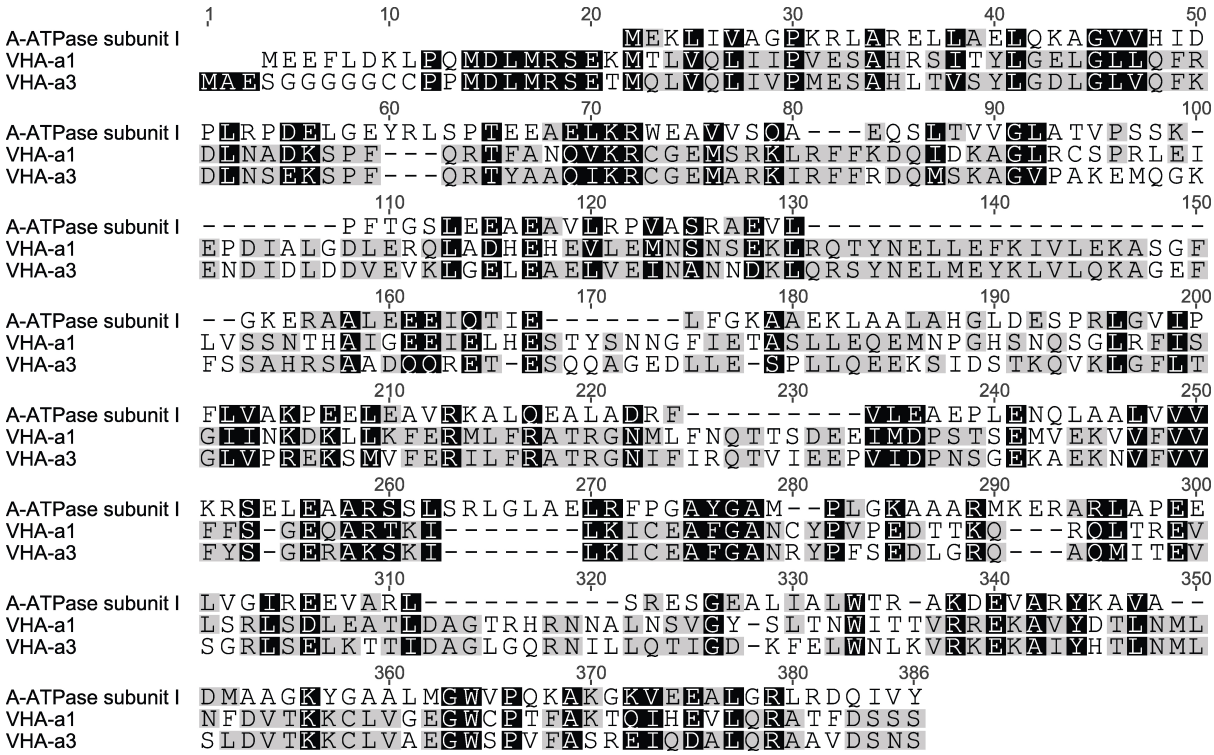

Figure S3. The amino acid sequence homology between Subunit I of *M. ruber* and *A. thaliana* subunits is low.

An alignment of amino acid sequences of VHA-a1 and VHA-a3 from *Arabidopsis* and *M. ruber* subunit I N-termini. The alignment is only up to 301 residues of subunit I because no electron density for the *M. ruber* subunit I was observed beyond residue 301. These sequences were used as inputs for the homology modelling. Sequence residues highlighted in black are similar between all proteins at the same position, in grey are similar between only two of the proteins at the same position and Un-highlighted residues are variable in all three sequences. The VHA-a1 and VHA-a3 aa sequences have an identity of 15% to the aa sequence of subunit I. Multiple sequence alignment was performed using Clustal Omega (Sievers et al., 2011).

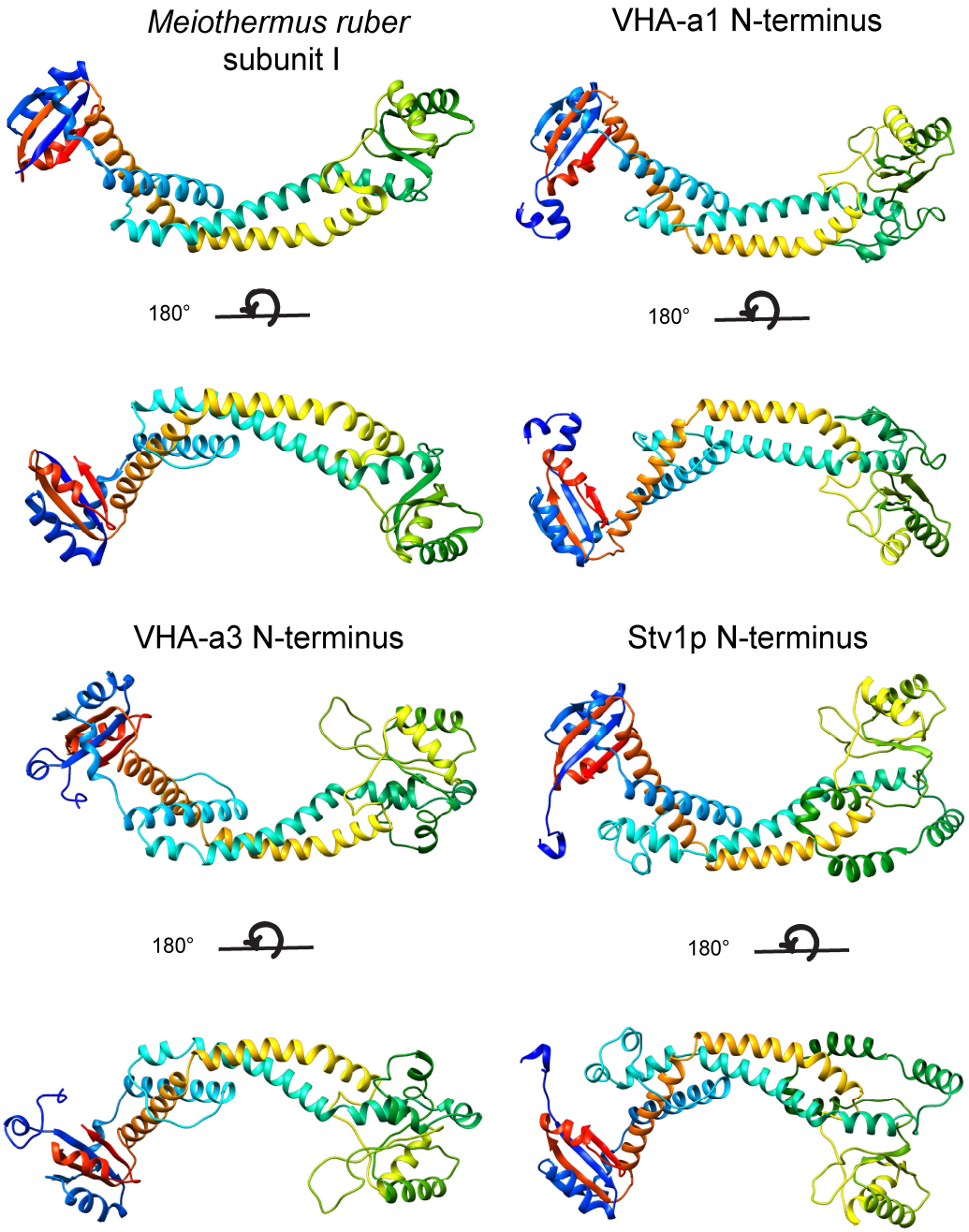

Figure S4. Three-dimensional homology modelling of the VHA-a1 and VHA-a3 N termini

Homology modelling of the N- termini of VHA-a1 and VHA-a3 was done using the coordinates of the N-terminus of subunit I of the A-ATPase from *M. ruber* (ProteinDataBankcode:3RRK) as a template. The models are colour ramped. The 3D models obtained for the N- termini of VHA-a1 and VHA-a3 are highly similar in topology to the model obtained for Stv1p (Finnigan et al., 2012a).

Table S1. Statistical support for the predicted structural homology models obtained from I-TASSER.

Subunit a N-terminal domain	Quality of Predicted Model	
	C-Score	TM-Score
VHA-a1	-0.85	0.61 ± 0.14
VHA-a3	-0.86	0.61 ± 0.14
Stv1p	-2.12	0.46 ± 0.15

The quality of the models generated using the online server I-TASSER is evaluated by using two criteria, C-score and the TM-score. The C-score is an estimate of the confidence of structure prediction, and ranges from − 5 to 2. Models with a higher score reflect a model of better quality. The TM-score is a measure of structural similarity between the predicted model and the template, and ranges from 0 to 1. A higher score indicates a better structural similarity (Roy et al., 2010).

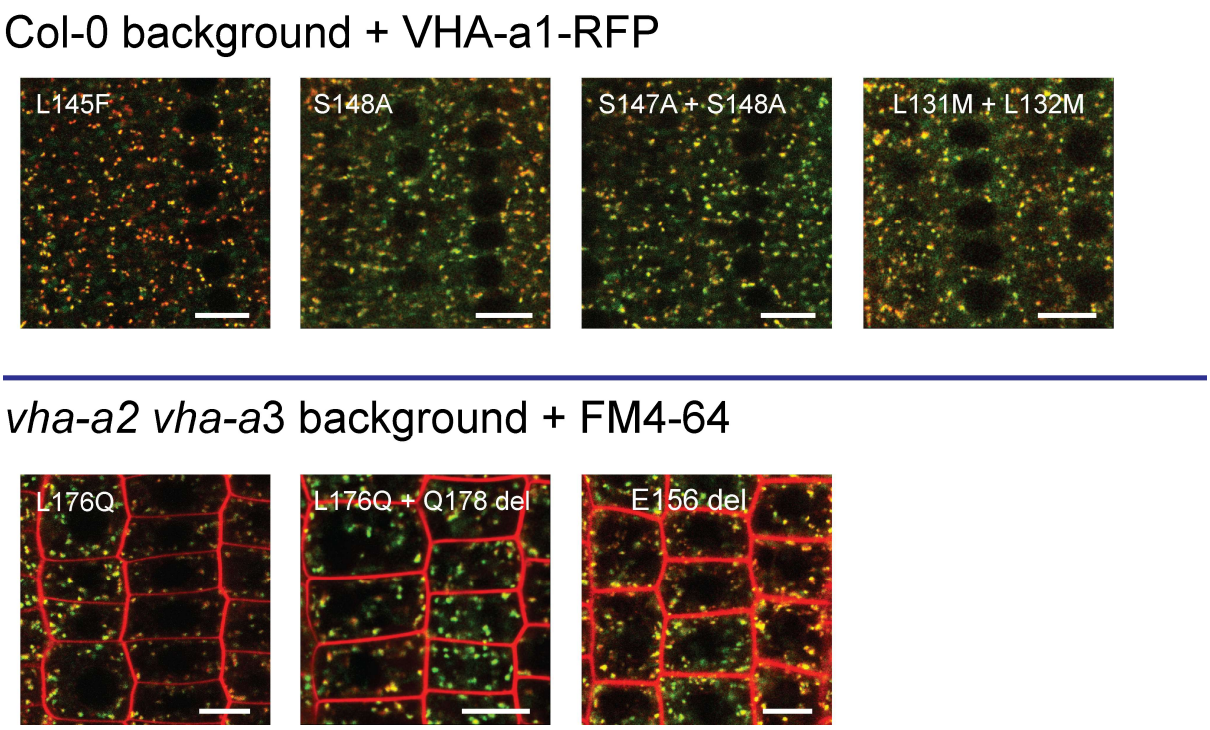

Figure S5. Additional amino acids that were mutated in VHA-a1 and that did not cause a change in the TGN localization of VHA-a1.

Conserved amino acids were mutated individually and combinatorially and the effect on the localization of GFP tagged VHA-a1 was analyzed in the wild type background and in the *vha-a2 vha-a3* double mutant background. Root tips of 6 day old seedlings were analyzed by CLSM. Scale bars = 10 µm

A Long Day: 22˚C, 16 hours light.

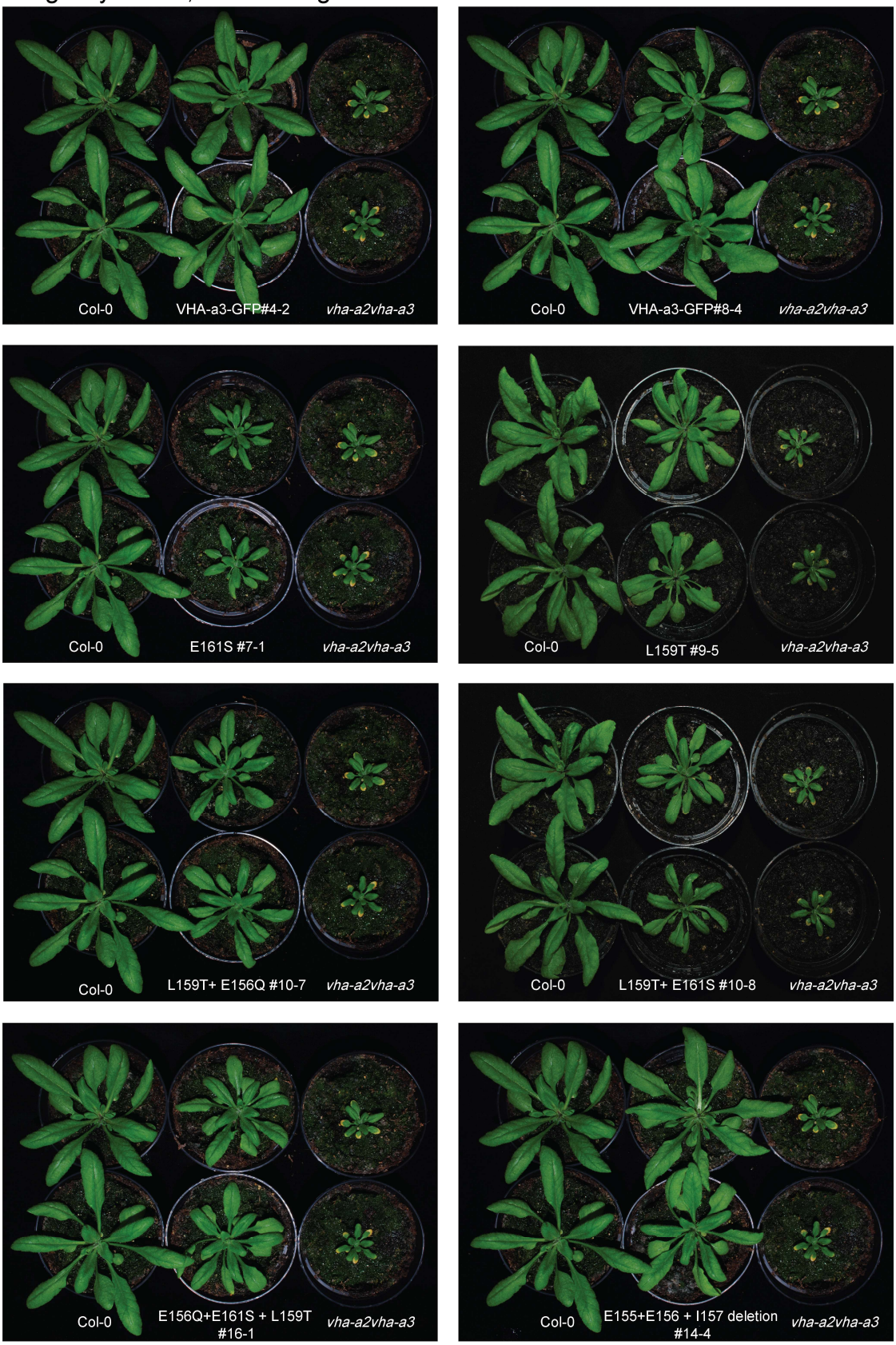

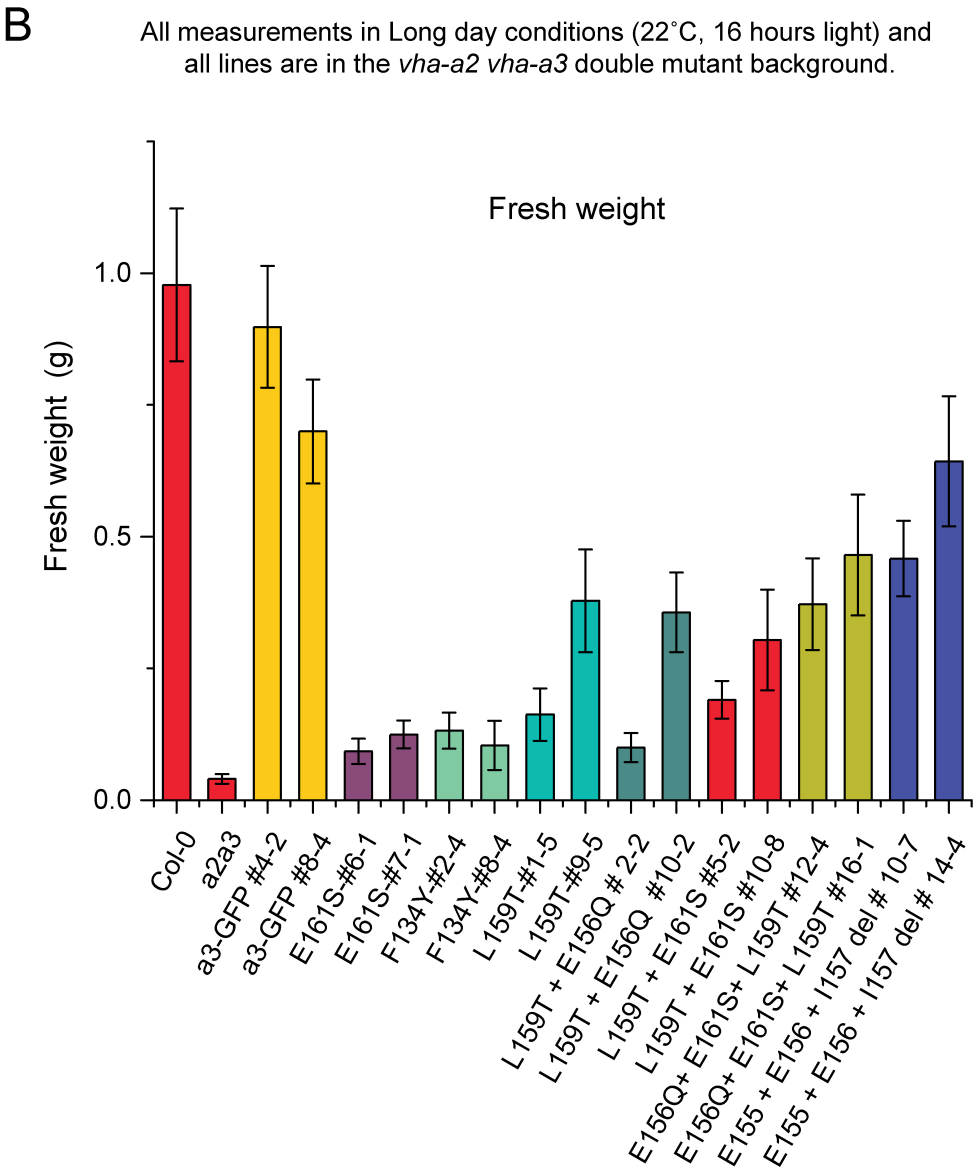

Figure S6. The mutated VHA-a1-GFP proteins complement the *vha-a2 vha-a3* double mutant to varying degrees in long day conditions.

(A) Plants were grown in long day conditions (22˚C and 16 hours light) for 4 weeks. All mutant variants of VHA-a1-GFP displayed bigger rosette size than the *vha-a2 vha-a3* double mutant. **E161S** which had a faint signal at the tonoplast in the *vha-a2 vha-a3* background (see **Figure 7 A**) also partially complemented the dwarf phenotype of the *vha-a2 vha-a3* double mutant. **(B)** Rosette fresh weight of 4 week old plants grown under long day conditions (n=12). Wild type rosette size is set to 100%. VHA-a1 with **E155+ E156 + I157** deletion complements the *vha-a2 vha-a3* double mutant the best.

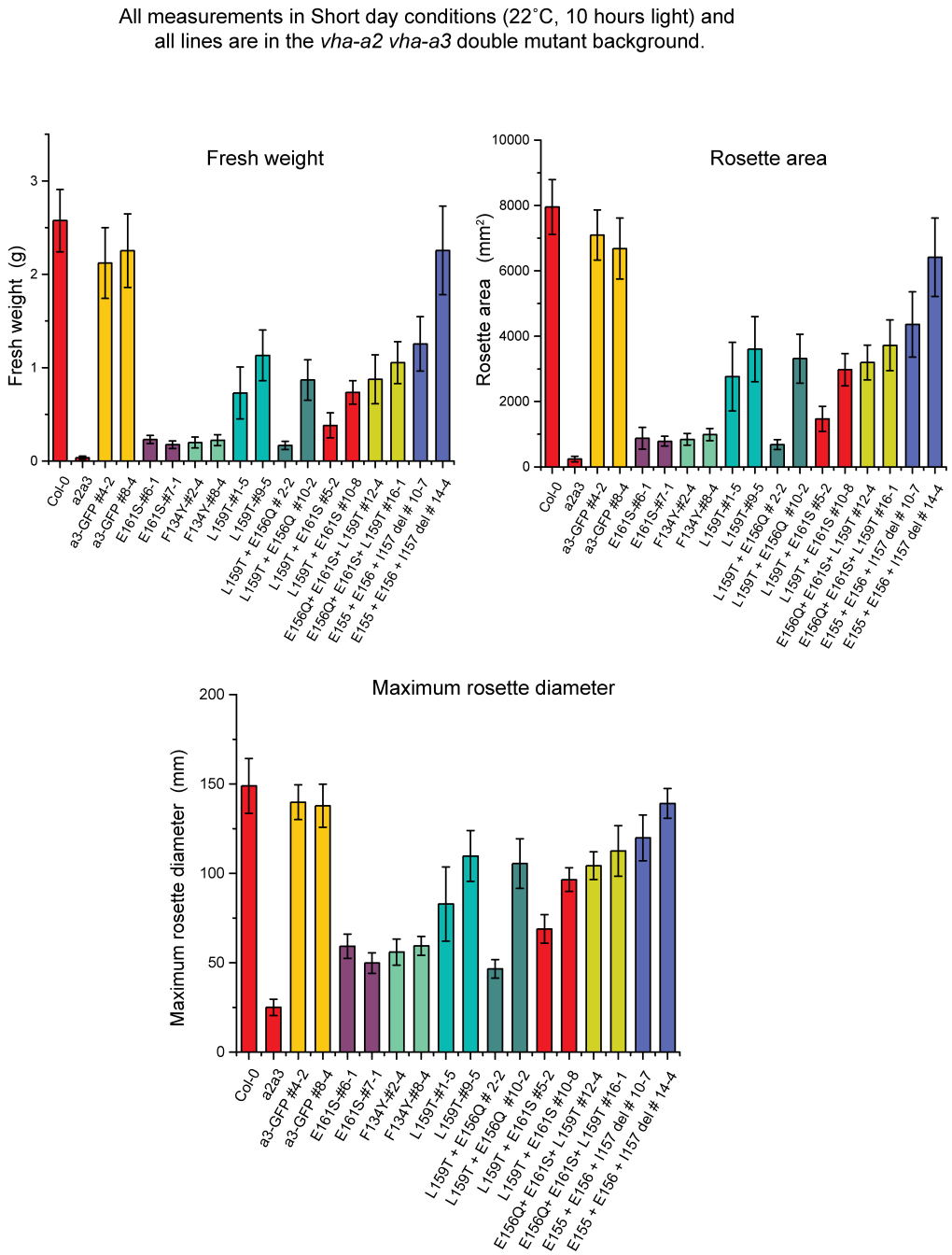

Figure S7. Measurements of rosette fresh weight, area and diameter for all mutations in short day conditions

Plants were grown under short day conditions (22˚C and 10 hours light). Mutations in VHA-a1-GFP are expressed in the *vha-a2 vha-a3* double mutant all under the *Ubiquitin10* promoter (*UBQ10*). Rosette fresh weight, area and diameter was measured of 6 week old plants (n=12).

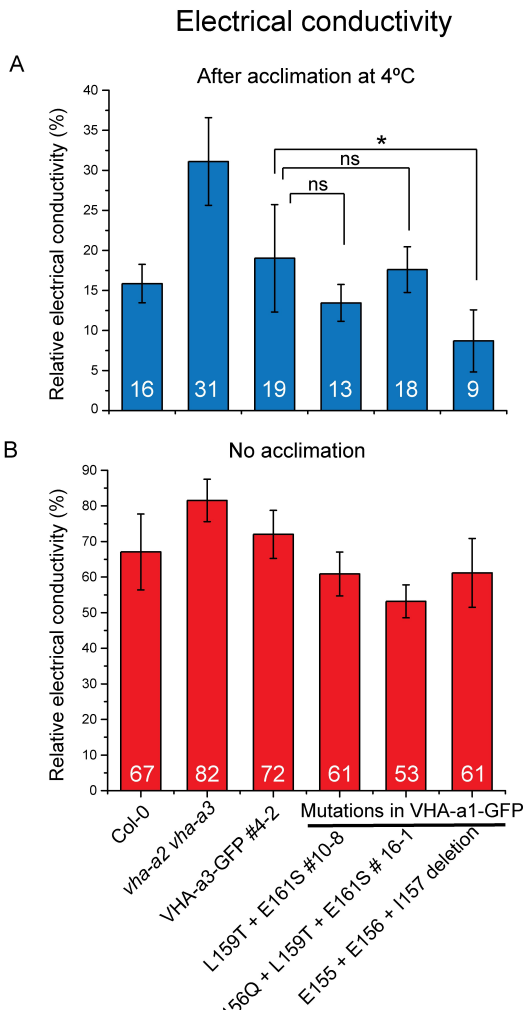

Figure S8. Freezing tolerance of *vha-a2 vha-a3* plants expressing mutated VHA-a1 subunits is comparable to wild type plants.

Three-week-old plants were cold adapted at 4˚C for 4 days, and electrolyte leakage was estimated by determining the electrical conductivity of the bathing solution of detached leaves frozen at -6˚C (n = 5). **(A)** Electrical conductivity measurements after cold acclimation. Leaves from *vha-a2 vha-a3* plants expressing VHA-a3-GFP, VHA-a1-GFP with mutations **L159T+ E161S** and **E156Q + L159T + E161S** showed comparable freezing tolerances to wild type leaves. Leaves from plants expressing VHA-a1-GFP with the **E155 + E156 + I157** deletion had the best freezing tolerance. Asterisks indicate a significant difference (*P < 0.05) according to Student's t test. (**B**) Electrical conductivity measurements were performed without any cold acclimation to show that it was the cold acclimation that is responsible for the freezing tolerance. Error bars represent SD of *n = 5* technical replicate

Table S2. Protein sequences used in the alignments in **Figure 4 and 16** an in the construction of the phylogenetic trees **in Figure 15 and S10**

No	Species	Database	Sequence ID	Modified
	Lower plants			
1	*K. flaccidum*	NCBI	kfl00005_0660_v1.1	Yes
2	*C. subellipsoidea*	Phytozome	estExt_GenewiseEukaryote.C_Chr_80030)	No
3	*O. lucimarinus*	Phytozome	estExt_GenewiseEukaryote.C_Chr_80030	No
4	*M. pusilla*	Phytozome	MicpuC2.e_gw1.5.60.1	No
5	*C. subellipsoidea*	Phytozome	estExt_Genewise1Plus.C_70184	No
6	*Micromonas sp RCC299*	Phytozome	fgenesh2_pm.C_Chr_08000065	No
7	*C.reinhardtii*	Phytozome	Cre11.g467705	No
8	*C.reinhardtii*	Phytozome	Cre09.g402500	No
9	*V. carteri*	Phytozome	Vocar.0008s0376	No
10	*D. salina*	Phytozome	Dusal.0182s00006	No
11	*V. carteri*	Phytozome	Vocar.0025s0074	No
12	*C.reinhardtii*	Phytozome	Cre04.g220350 1	No
13	*C.reinhardtii*	Phytozome	Cre04.g220350 2	No
14	*S. moellendorfii*	Phytozome	182335	No
15	*S. moellendorfii*	Phytozome	93837	No
16	*M. polymorpha*	Phytozome	Mapoly0004s0158 1	No
17	*M. polymorpha*	Phytozome	Mapoly0004s0158 2	No
18	*S. fallax*	Phytozome	Sphfalx0247s0020	No
19	*S. fallax*	Phytozome	Sphfalx0077s0094	No
20	*S. fallax*	Phytozome	Sphfalx0207s0012 1	No
21	*S. fallax*	Phytozome	Sphfalx0207s0012 2	No
22	*P. patens*	Phytozome	Pp3c26_10750 1	No
23	*P. patens*	Phytozome	Pp3c26_10750 2	No
24	*P. patens*	Phytozome	Pp3c4_24480) 1	No
25	*P. patens*	Phytozome	Pp3c4_24480) 2	No
26	*P. patens*	Phytozome	Pp3c4_24480) 3	No
27	*P. patens*	Phytozome	Pp3c3_6480 1	No
28	*P. patens*	Phytozome	Pp3c3_6480 2	No
29	*P. patens*	Phytozome	Pp3c13_3420 1	No
30	*P. patens*	Phytozome	Pp3c13_3420 2	No
31	*P. patens*	Phytozome	Pp3c13_3420 3	No
32	*P. patens*	Phytozome	Pp3c13_3420 4	No
33	*P. patens*	Phytozome	Pp3c13_3420 5	No
34	*P. patens*	Phytozome	Pp3c13_3420 6	No
35	*P. patens*	Phytozome	Pp3c13_3420 7	No
36	*P. patens*	Phytozome	Pp3c13_3420 8	No
37	*P. patens*	Phytozome	Pp3c13_3420 9	No
38	*P. patens*	Phytozome	Pp3c13_3420 10	No
	VHA-a1 related			
39	*P. taeda*	Pinerefseq	5A_I15_VO_L_1_T_29156/41278	yes
40	*Z. marina*	Phytozome	Zosma3g01360	No
41	*A. coerulea*	Phytozome	Aquca_046_00026 3	No
42	*A. trichopoda*	Phytozome	evm_27.TU.AmTr_v1.0_scaffold00080.37	No
43	*A. coerulea*	Phytozome	Aquca_046_00026 1	No
44	*A. coerulea*	Phytozome	Aquca_046_00026 2	No
45	*S. polyrhiza*	Phytozome	Spipo6G0067000	No

46	*M. acuminata*	Phytozome	GSMUA_Achr7G22660_001	No
47	*A. comosus*	Phytozome	Aco007033	No
48	*O. sativa*	Phytozome	LOC_Os01g61780	No
49	*B. distachyon*	Phytozome	Bradi2g54190 1	No
50	*B. stacei*	Phytozome	Brast01G098000	No
51	*T. aestivum*	Phytozome	Traes_3B_F1530FE81 1	No
52	*T. aestivum*	Phytozome	Traes_3B_F1530FE81 2	No
53	*S. bicolor*	Phytozome	Sobic.003G346400	No
54	*S. italica*	Phytozome	Seita.5G371100	No
55	*S. viridis*	Phytozome	Sevir.5G376500	No
56	*P. virgatum*	Phytozome	Pavir.Eb03637	No
57	*P. hallii*	Phytozome	Pahal.E01064	No
58	*P. virgatum*	Phytozome	Pavir.J03150	No
59	*M. guttatus*	Phytozome	Migut.D02174	No
60	*M. guttatus*	Phytozome	Migut.N02631	No
61	*S. lycopersicum*	Phytozome	(Solyc06g075400.2	No
62	*S. lycopersicum*	Phytozome	Solyc11g072530.1	No
63	*S. tuberosum*	Phytozome	PGSC0003DMG400025375	No
64	*E. grandis*	Phytozome	Eucgr.B02458	No
65	*E. grandis*	Phytozome	Eucgr.J00960	No
66	*K. marnieriana*	Phytozome	Kalax.0012s0214	No
67	*K. marnieriana*	Phytozome	Kalax.0294s0009	No
68	*K. marnieriana*	Phytozome	Kalax.0298s0062	No
69	*B. rapa*	Phytozome	Brara.C02406	No
70	*B. rapa*	Phytozome	Brara.G01384	No
71	*E. salsugineum*	Phytozome	(Thhalv10016255m.g	No
72	*C. grandiflora*	Phytozome	Cagra.1809s0001	No
73	*C. rubella*	Phytozome	Carubv10022649m.g	No
74	*A. thaliana*	Phytozome	AT2G28520	No
75	*B. stricta*	Phytozome	(Bostr.27991s0071	No
76	*A. lyrata*	Phytozome	933310	No
77	*A. halleri*	Phytozome	Araha.0947s0003	No
78	*L. usitatissimum*	Phytozome	Lus10018129.g	No
79	*L. usitatissimum*	Phytozome	Lus10036133.g	No
80	*P. vulgaris*	Phytozome	Phvul.011G071600)	No
81	*M. trancatula*	Phytozome	Medtr4g061090)	No
82	*G. max*	Phytozome	Glyma.12G072700) 3	No
83	*G. max*	Phytozome	Glyma.U021500	No
84	*M. trancatula*	Phytozome	Medtr2g093210) 1	No
85	*P. vulgaris*	Phytozome	Phvul.005G137800 1	No
86	*P. vulgaris*	Phytozome	Phvul.005G137800 2	No
87	*G. max*	Phytozome	Glyma.13G329100 1	No
88	*G. max*	Phytozome	Glyma.15G044700	No
89	*G. max:*	Phytozome	Glyma.13G329100 2	No
90	*V. vinifera*	Phytozome	GSVIVG01025116001	No
91	*C. sativus*	Phytozome	Cucsa.052610	No
92	*P. persica*	Phytozome	Prupe.6G092300	No
93	*C. clementina*	Phytozome	Ciclev10027830m.g	No
94	*C. sinensis*	Phytozome	orange1.1g003454m.g 1	No
95	*M. esculenta*	Phytozome	Manes.11G140100	No
96	*R. communis*	Phytozome	29688.t000006	No
97	*G. raimondii*	Phytozome	Gorai.006G119300 1	No
98	*G. raimondii*	Phytozome	Gorai.006G119300 3	No

99	*G. raimondii*	Phytozome	Gorai.006G119300 4	No
100	*G. raimondii*	Phytozome	Gorai.004G012600 1	No
101	*T. cacao*	Phytozome	Thecc1EG041113 5	No
102	*T. cacao*	Phytozome	Thecc1EG041113 4	No
103	*T. cacao*	Phytozome	Thecc1EG041113 6	No
			VHA-a3 related	
104	*G. montanum*	Gymno PLAZA	GMO00032493	No
105	*C. micholitzii*	Gymno PLAZA	CMI00015099	No
106	*T. baccata*	Gymno PLAZA	TBA00032038	No
107	*P. glauca*	Congenie	PGL00019274	No
108	*P. menziesii*	Gymno PLAZA	PME00001436	No
109	*P. sylvestris*	Congenie	PSY00015292	No
110	*P. pinaster*	Gymno PLAZA	PPI00050198	No
111	*P. taeda*	Pinerefseq	2A_I13_VO_L_1_T_44155/181601	No
112	*A. trichopoda*	Phytozome	evm_27.TU.AmTr_v1.0_scaffold00001.78	No
113	*S. polyrhiza*	Phytozome	Spipo1G0105500	No
114	*S. polyrhiza*	Phytozome	Spipo1G0105600	No
115	*A. comosus*	Phytozome	Aco014055	No
116	*M. acuminata*	Phytozome	GSMUA_Achr5G18710_001	No
117	*O. sativa*	Phytozome	LOC_Os10g10500	No
118	*B. stacei*	Phytozome	Brast03G107900	No
119	*B. distachyon*	Phytozome	Bradi3g22870) 1	No
120	*B. distachyon*	Phytozome	Bradi3g22870) 2	No
121	*O. sativa*	Phytozome	LOC_Os03g14690	No
122	*B. distachyon*	Phytozome	Bradi1g67960	No
123	*B. stacei*	Phytozome	Brast02G107000	No
124	*S. bicolor*	Phytozome	Sobic.001G435400	No
125	*Z. mays*	Phytozome	GRMZM2G058910	No
126	*S. italica*	Phytozome	Seita.9G468000	No
127	*S. viridis*	Phytozome	Sevir.9G471600	No
128	*P. virgatum*	Phytozome	Pavir.Ia03902	No
129	*P. hallii*	Phytozome	Pahal.A01364	No
130	*P. virgatum*	Phytozome	Pavir.Ib01048	No
131	*S. lycopersicum*	Phytozome	Solyc07g032080.2	No
132	*V. vinifera*	Phytozome	GSVIVG01009811001	No
133	*S. tuberosum*	Phytozome	PGSC0003DMG400027954	No
134	*M. trancatula*	Phytozome	Medtr3g112500	No
135	*G. max*	Phytozome	Glyma.06G027600	No
136	*P. vulgaris*	Phytozome	Phvul.002G179900	No
137	*M. domestica*	Phytozome	MDP0000220167	No
138	*P. persica*	Phytozome	Prupe.1G371400	No
139	*L. usitatissimum*	Phytozome	Lus10002104.g	No
140	*L. usitatissimum*	Phytozome	Lus10024304.g	No
141	*E. grandis*	Phytozome	Eucgr.F01613	No
142	*G. raimondii*	Phytozome	Gorai.002G125700 1	No
143	*G. raimondii*	Phytozome	Gorai.002G125700 2	No
144	*T. cacao*	Phytozome	Thecc1EG034141 3	No
145	*T. cacao*	Phytozome	Thecc1EG034141 1	No
146	*T. cacao*	Phytozome	Thecc1EG034141 2	No
147	*R. communis*	Phytozome	30170.t000535	No
148	*M. esculenta*	Phytozome	Manes.18G018300	No
149	*P. trichocarpa*	Phytozome	Potri.005G234100	No
150	*S. purpurea*	Phytozome	SapurV1A.0957s0050	No

151	*P. trichocarpa*	Phytozome	Potri.002G028600	No
152	*S. purpurea*	Phytozome	SapurV1A.0025s0850 1	No
153	*S. purpurea*	Phytozome	SapurV1A.0025s0850 2	No
154	*A. coerulea*	Phytozome	Aquca_007_00328 1	No
155	*V. vinifera*	Phytozome	GSVIVG01024208001	No
156	*A. coerulea*	Phytozome	Aquca_007_00328) 2	No
157	*E. grandis*	Phytozome	Eucgr.I01306 1	No
158	*E. grandis*	Phytozome	Eucgr.I01306) 2	No
159	*K. marnieriana*	Phytozome	Kalax.0053s0116	No
160	*K. marnieriana*	Phytozome	Kalax.0165s0060) 2	No
161	*K. marnieriana*	Phytozome	Kalax.0735s0023) 2	No
162	*K. marnieriana*	Phytozome	Kalax.0165s0060) 1	No
163	*K. marnieriana*	Phytozome	Kalax.0735s0023) 1	No
164	*G. raimondii*	Phytozome	Gorai.013G033700) 1	No
165	*G. raimondii*	Phytozome	Gorai.002G004800	No
166	*T. cacao*	Phytozome	Thecc1EG006818) 1	No
167	*T. cacao*	Phytozome	Thecc1EG006818) 3	No
168	*C. clementina*	Phytozome	Ciclev10027828m.g	No
169	*C. sinensis*	Phytozome	orange1.1g003392m.g) 1	No
170	*C. sinensis*	Phytozome	orange1.1g003392m.g) 2	No
171	*L. usitatissimum*	Phytozome	Lus10017490.g	No
172	*L. usitatissimum*	Phytozome	Lus10028796.g	No
173	*R. communis*	Phytozome	30131.t000251	No
174	*M. esculenta*	Phytozome	Manes.04G085500	No
175	*M. esculenta*	Phytozome	Manes.11G087300	No
176	*P. trichocarpa*	Phytozome	Potri.004G160400) 1	No
177	*P. trichocarpa*	Phytozome	Potri.004G160400) 2	No
178	*S. purpurea*	Phytozome	SapurV1A.0432s0230) 1	No
179	*S. purpurea*	Phytozome	SapurV1A.0432s0230) 2	No
180	*P. trichocarpa*	Phytozome	Potri.009G121400) 1	No
181	*P. trichocarpa*	Phytozome	Potri.009G121400) 2	No
182	*S. purpurea*	Phytozome	SapurV1A.0670s0160) 1	No
183	*S. purpurea*	Phytozome	SapurV1A.0670s0160) 2	No
184	*M. guttatus*	Phytozome	Migut.B00197	No
185	*S. lycopersicum*	Phytozome	Solyc01g110120.2	No
186	*C. sativus*	Phytozome	Cucsa.377810	No
187	*F. vesca*	Phytozome	gene01610-v1.0-hybrid	No
188	*P. persica*	Phytozome	Prupe.8G088600	No
189	*M. trancatula*	Phytozome	Medtr4g071070	No
190	*P. vulgaris*	Phytozome	Phvul.011G041500	No
191	*G. max*	Phytozome	Glyma.11G113400	No
192	*G. max*	Phytozome	Glyma.12G039300	No
193	*E. salsugineum*	Phytozome	Thhalv10000048m.g	No
194	*C. grandiflora*	Phytozome	Cagra.2961s0043	No
195	*B. stricta*	Phytozome	Bostr.5022s0091	No
196	*C. rubella*	Phytozome	Carubv10022648m.g) 1	No
197	*A. lyrata*	Phytozome	481007	No
198	*A. thaliana*	Phytozome	AT2G21410	No
199	*B. rapa*	Phytozome	(Brara.A00026	No
200	*B. rapa*	Phytozome	(Brara.H01826	No
201	*E. salsugineum*	Phytozome	Thhalv10024425m.g	No
202	*B. stricta*	Phytozome	Bostr.25542s0095	No
203	*A. lyrata*	Phytozome	490676	No

204	*A. thaliana*	Phytozome	AT4G39080	No
205	*C. grandiflora*	Phytozome	Cagra.1383s0085	No
206	*C. rubella*	Phytozome	Carubv10007773m.g	No

Figure S10. Phylogenetic analysis of the N-terminal sequences of VHA-a1 related proteins.

For each species all the VHA-a1 related protein sequences are shown. All sequences found for the chlorophytes, bryophytes, lycophytes were used for the analysis because it was not possible to classify them as VHA-a1-like or VHA-a3-like. Branch support is calculated on the basis of 500 bootstraps. Tree was constructed with Maximum likelihood (PHYML) (Guindon et al., 2010).

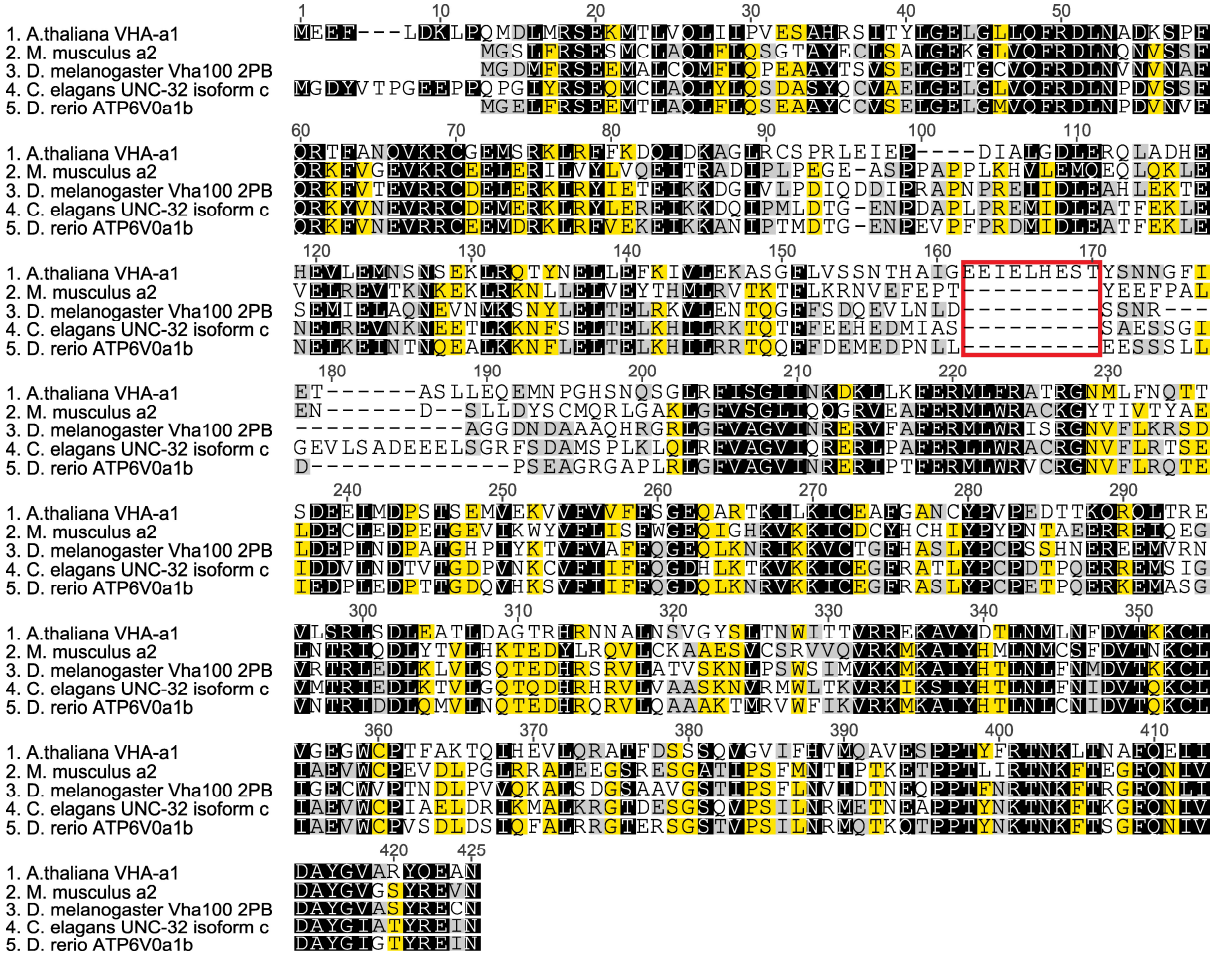

Figure S11. The a1-TD is unique to the plant kingdom

A. An alignment of amino acid sequences corresponding to the first 412 amino acids of VHA-a1 (the N-terminus) from mouse (a2 isoform), *C. elegans* (UNC-32 isoform c), *Drosophila melanogaster* (Vha100-2PB) and zebra fish (ATP6VO a1b). Sequence residues highlighted in black are similar between all proteins at the same position, in yellow are similar between four sequences at the same position, in grey are similar between only three of the proteins at the same position and Un-highlighted residues are variable in all sequences. The position of the acidic cluster of the a1-TD is indicated with a red box. Multiple sequence alignment was performed using Clustal Omega (Sievers et al., 2011).

Materials and Methods

Plant material and growth conditions

Arabidopsis thaliana, Columbia 0 (Col-0) ecotype was used in all experiments in this study. The *vha-a2 vha-a3* double mutant was characterized by Krebs et al., 2010. VHA-a1-GFP and VHA-a1-RFP lines were established by Dettmer et al., 2006. The VHP1-mGFP line is described by (Segami et al., 2014).

Growth of *Arabidopsis* seedlings for confocal microscopy was performed on plates. The standard growth medium used contained 1/2 Murashige and Skoog (MS), 0.5% sucrose, 0.5% phyto agar, and 10mM MES, and the pH was set to 5.8 using KOH. Agar and MS basal salt mixture were purchased from Duchefa. Seeds were surface sterilized with ethanol and stratified for 48h at 4°C. Plants were grown in long day conditions (LD) (16 h light/8 h dark) for 6 days.

For the rosette phenotype assays, seeds were stratified for 48 h at 4°C and then placed on soil. Seedlings were transferred to individual pots at 7 days after germination (DAG). Plants were grown either in LD or short day conditions (SD) (10 h light/14 h dark) for the required time.

Cold acclimation was performed with three-week-old plants. Plants were placed at 4˚C for 4 days in LD conditions.

Construct preparation

VHA-a1/VHA-a3 Chimeras

Five chimeric proteins were made which consisted of increasing lengths of the VHAa1 N-terminus (37aa, 85aa, 131aa, 179 aa and 228 aa) fused to decreasing lengths of the C-terminal domain of VHA-a3. The Greengate cloning system was used. Unique overhangs for each chimera were designed to allow seamless fusion of the VHA-a1 and VHA-a3 cDNA sequences (Table 1). The cDNA

sequences of VHA-a1 and VHA-a3 were amplified from pJET+a1 and a3+pBluscript plasmids respectively. The primers used are listed in **Table 2**.

Table 1. Unique overhangs for VHA-a1/VHA-a3 Chimeras

Chimera	Unique Overhang
a1NT**35***a3-GFP	-CTTA
a1NT**85***a3-GFP	-AAGC
a1NT**131***a3-GFP	-TATA
a1NT**179***a3-GFP	-CAGG
a1NT**288***a3-GFP	-TCAT

* The numbers in bold refer to the length of the VHA-a1 sequence

All PCR products were blunt end cloned into the pJET1.2 vector and verified by sequencing performed by eurofins. Verified clones were digested using *BglII* to release the PCR fragments. Digested fragments were purified using the Qiagen kit. To combine the VHA-a1 and VHA-a3 fragments, the Greengate cloning system was applied (Lampropoulos et al., 2013) . The following Greengate modules were used: pGGA006: UBQ10 promoter, pGGD001: linker-GFP, pGGE001: rbcS terminator, pGGF007: kanamycin resistance cassette and the destination vector pGGZ001.

Table 2: Primers used to amplify the VHA-a1 N-Termini and VHA-a3 C-Termini

No	PCR fragment	5' to 3'	Sequence
1	VHA-a1 NT 35 aa	Forward	GAT CGG TCT CGA ACA ATG GAG GAA TTC TTA GAT AA
		Reverse	GAA CGG TCT CGT AAG TGA TGG AAC GAT GAG CGG AT
2	VHA-a1 NT 85 aa	Forward	GAT CGG TCT CGA ACA ATG GAG GAA TTC TTA GAT AA
		Reverse	GAA CGG TCT CGG CTT TGT CAA TTT GAT CTT TAA AA
3	VHA-a1 NT 131 aa	Forward	GAT CGG TCT CGA ACA ATG GAG GAA TTC TTA GAT AA
		Reverse	GAA CGG TCT CGT ATA TGT CTG CCG AAG CTT TTC AC
4	VHA-a1 NT 179 aa	Forward	GAT CGG TCT CGA ACA ATG GAG GAA TTC TTA GAT AA
		Reverse	GAA CGG TCT CGC CTG CTC AAG TAA AGA GGC AGT CT
5	VHA-a1 NT 228 aa	Forward	GAT CGG TCT CGA ACA ATG GAG GAA TTC TTA GAT AA
		Reverse	GAA CGG TCT CGA TGA TTT CCT CAT CAG AGG TTG TT
6	VHA-a3 CT 2352 aa	Forward	GAT CGG TCT CGC TTA CCT TGG AGA TCT TGG CCT CG
		Reverse	GAA CGG TCT CGC TGA CTC GTC TTC GTT TGC CGT GA
7	VHA-a3 CT 2214 aa	Forward	GAT CGG TCT CGA AGC AGG AGT TCC AGC CAA GGA AA
		Reverse	GAA CGG TCT CGC TGA CTC GTC TTC GTT TGC CGT GA
8	VHA-a3 CT 2077 aa	Forward	GAT CGG TCT CGT ATA ATG AGC TTA TGG AGT ACA AG
		Reverse	GAA CGG TCT CGC TGA CTC GTC TTC GTT TGC CGT GA

9	VHA-a3 CT 1936 aa	Forward	GAT CGG TCT CGC AGG AAG AGA AGT CCA TTG ATT CG
		Reverse	GAA CGG TCT CGC TGA CTC GTC TTC GTT TGC CGT GA
10	VHA-a3 CT 1782 aa	Forward	GAT CGG TCT CGT CAT TGA TCC CAA CTC TGG GGA GA
		Reverse	GAA CGG TCT CGC TGA CTC GTC TTC GTT TGC CGT GA

Mutations in VHA-a1

A 535 bp fragment was amplified from *VHA-a1* cDNA using primers with *Eco31I sites* **(Table 3)**. This fragment was subcloned into the pJet1.2/blunt cloning vector generating the plasmid pJET+Ya1. PCR mediated site directed mutagenesis was performed on the pJET+Ya1 using primers indicated in **Table 4** and according to the manufacturer's protocol. All PCR products were verified by sequencing performed by Eurofins. Verified clones were digested using *BglII* to release the PCR fragments. Digested fragments were purified using the Qiagen kit. Greengate reactions were performed using the following Greengate modules: pGGA006: UBQ10 promoter, pGGD001: linker-GFP, pGGE001: rbcS terminator, pGGF005: hygromycin B resistance cassette, destination vector pGGZ001, the fragments containing the desired mutations, a connecting VHA-a1 fragment (Y2), VHA-a1 intron 10 fragment and a C-terminal fragment of VHA-a1.

Table 3. Primers used to amplify different fragments of VHA-a1.

No	PCR fragment	5' to 3'	Sequence
1	N-terminus of VHA-a1 (same as VHA-a1 NT 179 aa)	Forward	GAT CGG TCT CGA ACA ATG GAG GAA TTC TTA GAT AA
		Reverse	GAA CGG TCT CGC CTG CTC AAG TAA AGA GGC AGT CT
2	Connection Y2	Forward	GAT CGG TCT CGC AGG AAA TGA ATC CTG GAC ACT CT
		Reverse	AAC AGG TCT CAC GTA AGC ATC AAT AAT CTC CTG GAA
3	Intron 10	Forward	AAC AGG TCT CAT ACG GGT TAG TTC CAC TTT TGA TCA
		Reverse	AAC AGG TCT CAG CAA CAC TGC CAA GTA AGT ATC ATG
4	C-terminus of VHA-a1	Forward	AAC AGG TCT CAT TGC GAG ATA TCA AGA GGC AAA CC
		Reverse	GAA CGG TCT CGC TGA GAT TAA AGC GAA AGA GAA AG

Table 4. Primers used to for Site directed mutagenesis of VHA-a1

No	Mutation	5' to 3'	Sequence
1a	E156Q	Forward	CTC ATG CAA TTG GAG AAC AAA TTG AAC TAC ATG AAA GC
		Reverse	GCT TTC ATG TAG TTC AAT TTG TTC TCC AAT TGC ATG AG
2a	E161S	Forward	GAA GAA ATT GAA CTA CAT TCA AGC ACC TAC TCG AAT AAC GG
		Reverse	CCG TTA TTC GAG TAG GTG CTT GAA TGT AGT TCA ATT TCT TC
3a	F134Y	Forward	CAT ATA ACG AAC TTC TAG AAT ACA AGA TAG TTC TTG AAA AGG
		Reverse	CCT TTT CAA GAA CTA TCT TGT ATT CTA GAA GTT CGT TAT ATG
5a	L145F	Forward	GGC AAG TGG TTT CTT TGT CTC AAG TAA TAC TCA TG
		Reverse	CAT GAG TAT TAC TTG AGA CAA AGA AAC CAC TTG CC
6a	L159T	Forward	GGA GAA GAA ATT GAA ACA CAT GAA AGC ACC TAC TCG
		Reverse	CGA GTA GGT GCT TTC ATG TGT TTC AAT TTC TTC TCC
7a	S148A	Forward	GTG GTT TCC TTG TCT CAG CTA ATA CTC ATG CAA TTG
		Reverse	CAA TTG CAT GAG TAT TAG CTG AGA CAA GGA AAC CAC
1	E156Q + E161S + L159T	Forward	GCA ATT GGA GAA CAA ATT GAA ACA CAT TCA AGC ACC TAC TCG
		Reverse	CGA GTA GGT GCT TGA ATG TGT TTC AAT TTG TTC TCC AAT TGC
4	L159T + E156Q * template was 6a primers are for 1a	Forward	CTC ATG CAA TTG GAG AAC AAA TTG AAC TAC ATG AAA GC
		Reverse	CTC ATG CAA TTG GAG AAC AAA TTG AAC TAC ATG AAA GC

5	L159T + E161S * template was 6a primers are for 2a	Forward	GAA GAA ATT GAA CTA CAT TCA AGC ACC TAC TCG AAT AAC GG
		Reverse	CCG TTA TTC GAG TAG GTG CTT GAA TGT AGT TCA ATT TCT TC
6	S147A + S148A	Forward	GTG GTT TCC TTG TCG CAG CTA ATA CTC ATG CAA TTG
		Reverse	CAA TTG CAT GAG TAT TAG CTG CGA CAA GGA AAC CAC
7	L131M+ L132M	Forward	GAC ATA TAA CGA AAT GAT GGA ATT CAA GAT AGT TC
		Reverse	GAA CTA TCT TGA ATT CCA TCA TTT CGT TAT ATG TC
10	F134Y + I136L	Forward	CAT ATA ACG AAC TTC TAG AAT ACA AGC TAG TTC TTG AAA AGG
		Reverse	CCT TTT CAA GAA CTA GCT TGT ATT CTA GAA GTT CGT TAT ATG
12	L176Q	Forward	GAC TGC CTC TTT ACA AGA GCA GGA AAT GAA TCC TG
		Reverse	CAG GAT TCA TTT CCT GCT CTT GTA AAG AGG CAG TC
13	L176Q + Q178 del	Forward	GAC TGC CTC TTT ACA AGA GGA AAT GAA TCC TG
		Reverse	CAG GAT TCA TTT CCT CTT GTA AAG AGG CAG TC
16	E156 del	Forward	TAC TCA TGC AAT TGG AGA AAT TGA ACT ACA TGA AAG C
		Reverse	GCT TTC ATG TAG TTC AAT TTC TCC AAT TGC ATG AGT A
18	E156 + E155 + L157 del	Forward	AAT ACT CAT GCA ATT GGA GAA CTA CAT GAA AGC AC
		Reverse	GTG CTT TCA TGT AGT TCT CCA ATT GCA TGA GTA TT

Dexamethasone inducible Sar1H74L-CFP

Arabidopsis Sar1B cDNA sequence with the H74L mutation was synthesized by Eurofins. The synthesized fragment contained *Eco31I* at its 5' and 3' ends for subcloning. PCR was performed on the synthesized fragment and the PCR product was blunt end cloned into the pJET1.2 vector. The *Sar1H74L* sequence was verified by sequencing which was performed by Eurofins. Verified clones were digested using *BglII* to release the PCR fragments. Digested fragments were purified using the Qiagen kit. Two Greengate reactions were performed to create two intermediate vectors that were later combined on one T-DNA. The first intermediate vector consisted of 6 entry modules (pGGM000 empty vector, pGGA006:UBQ10; pGGB003 N-terminal-decoy; LhG4-GR; C-terminal-decoy; pGGE001:RBCS terminator and the FH adapter). The second intermediate vector consisted of 6 entry modules (pGGN000 empty vector, pGGA016: pOP6, *Sar1H74L* purified fragment, pGGD004: linker-CFP, pGGE001:rbcS, pGGF012: sulfadiazin resistance cassette and the HA adapter). The two intermediate vectors were combined on one final destination vector, pGGZ003.

Table 5. Primers used to amplify *Sar1H74L* synthesized fragment

	PCR fragment	**5' to 3'**	**Sequence**
1	*Sar1H74L*	Forward	AAC AGG TCT CAG GCT CAA CAA TGT TCT TGG TAG ATT GGT T
		Reverse	GAA CGG TCT CGC TGA CTT GAT ATA CTG AGA CAT CC

VHA-a3 with the a1-TD

The targeting domain of *VHA-a1* (*a1-TD*) was introduced in *VHA-a3* by PCR techniques. The N and C-termini of *VHA-a3* and the *a1-TD* were amplified using primers in **Table 6**. All PCR products were blunt end cloned into the pJET1.2 vector and verified by sequencing performed by eurofins. Verified clones were digested using *BglII* to release the PCR fragments. Digested fragments were purified using the Qiagen kit. The Greengate cloning system was applied to combine all fragments into the destination vector. The following Greengate modules were used: pGGA006: UBQ10 promoter, pGGD001: linker-GFP, pGGE001: rbcS terminator, pGGF012: sulfadiazin resistance cassette and the destination vector pGGZ001.

Table 6. Primers used to amplify *VHA-a3* N and C-terminal fragments and the *a1-TD*

	PCR fragment	**5' to 3'**	**Sequence**
1	*VHA-a3* N-terminus	Forward	TAT GGT CTC AGG CTC AAC AAT GGC GGA AAG TGG CGG TGG
		Reverse	AAC AGG TCT CAC CTT CTG AAG AAC CAA CTT GTA CT
2	*a1-TD*	Forward	AAC AGG TCT CAA AGG CAA GTG GTT TCC TTG TCT CA
		Reverse	AAC AGG TCT CAA AAG AGG CAG TCT CAA TAA AAC CG
3	*VHA-a3* C-terminus	Forward	AAC AGG TCT CAC TTT GTT AC AGG AAG AGA AGT CCA
		Reverse	GAA CGG TCT CGC TGA CTC GTC TTC GTT TGC CGT GA

Arabidopsis transformation

5 µl of the Greengate ligation reaction was transformed into DH5α cells and plated on LB plates containing spectinomycin for selection of correct plasmids. Colony PCR was performed to pre-screen colonies. Overnight cultures of positive clones were made. Mini preps of cultured bacteria were done with the Qiagen kit. Preped plasmids were test digested and correct binary plasmids were transformed into *A. tumefaciens* strain ASE1(pSOUP^{+}) and selected on 100 µg/ml spectinomycin, 5 µg/ml tetracycline (for pSOUP), 25 µg/ml chloramphenicol and 50 µg/ml kanamycin. *Arabidopsis* plants were transformed by the floral dip method as outlined by (Clough and Bent, 1998) and transgenic plants were selected on MS plates containing appropriate antibiotics.

Tonoplast vesicle preparation and enzyme assays

Preparation of tonoplast vesicles

Rosette leaf material (75 g) from plants grown under short day conditions was harvested. The leaf material was homogenized in homogenization buffer containing 0.4 M mannitol, 0.1 M Tris , 10% (vol/vol) glycerol, 3 mM Na2EDTA, 0.5% (wt/vol) BSA, 5% (vol/vol) PVP-10, 0.5 mM butylated hydroxytoluene, 0.3 mM dibucaine, 5 mM magnesium sulphate, 1 mM PMSF (phenylmethylsulphonyl fluoride), 1.3 mM benzamidine and 25 mM postassium metabisulfite. The homogenate was filtered through two layers of miracloth and centrifuged at 10,000 g for 20 min at 4°C. The supernatant was then centrifuged at 100,000 g for 45 min at 4°C. The microsomal membrane pellet was resuspended in resuspension buffer containing 0.4 M mannitol, 6 mM Tris-MES (pH 8) and 10% (vol/vol) glycerol. Tonoplast vesicles were obtained by performing a sucrose gradient with 22% sucrose. Centrifugation was performed at 97,000 g for 2 hours. Protein concentrations were determined as reported previously (Bradford, 1976).

ATP hydrolysis

ATP hydrolysis was measured at 28°C as described previously by (Krebs et al., 2010)

Proton translocation

The ATP-dependent proton transport activities were estimated from the initial rate of ATP-dependent fluorescence quenching in the presence of 3 mM ATP using the fluorescence dye ACMA (9-Amino-6-Chloro-2-Methoxyacridine). Excitation wavelength was 415 nm, and emission was measured at 485 nm in a microplate reader (Tecan Infinite M1000). Tonoplast vesicles were placed in a 96 well plate with a reaction buffer containing 0.25 M mannitol, 10 mM BTP-MES (pH 8), 100 mM tetramethylammonium chloride (TMA-Cl), 1 µM ACMA, 3 mM magnesium sulphate and 1 mM sodium vanadate. Measurements were started in the absence of ATP (1 measurement every 1 minute for 10 minutes). After 10 minutes, 6 µl of 100 mM ATP-BTP (pH 7.5) was added. Then 20 measurements were done every 25 seconds. The change in ACMA fluorescence over time after ATP addition was then calculated. Control measurements in the presence of 5 µm Concanamycin A were also performed.

SDS-PAGE and immunoblotting analysis

SDS-PAGE and immunoblotting were performed to determine protein levels in tonoplast membrane extracts. After electrophoresis, proteins were transferred to a nitrocellulose membrane (Whatman). The following primary antibodies were used: a GFP antibody (1:5000) and an anti-γ-Tip antibody (1:3000, against the C-terminal γ-Tip sequence CSRTHEQLPTTDY, (Jauh et al., 1998). Antigen on the membrane was detected with fluorescent labelled anti-rabbit antibodies from Mobitec (#MFP-A1008). Excitation (488 nm) and fluorescence detection was carried out using a cooled CCD camera system (Intas *ADVANCED* Fluoreszenz u. ECL Imager). Western blots were quantified with Fiji (based on ImageJ 1.47t).

pH measurements

Cell sap pH measurements were performed as previously described (Krebs et al., 2010).

Confocal microscopy

Confocal laser scanning microscopy was performed using a Leica TCS SP5II microscope equipped with a Leica HCX PL APO lambda blue 63.0x 1.20 UV water immersion objective. GFP was excited at 488 nm with a VIS-argon laser and fluorescence emission was detected between 500 and 555 nm. mRFP and FM4-64 were excited at 561 nm with a VIS-DPSS 561 laser diode and fluorescence emission was detected between 615 and 676 nm. CFP was excited using the 458 line of the argon laser and fluorescence emission was detected between 460 and 485 nm. The imaging parameters were as follows: image dimension: 512 X 512, pinhole: 1 airy unit, line average: 5. For image acquisition, the Leica Application Suite Advanced Fluorescence software was used. Processing of images was performed using Fiji (based on ImageJ 1.47t).

Pharmacological Treatments and Stains

Arabidopsis seedlings were incubated in liquid 1/2 MS medium with 0.5 % sucrose, pH 5.8, containing 50 µM BFA, 1 µM FM4-64, 60 µM DEX, or the equivalent amount of DMSO in control samples for the required time at room temperature. Stock solutions were prepared in DMSO.

Imaging

Pictures of rosettes for the soil phenotype assays were taken using a Nikon D60 digital camera. Images were processed using Adobe Photoshop (Cloud).

Homology modelling of the VHA-a N-termini

3D models of the VHA-a1 and VHA-a3 N-termini were obtained through homology modelling using the *M. ruber* subunit 1 (PDB:3RRK) crystal structure

as a template. Homology modelling was performed according to (Roy et al., 2010).

Phylogenetic analysis

The online platform at http://www.Phylogeny.fr was utilized (Dereeper et al., 2008). Phylogenetic analysis was performed as described in (Li, Yanbang, Provenzano et al., 2016). Trees were constructed with Maximum likelihood (PHYML) using the WAG amino acid replacement matrix substitution model (Guindon et al., 2010). Branch support was calculated on the basis of 500 bootstraps.

Multiple sequence alignments

Multiple sequence alignments were performed using Clustal omega (Sievers et al., 2011). Aligned sequences were analyzed in Geneious 8.1.5.

Chapter 2

Subunit a of the V-ATPase at the TGN as a putative pH-sensor

Scientific aim

The overexpression of the N-terminus of VHA-a1 results in reduction of cell expansion. It is suspected that this overexpression titrates endogenous VHA-a1 interacting proteins involved in vesicle trafficking thus this chapter aimed:

1. To determine protein interaction partners for the N-terminus of VHA-a1
2. To identify histidine residues in the C-terminus of VHA-a1 that could be involved in pH sensing.

Abstract

The TGN/EE (trans Golgi network / early endosome) of plants is a central organelle in cellular trafficking. It is an acidic compartment and the acidic pH of its lumen is mainly contributed by the vacuolar H^+-ATPase (V-ATPase) located on its membrane. We wanted to discover if the TGN localized V-ATPase not only fulfils its primary function of acidification, but whether it is also a component of the molecular machinery that senses the level of luminal acidification and can recruit cytosolic proteins involved in vesicle trafficking to the membrane. Here we show that overexpression of the N-terminus of the VHA-a1 subunit (VHA-a1NT), a component of the V_O subcomplex, causes a reduction in cell expansion and results in a serrated leaf phenotype. Biochemical analysis showed that VHA-a1NT associates with membranes because it is found in the microsomal membrane fraction. We also determined the three dimensional structure of the VHA-a1 C-terminus through homology modelling using yeast Vph1p as a template. This has allowed us to identify histidine residues in the VHA-a1 C-terminus that could be part of the pH sensing mechanism. Mass spectrometry analysis of VHA-a1NT co-immunoprecipitated proteins also identified potential interaction partners.

Introduction

The plant TGN is an organelle where endocytic, recycling and secretory pathways converge (Viotti et al., 2010). Because it receives endocytic and recycled proteins, the TGN also serves as the early endosome in plants (Viotti et al., 2010). The significance of this organelle in cellular trafficking cannot be understated as it performs vital functions that are needed for maintaining the integrity of the cell. By sorting receptors, transporters and other plasma membrane proteins either for recycling to the plasma membrane or for degradation at the lytic vacuoles, the TGN plays a key role in the way cells adapt to the prevailing environmental conditions (Reyes et al., 2011).

The TGN of plants is an acidic compartment (luminal pH = 5.66 (Luo et al., 2015)). It is acidified by the action of the vacuolar H^+-ATPase (V-ATPase). Failure to acidify the TGN leads to secretion and recycling defects (Luo et al., 2015). This inevitably means TGN function is tightly linked to its luminal pH. The vacuolar H^+-ATPase (V-ATPase) is a multisubunit complexes that is responsible for the acidification of various cellular compartments in all eukaryotic cells (Nishi and Forgac, 2002). They are multisubunit enzymes that consist of a membrane integral V_O subcomplex and a membrane peripheral V_1 subcomplex. ATP hydrolysis occurs on catalytic subunits of the V_1 subcomplex which drives the translocation of protons through the V_O subcomplex (Nishi and Forgac, 2002). Subunit a of the V_O subcomplex controls coupling of ATP hydrolysis to proton translocation as well as targeting of the complex in the cell (Kawasaki-Nishi et al., 2001; Dettmer et al., 2006). *A. thaliana* has three isoforms of subunit a, VHA-a1, VHA-a2 and VHA-a3. VHA-a1 targets the V-ATPase to the TGN whilst VHA-a2 and VHA-a3 target it to the limiting membrane of the vacuole (tonoplast) (Dettmer et al., 2006).

The sorting of proteins at the TGN involves the assembly of cytosol-oriented coat proteins which preferentially package cargo into vesicles. The coat proteins or coatomer also aid in vesicle formation by initiating and promoting membrane

curvature through protein interactions (Kirchhausen, 2000). The energy needed for vesicle formation is provided by small GTPases. Small GTPases are molecular switches that are active when in a GTP bound state and inactive in a GDP bound state. The conversion from active to inactive states is carried out by guanine-nucleotide exchange factors (GEFs) and conversion from inactive to active states by is carried out by GTPase activating proteins (GAPs) (Molendijk et al., 2004). Small GTPases are also involved in directing trafficking specificity to and facilitating vesicle docking on target membranes (Nielsen et al., 2008). Transport between different organelles employs specific sets of RAB and ARF (ADP-ribosylation factor) GTPases, which are members of the RAS-like family of small GTPases **(Figure 1)**

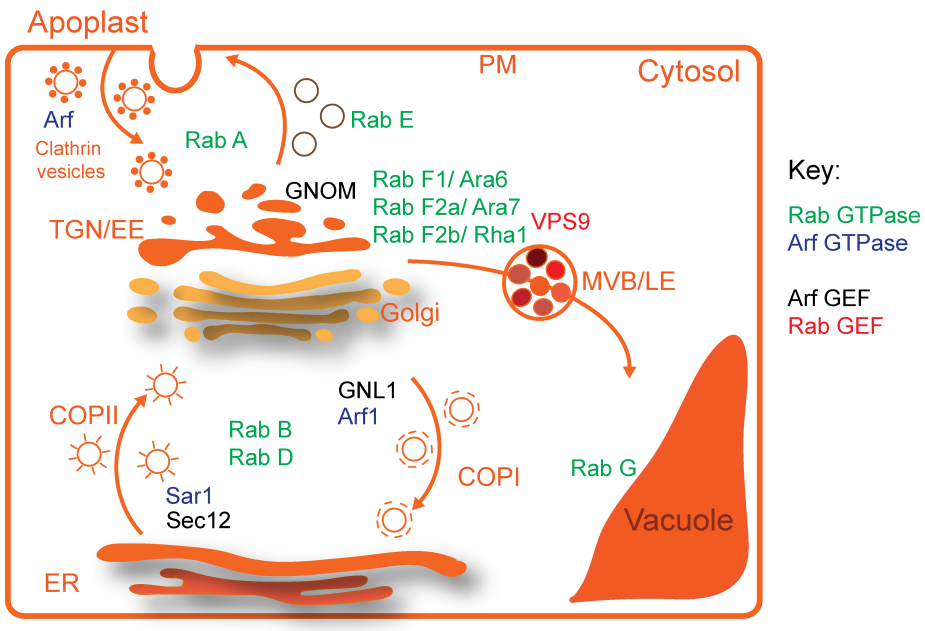

Figure 1: A schematic illustration for the RAB and ARF mediated vesicle transport pathways in plant cells.

Secretory, endocytic and recycling pathways employ specific sets of coat proteins, RAB and ARF GTPases as described by (Nielsen et al., 2008; Woollard and Moore, 2008). Characterized guanine exchange factors (GEFs) are also depicted (Geldner et al., 2003; Anders and Jürgens, 2008).

ARF (ADP-ribosylation factor), GNL1 (GNOM like 1), COP (coat protein complex), Sar1 (secretion-associated, Ras related protein 1), VPS9 (Vacuolar sorting protein 9),PM (Plasma membrane), ER (Endoplasmic reticulum) and MVB/LE (Multivesicular body/ Late endosome).

In mammalian cells it has been found that luminal acidification inside organelles not only serves to provide optimal pH conditions but it is also sensed by pH sensing proteins (PSPs) that can recruit cytosolic proteins to the membrane (Marshansky, 2007). Initial observations were made with studies involving a subset of COPs (coat proteins) which are present at endosomes. It was illustrated that βCOP and γCOP are recruited from the cytosol to endosomes in a luminal pH dependent manner and that their recruitment was thought to occur via a PSP located on the endosomal membrane (Aniento et al., 1996). Studies in mouse kidney cells finally identified this PSP. It was demonstrated that the subunit c and subunit a2 of the endosomal V-ATPase directly interact with the small GTPase Arf6 (ADP-ribosylation factor 6) and its GEF, ARNO (Arf nucleotide site opener), respectively and that this interaction is dependent on endosomal luminal pH (Zeuzem et al., 1992; Maranda et al., 2001; Hurtado-Lorenzo et al., 2006). Thus, the findings showed that the V-ATPase is not only responsible for endosomal acidification, but that it is also a component of the molecular machinery that senses the level of luminal acidification and can transmit the pH signal to effectors located on the cytosolic side of the membrane (Hurtado-Lorenzo et al., 2006). Intuitively, the V-ATPase is well suited as a pH sensor because the 100 kDa subunit a of the V_O subcomplex spans the entire membrane and has an extensive cytosolic N-terminus that could recruit cytosolic components.

It was then proposed that histidine residues located in the C-terminus of mouse subunit a2 are involved in the pH sensing mechanism. This is because it is the only amino acid whose pKa (pH at which it is 50% is protonated) is in the physiological range of the cell. Furthermore, histidine residues in other known pH sensing mammalian proteins have been identified as crucial components of their pH-sensing mechanism (Marshansky, 2007). Protein sensing proteins have been found and characterized in plants already. Examples include the water channel proteins (aquaporins) also known as plasma membrane intrinsic proteins or PIPs. These proteins exhibit cytosolic pH-dependent gating (Tournaire-Roux et al., 2003; Törnroth-Horsefield et al., 2006). The pH sensing in the aquaporins is

predicted to be achieved by a single histidine residue, His193, in the second cytoplasmic loop (D) of the protein (Törnroth-Horsefield et al., 2006). It is proposed that histidines in luminal loops or in the transmembrane domains in subunit a of the V-ATPase could be involved in the proton sensing. Thus it is vital to know the three dimensional (3D) structure of subunit a to identify the positioning of the histidines in the folded protein. Unfortunately, no crystal structure exists for any eukaryotic subunit a and this has hindered further investigations into the mechanisms of pH sensing by subunit a.

We wanted to investigate whether VHA-a1, the plant homologue of subunit a2, has the same pH sensing abilities in plants. Initial experiments in *Arabidopsis* involved overexpressing the N-terminus of VHA-a1 under an ethanol-inducible promoter to see if this evoked a cellular response. It was found that overexpression of the N-terminus of VHA-a1 resulted in inhibition of cell expansion and it was hypothesized that the VHA-a1NT competes with endogenous VHA-a1 interacting proteins involved in vesicle trafficking. It was also suggested that the VHA-a1NT exhibits properties of a membrane protein because of its punctate localization pattern as opposed to the expected homogenous cytosolic distribution (Liu, 2008).

In this study, we wanted to confirm the observations made with ethanol-inducible constructs using a dexamethasone-inducible system (Samalova et al., 2005) which is more desirable over the ethanol-inducible system because it has been reported that the ethanol-inducible system has background activity even in the absence of exogenously applied ethanol (Li et al., 2005). Such background activity makes propagation of transgenic lines very difficult if the transgene product inhibits plant growth. Neither the glucocorticoid receptor nor dexamethasone in the dexamethasone-inducible system are naturally present in plants, therefore eliminating the possibility of background activity (Moore et al., 1998).

We confirm that VHA-a1NT and not VHA-a3NT overexpression causes a strong inhibition of cell expansion and that VHA-a1NT associates with membranes because it is found in microsomal membrane fractions. We also investigated rosette phenotypes and found that VHA-a1NT overexpression results in a serrated leaf phenotype similar to the one brought about by inducible ami-VHA-a1(artificial micro RNA against VHA-a1) constructs (Kriegel, 2015). We also determined the 3D structure of the VHA-a1 C-terminus through homology modelling using a recently acquired model of Vph1p from yeast as a template. The yeast model was obtained from cryo-electron microscopy techniques (Schep et al., 2016; Mazhab-Jafari et al., 2016). Using our model, we predict seven of the eleven histidines located in the C-terminus of VHA-a1 to be involved in pH sensing due to their position in the 3D structure. Furthermore, co-immunoprecipitation(Co-IP) followed by mass spectrometry analysis were performed to identify VHA-a1NT interacting partners. A total of 48 candidate proteins that could be possible interaction partners were identified.

Results

Overexpression of the N-terminus of VHA-a1 (VHA-a1NT) inhibits cell expansion

Hypocotyl length of etiolated seedlings is generally used as an indicator for cell expansion because hypocotyl growth either in the light or the dark does not significantly involve cortical or epidermal cell divisions (Gendreau et al., 1997). We tested whether overexpression of the VHA-a1NT affects cell expansion in hypocotyls.

To overexpress the VHA-a1NT, we generated two constructs containing the first 412 or 198 amino acids of VHA-a1 linked to GFP (VHA-a1NT412-GFP and VHA-a1NT198-GFP). We also generated a construct to overexpress the N-terminal domain of VHA-a3 (VHA-a3NT412-GFP) to analyze if overexpression of VHA-a3NT also elicits a cellular response. All VHA-a N-termini were expressed under the control of the dexamethasone-inducible promoter (Samalova et al., 2005). We analyzed whether the reduction in hypocotyl growth is comparable to the previously published ethanol-inducible lines. We grew VHA-a1NT and VHA-a3NT lines for 4 days on medium supplemented with dexamethasone or DMSO and then measured hypocotyl length. DMSO-treated seedlings of all lines showed similar hypocotyl length indicating that the DEX-promoter system is not leaky **(Figure 1A).** The hypocotyl lengths of VHA-a1NT198-GFP lines were reduced by around 40% whereas VHA-a1NT412-GFP lines showed a reduction of 50% which is in agreement with the data obtained for the ethanol-inducible lines. Overexpression of VHA-a3NT412-GFP did not result in a significant decrease in hypocotyl length.

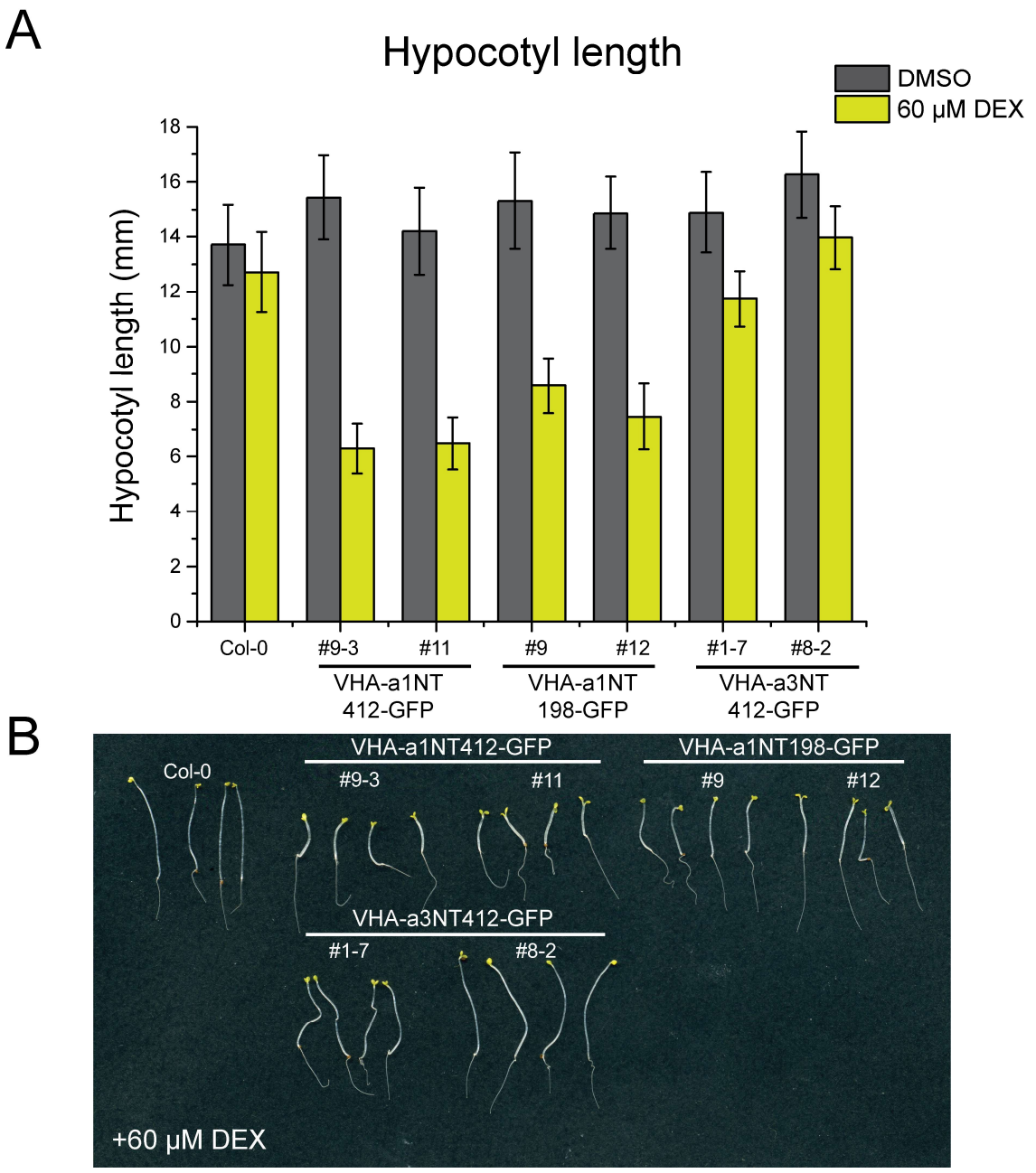

Figure 1. Plants expressing VHA-a1NT constructs show reduced hypocotyl length after DEX induction.

(A) Quantitative measurement of the hypocotyl length of DEX or DMSO treated wild type and two independent lines expressing VHA-a1NT412-GFP, VHA-a1NT198-GFP and VHA-a3NT412-GFP constructs. Etiolated seedlings were grown for 4 days on water agar containing either 60 µM dexamethasone or an equal amount of DMSO. Error bars represent SD of around 40 seedlings. **(B)** Morphological observation of etiolated seedlings after induction with 60 µM dexamethasone.

We also investigated rosette development to determine if overexpression of the VHA-a1NT has an effect on later developmental growth stages of the plant. Plants were grown on soil in standard growth conditions (long day, 16 hours light, 22˚C) for 3 weeks. Induction with dexamethasone was performed twice by spraying at 13 and 18 days after germination. It was observed that the rosette sizes of dexamethasone treated plants expressing VHA-a1NT412-GFP and VHA-a1NT198-GFP were strongly reduced compared to DMSO treated controls and to wild type plants **(Figure 2)**. Furthermore, newly formed leaves exhibited serrations at the leaf margins and at the end of the 3 week growth period some leaves had curled. These phenotypes were not observed in dexamethasone treated plants expressing VHA-a3NT412-GFP **(Figure 2).**

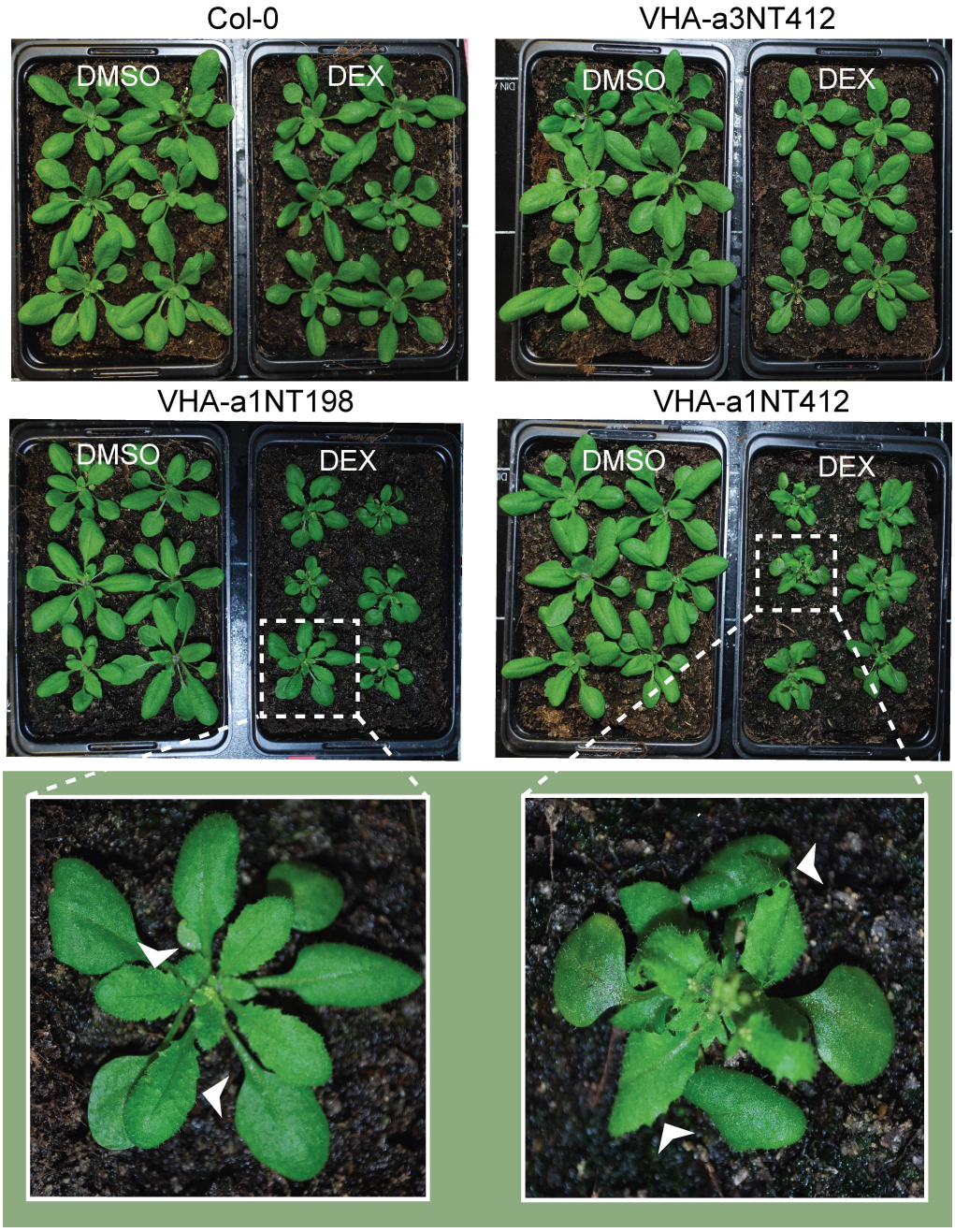

Figure 2. Plants expressing VHA-a1NT constructs show serrated leaf margins and curled leaf phenotypes.

Rosette growth phenotype of DEX or DMSO treated wild type and plants expressing VHA-a1NT412-GFP, VHA-a1NT198-GFP and VHA-a3NT412-GFP. After induction with DEX, only plants expressing VHA-a1NT412-GFP and VHA-a1NT198-GFP displayed smaller rosette sizes, serrated leaf margins and curled leaves. Plants were grown for 20 days under LD conditions at 22°C. Plants were sprayed with 60 µM DEX or DMSO at 13 and 18 days after germination.

The VHA-a1NT associates with membranes

In order to determine the localization of the VHA-a N-terminal proteins in the cell, we first performed transient expression in tobacco leaf cells. Plasmids were co-infiltrated with DEX and the plants were incubated for three days. It was observed that, in tobacco leaf cells VHA-a1NT198-GFP and VHA-a3NT412-GFP both are homogenously localized in the cytosol (**Figure 3 A, B and E**). But, aside from having a cytoplasmic localization pattern, VHA-a1NT412-GFP also accumulates in dots (**Figure 3C and D**).

The sorting information for VHA-a1 that is necessary and sufficient for targeting of VHA-a1 complexes to the TGN is located within a region in the N-terminus of VHA-a1 called the VHA-a1 targeting domain (a1-TD). We introduced the a1-TD into the N-terminus of VHA-a3 to determine if this sequence was responsible for the dot like localization pattern of VHA-a3NT412-GFP. The VHA-a3 N-terminus with this a1-TD (VHA-a3NTa1D-mVenus) is still homogenously localized in the cytosol like VHA-a3NT412-GFP **(Figure 3F).** This means that the dot like localization pattern of VHA-a1NT412-GFP is not due to the presence of the VHA-a1 targeting sequence in its sequence.

Ultimately we wanted to determine the localization of the VHA-a N-terminal proteins in *Arabidopsis*. Only the localization of VHA-a3NT412-GFP expressed under the control of the Ubiquitin 10 promoter (UBQ10) and VHA-a3NTa1D-mVenus expressed under a DEX inducible promoter could be determined in *Arabidopsis* root cells **(Figure 3 G and H)**. It is suspected that the other DEX inducible VHA-a N-terminal proteins are strongly degraded and localization studies should be performed in the presence of a proteosomal inhibitor.

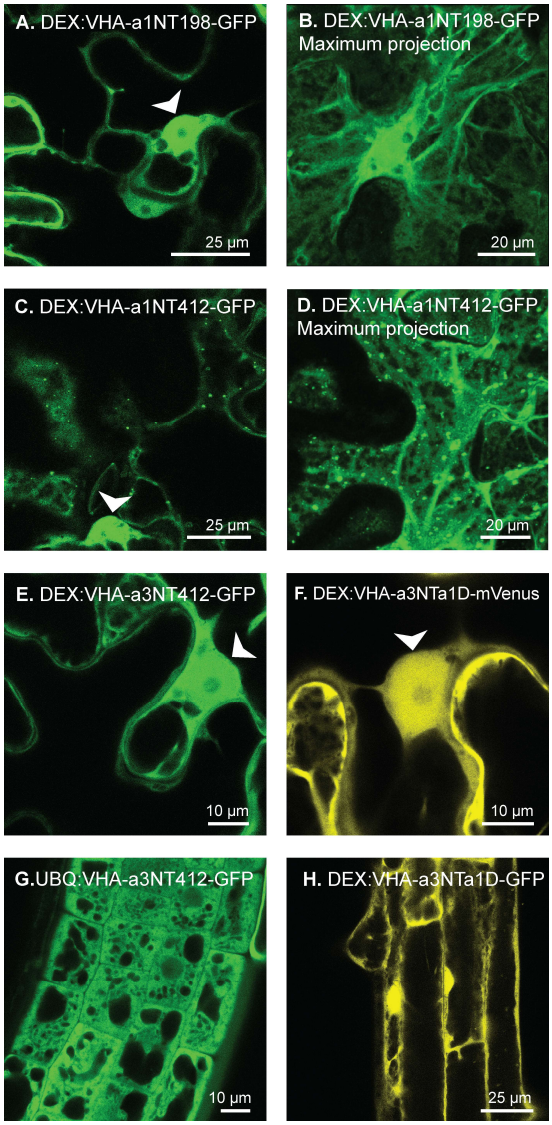

Figure 3. VHA-a1NT412-GFP accumulates in the cytosol and in dots in tobacco leaf cells.

The localization of the VHA-a N-terminal constructs were determined by CLSM in tobacco leaf cells. Plasmids were co-infiltrated with 60 µM dexamethasone and the plants were incubated for three days before CLSM analysis. **(A and B)** VHA-a1NT198-GFP is homogenously expressed in the cytosol. **(C and D)** VHA-a1NT412-GFP shows a cytoplasmic expression pattern but also accumulates in dots. **(E)** VHA-a3NT412-GFP is homogenously expressed in the cytosol. **(F)** The targeting motif of VHA-a1 (a1-TD) was introduced into the N terminus of VHA-a3. VHA-a3NTa1D-mVenus is still homogenously expressed in the cytosol. **(G)** VHA-a3NT412-GFP under the control of the Ubiquitin 10 promoter is homogenously expressed in the cytosol of *Arabidopsis* root cells. **(H)** VHA-a3NTa1D-mVenus is homogenously expressed in the cytosol of *Arabidopsis* root cells. The white arrows indicate nuclear localization which is typical for cytoplasmic localized proteins.

The dot like localization pattern of VHA-a1NT412-GFP suggests that it associates with membranes. To confirm that VHA-a1NT412-GFP possesses intrinsic membrane binding properties, we prepared microsomal membranes. Total protein extracts were prepared from 4 day old etiolated seedlings that had been grown on medium supplemented with 60 µM dexamethasone. The total proteins were then subjected to ultracentrifugation at 100,000 *g* to obtain microsomal membranes. The supernatants which represent the soluble protein fractions were also retained. Microsomal membranes and soluble protein fractions were analyzed by western blot. Our experiments show that the VHA-a1NT412-GFP protein is found predominately in the microsomal membrane fractions **(Figure 4).** VHA-a1NT198-GFP is found in both microsomal membranes and soluble protein fractions. Surprisingly, VHA-a3NT412-GFP could not be detected in any fraction. This could mean that the protein is not expressed or conditions have to be optimized for its detection.

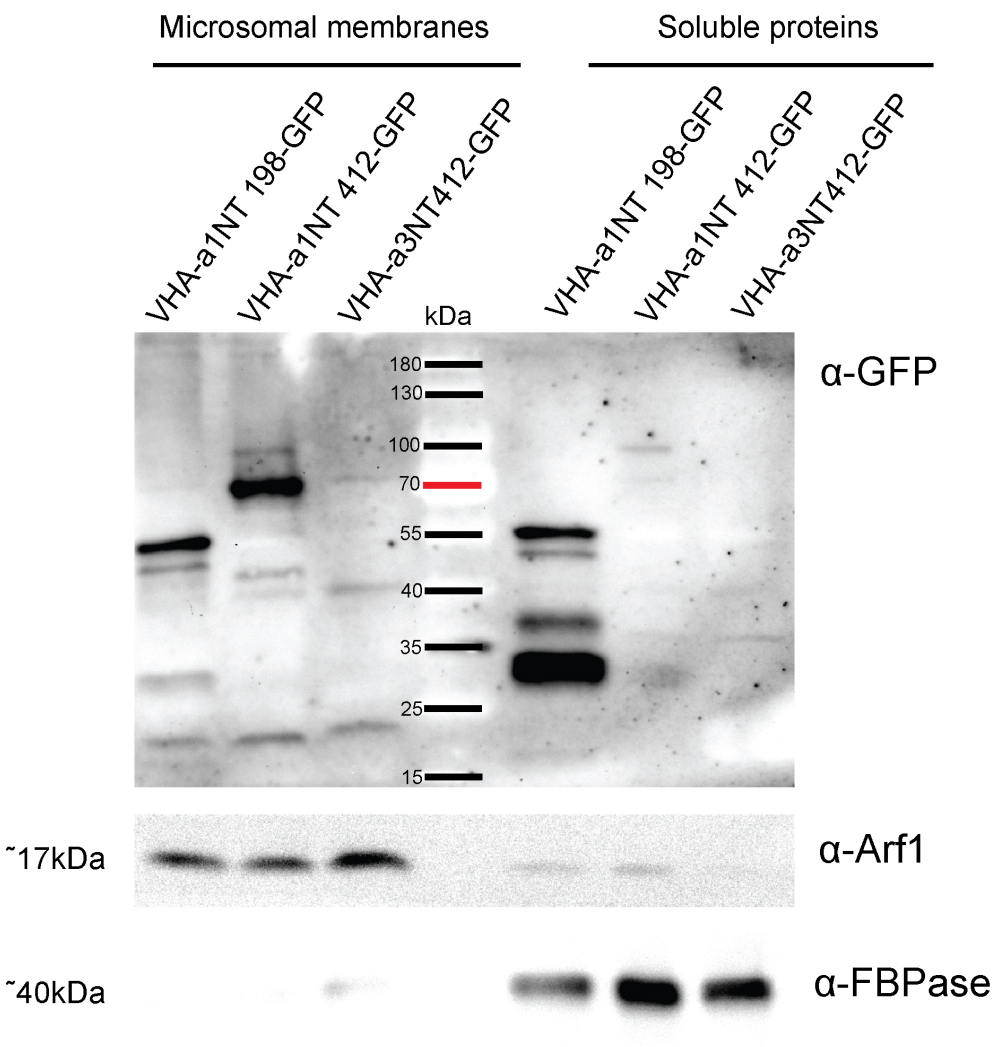

Figure 4. VHA-a1NT412-GFP is found predominately in the microsomal membrane fraction.

Total protein extracts were prepared from 4 day old etiolated seedlings that had been grown on medium supplemented with 60 µM dexamethasone. The total proteins were then subjected to ultracentrifugation at 100,000 *g* to obtain microsomal membranes. Western blot analysis of microsomal membrane and soluble protein fractions was performed using a GFP antibody. The expected sizes of the GFP tagged proteins are 73 kDa and 50 kDa for the 412 aa and 198 aa proteins respectively. VHA-a1NT412-GFP is found predominately in microsomal membrane fraction. VHA-a1NT198-GFP is found in both microsomal membranes and soluble protein fractions but displays multiple bands. This indicates that the protein is highly degraded. The band at 30 kDa in the soluble protein fraction is free GFP. VHA-a3NT412-GFP could not be detected in any fraction. Arf1 (ADP-ribosylation factor1) and FBPase (Fructose bisphosphatase) were used as loading controls for microsomal membranes and soluble protein fractions respectively.

Identification of histidines in the C-terminus of VHA-a1 that could be part of the pH sensing mechanism

The results obtained thus far when the VHA-a1NT is over expressed are similar to the observations made in mammalian cells when the N-terminus of subunit a2 is over expressed (Hurtado-Lorenzo et al., 2006). The overexpression of both VHA-a1 and subunit a2 N-termini evoke cellular responses and both N-terminal proteins are found to associate with membranes. This allowed us to agree with the previous working hypothesis that overexpression of the VHA-a1NT evokes a cellular response because it competes with endogenous VHA-a1 interacting proteins and we developed a second hypothesis that VHA-a1 also has pH sensing capabilities like subunit a2 from mouse.

It is known that histidines are important in the pH sensing mechanism of pH sensing proteins (PSPs) but there are several in the C-terminus of VHA-a1 (eleven) and subunit a2 (fourteen). It is important to know how these histidines are positioned in the folded protein so as to identify the ones involved in pH sensing. It is proposed that histidines on luminal loops and in the transmembrane domains should be the ones involved. At present, no crystal structure exists for any eukaryotic subunit a of the V-ATPase.

Recently a model of the C-terminus of Vph1p from *S. cerevisiae* was obtained through cryo-electron microscopy techniques (Mazhab-Jafari et al., 2016) (PDB=5TJ5). Vph1p is one of the two VHA-a homologous proteins present in yeast and has a sequence identity of 33% to VHA-a1. Homology modelling of VHA-a1, VHA-a3 and subunit a2 C-termini were performed using the model of the Vph1p C-terminus as a template to obtain 3D models (**Supplemental Figure S1 and S2**). Homology modelling was performed using the web based program I-TASSER(Roy et al., 2010). The models show that VHA-a1, VHA-a3 and subunit a2 C-termini have the same fold with 8 transmembrane domains of which two are highly tilted consistent and characteristic of rotary ATPases (Schep et al., 2016).

Next, we performed an alignment of VHA-a1 and subunit a2 C terminal sequences to identify histidines that are conserved in both proteins. The alignment revealed that of the eleven histidines in the N-terminus of VHA-a1, only six (H434, H665, H713, H738, H788 and H793) are conserved in position in the amino acid sequence alignment with histidines in subunit a2 **(Figure 5).** We then mapped these histidines in the 3D models to see if they occupy the same positions in the folded protein. Analysis of the 3D models showed that, these six histidines also occupy the same position in the three dimensional structure **(Figure 6).** Furthermore, all six histidines are conserved in the VHA-a1 clade **(Supplemental Figure S3).** H665 at position 12 in the alignment can be excluded because it is found on the cytoplasmic side of the protein **(Figure 6).** It is therefore proposed that H434, H713, H738, H788, H793 and other histidines primly situated in luminal loops (H494 and H613) in VHA-a1 should be investigated further.

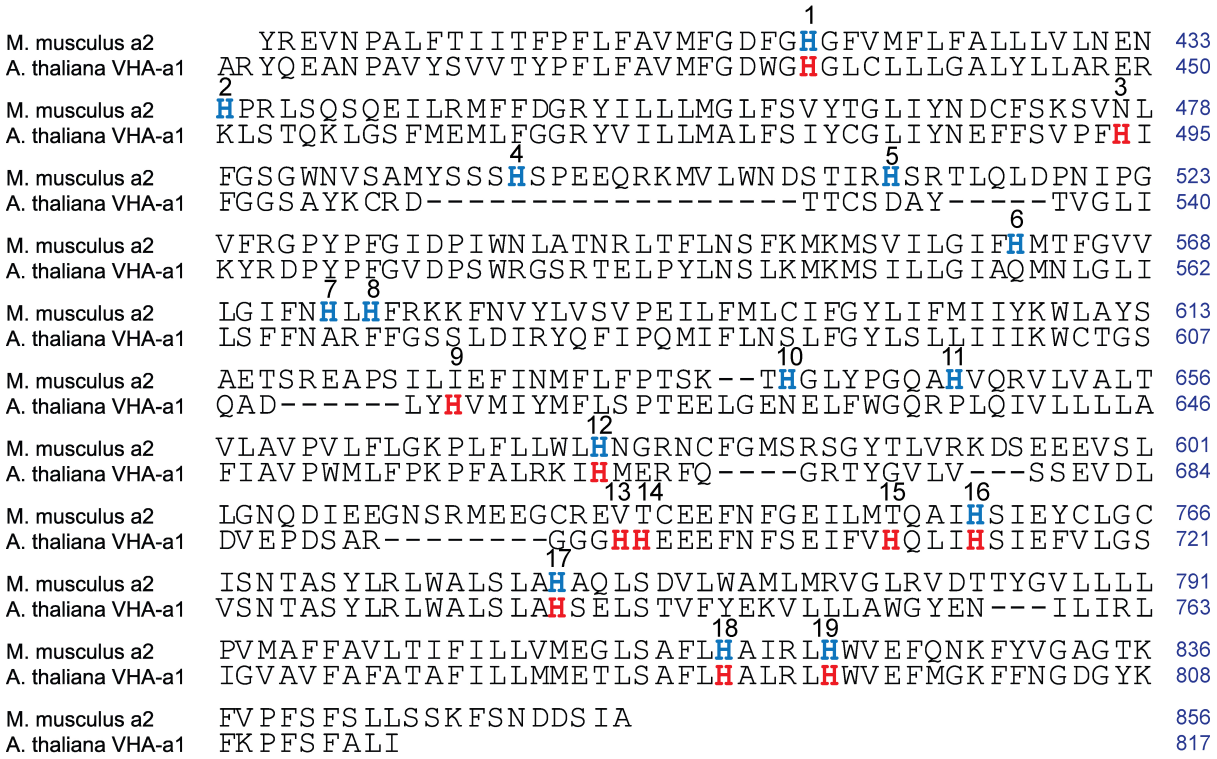

Figure 5. An alignment of VHA-a1 and mouse subunit a2 C-terminal amino acid sequences.

Histidines in VHA-a1 are depicted in red and those in subunit a2 are depicted in blue. Each position in the alignment that contains a histidine is numbered (black numbers). VHA-a1 has 11 histidines in the C-terminus and subunit a2 has 14. The numbers in blue to the right of the alignment indicate the amino acid numbers in the full length protein. Sequence alignment was performed using Clustal Omega (Sievers et al., 2011).

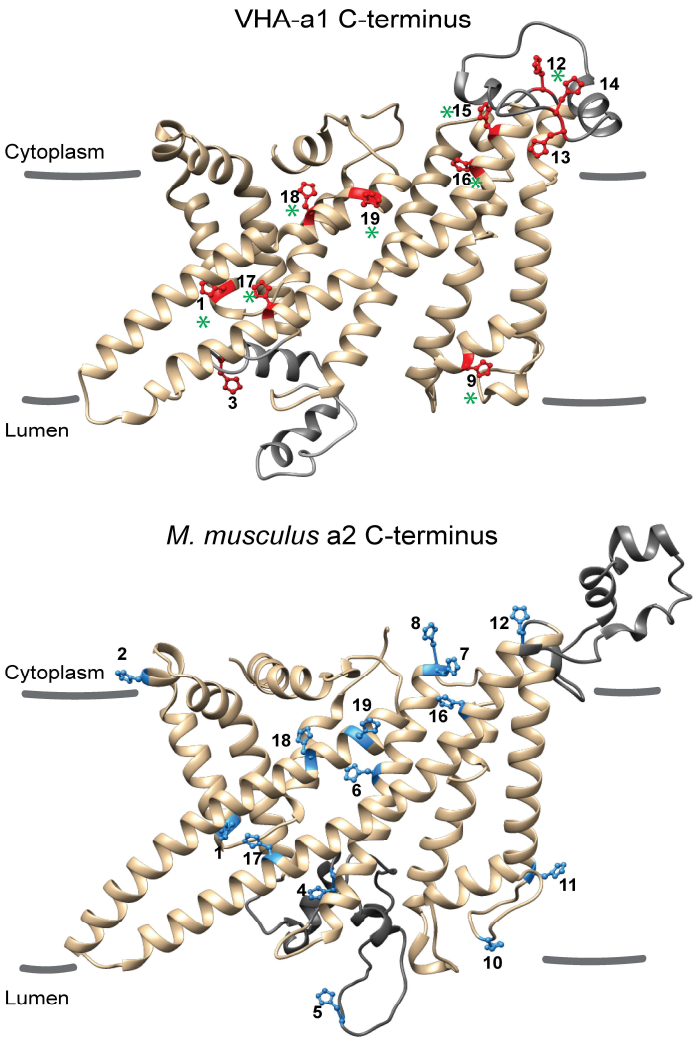

Figure 6. The position of histidines in the 3D structure of VHA-a1 and subunit a2 C-termini

Homology modelling of the C- termini of VHA-a1 and subunit a2 was performed using the coordinates of the C-terminus of Vph1p of the V-ATPase from *S. cerevisiae* (ProteinDataBankcode:5TJ5) as a template. The C-termini of VHA-a1 and subunit a2 contain eight membrane embedded α-helices. Two of these helices are long and highly-tilted. A more detailed description of the models is found in **Supplemental figure S1**. Histidine atoms are depicted in ball-and-stick representation and are coloured red in VHA-a1 and blue in subunit a2. The numbers in black indicate the position in the amino acid sequence alignment shown in **Figure 5**. Histidines at positions 1, 17, 18, 19, 16 and 12 in the alignment occupy similar positions in the 3D structure. Histidines that are conserved in the VHA-a1 clade are indicated with green asterisks in the VHA-a1 model.

Mass spectrometry reveals VHA-a1NT interacting proteins

Mouse subunit a2 participates in vesicle trafficking by recruiting a GTPase and its GEF to the membrane. *Arabidopsis* VHA-a1 may operate in a similar mechanism or it might employ a different mechanism that is unique to plant cells. We wanted to determine the proteins whose interaction with the N-terminus of VHA-a1are crucial for proper functioning of the V-ATPase at the TGN.

We performed co-immunoprecipitation (CO-IP) experiments using microsomal membranes which were extracted from 4 day old etiolated seedlings expressing VHA-a1NT412-GFP. Proteins were solubilized from membranes using NP-40 and a protein to detergent ratio of 1:25. The GFP-trap system was then applied to allow isolation of potential interaction partners from the solubilized proteins. GFP immuno purification performed in microsomal membrane extracts from etiolated seedlings expressing VHA-a3-GFP was used as a negative control. The presence of the VHA-a1NT412-GFP and VHA-a3-GFP was confirmed via SDS-PAGE followed by western blotting with a GFP antibody (**Figure 7**).

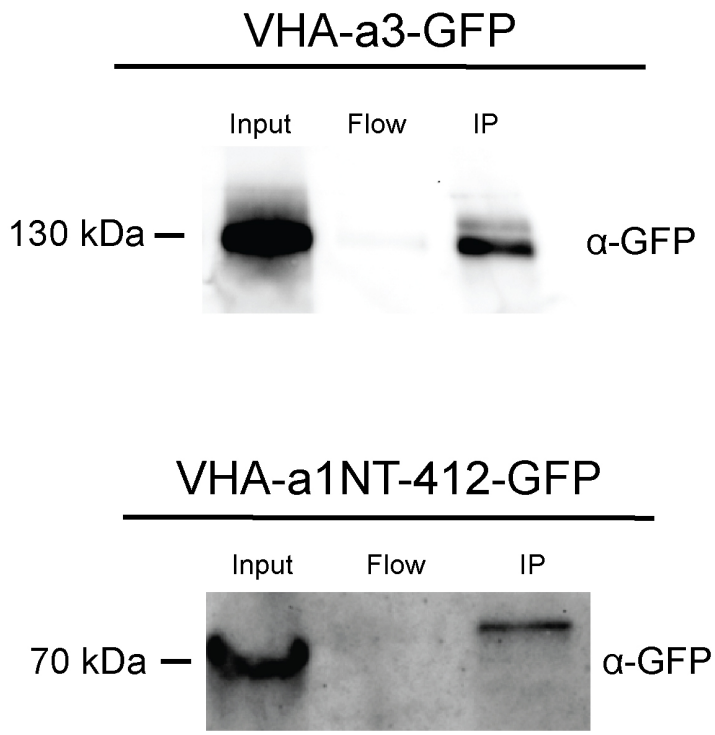

Figure 7. Western blot of CO-IP of VHA-a1NT412-GFP and VHA-a3-GFP

Microsomal membranes were extracted from 4 day old etiolated seedlings. Membrane proteins were solubilized from membranes with NP-40 (**Supplemental figure S4**). VHA-a1NT412-GFP and VHA-a3-GFP were immunoprecipitated from solubilized proteins (Input) with GFP trap nano bodies. Co-immunoprecipitated VHA-a1NT412-GFP and VHA-a3-GFP (IP) were detected by western blotting using a GFP antibody before being sent for mass spectrometry analysis. One representative blot out of four is shown for each line.

VHA-a1NT-GFP and VHA-a3-GFP co-purified proteins were then analyzed my mass spectrometry. A label-free quantification (LFQ) approach (Cox et al., 2014) was used to assess enrichment over the VHA-a3-GFP control. Over 1000 proteins were identified and quantified between the experiment and the control. using the MaxQuant platform (Cox et al., 2014).

Protein lists generated by MaxQuant were further analyzed by Perseus (version 1.5.4.41) (Tyanova et al., 2016). For each peptide a permutation-corrected (false discovery rate, FDR) t-test was applied to define significance between the control and the experiment. Only samples with valid LFQ values were considered. With

this approach 189 proteins were found to be significantly different and more than one fold abundant in the experiment (**Figure 8 A**)

Missing LFQ values may arise due to reasons which may include the following: (i) the peptide truly is present at an abundance the instrument should be able to detect, but is not detected or is incorrectly identified, (ii) the peptide truly is present but at an abundance below the instrument's detection limits, and (iii) the peptide is not present (Karpievitch et al., 2012).

The data set was filtered as to only include peptides with at least three LFQ values across all samples. Then the missing LFQ intensity values were imputed from a normal distribution (**Supplemental figure S5 B**) to simulate values at the lower limit of detection and the permutation-corrected (false discovery rate, FDR) t-test was applied again to define significance. With this approach 446 proteins were found to be significantly different and more than one fold abundant in the experiment (**Figure 8 B**).

A

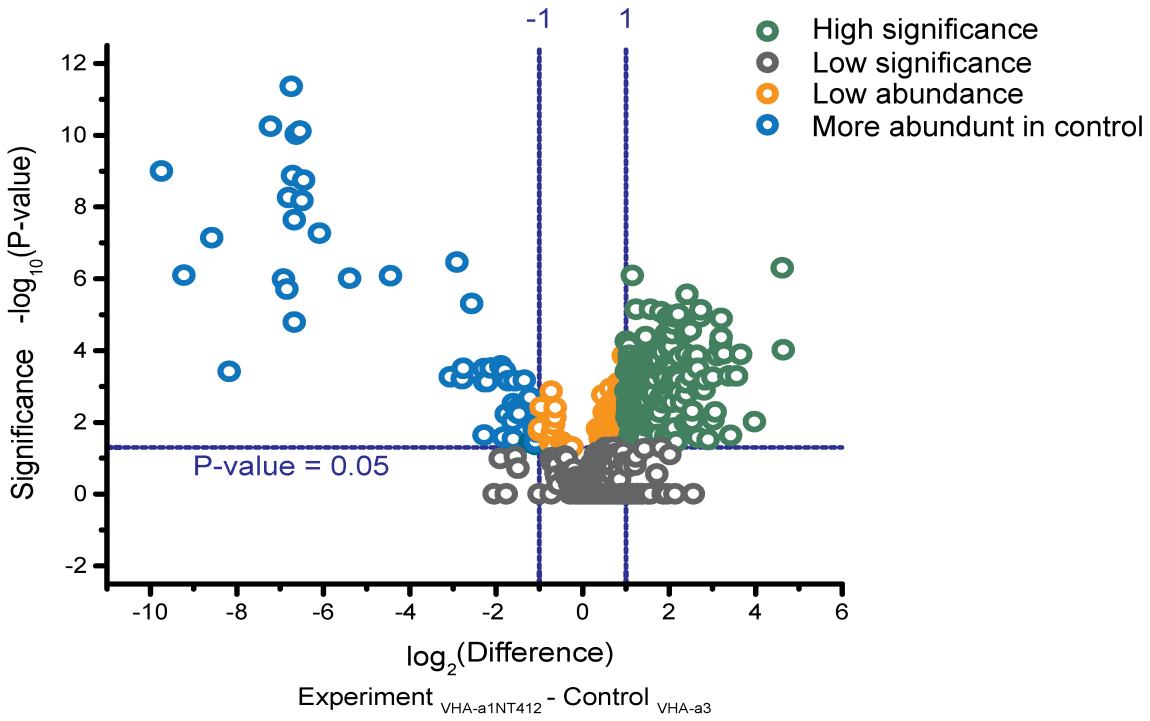
No imputation
-1
1
High significance
Low significance
Low abundance
More abundant in control
Significance -log10(P-value)
P-value = 0.05
log2(Difference)
Experiment VHA-a1NT412 - Control VHA-a3

B

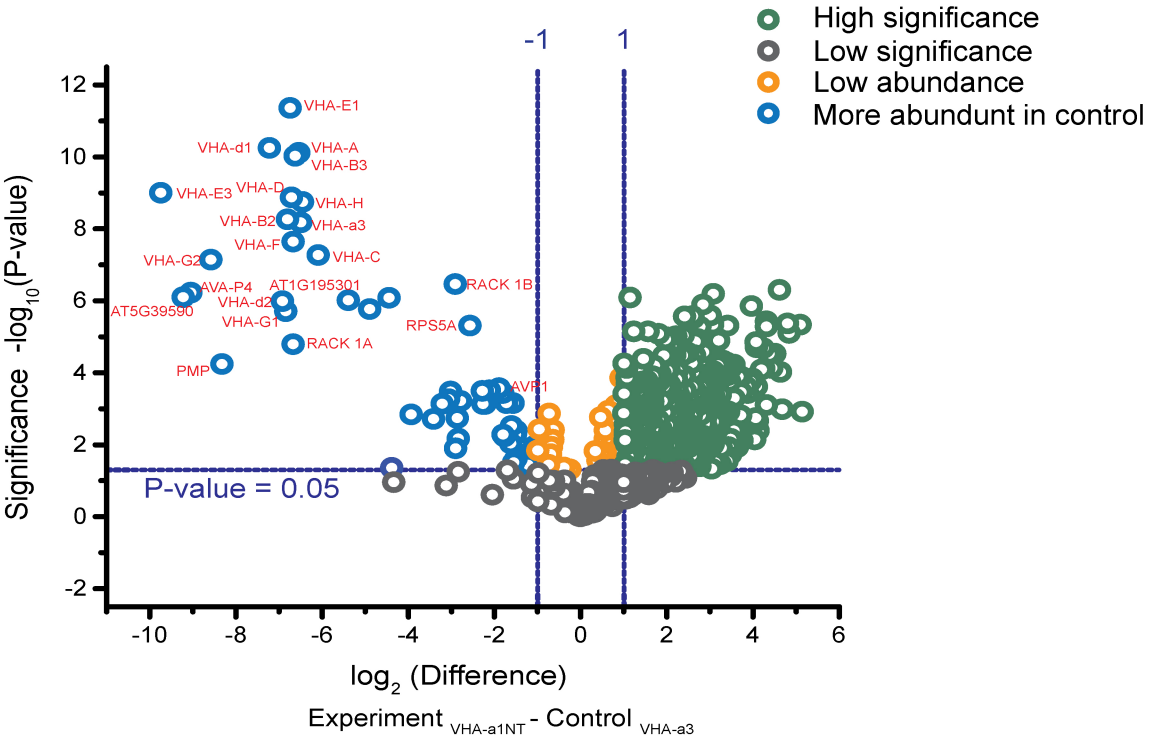
With imputation
-1
1
High significance
Low significance
Low abundance
More abundant in control
VHA-E1
VHA-d1
VHA-A
VHA-B3
VHA-E3
VHA-D
VHA-H
VHA-B2
VHA-a3
VHA-F
VHA-C
VHA-G2
AVA-P4
AT1G195301
RACK 1B
AT5G39590
VHA-d2
VHA-G1
RPS5A
RACK 1A
PMP
AVP1
Significance -log10(P-value)
P-value = 0.05
log2 (Difference)
Experiment VHA-a1NT - Control VHA-a3

Figure 8. Statistical analysis of proteins detected by mass spectrometry

The -log of the p-values obtained from the two sample t-tests were plotted against the differences between the LFQ means to visualize and identify proteins that were significantly different between the control and the experiment. **(A)** Volcano plot showing the results of a two-sample t test(FDR 0.05, S0 0.1) applied to LFQ intensities to assess enrichment in VHA-a1NT412-GFP samples over VHA-a3-GFP controls. Only samples with valid LFQ values were considered. 189 proteins (green circles) were found to be significantly different and more than one fold abundant between the control and the experiment. **(B)** Missing LFQ values were imputed from normal distribution curves for each sample. Only peptides with at least three LFQ values across all samples were considered. The volcano plot shows the differences between the means (x-axis) versus the −log p-values (y-axis) from a two-sample t-test (FDR 0.05, S0 0.1). 446 proteins (green circles) were found to be significantly different and more than one fold abundant between the control and the experiment. Proteins which are known to interact with VHA-a3 such as the subunits of the V-ATPase are more abundant in the VHA-a3-GFP samples and are indicated in red. Data analysis was performed using the Perseus computational software (Tyanova et al., 2016)

The proteins identified to be significantly more abundant in the VHA-a1NT412-GFP samples after imputation were classified according to protein class using the PANTHER classification system (Mi et al., 2016) **(Figure 9)**. The class of proteins that was enriched the most in the VHA-a1NT412-GFP samples was the class of oxidoreductases. Only 2.8% of the enriched proteins were classified as membrane traffic proteins. None the less, all the proteins identified to be significantly more abundant in the VHA-a1NT412-GFP samples were individually assessed and 48 proteins which could be potential interaction partners for the VHA-a1NT were selected **(Figure 10 and Supplemental table S2).** Proteins were selected based on significance of abundance in the VHA-a1NT412-GFP samples, based on the p-value of the t-test statistic, and relevance to the TGN compartment in terms of spatial localization, signaling and trafficking. Uncharacterized proteins were also included in the final list.

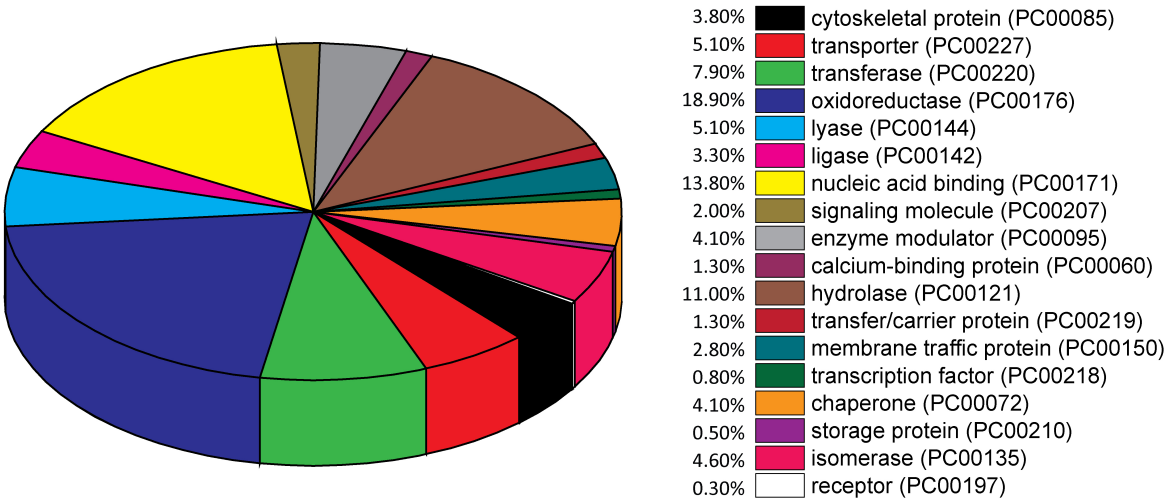

Figure 9. Classification of proteins that were significantly enriched in the VHA-a1NT412-GFP samples according to protein class

The protein classes were assigned using the PANTHER classification system (Mi et al., 2016). 2.8% of the proteins were classified to be involved in membrane trafficking.

Figure 10. Z-score normalized LFQ intensity values across four replicates of selected proteins of interest.

Hierarchical clustering of z-score normalized LFQ values was performed using a Euclidian distance method. The z-score normalized values are shown in a heat map that represents the variation in protein abundance between the analyzed samples. Columns indicate the samples, and rows indicate the proteins. Intensity ranges from highest intensity (purple) to lowest (blue). The selected proteins include uncharacterized proteins, proteins involved in vesicle transport and the GTPases: ARF C1, ARF 2-A, 2-B and Protein ROOT HAIR DEFECTIVE 3. VHA-a1 is included for comparison purposes. The gene names and protein IDs are presented in **supplemental table S2.**

Discussion

Subunit a of the V-ATPase is central to the functioning of the V-ATPase complex. It has been shown to control targeting of the complex in cell, coupling of ATP hydrolysis to proton transport and it contains hemi channels through which protons pass from the cytosol to the lumen(Kawasaki-Nishi et al., 2001; Leng et al., 1998; Forgac, 2007). It was revealed that in mammalian kidney cells, subunit a interacts and recruits a guanine exchange factor (GEF) called ARNO (Arf nucleotide site opener) to the membrane in a pH dependent manner (Hurtado-Lorenzo et al., 2006). This finding added a new feature to subunit a as a pH sensing protein. Mammalian subunit a1, a3 and a4 isoforms were also reported to interact with ARNO therefore interaction with components of the vesicle trafficking machinery may be a general feature of subunit a function (Hurtado-Lorenzo et al., 2006). We investigated whether *Arabidopsis* VHA-a1 participates in vesicle trafficking in a similar way as observed for its mammalian homologue.

In this study, we utilized a long (412 aa) and short (198aa) version of the VHA-a1 N-terminus (VHA-a1NT) to show that VHA-a1NT overexpression causes inhibition of cell expansion in etiolated hypocotyls and causes a serrated leaf phenotype. These phenotypes can be attributed to aberration of VHA-a1 function because they are the same phenotypes brought about by inducible ami-VHA-a1(artificial micro RNA against VHA-a1) constructs (Kriegel, 2015). VHA-a1NT412-GFP overexpression results in a more severe inhibition of hypocotyl expansion and reduces the rosette area more severely than overexpression of VHA-a1NT198-GFP. In addition, VHA-a1NT412-GFP is found predominately in membrane fractions while VHA-a1NT198-GFP is partitioned comparably between membrane and soluble fractions. Furthermore, through localization studies in tobacco leaf cells, we show that the association of VHA-a1NT412-GFP to membranes is not due the presence of the VHA-a1 targeting domain (K140-S174) in its sequence.

It is unlikely that the VHA-a3NT participates in vesicle trafficking events because the *vha-a2 vha-a3* double mutant is dwarfed and shows a day length dependent phenotype but it does not show any phenotype related to defective vesicle trafficking (Krebs et al., 2010).

Expression in *Arabidopsis* root cells has to be optimized. It is suspected that the VHA-a constructs are strongly degraded hence the lack of fluorescence. This could be circumvented by applying the use of the proteosomal inhibitor, MG132(Lee, 1998). VHA-a3NT412-GFP could not be detected in *Arabidopsis* root cells and on the western blot. This may be due to problems in induction times because the fluorescence detection in tobacco leaves suggests that the transgenic protein is expressed.

Mass spectrometry analysis revealed potential VHA-a1NT interaction partners. These proteins include uncharacterized proteins as well as characterized proteins, a subset of which are involved in vesicle trafficking. The interactions have to be confirmed with other techniques such as bimolecular fluorescence complementation (BiFC) and the yeast two hybrid method (Kerppola, 2008; Brückner et al., 2009). Noticeably, the mass spectrometry results also showed that there was a lot of background noise (house keeping proteins) such as ribosomal proteins and chloroplastic proteins that were part of the final result. Background noise may have been caused by unspecific binding to the GFP trap nano body, which was used for the CO-IPs. Repetition of the CO-IP experiments using a verified GFP antibody coupled to beads may reduce unspecific binding.

Homology modelling of the C-termini of the plant VHA-a subunits allowed the 3D structure of this important subunit to be visualized. This has allowed us to identify histidine residues based on their position in the folded protein that may be involved in pH sensing. These histidines can be further investigated by mutational studies. The models also allow us to know the amino acid environment around the histidines. The pKa value of an amino acid varies depending on the amino acid environment in the protein. This is because the amino acid environment

determines the electrostatic potential and solvent accessibility of side chains (Srivastava et al., 2007). Estimation of the pKa of each of the potential histidines may help in identifying the ones that may be involved in pH sensing.

Overall the study has provided further evidence that subunit a of the V-ATPase at the TGN may act as a pH sensing protein. We have identified histidines in VHA-a1 that could be involved in the molecular pH sensing mechanism. Potential interaction partners for VHA-a1NT have been identified and we have provided 3D models that may be useful in studying other aspects related to subunit a function.

Supplemental material

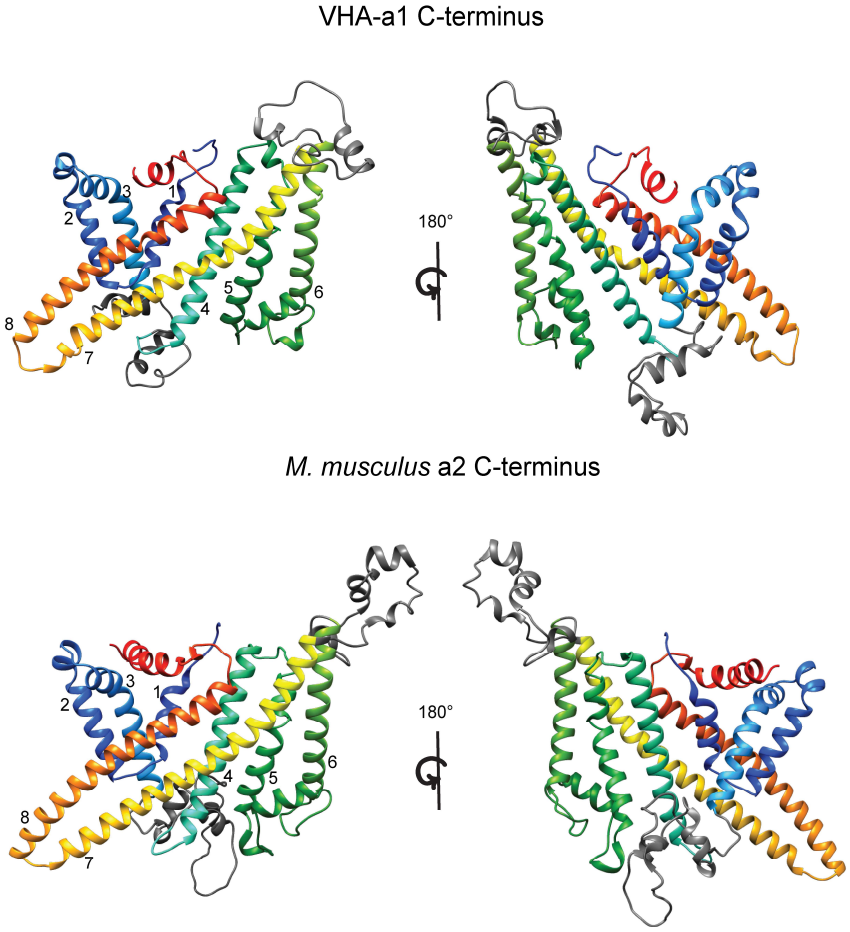

Figure S1. 3D structure of VHA-a1 and subunit a2 C-termini

Homology modelling of the C- termini of VHA-a1 and subunit a2 was performed using the coordinates of the C-terminus of Vph1p of the V-ATPase from *S. cerevisiae* (Protein Data Bank code: 5TJ5) as a template. The C-termini of VHA-a1 and subunit a2 contain eight membrane embedded α-helices. The membrane embedded domain of subunit a starts with a pair of short α-helices that do not fully cross the lipid bilayer(1 and 2).Four subsequent transmembrane α -helices (3 to 6) produce a central layer in the subunit structure. The last two helices (7 and 8) are long and highly-tilted. The loops depicted in dark grey (residues and 487-532 and 664-704 in VHA-a1 and residues 470-538 and 674-729 in mouse subunit a2) were not modelled because they were not available in the Vph1p model due to no density detection.

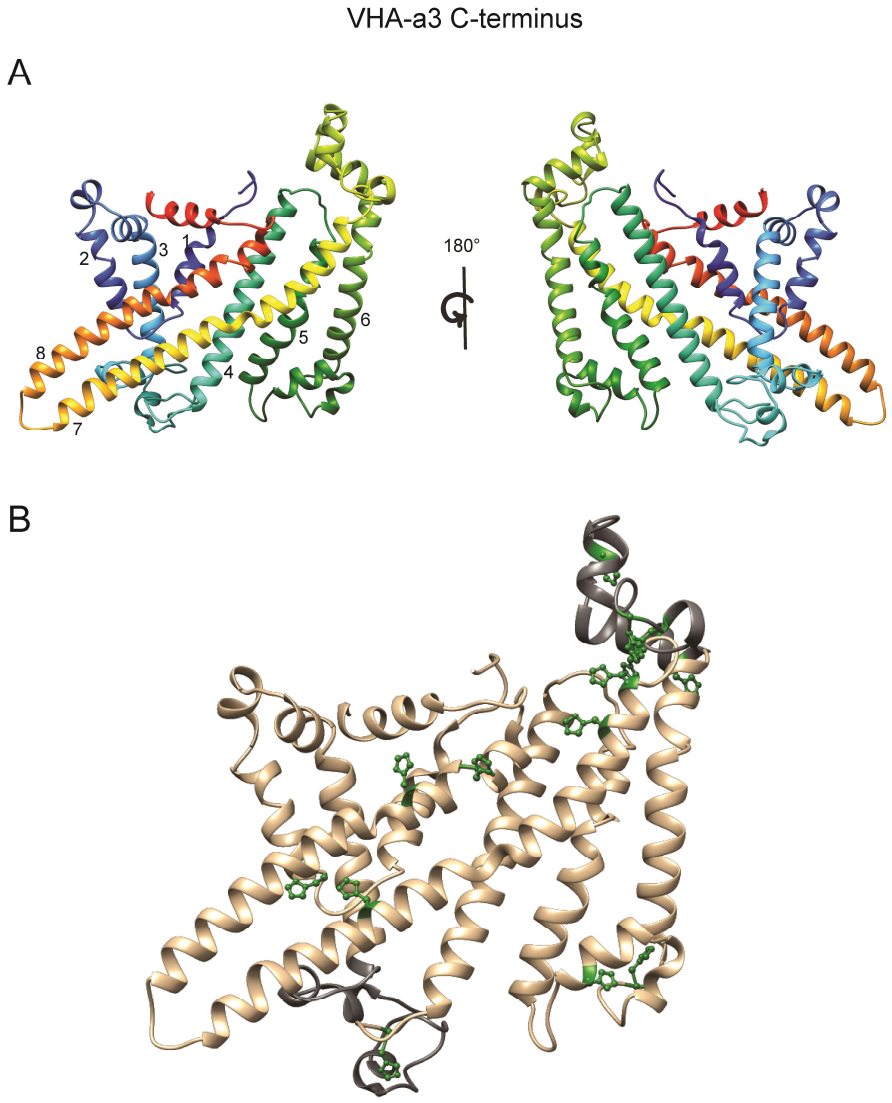

Figure S2. 3D structure of the VHA-a3 C-terminus

(A) Homology modelling of the C- termini of VHA-a1 and subunit a2 was performed using the coordinates of the C-terminus of Vph1p of the V-ATPase from *S. cerevisiae* (Protein Data Bankcode: 5TJ5) as a template. The loops depicted in dark grey (residues and 488-533 and 665-703) were not modelled because they were not available in the Vph1p model due to no density detection. The VHA-a3 C-terminus has 14 Histidines which are depicted in ball-and-stick representation and are coloured green. Some of these histidines occupy the same position in the 3D structure as histidines in VHA-a1 and subunit a2 C-termini.

Table S1. Statistical support for the predicted structural homology models obtained from I-TASSER.

Subunit a C-terminal domain	Quality of Predicted Model	
	C-Score	TM-Score
VHA-a1	-0.78	0.61 ± 0.14
VHA-a3	-0.78	0.61 ± 0.14
M.musculus subunit a2	-1.33	0.55 ± 0.15

The quality of the models generated using the online server I-TASSER is evaluated by using two criteria, C-score and the TM-score. The C-score is an estimate of the confidence of structure prediction, and ranges from − 5 to 2. Models with a higher score reflect a model of better quality. The TM-score is a measure of structural similarity between the predicted model and the template, and ranges from 0 to 1. A higher score indicates a better structural similarity (Roy et al., 2010)

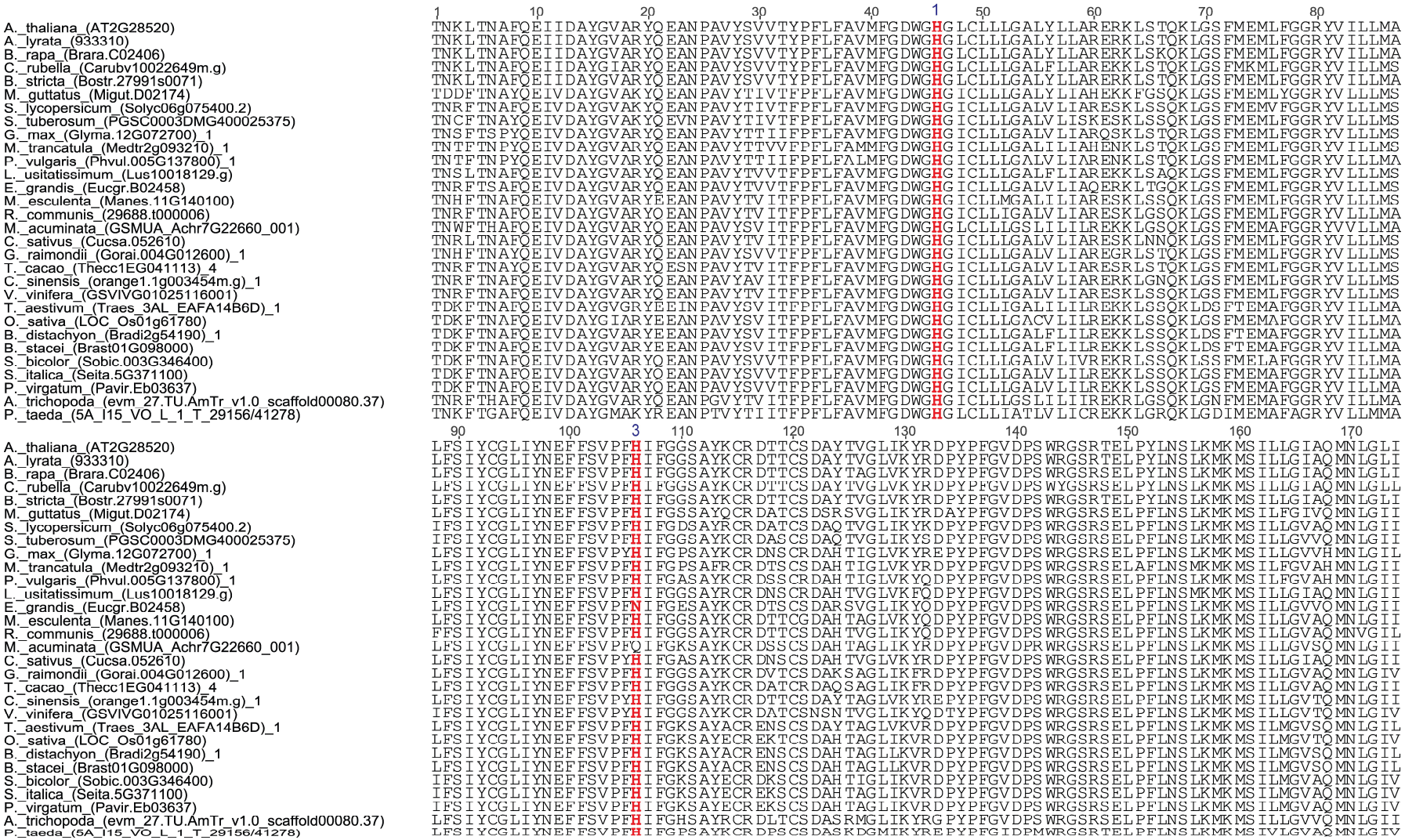
1 10 20 30 40 1 50 60 70 80
A._thaliana_(AT2G28520)
A._lyrata_(933310)
B._rapa_(Brara.C02406)
C._rubella_(Carubv10022649m.g)
B._stricta_(Bostr.27991s0071)
M._guttatus_(Migut.D02174)
S._lycopersicum_(Solyc06g075400.2)
S._tuberosum_(PGSC0003DMG400025375)
G._max_(Glyma.12G072700)_1
M._trancatula_(Medtr2g093210)_1
P._vulgaris_(Phvul.005G137800)_1
L._usitatissimum_(Lus10018129.g)
E._grandis_(Eucgr.B02458)
M._esculenta_(Manes.11G140100)
R._communis_(29688.t000006)
M._acuminata_(GSMUA_Achr7G22660_001)
C._sativus_(Cucsa.052610)
G._raimondii_(Gorai.004G012600)_1
T._cacao_(Thecc1EG041113)_4
C._sinensis_(orange1.1g003454m.g)_1
V._vinifera_(GSVIVG01025116001)
T._aestivum_(Traes_3AL_EAFA14B6D)_1
O._sativa_(LOC_Os01g61780)
B._distachyon_(Bradi2g54190)_1
B._stacei_(Brast01G098000)
S._bicolor_(Sobic.003G346400)
S._italica_(Seita.5G371100)
P._virgatum_(Pavir.Eb03637)
A._trichopoda_(evm_27.TU.AmTr_v1.0_scaffold00080.37)
P._taeda_(5A_I15_VO_L_1_T_29156/41278)
90 100 3 110 120 130 140 150 160 170
A._thaliana_(AT2G28520)
A._lyrata_(933310)
B._rapa_(Brara.C02406)
C._rubella_(Carubv10022649m.g)
B._stricta_(Bostr.27991s0071)
M._guttatus_(Migut.D02174)
S._lycopersicum_(Solyc06g075400.2)
S._tuberosum_(PGSC0003DMG400025375)
G._max_(Glyma.12G072700)_1
M._trancatula_(Medtr2g093210)_1
P._vulgaris_(Phvul.005G137800)_1
L._usitatissimum_(Lus10018129.g)
E._grandis_(Eucgr.B02458)
M._esculenta_(Manes.11G140100)
R._communis_(29688.t000006)
M._acuminata_(GSMUA_Achr7G22660_001)
C._sativus_(Cucsa.052610)
G._raimondii_(Gorai.004G012600)_1
T._cacao_(Thecc1EG041113)_4
C._sinensis_(orange1.1g003454m.g)_1
V._vinifera_(GSVIVG01025116001)
T._aestivum_(Traes_3AL_EAFA14B6D)_1
O._sativa_(LOC_Os01g61780)
B._distachyon_(Bradi2g54190)_1
B._stacei_(Brast01G098000)
S._bicolor_(Sobic.003G346400)
S._italica_(Seita.5G371100)
P._virgatum_(Pavir.Eb03637)
A._trichopoda_(evm_27.TU.AmTr_v1.0_scaffold00080.37)
P._taeda_(5A_I15_VO_L_1_T_29156/41278)

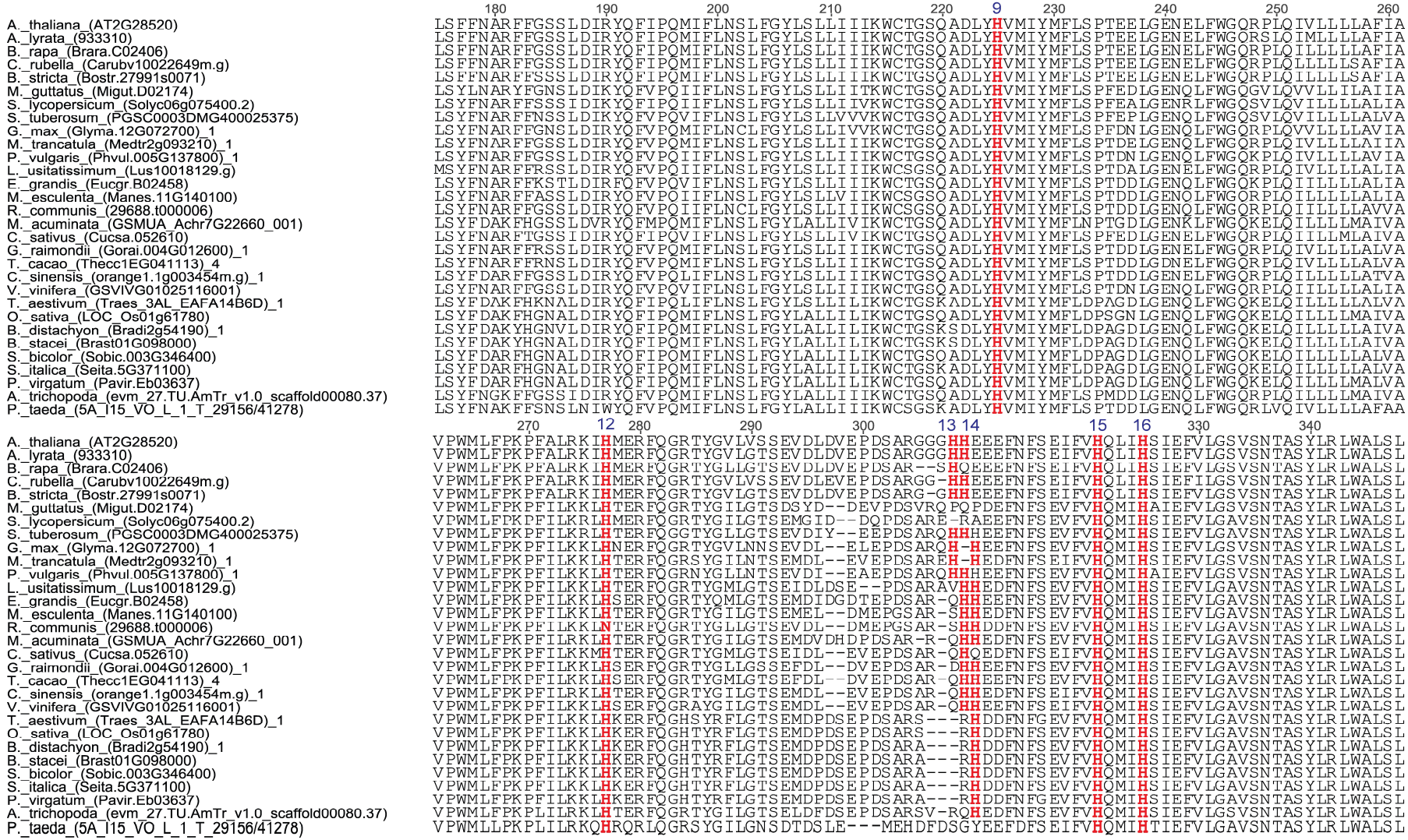
180 190 200 210 220 9 230 240 250 260
A._thaliana_(AT2G28520) LSFFNARFFGSSLDIRYQFIPQMIFLNSLFGYLSLLIIIKWCTGSQADLYHVMIYMFLSPTEELGENELFWGQRPLQIVLLLLAFIA
A._lyrata_(933310) LSFFNARFFGSSLDIRYQFIPQMIFLNSLFGYLSLLIIIKWCTGSQADLYHVMIYMFLSPTEELGENELFWGQRSLQIMLLLLAFIA
B._rapa_(Brara.C02406) LSFFNARFFGSSLDIRYQFIPQMIFLNSLFGYLSLLIIIKWCTGSQADLYHVMIYMFLSPTEELGENELFWGQRPLQILLLLLAFIA
C._rubella_(Carubv10022649m.g) LSFFNARFFGSSLDIRYQFIPQMIFLNSLFGYLSLLIIIKWCTGSQADLYHVMIYMFLSPTEELGENELFWGQRPLQLLLLLSAFIA
B._stricta_(Bostr.27991s0071) LSFFNARFFSSSLDIRYQFIPQMIFLNSLFGYLSLLIIIKWCTGSQADLYHVMIYMFLSPTEELGENELFWGQRPLQILLLLSAFIA
M._guttatus_(Migut.D02174) LSYLNARYFGNSLDIKYQFVPQIIFLNSLFGYLSLLIITKWCTGSQADLYHVMIYMFLSPFEDLGENQLFWGQGVLQVVLLILAIIA
S._lycopersicum_(Solyc06g075400.2) LSYFNARFFSSSIDIKYQFIPQIIFLNSLFGYLSLLIIVKWCTGSQADLYHVMIYMFLSPFEALGENRLFWGQSVLQVILLLLALIA
S._tuberosum_(PGSC0003DMG400025375) LSYFNARFFNSSLDIKYQFVPQVIFLNSLFGYLSLLVVVKWCTGSQADLYHVMIYMFLSPFEPLGENQLFWGQSVLQVILLLLALVA
G._max_(Glyma.12G072700)_1 LSYFNARFFGNSLDIRYQFVPQMIFLNCLFGYLSLLIVVKWCTGSQADLYHVMIYMFLSPFDNLGENQLFWGQRPLQVVLLLLAVIA
M._trancatula_(Medtr2g093210)_1 LSYFNARFFGSSLDIRYQFVPQMIFLNSLFGYLSLLIIIKWCTGSQADLYHVMIYMFLSPTDELGENQLFWGQRPLQIVLLLLAIIA
P._vulgaris_(Phvul.005G137800)_1 LSYFNARFFGSSLDIRYQFVPQIIFLNSLFGYLSLLIIIKWCTGSQADLYHVMIYMFLSPTDNLGENQLFWGQKPLQIVLLLLAVIA
L._usitatissimum_(Lus10018129.g) MSYFNARFFRSSLDIRYQFVPQIIFLNSLFGYLSLLIIIKWCSGSQADLYHVMIYMFLSPTDALGENELFWGQRPLQIVLLLLALIA
E._grandis_(Eucgr.B02458) LSYFNARFFKSTLDIRFQFVPQVIFLNSLFGYLSLLIIIKWCTGSQADLYHVMIYMFLSPTDDLGENQLFWGQKPLQIILLLLALIA
M._esculenta_(Manes.11G140100) LSYFNARFFASSLDIRYQFVPQIIFLNSLFGYLSLLVIIKWCSGSQADLYHVMIYMFLSPTDDLGENQLFWGQRPLQIILLLLALIA
R._communis_(29688.t000006) LSYFNARFFGSSLDIRYQFVPQIIFLNCLFGYLSLLIIIKWCSGSQADLYHVMIYMFLSPTDDLGENQLFWGQRPLQIILLLLAVVA
M._acuminata_(GSMUA_Achr7G22660_001) LSYFDAKFHGSSLDVRYQFMPQMIFLNSLFGYLALLIVIKWCTGSQADLYHVMIYMFLNPTGDLGENKLFWGQKELQILLLLMAIVA
C._sativus_(Cucsa.052610) LSYFNARFTGSSIDIRYQFIPQVIFLNSLFGYLSLLIVIKWCTGSQADLYHVMIYMFLSPFEDLGENELFWGQRPLQIILLMLAIVA
G._raimondii_(Gorai.004G012600)_1 LSYFNARFFRSSLDIRYQFVPQMIFLNSLFGYLSLLIIIKWCTGSQADLYHVMIYMFLSPTDDLGENELFWGQRPLQIVLLLLALVA
T._cacao_(Thecc1EG041113)_4 LSYFNARFFRNSLDIRYQFVPQMIFLNSLFGYLSLLIIIKWCTGSQADLYHVMIYMFLSPTDDLGDNELFWGQRPLQIVLLLLALVA
C._sinensis_(orange1.1g003454m.g)_1 LSYFDARFFGSSLDIRYQFVPQLIFLNSLFGYLSLLIIIKWCTGSQADLYHVMIYMFLSPTDDLGENELFWGQRPLQILLLLLATVA
V._vinifera_(GSVIVG01025116001) LSYFNARFFGSSLDIRYQFVPQVIFLNSLFGYLSLLIIIKWCTGSQADLYHVMIYMFLSPTDNLGENQLFWGQRPLQIILLLLALIA
T._aestivum_(Traes_3AL_EAFA14B6D)_1 LSYFDAKFHKNALDIRYQFIPQLIFLNSLFGYLSLLILKWCTGSKADLYHVMIYMFLDPAGDLGENQLFWGQKELQILLLLLALVA
O._sativa_(LOC_Os01g61780) LSYFDAKFHGNALDIRYQFIPQMIFLNSLFGYLALLILKWCTGSQADLYHVMIYMFLDPSGNLGENQLFWGQKELQILLLLMAIVA
B._distachyon_(Bradi2g54190)_1 LSYFDAKYHGNVLDIRYQFIPQMIFLNSLFGYLALLILKWCTGSKSDLYHVMIYMFLDPAGDLGENQLFWGQKELQILLLLLAIVA
B._stacei_(Brast01G098000) LSYFDAKYHGNALDIRYQFIPQMIFLNSLFGYLALLILKWCTGSKSDLYHVMIYMFLDPAGDLGENQLFWGQKELQILLLLLAIVA
S._bicolor_(Sobic.003G346400) LSYFDARFHGNALDIRYQFIPQMIFLNSLFGYLALLILKWCTGSQADLYHVMIYMFLDPAGDLGENQLFWGQKELQILLLLLALVA
S._italica_(Seita.5G371100) LSYFDARFHGNALDIRYQFIPQMIFLNSLFGYLALLILKWCTGSKADLYHVMIYMFLDPAGDLGENQLFWGQKELQILLLLLALVA
P._virgatum_(Pavir.Eb03637) LSYFDARFHGNALDIRYQFIPQMIFLNSLFGYLALLILKWCTGSQADLYHVMIYMFLDPAGDLGENQLFWGQKELQILLLLLALVA
A._trichopoda_(evm_27.TU.AmTr_v1.0_scaffold00080.37) LSYFNGKFFGSSIDIRYQFVPQMIFLNSLFGYLALLIIIKWCTGSQADLYHVMIYMFLSPMDDLGENQLFWGQRPLQILLLLMAIVA
P._taeda_(5A_115_VO_L_1_T_29156/41278) LSYFNAKFFSNSLNIWYQFVPQMIFLNSLFGYLALLIIIKWCSGSKADLYHVMIYMFLSPTDDLGENQLFWGQRLVQIVLLLLAFAA
270 12 280 290 13 14 300 15 16 330 340
A._thaliana_(AT2G28520) VPWMLFPKPFALRKIHMERFQGRTYGVLVSSEVDLDVEPDSARGGGHHEEEEFNFSEIFVHQLIHSIEFVLGSVSNTASYLRLWALSL
A._lyrata_(933310) VPWMLFPKPFALRKIHMERFQGRTYGVLGTSEVDLDVEPDSARGGGHHEEEEFNFSEIFVHQLIHSIEFVLGSVSNTASYLRLWALSL
B._rapa_(Brara.C02406) VPWMLFPKPFALRKIHMERFQGRTYGLLGTSEVDLDVEPDSAR--SHQEEEEFNFSEIFVHQLIHSIEFVLGSVSNTASYLRLWALSL
C._rubella_(Carubv10022649m.g) VPWMLFPKPFALRKIHMERFQGRTYGVLVSSEVDLEVEPDSARGG-HHEEEEFNFSEIFVHQLIHSIEFILGSVSNTASYLRLWALSL
B._stricta_(Bostr.27991s0071) VPWMLFPKPFALRKIHMERFQGRTYGVLGTSEVDLDVEPDSARG-GHHEEEEFNFSEIFVHQLIHSIEFVLGSVSNTASYLRLWALSL
M._guttatus_(Migut.D02174) VPWMLFPKPFILKKLHTERFQGRTYGILGTSDSYD--DEVPDSVRQPQPDEFNFSEVFVHQMIHAIEFVLGSVSNTASYLRLWALSL
S._lycopersicum_(Solyc06g075400.2) VPWMLFPKPFILKRLHMERFQGRTYGILGTSEMGID--DQPDSARE-RAEEFNFSEVFVHQMIHSIEFVLGAVSNTASYLRLWALSL
S._tuberosum_(PGSC0003DMG400025375) VPWMLFPKPFILKRLHTERFQGGTYGLLGTSEVDIY--EEPDSARQHHHEEFNFSEVFVHQMIHSIEFVLGAVSNTASYLRLWALSL
G._max_(Glyma.12G072700)_1 VPWMLFPKPFILKKLHNERFQGRTYGVLNNSEVDL--ELEPDSARQH-HEEFNFSEVFVHQMIHSIEFVLGSVSNTASYLRLWALSL
M._trancatula_(Medtr2g093210)_1 VPWMLFPKPFILKKLHTERFQGRSYGILNTSEMDL--EVEPDSAREH-HEDFNFSEIFVHQMIHSIEFVLGSVSNTASYLRLWALSL
P._vulgaris_(Phvul.005G137800)_1 VPWMLFPKPFILKKLHTERFQGRNYGLLNTSEVDI--EAEPDSARQHHHEEFNFSEVFVHQMIHAIEFVLGSVSNTASYLRLWALSL
L._usitatissimum_(Lus10018129.g) VPWMLFPKPFILKKLHTERFQGRTYGMLGTSEIDLDSE--PDSARAVHHEDFNFSEVFVHQMIHSIEFVLGAVSNTASYLRLWALSL
E._grandis_(Eucgr.B02458) VPWMLFPKPFILKKLHSERFQGRTYQMLGTSEMDIDGDTEPDSAR-QHHEEFNFSEVFVHQMIHSIEFVLGAVSNTASYLRLWALSL
M._esculenta_(Manes.11G140100) VPWMLFPKPFILKKLHTERFQGRTYGILGTSEMEL--DMEPGSAR-SHHEDFNFSEVFVHQMIHSIEFVLGAVSNTASYLRLWALSL
R._communis_(29688.t000006) VPWMLFPKPFILKKLNTERFQGRTYGLLGTSEVDL--DMEPGSAR-SHHDDFNFSEVFVHQMIHSIEFVLGAVSNTASYLRLWALSL
M._acuminata_(GSMUA_Achr7G22660_001) VPWMLFPKPFILRKLHTERFQGRTYGILGTSEMDVDHDPDSAR-R-QHHEDFNFSEVFVHQMIHSIEFVLGAVSNTASYLRLWALSL
C._sativus_(Cucsa.052610) VPWMLFPKPFILKKMHTERFQGRTYGMLGTSEIDL--EVEPDSAR-QHQEDFNFSEIFVHQMIHSIEFVLGAVSNTASYLRLWALSL
G._raimondii_(Gorai.004G012600)_1 VPWMLFPKPFILKKLHSERFQGRTYGLLGSSEFDL--DVEPDSAR-DHHEEFNFSEVFVHQMIHSIEFVLGAVSNTASYLRLWALSL
T._cacao_(Thecc1EG041113)_4 VPWMLFPKPFILKKLHSERFQGRTYGMLGTSEFDL--DVEPDSAR-QHHEEFNFSEVFVHQMIHSIEFVLGAVSNTASYLRLWALSL
C._sinensis_(orange1.1g003454m.g)_1 VPWMLFPKPFILRKLHTERFQGRTYGILGTSEMDL--EVEPDSAR-QHHEDFNFSEIFVHQMIHSIEFVLGAVSNTASYLRLWALSL
V._vinifera_(GSVIVG01025116001) VPWMLFPKPFILKKLHSERFQGRAYGILGTSEMDL--EVEPDSAR-QHHEEFNFSEIFVHQMIHSIEFVLGAVSNTASYLRLWALSL
T._aestivum_(Traes_3AL_EAFA14B6D)_1 VPWMLFPKPFILKKLHKERFQGHSYRFLGTSEMDPDSEPDSARS---RHDDFNFGEVFVHQMIHSIEFVLGAVSNTASYLRLWALSL
O._sativa_(LOC_Os01g61780) VPWMLFPKPFILKKLHKERFQGHTYRFLGTSEMDPDSEPDSARS---RHDDFNFSEVFVHQMIHSIEFVLGAVSNTASYLRLWALSL
B._distachyon_(Bradi2g54190)_1 VPWMLFPKPFILKKLHKERFQGHTYRFLGTSEMDPDSEPDSARA---RHDDFNFSEVFVHQMIHSIEFVLGAVSNTASYLRLWALSL
B._stacei_(Brast01G098000) VPWMLFPKPFILKKLHKERFQGHTYRFLGTSEMDPDSEPDSARA---RHDDFNFSEVFVHQMIHSIEFVLGAVSNTASYLRLWALSL
S._bicolor_(Sobic.003G346400) VPWMLFPKPFILKKLHKERFQGHTYRFLGTSEMDPDSEPDSARA---RHDDFNFSEVFVHQMIHSIEFVLGAVSNTASYLRLWALSL
S._italica_(Seita.5G371100) VPWMLFPKPFILKKLHKERFQGHTYRFLGTSEMDPDSEPDSARA---RHDDFNFSEVFVHQMIHSIEFVLGAVSNTASYLRLWALSL
P._virgatum_(Pavir.Eb03637) VPWMLFPKPFILKKLHKERFQGHTYRFLGTSEMDPDSEPDSARA---RHDDFNFGEVFVHQMIHSIEFVLGAVSNTASYLRLWALSL
A._trichopoda_(evm_27.TU.AmTr_v1.0_scaffold00080.37) VPWMLFPKPFILRKLHTERFQGRTYGILGTSELDFDSEPDSARSV-RQHEEFNFSEVFVHQMIHSIEFVLGSVSNTASYLRLWALSL
P._taeda_(5A_115_VO_L_1_T_29156/41278) VPWMLLPKPLILRKQHRQRLQGRSYGILGNSDTDSLE---MEHDFDSGYEEFDFSEIFVHQMIHTIEFVLGAVSNTASYLRLWALSL

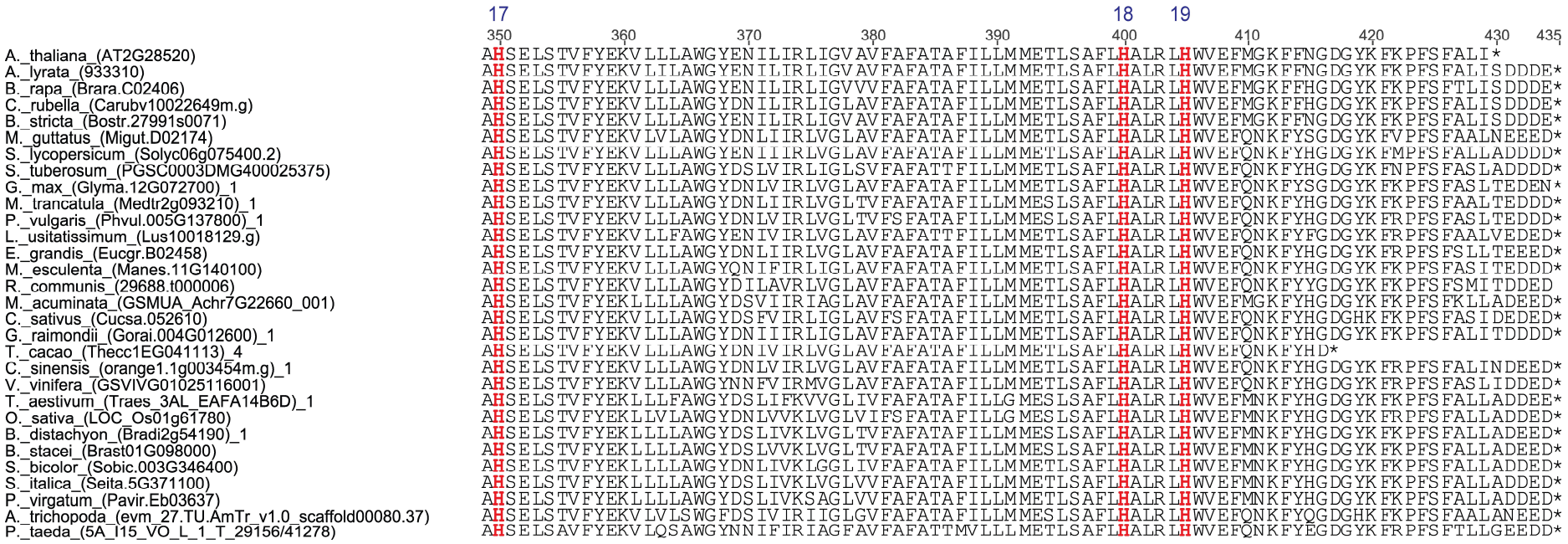

Figure S3. An alignment of C-terminal sequences from selected species from the VHA-a1 clade

Histidines are depicted in red. Only histidines that appear in *Arabidopsis* VHA-a1 were considered. The sequence numbers in blue are in reference to the position of the histidines in the alignment between *A. thaliana* VHA-a1 and *M. musculus* subunit a2 **(Figure 6)**. All the histidines in the C-terminal domain of AtVHA-a1 are conserved with the exception of H494(3), H696(13) and H697(14).

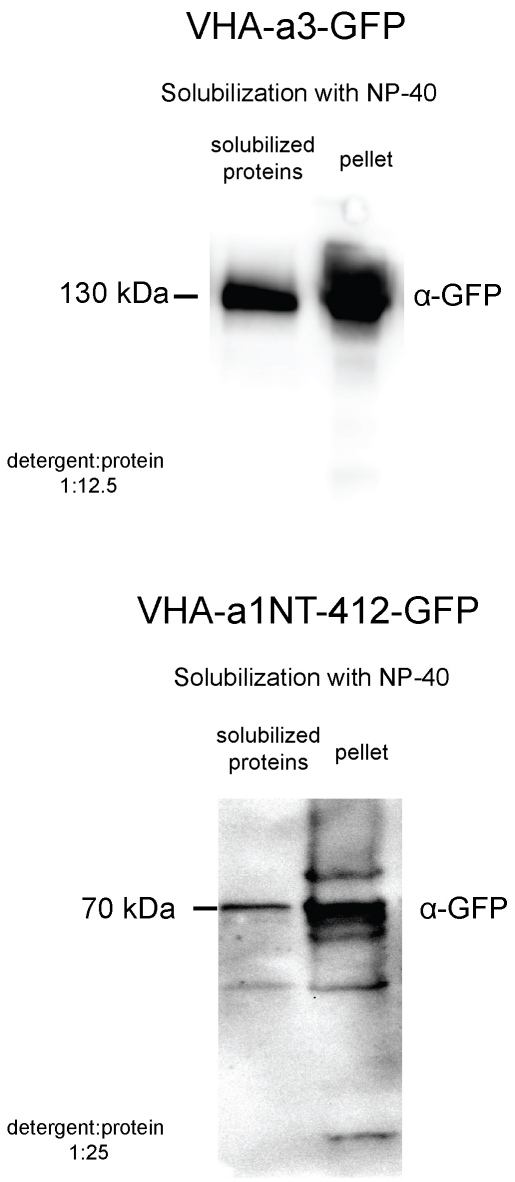

Figure S4. Solubilization of membrane proteins with NP-40.

Membrane proteins were solubilized from microsomal membranes with NP-40 detergent using the indicated detergent to protein ratios. A total of 100 and 600 µg of protein (microsomal membranes) were used for solubilization of VHA-a3-GFP and VHA-a1NT412-GFP respectively.

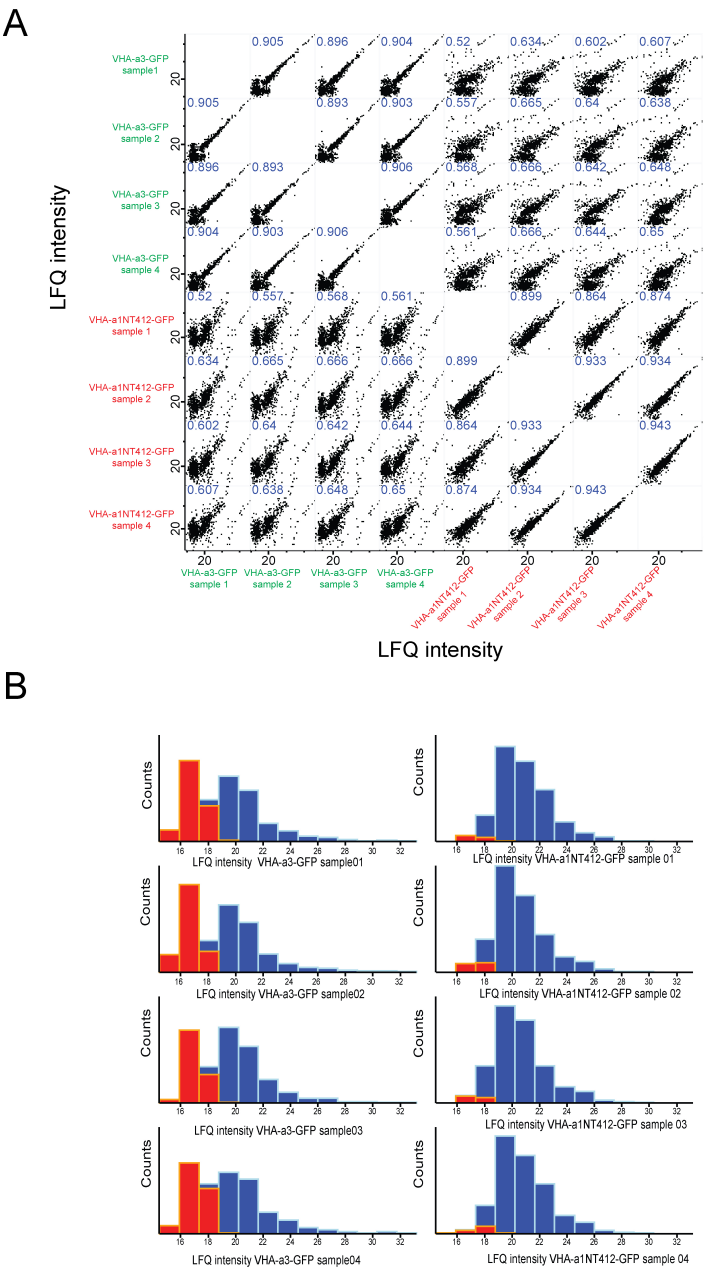

Figure S5. Mass spectrometry data quality

(A) LFQ-intensity correlations of the four technical replicates of VHA-a3-GFP and VHA-a1NT412-GFP samples. Log_2 (LFQ intensity) is plotted after imputation of missing values. The diagram shows there is a high correlation among the technical replicates. Light blue numbers represent the Pearson's correlation values for each dot-plot. **(B)** Histogram plots of LFQ intensities for each sample. In blue are the intensity distributions before imputation of missing values. The plots show that the intensities are more or less normally distributed. In red are the distributions of the imputed values.

Table S2: Potential VHA-a1NT interaction partners

Proteins are listed according to their gene ontology (GO) annotations. VHA-a1 is included for comparison purposes.

No	Protein name	Gene name	-Log (P-value)	Log_2 Difference (experiment-control)	Protein IDs
	Enzyme modulator				
1	Arf C1	*Arf C1*	3.044339409	1.682935	Q9LIK1
2	Arf 2-A;2-B, 1	*Arf 2-A, 2-B,1*	1.107875224	0.295967	*Q9M1P5;Q6ID97;Q9LYJ3;Q9LQC8;P36397;P0DH91
3	GTP-binding nuclear protein Ran-1;GTP-binding nuclear protein Ran-3;GTP-binding nuclear protein Ran-2	*RAN1; RAN3; RAN2*	2.815648956	1.648046	P41916;Q8H156;P41917
4	Protein ROOT HAIR DEFECTIVE 3	*RHD3*	3.70771235	1.313676	P93042
5	Ras-related protein RABB1b	*RABB1B*	2.342522621	0.607552	Q38922
6	Ras-related protein RABD2b;Ras-related protein RABD2c	*RABD2B;RABD2C*	2.393771617	0.575064	Q9FPJ4;Q9SEH3;P28188
7	Ras-related protein RABE1c	*RABE1C*	1.295116707	0.533969	P28186
8	Ras-related protein RABA2a	*RABA2A*	1.469821013	0.476317	O04486
9	Ras-related protein RABB1c	*RABB1C*	1.147432382	0.326992	P92963; O23561
	Membrane traffic				
10	Dynamin-related protein 3A	*DRP3A*	2.387015929	3.562909	F4JJ15;Q8S944
11	Protein transport protein SEC31 homolog B	At3g63460	5.328630169	3.071909	F4J109;Q8L611;F4J110
12	Clathrin heavy chain 2	*CHC2*	1.688390484	2.5699	Q0WLB5
13	Trafficking protein particle complex II-specific subunit 130 homolog	*TRS130*	3.917011824	2.415949	F4K0C4
14	Vesicle-associated protein 1-1, N-terminally processed	*PVA11*	1.127213177	2.363873	Q8VZ95
15	SNARE-like superfamily protein	AT1G51160	2.217348625	2.321127	Q9SYB8
16	Trafficking protein particle complex II-specific subunit 120 homolog	*TRS120*	2.967025603	2.26202	Q9FY61
17	Vacuolar protein sorting-associated protein 26B	*VPS26B*	1.527829079	1.154666	F4JJR0;Q9T091;Q9FJD0
18	Clathrin heavy chain 1	*CHC1*	3.051384251	1.098716	Q0WNJ6
19	Vesicle-associated protein 1-2; N-terminally processed	*PVA12*	2.005545876	1.072913	Q9SHC8
20	Vesicle-associated membrane protein 711	*VAMP711*	2.555951435	1.06858	O49377

21	Vacuolar protein-sorting-associated protein 33 homolog	*ATVPS33;VPS33*	2.237064317	1.856566	F4JE40; Q94KJ7
22	Zinc ion binding protein	At1g12470	2.505348152	1.699886	F4IDS7
23	Coatomer subunit alpha-2	At2g21390	3.89348188	1.680211	Q9SJT9
24	Coatomer subunit gamma		2.235626761	1.210904	Q0WW26
25	Vessicle transport	At5g54750	1.497509607	2.02157	Q9FFV2; F4K1U5
26	SNARE-like protein		1.900032	2.18061	F4HTY0
27	Transmembrane 9 superfamily member 9 and 8	At5g25100	3.101037949	2.758275	F4KIM7;Q9C5N2;F4KIB2
	Transport				
28	Mechanosensitive ion channel protein 9	*MSL9*	3.607246628	4.088155	Q84M97
29	V-type proton ATPase subunit a1	*VHA-a1*	5.333889442	5.103902	Q8RWZ7
	Lipid binding				
30	Calcium-dependent phospholipid binding protein	At4g34150	1.946937249	2.469962	Q945K9
31	Membrane steroid-binding protein 2	*MSBP2*	2.695413401	2.378972	Q9M2Z4
32	MLP-like protein 28	*MLP28*	2.566157565	1.048123	Q9SSK9;A8MR6; B3H4F3;A8MRH; F4I6Y3
	Kinase				
33	PTI1-like tyrosine-protein kinase 1	*PTI11*	2.942008366	0.644911	Q8H1G6
	Uncharacterized				
34	Uncharacterized protein	At1g27020	3.753251081	3.941407	O04551
35	Uncharacterized protein	At5g58030	3.753459799	3.204395	Q9FGU1
36	Uncharacterized protein	At1g71500	2.412377419	3.180191	Q9C9I7
37	Uncharacterized protein	At4g39820	2.808360079	2.778302	Q5XF35
38	Uncharacterized protein	At2g32240	1.553939631	2.738505	F4ISU2
39	Uncharacterized protein	At4g34180	3.601555059	2.583998	Q93V74
40	Uncharacterized protein	At3g17900	2.298927086	2.458985	Q9ASZ4
41	Uncharacterized protein	At4g12590	1.273011745	2.339843	Q9SU27
42	Uncharacterized protein	At2g44060	1.070065452	2.326069	O80576
43	Uncharacterized protein	At2g47960	1.37548724	2.235386	O82263
44	Uncharacterized protein	At5g62200	0.96392666	2.215509	Q6NPM5
45	Uncharacterized protein	AT5g11680	2.037871401	2.156443	Q9LYG2
46	Uncharacterized protein	At5g65950	4.195553539	1.719878	F4JXM9
47	Uncharacterized protein	AT5g08060	1.49938357	1.560574	Q9SD78
48	Uncharacterized protein	At5g11560	2.691286103	0.907655	F4JXW9
49	Tetratricopeptide repeat (TPR)-like superfamily protein	At5g16280	2.362014137	2.170833	F4KCQ9;F4KCR0

***** A protein has several UniProt identifiers if the detected peptides do not allow distinguishing between these identifiers.

Materials and Methods

Plant material and growth conditions

Arabidopsis thaliana, Columbia 0 (Col-0) ecotype was used in all experiments in this study. The VHA-a3-GFP expressing line was established by Dettmer et al., 2006.

Growth of *Arabidopsis* seedlings for confocal microscopy was performed on plates. The standard growth medium used contained 1/2 Murashige and Skoog (MS), 0.5% sucrose, 0.5% phyto agar, and 10mM MES, and the pH was set to 5.8 using KOH. Agar and MS basal salt mixture were purchased from Duchefa. Seeds were surface sterilized with ethanol and stratified for 48h at 4°C. Plants were grown in long day conditions (LD) (16 h light/8 h dark) for 6 days.

For the rosette phenotype assays, seeds were stratified for 48 h at 4°C and then placed on soil. Seedlings were transferred to individual pots at 7 days after germination (DAG). Plants were grown in LD conditions.

Etiolated seedlings were grown on vertical plates with medium containing 1/2 MS, 0.5% sucrose, 0.7% phyto agar, and 10mM MES, and the pH was set to 5.8 using KOH. After seed sterilization and stratification, plates were exposed to light for 4 h, wrapped in two layers of aluminium foil and then kept at 22°C for 4 days.

Nicotiana benthamiana plants for infiltration experiments were cultivated in LD conditions at 28°C.

Construct preparation

Dexamethasone inducible VHA-a N-termini

VHA-a1 and *VHA-a3* N-termini cDNA sequences were amplified from pJET+a1 and a3+pBluscript plasmids respectively. *VHA-a3NT-a1D* was amplified from pVHA-a3-a1D-GFP created in chapter 1. The primers used are listed in **Table 1**. The primers contained *Eco31I* sites to allow the Greengate system to be used. PCR products were blunt end cloned into the pJET1.2 vector. The sequences were verified by sequencing which was performed by Eurofins. Verified clones were digested using *BglII* to release the PCR fragments. Digested fragments were purified using the Qiagen kit. Two Greengate reactions were performed to create two intermediate vectors that were later combined on one T-DNA. The first intermediate vector consisted of 6 entry modules (pGGM000 empty vector, pGGA006:UBQ10; pGGB003 N-terminal-decoy; LhG4-GR; C-terminal-decoy; pGGE001:RBCS terminator and the FH adapter). The second intermediate vector consisted of 6 entry modules (pGGN000 empty vector, pGGA016: pOP6, *VHA-a-NT* purified fragment, pGGD001: linker-GFP or pGGD: linker-mVenus, pGGE001:rbcS, pGGF005: hygromycin B resistance cassette and the HA adapter). The two intermediate vectors were combined on one final destination vector, pGGZ003.

To create a non DEX inducible version of VHA-a3NT, a Greengate reaction was performed using the following modules: pGGA006: UBQ10 promoter, pGGD001: linker-GFP, pGGE001: rbcS terminator, pGGF001: Basta resistance cassette and the destination vector pGGZ001.

Table 1. Primers used to amplify the different *VHA-a* N-termini

No	PCR fragment	5' to 3'	Sequence
1	*VHA-a1NT198*	Forward	GAT CGG TCT CGG GCT CAA CAA TGG AGG AAT TCT TAG ATA A
		Reverse	AAC AGG TCT CAC TGA GTT GAT GAT TCC ACT AAT AA
2	*VHA-a1NT412*	Forward	GAT CGG TCT CGG GCT CAA CAA TGG AGG AAT TCT TAG ATA A
		Reverse	AAC AGG TCT CTC TGA AGG GTT TGC CTC TTG ATA TC
3	*VHA-a3NT412*	Forward	TAT GGT CTC AGG CTC AAC AAT GGC GGA AAG TGG CGG TGG
		Reverse	AAC AGG TCT CTC TGA TGG ATT GGC TTC CTG ATA CT
4	*VHA-a3NT-a1D*	Forward	TAT GGT CTC AGG CTC AAC AAT GGC GGA AAG TGG CGG TGG
		Reverse	AAC AGG TCT CTC TGA TGG ATT GGC TTC CTG ATA CT

Arabidopsis transformation

5 µl of the Greengate ligation reaction was transformed into DH5α cells and plated on LB plates containing spectinomycin for selection of correct plasmids. Colony PCR was performed to pre-screen colonies. Overnight cultures of positive clones were made. Mini preps of cultured bacteria were done with the Qiagen kit. Preped plasmids were test digested and correct binary plasmids were transformed into *A. tumefaciens* strain ASE1(pSOUP^{+}) and selected on 100 µg/ml spectinomycin, 5 µg/ml tetracycline (for pSOUP), 25 µg/ml chloramphenicol and 50 µg/ml kanamycin. *Arabidopsis* plants were transformed by the floral dip method as outlined by (Clough and Bent, 1998) and transgenic plants were selected on MS plates containing appropriate antibiotics

Transient expression in *N. benthamiana*

Transient in planta protein expression was performed in *N. benthamiana* leaves that were infiltrated with *the A. tumefaciens* strain ASE1(pSOUP^{+}) habouring plasmids of interest. An *A. tumefaciens* strain GV3101 pMP90 carrying the 19K plasmid to suppresses posttranscriptional gene silencing and therefore increase transformation efficiency was co-infiltrated. Leaves were analyzed by confocal microscopy 3 to 4 days after infiltration.

Preparation of microsomal membranes

Etiolated seedlings were prepared and microsomal membranes were isolated with extraction buffer that contained 50 mM Tris-HCL pH 8, 50 mM NaCl, 10% (vol/vol) Glycerol, 1x complete protease inhibitor cocktail (Roche). Seedlings were ground in extraction buffer. The homogenate was filtered through two layers of miracloth and centrifuged at 10,000 g for 10 min at 4°C. The supernatant was filtered through miracloth again and then centrifuged at 150,000 g for 30 min at 4°C. The microsomal membrane pellet was resuspended in extraction buffer. Protein concentrations were determined as reported previously (Bradford, 1976) and aliquots were stored at -80˚C.

Co-immunopreciptiation

Proteins were solubilized from membranes using an extraction buffer that contained 50 mM Tris-HCL pH8, 50 mM NaCl, 10% (vol/vol) Glycerol, 1x complete protease inhibitor cocktail (Roche) and NP-40 detergent. Protein to detergent ratios of 1:25 for VHA-a1NT412-GFP and 1:12.5 for VHA-a3-GFP were used. The protein amounts used for solubilization were, 100 µg and 600 µg for VHA-a3-GFP and VHA-a1NT412-GFP samples respectively. Microsomal membrane preparations were incubated for 1 h at 4°C with NP-40. Solubilized proteins were separated from non-solubilized proteins by centrifugation at 150.000 *g* for 30 min. The supernatant was loaded on GFP-Trap® coupled to agarose beads (ChromoTek GmbH, München, Germany) and incubated for 4h at 4°C on a roller table. Beads were washed three times with extraction buffer and

then proteins were eluted with SDS-(4 % SDS, 140 mM Tris-HCl pH 6.8, 20 % Glycerol, 0.01 % Bromophenol blue, 10 % ß-Mercaptoethanol) at 50°C for 5 min.

SDS-PAGE and immunoblotting analysis

SDS-PAGE and immunoblotting were performed to determine protein levels in tonoplast membrane extracts. After electrophoresis, proteins were transferred to a nitrocellulose membrane (Whatman). The following primary antibodies were used: a GFP antibody (1:5000), cFBPase antibody (Agrisera, 1:5000) and an Arf1 antibody (1:5000). Antigen on the membrane was detected with horseradish peroxidase-coupled anti-rabbit IgG (Promega) and chemiluminescent substrate (Peqlab). Detection was carried out using a cooled CCD camera system (Intas *ADVANCED* Fluoreszenz u. ECL Imager).

Mass spectrometry analysis

Sample preparation for MS analysis of four technical replicates for each experimental condition was performed by the core facility for mass spectrometry & proteomics (CFMP) at the ZMBH. A Label-free quantification (LFQ) approach was undertaken using the MaxQuant platform (Cox et al., 2014). All MS data processing in MaxQuant was performed by CFMP.

Protein lists generated by MaxQuant were further analyzed by Perseus (version 1.5.4.41)(Tyanova et al., 2016). Contaminants were filtered out and all the LFQ intensities were log2 transformed. Scatter plots were generated for each experimental condition to compare the differences between replicates and to compute Pearson correlation coefficients.

The data was filtered to require three valid values across all samples and empty values were imputed with random numbers from a normal distribution, whose mean and SD were chosen to simulate low abundance values close to noise level

(imputation criteria: width 0.3, downshift 1.8). A modified t-test with permutation-based FDR statistics was applied (250 permutations; FDR 0.05; S0 0.1).
Volcano plots to demonstrate significant changes in protein abundance between the control and experiment were created by plotting the -log of the p-values obtained from the two sample t-tests against the differences between the log2 transformed LFQ means. For heat maps, the log2 ratios of LFQ intensities were plotted by hierarchical clustering to compare the technical replicates.

The proteins identified to be significantly more abundant in the VHA-a1NT412-GFP samples after imputation were classified according to protein class using the PANTHER classification system (Mi et al., 2016).

Confocal microscopy

Confocal laser scanning microscopy was performed using a Leica TCS SP5II microscope equipped with a Leica HCX PL APO lambda blue 63.0x 1.20 UV water immersion objective. GFP was excited at 488 nm with a VIS-argon laser and fluorescence emission was detected between 500 and 555 nm. mRFP was excited at 561 nm with a VIS-DPSS 561 laser diode and fluorescence emission was detected between 615 and 676 nm. mVenus was excited using the 514 line of the argon laser and fluorescence emission was detected between 540 and 585 nm. The imaging parameters were as follows: image dimension: 512 X 512, pinhole: 1 airy unit, line average: 5. For image acquisition, the Leica Application Suite Advanced Fluorescence software was used. Processing of images was performed using Fiji (based on ImageJ 1.47t).

Pharmacological Treatments

Dexamethasone was purchased from Sigma, dissolved in DMSO and stored as 30 mM working aliquots at -20°C.

Etiolated seedlings were prepared on plates containing 1/2 MS medium with 0.5% sucrose, 0.7% phyto agar and pH 5.8, 60 µM DEX, or the equivalent amount of DMSO in control samples.

For the rosette phenotype assays, seedlings were transferred to individual pots at 7 days after germination (DAG). Induction with 60 µM DEX was performed twice by spraying at 13 and 18 days after germination.

Imaging

Pictures of rosettes for the soil phenotype assays and plates for the hypocotyl length measurements were taken using a Nikon D60 digital camera. Images were processed using Adobe Photoshop (Cloud).

Homology modelling of the VHA-a C-termini

3D models of the VHA-a1, *M. musculus* subunit a2 and VHA-a3 C-termini were obtained through homology modelling using the yeast model of Vph1p (PDB: 5TJ5) as a template. Homology modelling was performed according to (Roy et al., 2010)

Chapter 3

Regulation of the plant V-ATPase by S-acylation

Scientific aim

The function of the S-acylation of the V-ATPase subunit, VHA-a3, has not been determined and this chapter thus aimed:

1. To determine the function of the S-acylation of VHA-a3 in *A. thaliana*

Abstract

The vacuolar H^+-ATPases (V-ATPases) are multisubunit complexes that are responsible for the acidification of various cellular compartments in all eukaryotic cells. We have discovered a new form of modification of this highly conserved eukaryotic protein pump that is unique to plants. We show that the tonoplast localized isoform (VHA-a3) and not the endosomal localized isoform (VHA-a1) is S-acylated. Two cysteine residues found in the N-terminus of all plant VHA-a3-related sequences are the site of the S-acylation in VHA-a3. We show that S-acylation is not involved in targeting of VHA-a3 to the tonoplast and that V-ATPase activity is not compromised by a lack of S-acylation in standard growth conditions, in reduced day length conditions and in the presence of high concentrations of zinc. Furthermore, we show that a mutant form of VHA-a3 (VHA-a3 R729N), whose exit from the Endoplasmic reticulum (ER) is compromised, is less S-acylated. This implies that the site of S-acylation of VHA-a3 in the cell is the tonoplast. However, we show that the two tonoplast localized protein S-acyl transferases (PATs) are not responsible for S-acylation of VHA-a3. The study provides the first insights into the function of this new form of modification in the regulation of the V-ATPase at the tonoplast.

Introduction

S-acylation in plants: Occurrence

Amino acids which are the building blocks of proteins have many side chains which can be modified by an array of biochemical reactions. One form of protein modification is protein lipidation. Protein lipidation describes the addition of any form of a hydrophobic moieties to a protein (Hemsley, 2015). The hydrophobic moieties come in different forms (**Table 1**) and each imparts unique properties to the protein and its immediate micro environment (Hemsley, 2015). These properties clearly include an increase in the proteins hydrophobicity which facilitates its interaction with the inner core of the phospholipid bilayer of membranes which is hydrophobic in nature (Alberts,et al., 2002).Consequently protein lipidation has been shown to regulate intracellular trafficking, subcellular localization, protein-protein and protein-lipid interactions (Resh, 2016).

S-acylation also known as palmitoylation is one of the protein lipid modifications that has gained interest in the plant field after it was shown to be more prevalent in plants than any other form of protein lipid modification (Hemsley et al., 2013). This form of protein lipid modification has been more extensively studied in mammalian cells than in plant cells (Resh, 2016; Greaves and Chamberlain, 2010). S-acylation occurs post-translationally and affects proteins involved in diverse cellular processes from receptor kinases to membrane integral transporters (Hemsley et al., 2013). It occurs on soluble and integral membrane proteins and involves the conjugation of saturated fatty acids, usually palmitate or stearate to a cysteine residue of a protein through a thioester bond (Greaves and Chamberlain, 2010).

The lack of a consensus sequence for S-acylation makes prediction of S-acylation targets very difficult. However, several prediction programs do exist but all predictions have to be experimentally verified (Ren et al., 2008). In vitro and in vivo techniques have been developed to detect protein lipidation. In vivo

methods from the animal field include cell culture with azido-fatty acids as probes for protein myristoylation and/or palmitoylation (Chan et al., 2010). The disadvantages of these methods are that they require cell culture, they use non-natural lipids and introduce an element of toxicity to the cells (Hemsley, 2013).

Table 1. Different forms of protein lipidation reported in plants.

Lipid modification	Lipid moiety added	Example in plants	Reference
S-acylation	Saturated fatty acids: Palmitate or Stearate	Cellulose synthase A subunits of the cellulose synthase complex (CSC)	(Kumar et al., 2016)
N- myristoylation	14 carbon Myristol chain	Calcineurin B–like proteins (CBLs)	(Batistic et al., 2008)
Prenylation: Farnesylation and Geranylgeranylation	Polyisoprene lipids	Adenosine phosphate-isopentenyl-transferase 3 (AtIPT3) involved in cytokinin biosynthesis	(Galichet et al., 2008)
Glycosylphosphatidyl inositol (GPI) anchor and Glycosylinositolphos phorylceramide (GIPC) anchor	Glycolipids	Plasmodesmata callose binding proteins (PDCBs)	(Simpson et al., 2009)

A proteomics study identified approximately 500 proteins to be S-acylated in plants (Hemsley et al., 2013). Interestingly, one of these was VHA-a3, a subunit of the V-ATPase. The vacuolar H^+-ATPases (V-ATPases) are multisubunit complexes that are responsible for the acidification of various cellular compartments in all eukaryotic cells(Nishi and Forgac, 2002). They are multisubunit enzymes that consist of a membrane integral V_O subcomplex and a membrane peripheral V_1 subcomplex. ATP hydrolysis occurs on catalytic subunits of the V_1 subcomplex which drives the translocation of protons through the V_O subcomplex (Nishi and Forgac, 2002). Subunit a of the V_O subcomplex controls coupling of ATP hydrolysis to proton translocation as well as targeting of the complex in the cell (Kawasaki-Nishi et al., 2001; Dettmer et al., 2006). *A.*

thaliana has three isoforms of subunit a, VHA-a1, VHA-a2 and VHA-a3. VHA-a1 targets the V-ATPase to the TGN whilst VHA-a2 and VHA-a3 target it to the limiting membrane of the vacuole (tonoplast) (Dettmer et al., 2006).
The S-acylation of VHA-a3 was experimentally verified using a robust in vitro method called the biotin switch assay (BSA) which has been adapted to detect S-acylation of plant proteins (Hemsley, 2013; Forrester et al., 2009). In this method, total proteins are extracted from any tissue in the plant in the absence of reducing agents. Free cysteines are blocked with the thiol reactive reagent N-ethylmaleimide (NEM). Hydroxylamine is then used to cleave all S-acyl groups. The generated free thiols are then labelled with thiol reactive biotin. The degree of biotinylation (and hence S-acylation) is determined by neutravidin pull down followed by immunoblotting for the protein(s) of interest. Using the biotin switch assay, it was confirmed that VHA-a3 is indeed S-acylated whereas the TGN localized isoform VHA-a1 is not (Fink, 2012). This has instigated investigations into what could be the possible function of the S-acylation of the VHA-a3 isoform.

S-acylation in plants function and regulation

In the context of the V-ATPase, one can speculate about the possible functions of S-acylation of VHA-a3. Three possibilities seem plausible. First, it could be the sorting signal in VHA-a3 that targets the V-ATPase to the tonoplast. S-acylation has been shown to change a proteins subcellular localization. This is finely illustrated by the Rho GTPases of plants (ROPs). ROPs belong to the Ras super family of small GTP-binding proteins and are involved in various signaling pathways in the cell (Berken and Wittinghofer, 2008). They are classified as Type-I or Type-II depending on sequences in their C-terminal domain (Berken and Wittinghofer, 2008). Type-II ROPS are S-acylated on their C-terminus which facilitates their attachment to the plasma membrane where they perform their function (Lavy and Yalovsky, 2006). On the other hand for Type-I ROPs, the S-acylation status changes depending on the active state. The inactive GDP bound form is only geranylgeranylated which tethers it to the plasma membrane. In the

GTP bound active form, they are geranylgeranylated and S-acylated (Sorek et al., 2007).
Secondly, S-acylation is reversible, it could be a molecular switch that transforms the activity of the V-ATPase from active to inactive states. Finally, S-acylation could be used to move the V-ATPase to different domains within the membrane. This is true for Type-I ROPs where S-acylation was shown to act as a regulatory mechanism to move active or inactive Type-I ROP between detergent resistant and soluble membrane fractions rather than providing attachment to the membrane (Sorek et al., 2011).

Double lipid modifications such as those of the Type-I ROPs is a recurring theme in the plant proteome that applies to several other plant proteins such as calcineurin B–like protein 1 (CBL1) that is dually myristoylated and S-acylated (Batistic et al., 2008).This dual modification of a protein with different forms of lipid modifications is due to another important attribute of S-acylation. It is stable. It has a membrane affinity half life which is longer than that of myrisotoylation and prenylation (Shahinian and Silvius, 1995). Another important factor is that, the protein S-acyl transferases (PATs)that are responsible for catalyzing the S-acylation reaction are membrane bound only (Batistic, 2012). Therefore soluble proteins need to be recruited to the membrane to be S-acylated even if it is by weak membrane anchors such as N-myristoylation or farnesylation (Hemsley, 2015).

Arabidopsis has 25 PATs (AtPATs) which are localized mainly at the plasma membrane and to other endomembranes in the cell excluding those of the mitochondria and chloroplasts (Batistic, 2012) (**Figure 1**). PATs are multiple membrane spanning proteins and possess a DHHC-CRD domain (Asp-His-His-Cys within a Cys-rich domain) which is the active site (Greaves and Chamberlain, 2010). The existence of a large number of AtPATs is believed to stem from the fact there is no consensus sequence for modification by the PAT enzymes and therefore a large number of PATs are required to cater to the multitude of S-acylation sites found on different proteins. In addition, the requirement that

substrates to be S-acylated must be recruited to membranes means that different PATs with different adaptations to different membranes and microdomain environments must be present in the cell (Hemsley, 2015). Of all the known AtPATs, only three have been fully characterized. The homozygous mutants of PATs 10, 14 and 24 show pleiotropic phenotypesrelating to growth, development, and stress responses(Li et al., 2016; Qi et al., 2013; Zhou et al., 2013; Hemsley et al., 2005). The pleiotropic phenotypes indicate that they likely S-acylate a diverse range of proteins (Hemsley, 2015).

The only PATs that VHA-a3 containing V-ATPases come into contact with are Endoplasmic reticulum (ER) and tonoplast localized PATs. This is because VHA-a3 containing V-ATPases can be delivered directly from the ER to the vacuole via structures known as provacuoles (Viotti et al., 2013).Therefore, the ER and tonoplast localized PATs should be investigated to determine if they are responsible for the S-acylation of VHA-a3.

De-S-acylation is regulated by two distinct serine hydrolases; acyl protein thioesterases (APT) and palmitoyl protein thioesterases (PPT) (Hemsley, 2015). In mammals, APTs are cytosolic and PPTs are localised at the lysosomes (Hornemann, 2014). No APTs or PPTs have been characterized in plants but their existence is highly probable and their significance should be like in animals where it is clear that palmitoylation and depalmitoylation cycles are import for proper functioning of an S-acylated protein (Hornemann, 2014). Any interference to these cycles has detrimental effects. For example some human diseases such as schizophrenia have been linked to palmitoylation/depalmitoylation defects (Hornemann, 2014).

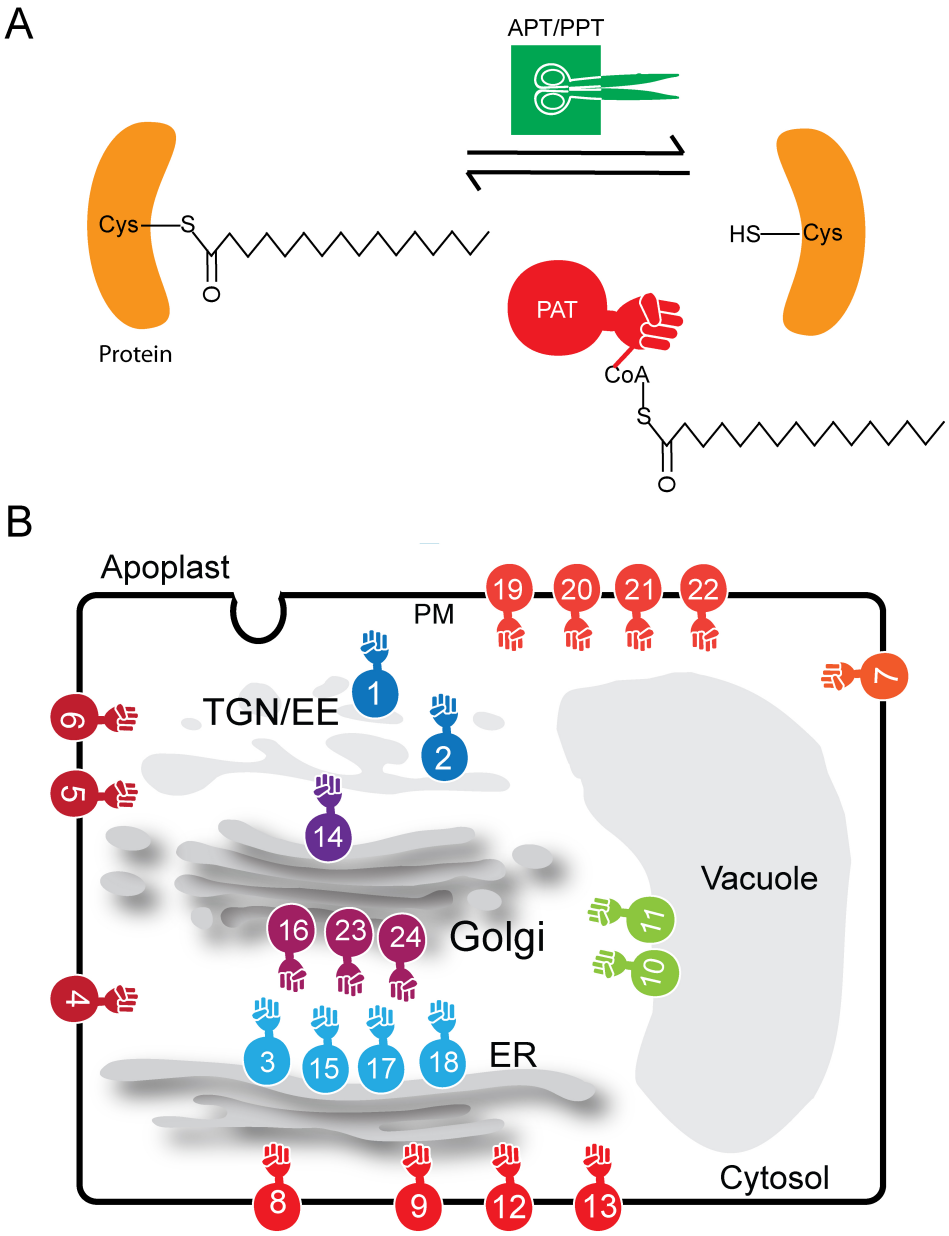

Figure 1: The localizations of the 24AtPATs (protein S-acyl transferases).

(A) The S-acylation reaction is catalyzed by PATs (16 carbon palmitate is shown). S-acylation is reversible. The acyl group is removed by serine hydrolases; acyl protein thioesterases (APT) and palmitoyl protein thioesterases (PPT). **(B)** The localization of AtPATs based on a study in tobacco cells (Batistic, 2012). The majority of AtPATs are plasma membrane localized. Two PATs are tonoplast localized, PAT10 and 11. It should be noted that PAT10 was also shown to have a Golgi localization. Of the four Golgi localized PATs, PAT14 was found to be located on the Trans side of the Golgi.

In this study, mutant forms of VHA-a3 were used to uncover the function of S-acylation of this vital subunit of the V-ATPase complex. A mutant form of VHA-a3 that cannot be S-acylated(VHA-a3SS) revealed that S-acylation is not involved in the targeting of the V-ATPase to the tonoplast and that S-acylation is also not important for sequestration of heavy metals into the vacuole. Another mutant form of VHA-a3 (VHA-a3 R729N), whose exit from the Endoplasmic reticulum (ER) is compromised, is less S-acylated. This implies that the site of S-acylation of VHA-a3 in the cell is the tonoplast. This study showcases the first attempts to determine the function of S-acylation of the tonoplast localized V-ATPase.

Results

S-acylation is not involved in targeting of the V-ATPase complex to the tonoplast

When the N-terminal sequences of VHA-a3 related proteins were examined, it could be seen that there were two cysteines and a string of glycines that are highly conserved (**Figure1**). We wondered if the site of S-acylation could be these two conserved cysteines. The two conserved cysteines were mutated to serines in VHA-a3 (VHA-a3SS: C10S + C11S) and the effect on S-acylation was determined using the biotin switch assay.

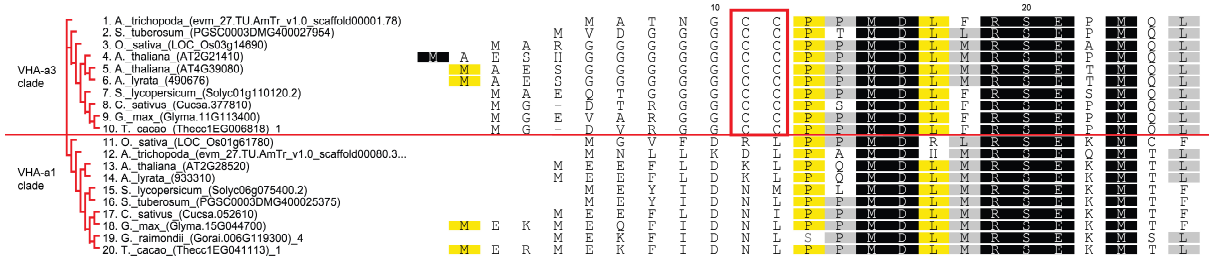

Figure1. Two cysteines are conserved in the N-terminus of VHA-a3-related sequences but are absent from VHA-a1 clade

Amino acid sequence alignment of representative sequences from the VHA-a1 and VHA-a3 clades. Residues similar between all proteins at the same position are shown against a black background. Residues similar in 18 or more sequences at the same position are shown against a yellow background. Residues similar in 14 or more sequences at the same position are shown against a grey background. Un-highlighted residues are variable in all sequences at the same position. The position of the conserved cysteines is indicated with a red box. Multiple sequence alignment was performed with Clustal omega (Sievers et al., 2011).

The mutations in VHA-a3 abolished S-acylation (**Figure2 A**). Therefore it could be concluded that the two cysteines are the site of S-acylation in VHA-a3 and quite possibly in the other VHA-a3 related sequences as well.

Protein modification by S-acylation has been shown to be responsible for the recruitment of cytosolic proteins to membranes (Lavy and Yalovsky, 2006) or to act as the targeting signal of a protein to target it to a specific membrane(Kumar et al., 2016). We examined if S-acylation of VHA-a3 was responsible for its trafficking and targeting to the tonoplast. VHA-a3SS was fused to GFP and the localization of the fusion protein was examined by CLSM in *Arabidopsis*. The localization VHA-a3SS-GFP was not different from that of VHA-a3-GFP (**Figure 2 B**). Furthermore, the introduction of the double cysteine motif into the N-terminus of VHA-a1 did not change its TGN localization nor was it sufficient to cause S-acylation of the chimeric protein **(Supplemental figure 6)**. Therefore it was concluded that the trafficking and tonoplast localization of VHA-a3 are independent of S-acylation.

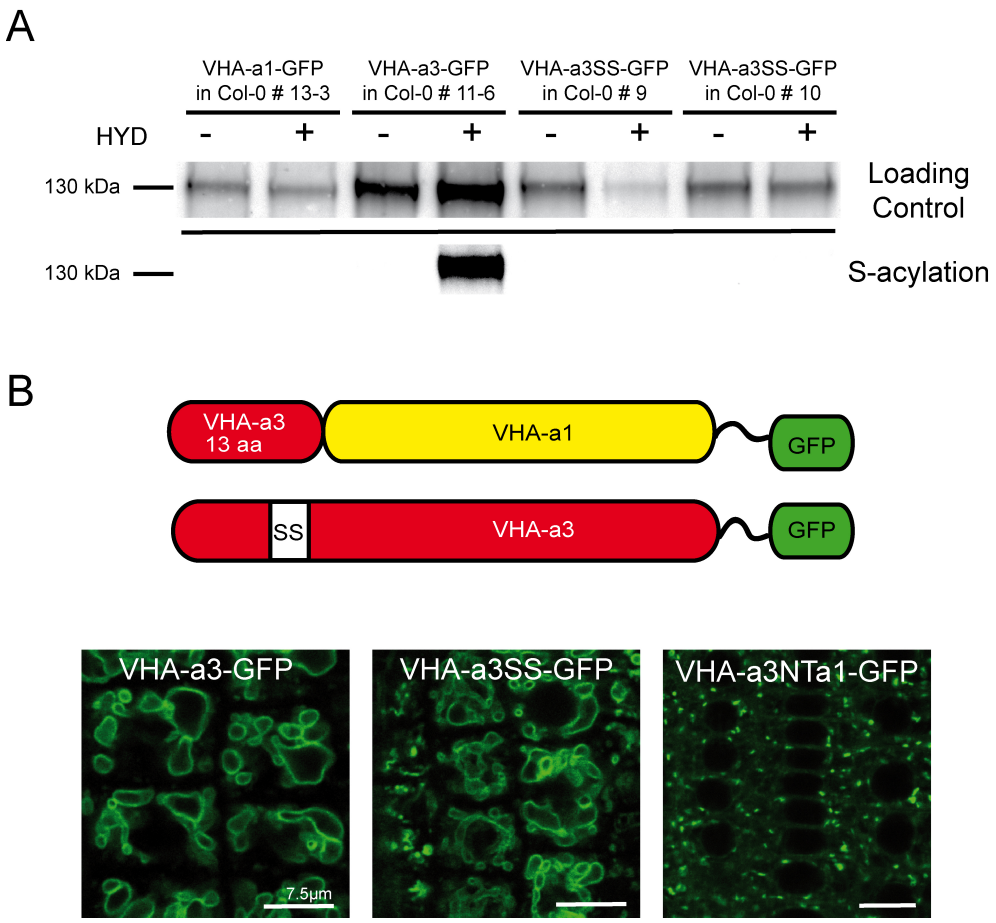

Figure 2. Two cysteines in the N-terminus of VHA-a3 are the site of S-acylation

(A). Cys 10 and 11 in the N-terminus of VHA-a3 were mutated to serines (VHA-a3SS). The effect of these mutations on S-acylation was determined by the biotin switch assay followed by immunoblotting with a GFP antibody using two independent lines. Total membranes were isolated from *Arabidopsis* plants expressing VHA-a3-GFP or VHA-a3SS-GFP. Free thiols were first blocked with NEM. Samples were then treated with (HYD+) or without (HYD-), the thioester cleavage reagent hydroxylamine. HYD+ and HYD- samples were treated with sulfhydryl reactive biotin and then combined with neutravidin beads which have a high affinity for biotin. The loading controls show that comparable amounts of protein were loaded onto neutravidin beads for each line. The row labelled 'S-acylation' shows the levels of VHA-a3-GFP and VHA-a3SS-GFP recovered from neutravidin beads, and therefore originally S-acylated. VHA-a3-GFP has a mass of approximately 130 kDa. The results indicate that VHA-a3 with the C10S and C11S mutations is no longer S-acylated. **(B)** The effect of removing the S-acylation on targeting was examined by CLSM. Non S-acylated VHA-a3SS-GFP still localized correctly to the tonoplast like VHA-a3-GFP. In addition, introducing the double cysteine motif into VHA-a1 (VHA-a3NTa1-GFP) did not change the TGN localization of VHA-1. Error bars= 10 µm unless otherwise indicated

The double cysteine motif and hence S-acylation is highly conserved in the VHA-a3 clade

In order to assess how prevalent S-acylation was in the plant kingdom; we collected additional VHA-a3 related sequences from higher plants, lower plants and algae. The presence of the double cysteine motif was used as an indicator of S-acylation and we aimed to determine the conservancy of the double cysteine motif and to possibly trace its phylogenetic origin. The sequences collected included predicted protein sequences as wells as cDNA sequences. The C-terminus of subunit a of the V-ATPase is considered to be more conserved in terms of amino acid sequence than the N-terminus (Kawasaki-Nishi et al., 2001). For this reason, and the fact that the double cysteine motif is found in the N-terminus of AtVHA-a3, phylogenetic analysis was performed on N-terminal sequences only (corresponding to the first 369 aa of AtVHA-a3). A total of 141 sequences were analyzed **(Supplemental figure 1)**.

In general all species possess several VHA-a3 related sequences which could represent different isoforms like VHA-a2 and VHA-a3 in *A. thaliana* (**Figure 3**). However, this has to be experimentally verified. Phylogenetic analysis of the collected sequences showed that the double cysteine motif is absent in the lower plants, charophyte and chlorophytes but it is highly conserved in the higher plants and it originated with the gymnosperms (**Figure 3 and 4**).

Figure 3. Phylogenetic analysis of the N-terminal sequences of VHA-a3 related proteins.

For each species all the VHA-a3 related protein sequences are shown. All sequences found for the chlorophytes, bryophytes, lycophytes were used for the analysis because it was not possible to classify them as VHA-a1-like or VHA-a3-like. Branch support is calculated on the basis of 500 bootstraps. The node values are shown. Tree was constructed with Maximum likelihood (PHYML) (Guindon et al., 2010).

A closer analysis of the sequences showed that the species analyzed could be grouped into four groups based on the number of cysteines they contain (**Table 1**). Overall, it can be stated that the double (sometimes single) cysteine motif and hence S-acylation is found in all the species analyzed with only one exception, *M. accuminata* (Banana).

Table 1. The distribution of the double cysteine motif in the plant kingdom

Group		Examples	Percentage of sequences
1	Species that possess several VHA-a3 related sequences and **all** contain the double cysteine motif.	*C.sinensis* (Orange) *O. sativa* (Rice) *A.comosus* (Pineapple)	*86.5%*
2	Species that possess several VHA-a3 related sequences and **some** contain the double cysteine motif and others contain only one cysteine.	*T. baccata* (Conifer: English yew) *E. salsugineum* (Salt cres) *M. esculenta* (Cassava) *B. distachyon* (grass: Purple false brome)	*5 %*
3	Species that possess several VHA-a3 related sequences and **some** contain the double cysteine motif and others do not.	*L. usitatissimum* (Flax) *P. trichocarpa* (Poplar tree) *G. raimondii* (Cotton) *G. max* (Soy bean)	*7.8 %*
4	Species that possess a VHA-a3 related sequence and it does **not** contain any N-terminal cysteines.	*M. accuminata* (Banana)	*0.7%*

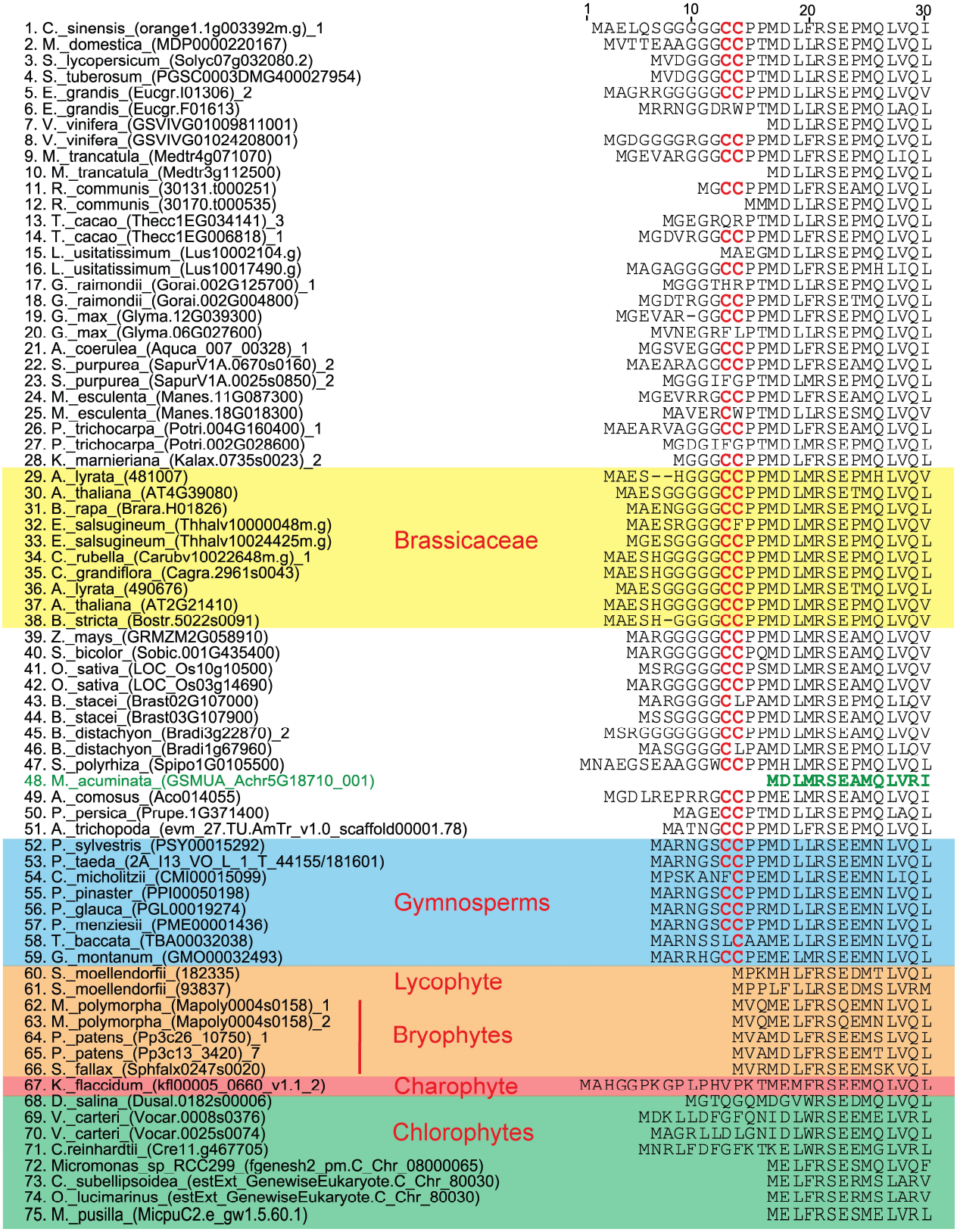
1 10 20 30
1. C._sinensis_(orange1.1g003392m.g)_1 MAELQSGGGGGCCPPMDLFRSEPMQLVQI
2. M._domestica_(MDP0000220167) MVTTEAAGGGCCPTMDLLRSEPMQLVQL
3. S._lycopersicum_(Solyc07g032080.2) MVDGGGCCPTMDLLRSEPMQLVQL
4. S._tuberosum_(PGSC0003DMG400027954) MVDGGGCCPTMDLLRSEPMQLVQL
5. E._grandis_(Eucgr.I01306)_2 MAGRRGGGGGCCPPMDLLRSEPMQLVQV
6. E._grandis_(Eucgr.F01613) MRRNGGDRWPTMDLLRSEPMQLAQL
7. V._vinifera_(GSVIVG01009811001) MDLLRSEPMQLVQL
8. V._vinifera_(GSVIVG01024208001) MGDGGGGRGGCCPPMDLFRSEPMQLVQL
9. M._trancatula_(Medtr4g071070) MGEVARGGGCCPPMDLFRSEPMQLIQL
10. M._trancatula_(Medtr3g112500) MDLLRSEPMQLVQL
11. R._communis_(30131.t000251) MGCCPPMDLFRSEAMQLVQL
12. R._communis_(30170.t000535) MMMDLLRSEPMQLVQL
13. T._cacao_(Thecc1EG034141)_3 MGEGRQRPTMDLLRSEPMQLVQL
14. T._cacao_(Thecc1EG006818)_1 MGDVRGGCCPPMDLFRSEPMQLVQL
15. L._usitatissimum_(Lus10002104.g) MAEGMDLLRSEPMQLVQL
16. L._usitatissimum_(Lus10017490.g) MAGAGGGGCCPPMDLFRSEPMHLIQL
17. G._raimondii_(Gorai.002G125700)_1 MGGGTHRPTMDLLRSEPMQLVQL
18. G._raimondii_(Gorai.002G004800) MGDTRGGCCPPMDLFRSETMQLVQL
19. G._max_(Glyma.12G039300) MGEVAR-GGCCPPMDLFRSEPMQLVQL
20. G._max_(Glyma.06G027600) MVNEGRFLPTMDLLRSEPMQLVQL
21. A._coerulea_(Aquca_007_00328)_1 MGSVEGGCCPPMDLFRSEPMQLVQI
22. S._purpurea_(SapurV1A.0670s0160)_2 MAEARAGCCPPMDLFRSEAMQLVQL
23. S._purpurea_(SapurV1A.0025s0850)_2 MGGGIFGPTMDLMRSEPMQLVQL
24. M._esculenta_(Manes.11G087300) MGEVRRGCCPPMDLFRSEAMQLVQL
25. M._esculenta_(Manes.18G018300) MAVERCWPTMDLLRSESMQLVQV
26. P._trichocarpa_(Potri.004G160400)_1 MAEARVAGGGCCPPMDLFRSEAMQLVQL
27. P._trichocarpa_(Potri.002G028600) MGDGIFGPTMDLMRSEPMQLVQL
28. K._marnieriana_(Kalax.0735s0023)_2 MGGGCCPPMDLFRSEPMQLVQL
29. A._lyrata_(481007) MAES--HGGGCCPPMDLMRSEPMHLVQV
30. A._thaliana_(AT4G39080) MAESGGGGGCCPPMDLMRSETMQLVQL
31. B._rapa_(Brara.H01826) MAENGGGGCCPPMDLMRSEPMQLVQL
32. E._salsugineum_(Thhalv10000048m.g) MAESRGGGCFPPMDLMRSEPMQLVQV
33. E._salsugineum_(Thhalv10024425m.g) MGESGGGGCCPPMDLMRSEPMQLVQL
34. C._rubella_(Carubv10022648m.g)_1 MAESHGGGGGCCPPMDLMRSEPMQLVQL
35. C._grandiflora_(Cagra.2961s0043) MAESHGGGGGCCPPMDLMRSEPMQLVQL
36. A._lyrata_(490676) MAESGGGGGCCPPMDLMRSETMQLVQL
37. A._thaliana_(AT2G21410) MAESHGGGGGCCPPMDLMRSEPMQLVQV
38. B._stricta_(Bostr.5022s0091) MAESH-GGGGCCPPMDLMRSEPMQLVQV
39. Z._mays_(GRMZM2G058910) MARGGGGGCCPPMDLMRSEAMQLVQV
40. S._bicolor_(Sobic.001G435400) MARGGGGGCCPQMDLMRSEAMQLVQV
41. O._sativa_(LOC_Os10g10500) MSRGGGGCCPSMDLMRSEAMQLVQV
42. O._sativa_(LOC_Os03g14690) MARGGGGGCCPPMDLMRSEAMQLVQV
43. B._stacei_(Brast02G107000) MARGGGGCLPAMDLMRSEPMQLLQV
44. B._stacei_(Brast03G107900) MSSGGGGCCPPMDLMRSEAMQLVQV
45. B._distachyon_(Bradi3g22870)_2 MSRGGGGGGGCCPPMDLMRSEAMQLVQV
46. B._distachyon_(Bradi1g67960) MASGGGGCLPAMDLMRSEPMQLLQV
47. S._polyrhiza_(Spipo1G0105500) MNAEGSEAAGGWCCPPMHLMRSEPMQLVQL
48. M._acuminata_(GSMUA_Achr5G18710_001) MDLMRSEAMQLVRI
49. A._comosus_(Aco014055) MGDLREPRRGCCPPMELMRSEAMQLVQI
50. P._persica_(Prupe.1G371400) MAGECCPTMDLLRSEPMQLAQL
51. A._trichopoda_(evm_27.TU.AmTr_v1.0_scaffold00001.78) MATNGCCPPMDLFRSEPMQLVQL
52. P._sylvestris_(PSY00015292) MARNGSCCPPMDLLRSEEMNLVQL
53. P._taeda_(2A_I13_VO_L_1_T_44155/181601) MARNGSCCPPMDLLRSEEMNLVQL
54. C._micholitzii_(CMI00015099) MPSKANFCPEMDLLRSEEMNLIQL
55. P._pinaster_(PPI00050198) MARNGSCCPPMDLLRSEEMNLVQL
56. P._glauca_(PGL00019274) MARNGSCCPRMDLLRSEEMNLVQL
57. P._menziesii_(PME00001436) MARNGSCCPPMDLLRSEEMNLVQL
58. T._baccata_(TBA00032038) MARNSSLCAAMELLRSEEMNLVQL
59. G._montanum_(GMO00032493) MARRHGCCPEMELMRSEEMNLVQL
60. S._moellendorfii_(182335) MPKMHLFRSEDMTLVQL
61. S._moellendorfii_(93837) MPPLFLLRSEDMSLVRM
62. M._polymorpha_(Mapoly0004s0158)_1 MVQMELFRSQEMNLVQL
63. M._polymorpha_(Mapoly0004s0158)_2 MVQMELFRSQEMNLVQL
64. P._patens_(Pp3c26_10750)_1 MVAMDLFRSEEMSLVQL
65. P._patens_(Pp3c13_3420)_7 MVAMDLFRSEEMTLVQL
66. S._fallax_(Sphfalx0247s0020) MVRMDLFRSEEMSKVQL
67. K._flaccidum_(kfl00005_0660_v1.1_2) MAHGGPKGPLPHVPKTMEMFRSEEMQLVQL
68. D._salina_(Dusal.0182s00006) MGTQGQMDGVWRSEDMQLVQL
69. V._carteri_(Vocar.0008s0376) MDKLLDFGFQNIDLWRSEEMELVRL
70. V._carteri_(Vocar.0025s0074) MAGRLLDLGNIDLWRSEEMQLVQL
71. C.reinhardtii_(Cre11.g467705) MNRLFDFGFKTKELWRSEEMGLVRL
72. Micromonas_sp_RCC299_(fgenesh2_pm.C_Chr_08000065) MELFRSESMQLVQF
73. C._subellipsoidea_(estExt_GenewiseEukaryote.C_Chr_80030) MELFRSERMSLARV
74. O._lucimarinus_(estExt_GenewiseEukaryote.C_Chr_80030) MELFRSERMSLARV
75. M._pusilla_(MicpuC2.e_gw1.5.60.1) MELFRSESMELVRL
Brassicaceae
Gymnosperms
Lycophyte
Bryophytes
Charophyte
Chlorophytes

Figure 4. The double cysteine motif is conserved in higher plants and absent in chlorophytes.

The double cysteine motif is indicated in red. It is absent from the chlorophytes, bryophytes and lycophytes. The motif emerges in the gymnosperm sequences. Some species possess several VHA-a3 related sequences and some have only one cysteine while others have none. *M. acuminata* (Banana) was the only species that possessed a VHA-a3 related sequence that does not contain any N- terminal cysteines (green). Multiple sequence alignment was performed with Clustal omega (Sievers et al., 2011).

The species in group 3 that possess several VHA-a3 related sequences of which some contain the double cysteine motif while others do not were analyzed further to see if they have a common attribute. No common denominator could be discernible amongst the species aside from that four of them belong to the order Malphigiales (**Figure 5**).

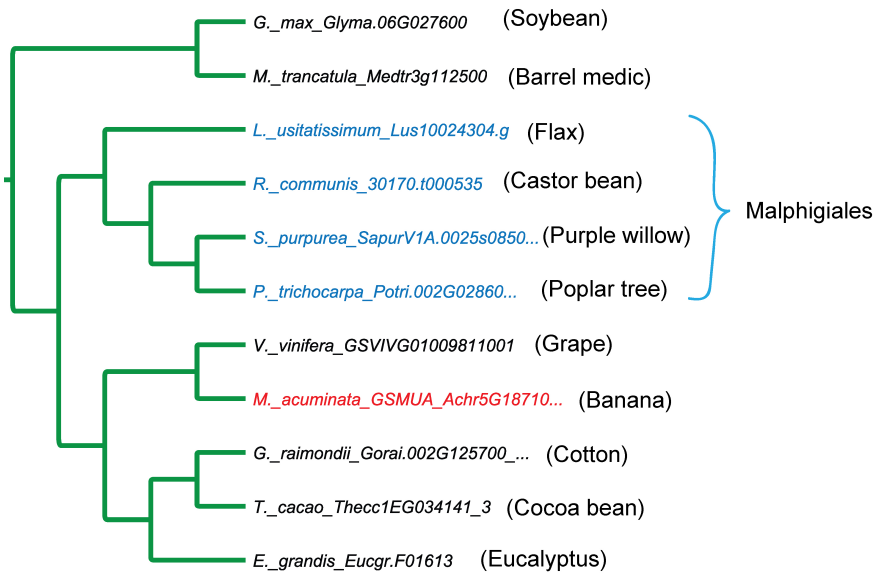

Figure 5. Species that possess VHA-a3 like sequences which do not contain N-terminal cysteines.

Species that possess multiple VHA-a3 related sequences and some of which do not contain N-terminal cysteines were analyzed for a common denominator. Four of these species belong to the order Malphigiales. The remainder of the species come from different phylogenetic groups and do not seem to have anything in common. *M. acuminata* (Banana) is indicated in red as it is the only species that possessed a VHA-a3 related sequence with no N- terminal cysteines.

V-ATPase activity is not compromised by a lack of S-acylation

After determining that the double cysteine motif was highly conserved in the plant kingdom, it was reasonable to assume that S-acylation of a V-ATPase subunit must serve some sort of purpose.

Since we showed that S-acylation is not involved in targeting, the next aspect we considered was that S-acylation is related to the function of the V-ATPase pump. That is, S-acylation is used to switch between active and inactive states of the enzyme. In order to determine whether V-ATPases that incorporate non S-acylated VHA-a3 subunits are functional, we expressed GFP fusion constructs of the mutated and non mutated forms of VHA-a3 in the *vha-a2 vha-a3* double mutant. The *vha-a2 vha-a3* double mutant lacks V-ATPases at the tonoplast and has a dwarfed phenotype and a more alkaline vacuolar pH (Krebs et al., 2010). Two independent lines were chosen for each fusion construct. VHA-a3SS-GFP localized to the tonoplast in the *vha-a2 vha-a3* double mutant like in the wild type background (**Figure 6 B**).

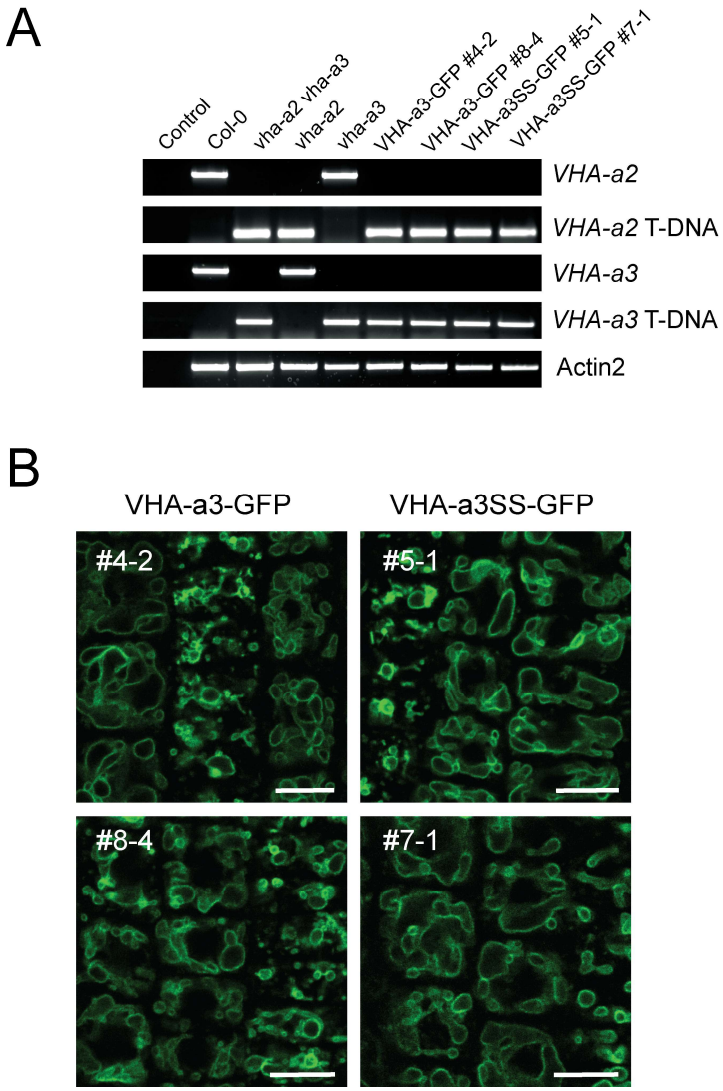

Figure 6. VHA-a3SS-GFP is correctly localized at the tonoplast in the *vha-a2 vha-a3* double mutant.

VHA-a3-GFP and VHA-a3SS-GFP were expressed in the*vha-a2 vha-a3* double mutant. Two independent lines were selected for each construct. **(A)** The lines were genotyped to confirm that they were in the *vha-a2 vha-a3* double mutant. **(B)** The localization of the fusion constructs was analyzed by CLSM. VHA-a3-GFP and VHA-a3SS-GFP both localized at the tonoplast in the *vha-a2 vha-a3* double mutant. Scale bars = 10 µm.

We then investigated whether we could detect differences in complementation of the *vha-a2 vha-a3* double mutant phenotype between complexes that incorporated VHA-a3-GFP and VHA-a3SS-GFP. Phenotype assays were performed in standard long day conditions (22˚C and 16 hours light). In these growth conditions, there was no significant difference between the VHA-a3-GFP and VHA-a3SS-GFP lines. Both constructs were able to complement the dwarf phenotype of the double mutant to the similar levels **(Supplemental figure S2).**

The growth phenotype of the *vha-a2 vha-a3* double mutant shows day-length-dependent growth retardation and is more severe in short day conditions (Krebs et al., 2010). Therefore, phenotype assays were also performed in short day conditions (22˚C and 10 hours light). We observed that in these short day length conditions, there was also no significant difference in the complementation of the *vha-a2 vha-a3* phenotype between the VHA-a3-GFP and VHA-a3SS-GFP lines **(Figure 7A and B)**.

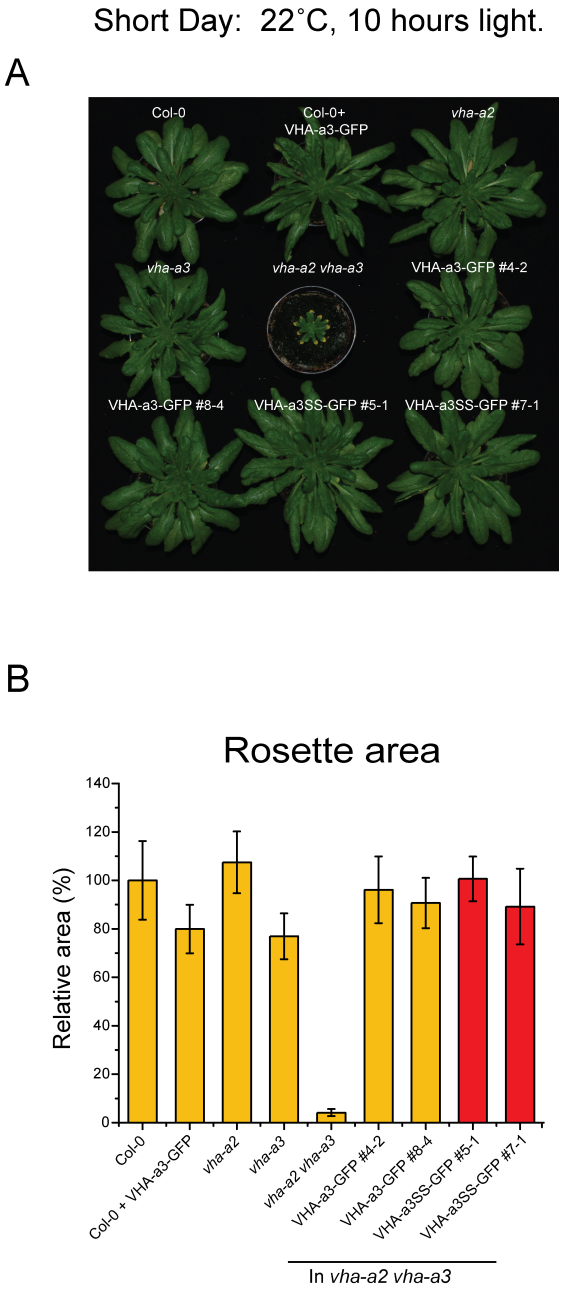

Figure 7. V-ATPases that incorporate mutated and non mutated VHA-a3 subunits complement the *vha-a2 vha-a3*double mutant phenotype to similar levels in short day conditions

Plants were grown under short day conditions (22˚C and 10 hours light) for 6 weeks. **(A)** Plants expressing VHA-a3-GFP and VHA-a3SS-GFP displayed bigger rosette sizes than the *vha-a2 vha-a3* double mutant. Both constructs were able to complement the dwarf phenotype of the double mutant to similar levels. **(B)** The rosette area was measured using rosette tracker on Fiji. Wild type rosette area is set to 100%. Rosette diameter and fresh weight are reported in **Supplemental figure 1.**

Loss of S-acylation does not impair vacuolar V-ATPase function under cold and zinc metal stress conditions

After observing that V-ATPases that incorporate VHA-a3SS-GFP were still able to complement the *vha-a2 vha-a3* double mutant in long day and short day conditions, we postulated that S-acylation may become important under stress conditions. That is, S-acylation is a means to regulate the activity of the V-ATPase in response to a prevailing stress condition. We investigated stress conditions that severely worsen the phenotype of the *vha-a2 vha-a3* double mutant and conditions where increased V-ATPase activity is required.

The first condition we investigated was zinc metal stress. The *vha-a2 vha-a3* double mutant shows an increased sensitivity to zinc compared to the wild type due to reduced proton-coupled vacuolar uptake (Krebs et al., 2010). Zinc is an essential micronutrient required for a wide range of physiological processes in all plant organs for the activities of various metal-dependent enzymes and proteins (Krämer et al., 2007). However, at elevated levels it becomes toxic to the plant. Thus, we examined the growth of the *vha-a2 vha-a3* double mutant expressing either VHA-a3-GFP or VHA-a3SS-GFP under different zinc concentrations.

Growth assays were performed on plates containing different concentrations of $ZnCl_2$ **(Figure 8 A and B and Supplemental figure S3).** The root lengths of the seedlings were measured to quantify growth. The results show that *vha-a2 vha-a3* plants expressing either VHA-a3-GFP or VHA-a3SS-GFP had the same concentration dependent sensitivity to zinc (**Figure 8 C**). Therefore, it was concluded that S-acylation does not play a role in the proton gradient dependent sequestration of zinc metal into the vacuole.

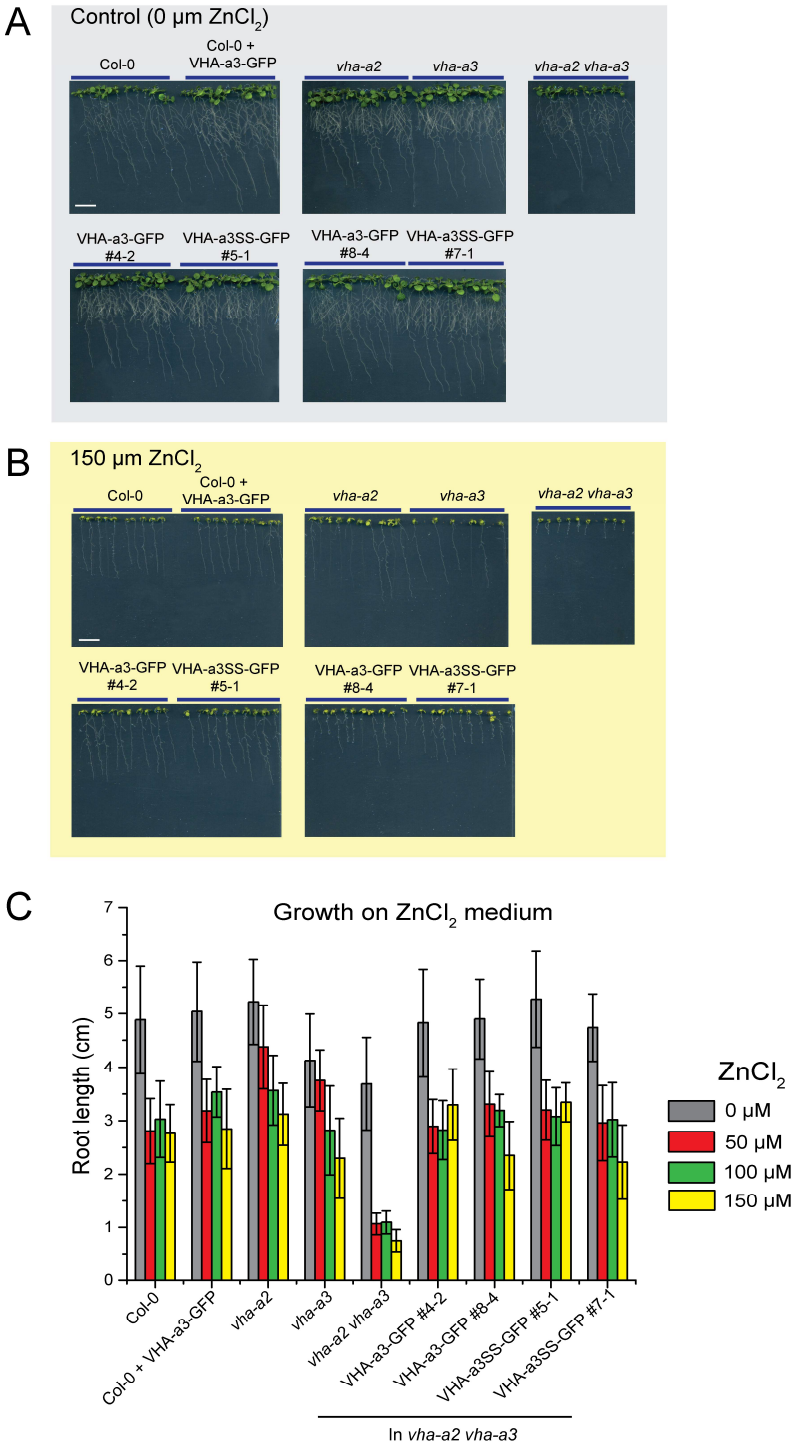

Figure 8. S-acylation is not required for vacuolar sequestration of Zinc metal.

(A and B) Seedlings were grown for 12 days on plates containing the indicated concentrations of $ZnCl_2$. Growth on 50 and 100 µM concentrations of Zinc are reported in **Supplemental figure 5**. Scale bars = 1 cm. **(C)** Averaged root lengths under different concentrations of $ZnCl_2$ for one representative experiment. Error bars represent the Standard deviation with n =40

The rosette phenotype assays showed that S-acylation is not a molecular on and off switch for the V-ATPase because V-ATPases that incorporate VHA-a3SS-GFP subunits are functional. Therefore, we postulated that S-acylation might be important for adjusting the activity of the V-ATPase since it is reversible. And we developed the following hypothesis, that S-acylation is a break that slows down the activity of the V-ATPase.

In order to investigate this hypothesis, we first set out to determine if there were any differences in ATP hydrolysis and proton translocation activities between V-ATPases that incorporate VHA-a3-GFP and VHA-a3SS-GFP subunits. Concurrently to this, we also wanted to determine whether VHA-a3-GFP and VHA-a3SS-GFP containing V-ATPases respond differently to cold acclimation. Cold acclimation is a process whereby plants acquire increased freezing tolerance after being exposed to low non freezing temperatures for days or weeks depending on the species (Xin and Browse, 2000). Cold acclimation was performed at 4˚C for 4 days with six-week-old plants that had been grown in SD conditions.

Tonoplast vesicles were prepared from rosette leaves of cold acclimated and non cold acclimated plants which had been grown for 6 week in SD conditions. The ATP hydrolysis and proton translocation activities were measured. It was observed that the VHA-a3SS-GFP lines exhibited higher ATP hydrolysis and proton translocation activities at 22˚C than the VHA-a3GFP line #4-2 despite having the same or less amount of protein **(Figure 9 A, B, D and E)**. According to our hypothesis, the VHA-a3GFP line #8-4 shows higher activities at 22˚C than the VHA-a3GFP line #4-2 probably because it is less S-acylated **(Figure 8 C).**

After cold acclimation, the wild type ATP hydrolysis activity underwent a cold induced increase which is consistent to what has been previously reported (Kriegel et al., 2015) (**Figure 9 A)**. The VHA-a3SS-GFP lines also exhibited a cold induced increase in ATP hydrolysis activity but much less than the VHA-a3-GFP line #4-2. VHA-a3GFP line #8-4 did not show a cold induced increase in

ATP hydrolysis activity probably because it has less protein at 4˚C. All lines exhibited a cold induced increase in proton translocation activity (**Figure 9 B).**

We then investigated if these differences in V-ATPase activity are reflected in the vacuolar pH since the V-ATPase is the main contributor to vacuolar pH (Kriegel et al., 2015). In fully expanded cells, the cell sap pH is generally accepted to represent the vacuolar pH because in mature cells the vacuolar lumen accounts for 80-90% of the whole cell volume (Kurkdjian and Guern, 1981). Thus, cell sap pH measurements were performed using rosette leaves from plants which were grown for 6 weeks under short day conditions at 22°C. Non acclimated wild type leaves had a cell sap pH of 5.82 and the *vha-a2 vha-a3* double mutant leaves had a more alkaline pH of 6.51. After cold acclimation, there was a small reduction in cell sap pH from 5.82 to 5.73 in the wild type **(Figure 9 F)**, consistent with the observed increases in ATP hydrolysis and proton translocation activities. VHA-a3SS-GFP lines have slightly more acidic cell sap pH values than VHA-a3-GFP lines at 22˚C. After cold acclimation, the VHA-a3-GFP and VHA-a3SS-GFP lines both exhibited cold induced drops in cell sap pH. However, the drop in cell sap pH was greater in the VHA-a3-GFP lines.

The increased V-ATPase activity after cold acclimation is required for increased loading of solutes into the vacuole which are required for fortifying the cell against freezing (Schulze et al., 2012). We investigated how the observed changes in V-ATPase activity influence the freezing tolerance. Cell damage due to freezing can be estimated by measuring the release of electrolytes from frozen leaves, which is an indicator for the amount of destroyed cells (Ristic and Ashworth, 1993). Therefore, three-week-old plants were cold adapted at 4˚C for 4 days, and electrolyte leakage was estimated by determining the electrical conductivity of the bathing solution of detached leaves frozen gradually to -6˚C.

At -6°C, wild-type leaves released 23.6% of their total electrolytes consistent to what has been reported (Klemens et al., 2013). The leaves of the VHA-a3SS-GFP lines released approximately 25% of their electrolytes, which indicates

comparable freezing tolerance to wild type leaves. The VHA-a3-GFP lines #4-2 and #8-4 released 37% and 32% of their electrolytes respectively. The results indicate that these leaves are less tolerant to freezing than wild type leaves and leaves of the VHA-a3SS-GFP lines **(Figure 9 G)**.

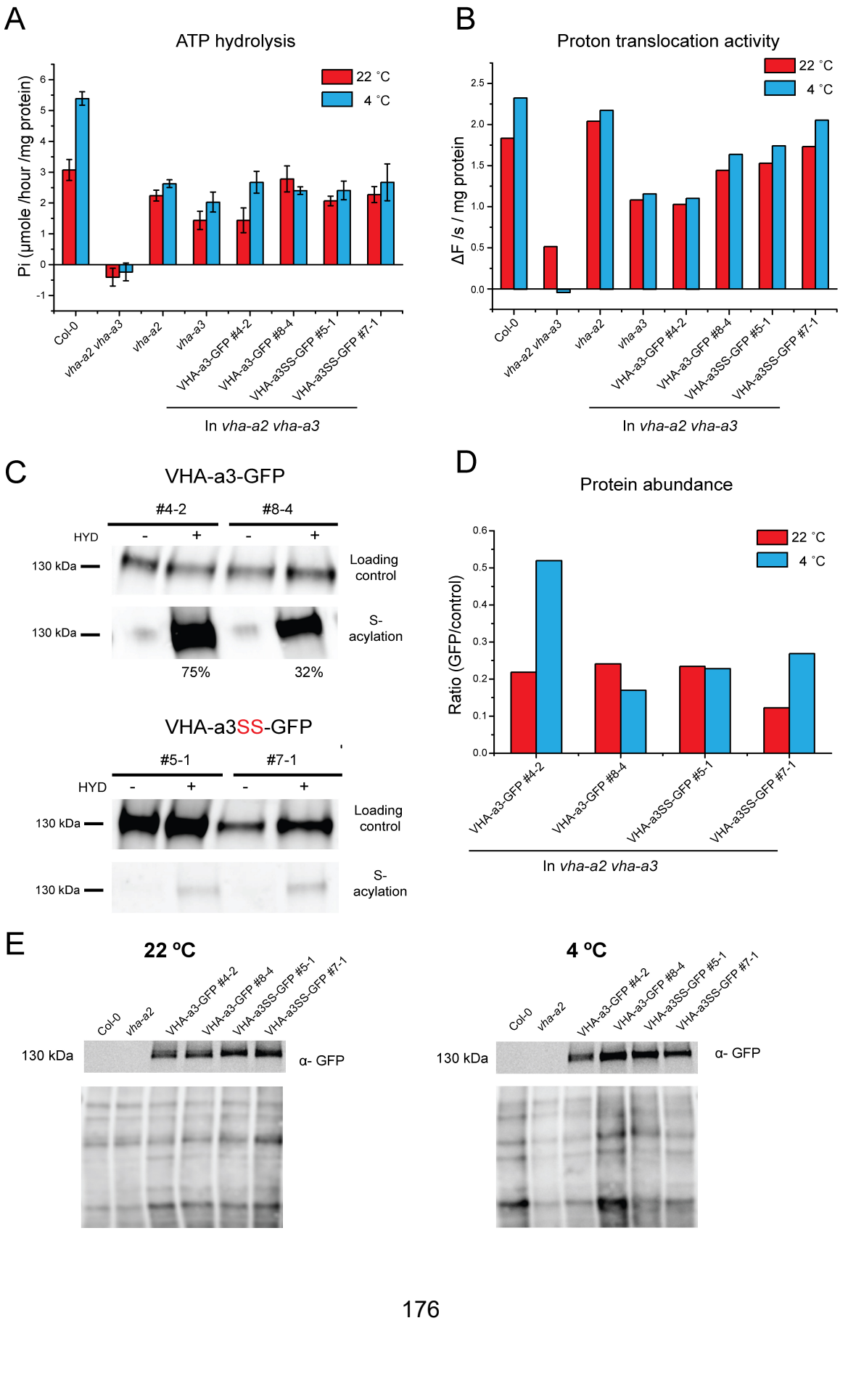
A
ATP hydrolysis
Pi (µmole /hour /mg protein)
22 °C
4 °C
Col-0
vha-a2 vha-a3
vha-a2
vha-a3
VHA-a3-GFP #4-2
VHA-a3-GFP #8-4
VHA-a3SS-GFP #5-1
VHA-a3SS-GFP #7-1
In vha-a2 vha-a3
B
Proton translocation activity
ΔF /s / mg protein
22 °C
4 °C
In vha-a2 vha-a3
C
VHA-a3-GFP
#4-2
#8-4
HYD
130 kDa
Loading control
S-acylation
75%
32%
VHA-a3SS-GFP
#5-1
#7-1
D
Protein abundance
Ratio (GFP/control)
22 °C
4 °C
In vha-a2 vha-a3
E
22 ºC
4 ºC
130 kDa
α- GFP

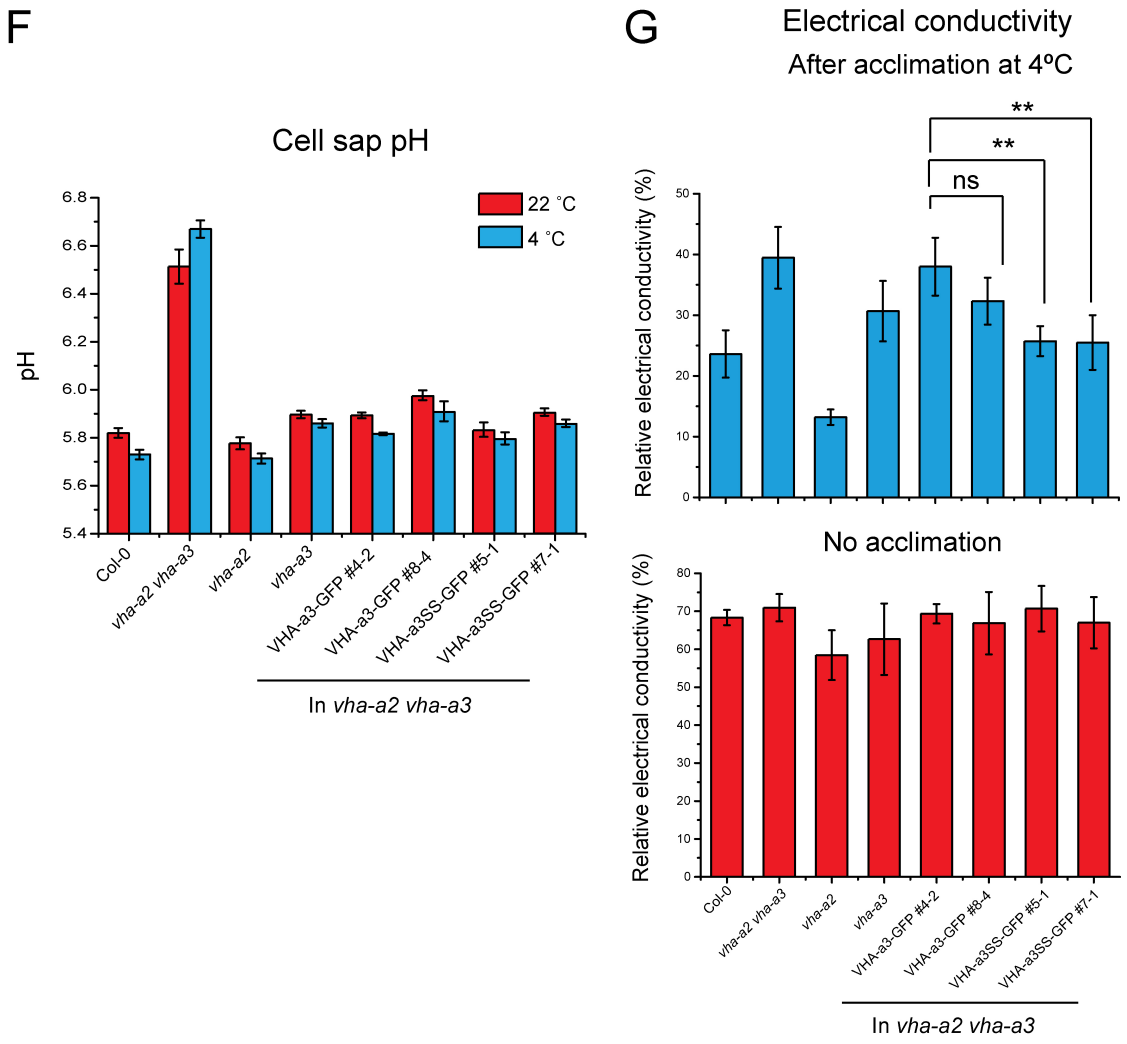

Figure 9. A lack of S-acylation may render the V-ATPase more active

The results presented are of one biological replicate.**(A)** ATP hydrolysis measurements. Tonoplast vesicles were prepared from 6 week old plants grown under short day conditions at 22°C. Tonoplast vesicles were supplied with 3 mM ATP and the KNO_3-inhibited V-ATPase activity was estimated by measuring the amount of Pi released. **(B)** The ATP-dependent proton transport activities were estimated from the initial rate of ATP-dependent fluorescence quenching in the presence of 3 mM ATP using the fluorescence dye ACMA (9-Amino-6-Chloro-2-Methoxyacridine). Measurements were performed in the presence of the P-type ATPase inhibitor, sodium vanadate. Approximately 25 µg of protein was used for these assays. **(C)** S-acylation was determined by the acyl RAC method followed by immunoblotting with a GFP antibody. Total membranes were isolated from *Arabidopsis* plants expressing VHA-a3-GFP and VHA-a3SS-GFP and were subjected to the acyl resin-assisted capture (acyl-RAC) method. Free thiols were first blocked with NEM. Samples were then treated with (HYD+) or without (HYD-) the thioester cleavage reagent hydroxylamine. Samples were then combined with a thiol-reactive

sepharose resin to capture free acyl groups. The row labelled 'S-acylation' shows the levels of VHA-a3-GFP and VHA-a3SS-GFP recovered from beads, and therefore originally S-acylated. VHA-a3-GFP and VHA-a3SS-GFP have masses of approximately 130 kDa. The results indicate that VHA-a3-GFP is S-acylated and VHA-a3SS-GFP is not. **(D)** Abundance of the GFP tagged proteins was determined via western blot.Tonoplast membrane proteins from the same preparations used for the activity assays were separated by SDS-PAGE and subsequently immunoblotted with an anti-GFP antibody. Equal protein loading was determined by staining all proteins with the Smartalyzer dye. Protein levels were measured using Fiji and normalized to whole lane Smartalyzer dye staining. Bar charts represent quantification of one representative immunoblot. **(E)** Western blots that were used for the quantification in D. **(F)** VHA-a3SS-GFP lines have slightly more acidic cell sap pH values than VHA-a3-GFP lines at 22˚C. All lines display a drop in cell sap pH after cold acclimation with the exception of the *vha-a2 vha-a3* double mutant. Plants for cell sap pH measurements were grown for 6 weeks under short-day conditions at 22°C. Cold acclimation was performed at 4˚C for 4 days. Cell sap pH measurements were performed at the same time for both temperature conditions. Error bars represent SD of *n = 3* technical replicates. **(G)** Freezing tolerance of VHA-a3SS-GFP lines is comparable to wild type plants and better than VHA-a3-GFP lines. Three-week-old plants were cold adapted at 4˚C for 4 days, and electrolyte leakage was estimated by determining the electrical conductivity of the bathing solution of detached leaves frozen at -6˚C (n = 5). Asterisks indicate a significant difference (*P < 0.05) according to Student’s t test. Electrical conductivity measurements were performed without any cold acclimation to show that it was the cold acclimation that is responsible for the freezing tolerance. Error bars represent SD of *n = 5* technical replicates.

Tonoplast localized protein S-acyl transferases (PATs) are not involved in S-acylation of VHA-a3

In order to unravel how S-acylation is involved in the spatial and temporal regulation of the V-ATPase complex, it is important to know where S-acylation of VHA-a3 takes place and the enzymes involved. The most likely PAT candidates are the ER and tonoplast localized PATs. This is because these PATs are the ones that VHA-a3 containing V-ATPases come into contact with since VHA-a3 containing V-ATPases can be transported directly from the ER to the vacuole via provacuoles (Viotti et al., 2013).

We utilized a mutant form of VHA-a3 (VHA-a3-R729N) to discern if ER or tonoplast localized PATs are involved in the S-acylation of VHA-a3.VHA-a3 with a R729N mutation allows proper assembly of the V-ATPase complex but renders the complex inactive (Neubert, 2011). In the wild type background where both endogenous VHA-a2 and VHA-a3 are present, VHA-a3-R729N is predominately retained at the ER and only a few complexes that incorporate this mutated subunit reach the tonoplast **(Figure 10 A)**. But in the *vha-a2 vha-a3* double mutant which lacks VHA-a2 and VHA-a3, complexes that incorporate VHA-a3-R729N are transported more efficiently to the tonoplast **(Figure 10 B)**. It is hypothesized that this occurs because the competition created by VHA-a2 and VHA-a3 containing complexes to enter provacuoles is absent.

S-acylation of VHA-a3-R729N was determined in the wild type and *vha-a2 vha-a3* double mutant using the biotin switch assay. It was seen that VHA-a3-R729N is less S-acylated in the wild type background **(Figure 10 C)**. This implied that the site of S-acylation of VHA-a3 in the cell is the tonoplast.A*pat10* mutant (Zhou et al., 2013)was obtained and crossed to a *pat11* mutant to create a *pat10 pat11* double mutant. VHA-a3-GFP correctly localizes to the tonoplast in the *pat10 pat11* double mutant **(Figure 10 D)**. When the S-acylation status of VHA-a3-GFP was analyzed in the *pat10 pat11* double mutant it was found that VHA-a3-GFP is still s-acylated in the double mutant **(Figure 10 E)**. This means that the two tonoplast localized PATs are not responsible for S-acylation of VHA-a3.

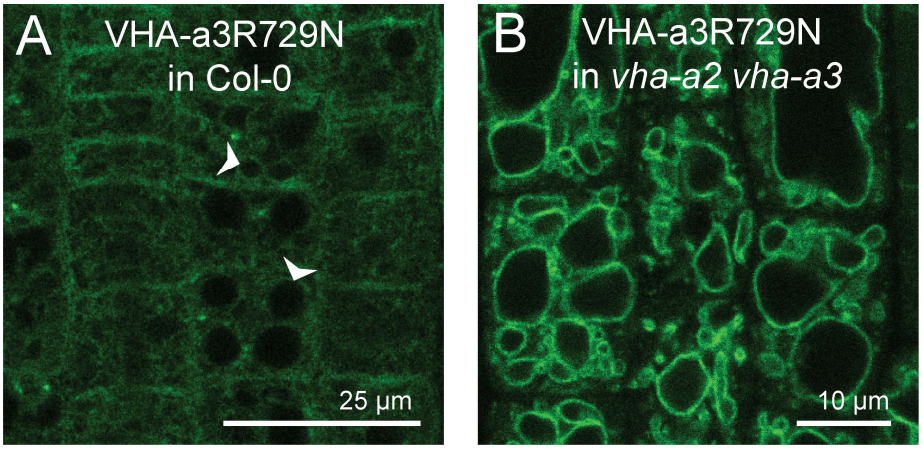
A
VHA-a3R729N
in Col-0
25 µm
B
VHA-a3R729N
in vha-a2 vha-a3
10 µm

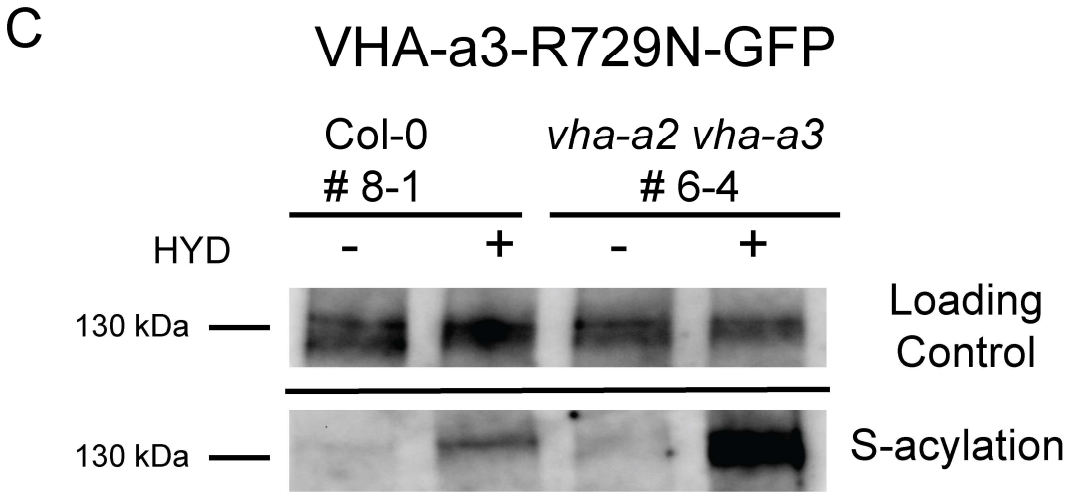
C
VHA-a3-R729N-GFP
Col-0
8-1
vha-a2 vha-a3
6-4
HYD
-
+
-
+
130 kDa
Loading
Control
130 kDa
S-acylation

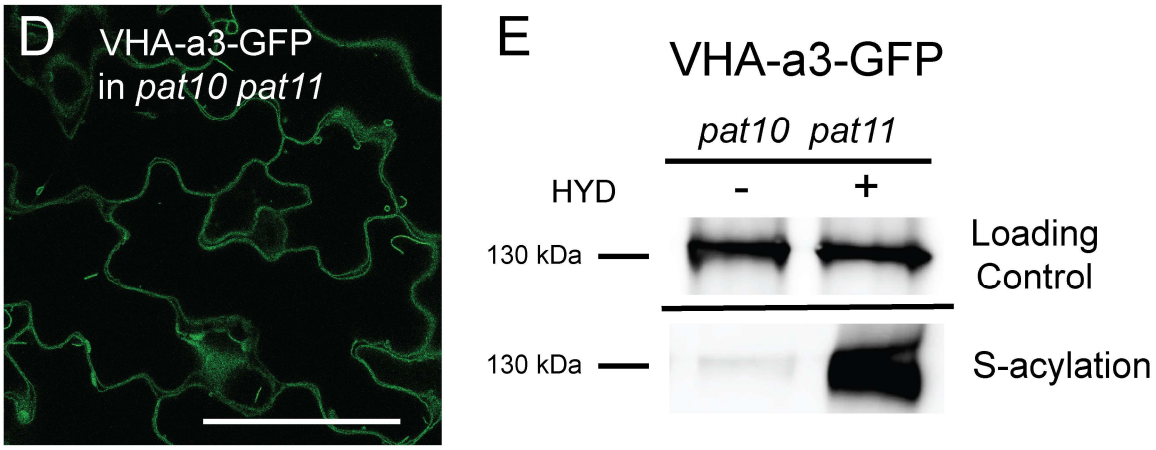
D
VHA-a3-GFP
in pat10 pat11
E
VHA-a3-GFP
pat10 pat11
HYD
-
+
130 kDa
Loading
Control
130 kDa
S-acylation

Figure 10. Tonoplast localized protein S-acyl transferases (PATs), PAT10 and 11, are not involved in S-acylation of VHA-a3

(A) VHA-a3-R729N-GFP is predominately retained in the ER in the wild type background and very little protein is found at the tonoplast indicated by white arrows. **(B)** VHA-a3-R729N-GFP is transported more efficiently to the tonoplast in the *vha-a2 vha-a3* double mutant. **(C)** S-acylation was determined by the biotin switch assay, as described by (Hemsley, 2013), followed by immunoblotting with a GFP antibody. Total membranes were isolated from *Arabidopsis* plants expressing VHA-a3-R729N-GFP. Free thiols were first blocked with NEM. Samples were then treated with (HYD+) or without (HYD-), the thioester cleavage reagent hydroxylamine. HYD+ and HYD- samples were treated with sulfhydryl reactive biotin and then combined with neutravidin beads which have a high affinity for biotin. The loading controls show that comparable amounts of protein were loaded onto neutravidin beads for each line. The row labelled 'S-acylation' shows the levels of VHA-a3-R729N-GFP recovered from neutravidin beads, and therefore originally S-acylated. VHA-a3-R729N-GFP has a mass of approximately 130kDa. The results indicate that VHA-a3-R729N-GFP is less S-acylated in the wild type background. **(D)** VHA-a3-GFP correctly localizes to the tonoplast in the *pat10 pat11* double mutant. **(E)** Total membranes were isolated from *Arabidopsispat10 pat11* plants expressing VHA-a3-GFP and were subjected to the biotin switch assay. The row labelled 'S-acylation' shows the levels of VHA-a3-GFP recovered from neutravidin beads, and therefore originally S-acylated. VHA-a3-GFP has a mass of approximately 130 kDa. The results indicate that VHA-a3-GFP is S-acylated in the *pat10 pat11* double mutant

Discussion

Plants because of their sessile lifestyle and their unique vacuole which occupies most of the cell volume may require another level of regulation of their V-ATPase at the tonoplast. The activity of the V-ATPase pump has been shown to change depending on environmental conditions. For instance, V-ATPase activity has also been shown to increase when the plant is exposed to low temperatures (Schulze et al., 2012; Kriegel et al., 2015). The ability to change activities is due the inherent nature of the V-ATPase complex. The V-ATPase complex differs from other ATPases because it can adjust its coupling of ATP hydrolysis to proton translocation depending on the electrical gradient across the membrane (Rienmüller et al., 2012). The pump is most active when the gradient is low and slows down when the luminal pH becomes more acidic (Rienmüller et al., 2012). The mechanisms of how the V-ATPase activity is regulated has not been fully elucidated.

We have investigated a new form of a post translational modification of one of the subunits of the plant V-ATPase complex. Subunit a has important functions relating to the functioning of the V-ATPase pump. Subunit a controls cellular targeting and coupling of ATP hydrolysis to proton translocation (Dettmer et al., 2006; Kawasaki-Nishi et al., 2001). We show that the tonoplast targeting isoform VHA-a3 is S-acylated while the TGN/endosomal targeting isoform VHA-a1 is not. We also found the site of S-acylation to be cysteines (C10 and C11) in the N-terminus of VHA-a3. This double cysteine motif is highly conserved in the plant kingdom and originates within the gymnosperm sequences. All plant species analyzed in this study possess at least one sequence with the double cysteine motif with the exception of *M. accuminata* (banana).

We show that S-acylation is not involved in targeting of VHA-a3 complexes to the tonoplast. In addition, the first 13 amino acids from the N-terminus of VHA-a3 are insufficient to not only change the TGN localization of VHA-a1 but they are also insufficient to bring about S-acylation. This might be because further downstream

sequences in VHA-a3 are needed to maintain the proper 3D conformation needed for interaction with a PAT (Protein S-acyl transferase) or TGN localized PATs cannot S-acylate VHA-a3. By showing that VHA-a3-GFP is still S-acylated in the *pat10 pat11* double mutant, we can exclude the known tonoplast PATs for being responsible for S-acylation of VHA-a3. We postulate that, it is either a yet unknown tonoplast PAT or an ER localized PAT that is involved in S-acylating of VHA-a3.

We also found that S-acylation is not required for activity of the V-ATPase. This is because V-ATPases that incorporate VHA-a3SS-GFP subunits are able to complement the *vha-a2 vha-a3* double mutant to comparable levels as V-ATPases that incorporate VHA-a3-GFP in standard growth conditions and even in the presence of high concentrations of zinc. However, although the level of complementation is the same, VHA-a3SS-GFP containing V-ATPases exhibit higher V-ATPase activities. The higher activities in the VHA-a3SS-GFP lines are not due to the presence of more transgenic protein in these lines. Furthermore, the cell sap pH of VHA-a3SS-GFP lines does not drop as much as that of the VHA-a3-GFP lines after the plants are exposed to low temperatures. This implies that the VHA-a3SS containing pumps are always operating at their maximum capacity.

A curious observation was made with the *vha-a2* single mutant. The *vha-a2* mutant shows very efficient coupling of ATP hydrolysis to proton translocation, exhibits bigger rosette sizes and has a slightly more acidic cell sap pH than the complementation lines in SD conditions. In addition, it shows a better tolerance to zinc than wild type. All these observations may be due to a compensatory mechanism that is present in the mutant.

Repetitions of these experiments with more biological replicates have to performed in order to confirm the observations made. It also has to be considered that palmitoylation and depalmitoylation cycles are import for proper functioning of S-acylated proteins (Hornemann, 2014). Maybe greater differences in V-

ATPase activity and hence cell sap pH can be observed if the cycles are interrupted by inhibiting de-S-acylation with inhibitors. Kinetic experiments which would show how V-ATPase activities change over time may be more insightful in revealing differences between VHA-a3-GFP and VHA-a3SS-GFP containing V-ATPases than end point measurements. None the less, the data from our experiments imply that reducing or removing S-acylation increases the activity of the V-ATPase. And we have developed the following hypothesis, that S-acylation is not a molecular switch to turn on and off the activity of the V-ATPase but it may rather be used to regulate the activity of the V-ATPase.

We have also considered how S-acylation may be changing the activity of the V-ATPase. S-acylation occurs at the N-terminus of VHA-a3. It has been reported that the N-terminus of subunit a of the yeast V-ATPase is mobile and not static. It moves along the plane of the membrane as the V-ATPase is functioning (Zhao et al., 2015). We postulate that S-acylation at the N-terminus of VHA-a3 could be a means to anchor VHA-a3 to the membrane **(Figure1)**. This would interfere with the activity of the complex.

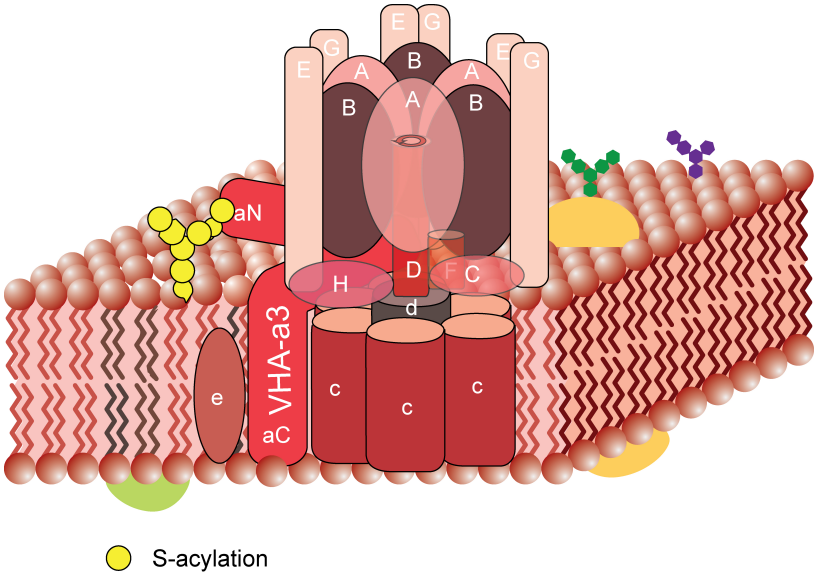

Figure 1. S-acylation of VHA-a3 can be used to anchor the N-terminus to the membrane

The N-terminus of VHA-a3 lies parallel to the membrane and therefore can be anchored into the membrane by S-acylation.

Another possible function of anchoring the N-terminus onto the membrane would be to partition the V-ATPase into microdomains with high sterol content in the tonoplast membrane. It has been shown that sterols are present at the tonoplast and that VHA-a3 is present in sterol enriched membranes (Viotti et al., 2013). One way to study microdomains enriched in sphingolipid and sterol content and the proteins associated with them is to isolate detergent resistant membranes (DRMs). DRMs are resistant to solubilisation by non-ionic detergents at low temperature and float to low density during sucrose gradient centrifugation (Borner et al., 2005). It is plausible to speculate that microdomain partitioning may regulate the activity of the V-ATPase. Therefore the presence of VHA-a3 containing V-ATPases in DRMs and the absence of VHA-a3SS V-ATPases thereof has to be investigated.

Overall, the study has investigated a new form of post-translational modification that is unique to the plant V-ATPase. Our data implies that the mode of action of S-acylation is not a molecular switch to turn on and off the V-ATPase complex but is rather a knob for fine tuning the activity of the V-ATPase in response to an environmental stimuli.

Supplemental material

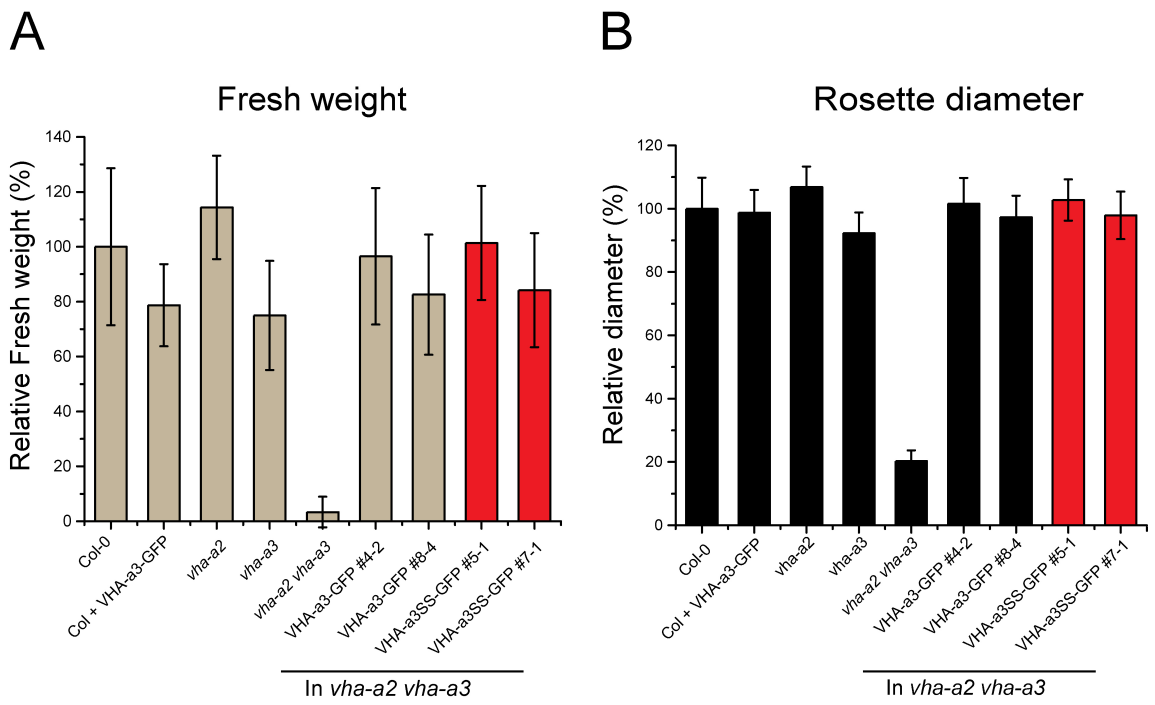

Figure S1. V-ATPases that incorporate mutated and non mutated VHA-a3 subunits complement the *vha-a2 vha-a3* double phenotype to similar levels in short day conditions

Plants were grown under short day conditions (22˚C and 10 hours light) for 6 weeks. **(A)** Rosette fresh weight. **(B)** The rosette diameter was measured using rosette tracker on Image J. Wild type rosette fresh weight and diameter are set to 100%.

Long Day: 22˚C, 16 hours light.

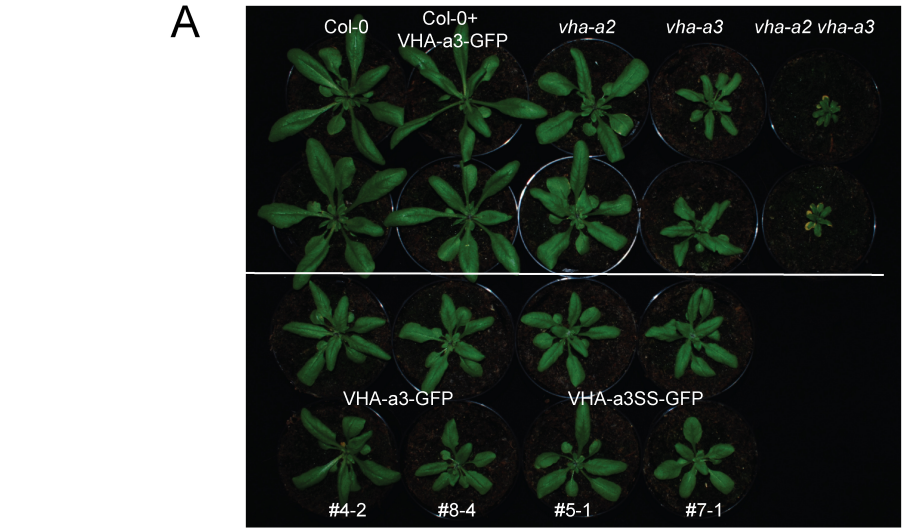

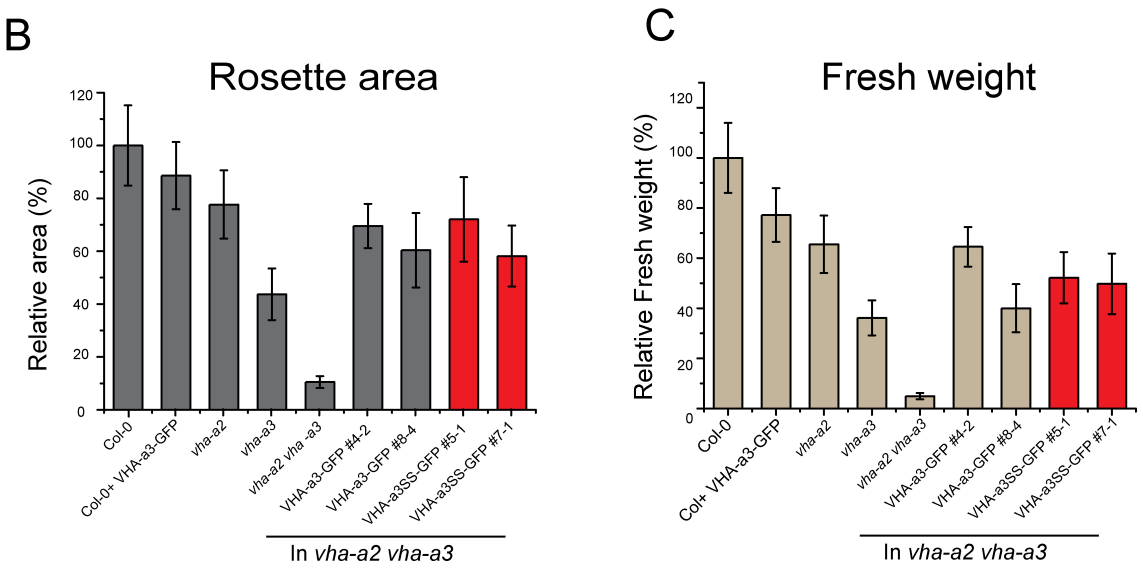

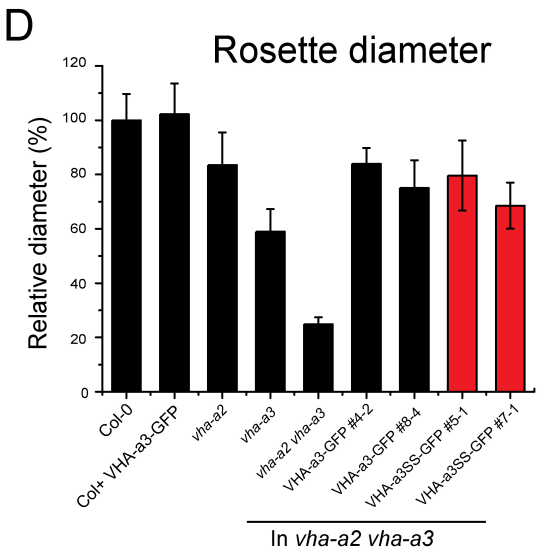

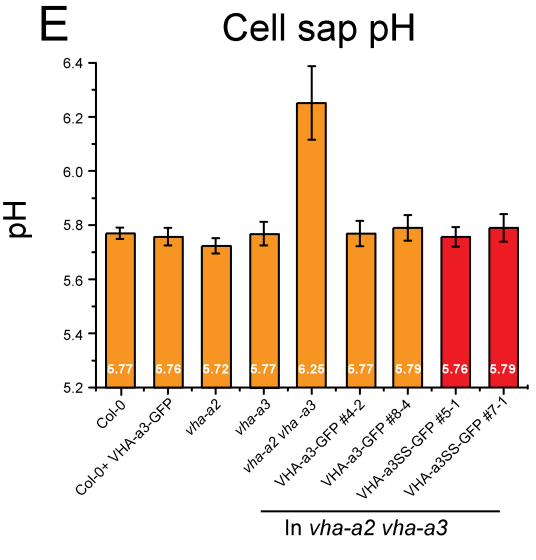

Figure S2. V-ATPases that VHA-a3-GFP and VHA-a3-SS-GFP subunits complement the *vha-a2 vha-a3* double phenotype to similar levels in long day conditions.

Plants were grown under standard long day conditions (22˚C and 16 hours light) for 4 weeks. **(A)** Plants expressing VHA-a3-GFP and VHA-a3SS-GFP displayed bigger rosette sizes than the *vha-a2 vha-a3* double mutant. Both constructs were able to complement the dwarf phenotype of the double mutant to similar levels. **(B)** Rosette area. **(C)** Rosette fresh weight. **(D)** Rosette diameter. Rosette was measured using rosette tracker on Image J. Wild type rosette area is set to 100%**.** (**E)** Cell sap pH is equivalent to vacuolar pH for plant cells because vacuoles occupy 90 % of the cell (Kurkdjian and Guern, 1981). Cell sap pH measurements were conducted using 4 week old rosettes. V-ATPases that incorporate mutated and non mutated VHA-a3 subunits were able to acidify vacuoles to wild type levels.

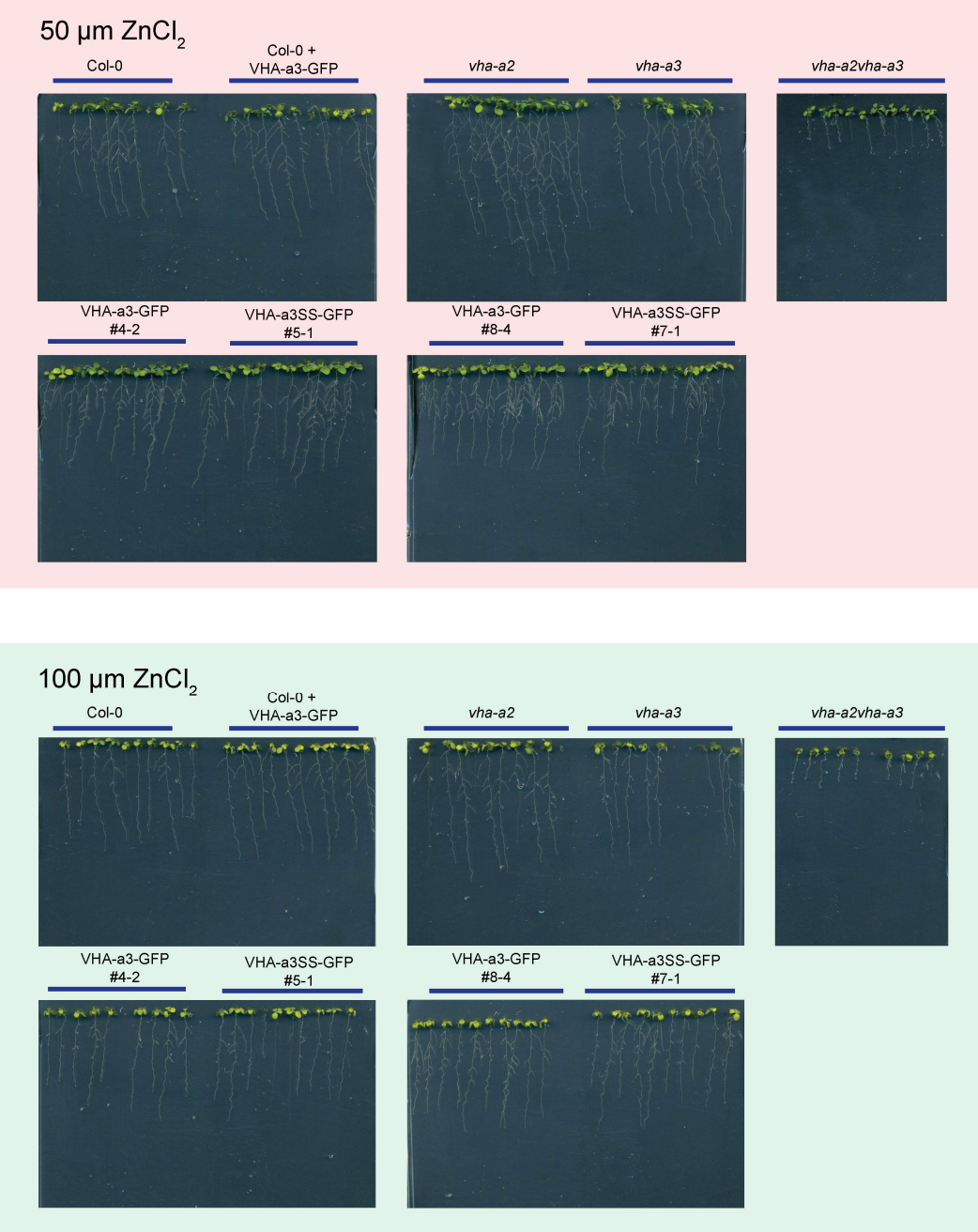

Figure S3. S-acylation is not required for vacuolar sequestration of Zinc metal.

Seedlings were grown for 12 days on plates containing the indicated concentrations of 50 and 100 µM concentrations $ZnCl_2$.

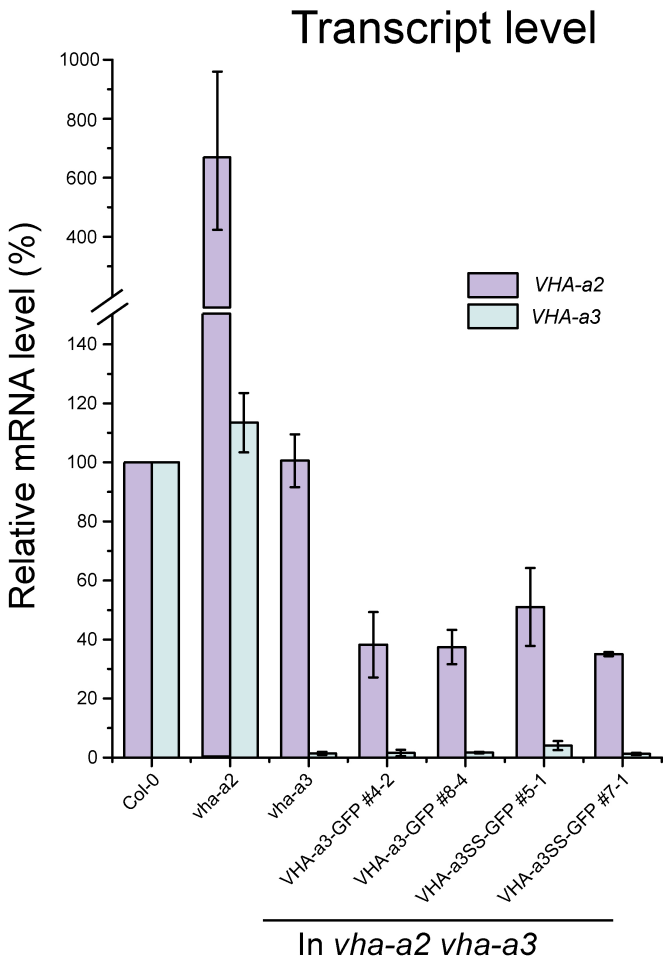

Figure S4. *VHA-a2* and *VHA-a3* transcript levels in the selected VHA-a3-GFP and VHA-a3SS-GFP lines in the *vha-a2 vha-a3* background.

The transcript level of *VHA-a2* and *VHA-a3* was measured by qRT-PCR in 6-week-old rosette leaves of plants grown under short day conditions. The *vha-a2* mutant expresses high levels of a truncated transcript that is not functional (Krebs et al., 2010). VHA-a3-GFP and VHA-a3SS-GFP lines in the *vha-a2 vha-a3* background express comparable levels of this truncated transcript. Error bars indicate SD of n = 3 biological replicates

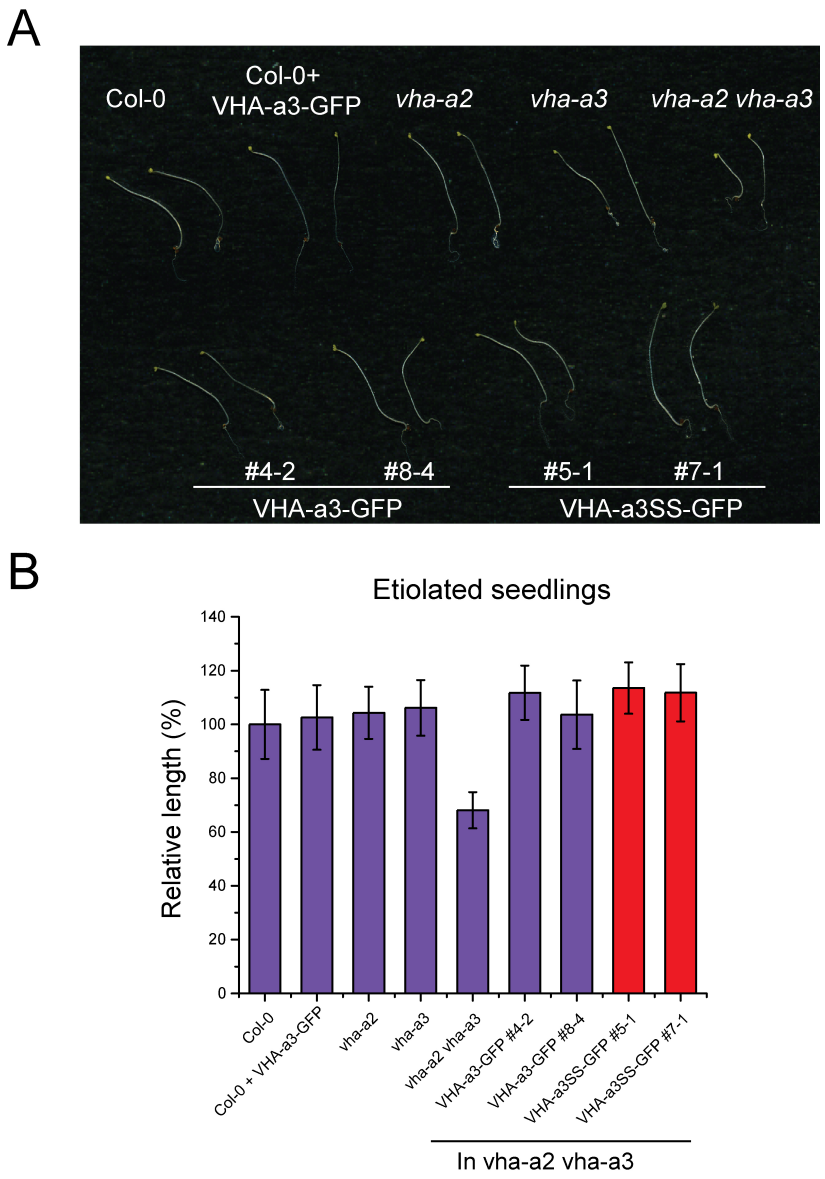

Figure S5. VHA-a3-GFP and VHA-a3SS-GFP lines have comparable cell expansion levels.

(A) Morphological observation. **(B)** Quantitative measurement of the hypocotyl length. Etiolated seedlings were grown for 4 days on vertical plates. Error bars represent SD of around 40 seedlings.

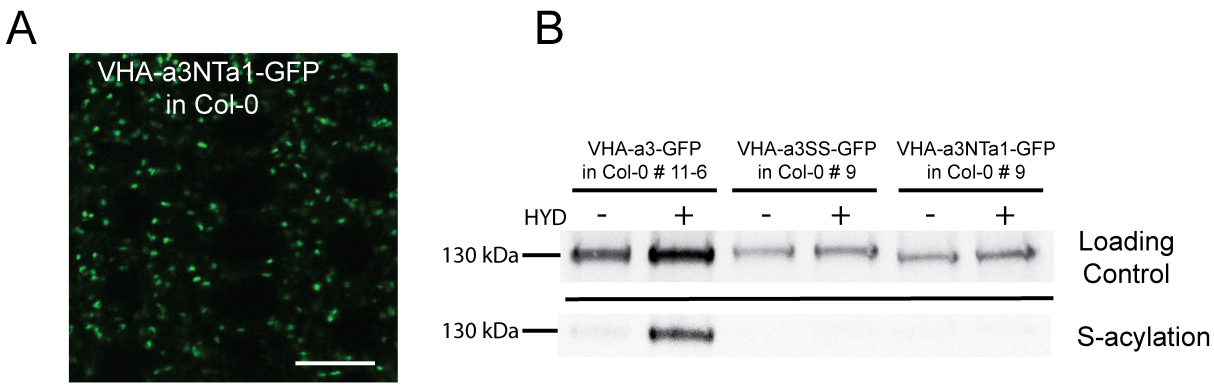

Figure S7. Introducing the double cysteine motif into VHA-a1 (VHA-a3NTa1-GFP) does not change the TGN localization of VHA-1 and it is not enough for S-acylation to place.

(A) The first 13 amino acids containing the double cysteine motif of VHA-a3 were introduced on to the N-terminus of VHA-a1. This chimeric protein still localized at the TGN localization like VHA-a1. Error bars= 10 µm.**(B)** Total membranes were isolated from *Arabidopsis* plants expressing VHA-a3-GFP, VHA-a3SS-GFP and VHA-a3NTa1-GFP. Free thiols were first blocked with NEM. Samples were then treated with (HYD+) or without (HYD-) the thioester cleavage reagent hydroxylamine. HYD+ and HYD- samples were treated with sulfhydryl reactive biotin and then combined with neutravidin beads which have a high affinity for biotin. The loading controls show that comparable amounts of protein were loaded onto neutravidin beads for each line. The row labelled 'S-acylation' shows the levels of VHA-a3-GFP, VHA-a3SS-GFP and VHA-a3NTa1-GFP recovered from neutravidin beads, and therefore originally S-acylated. VHA-a3-GFP has a mass of approximately 130kDa. The results indicate that VHA-a3NTa1-GFPis not S-acylated.

Materials and Methods

Plant material and growth conditions

Arabidopsis thaliana, Columbia 0 (Col-0) ecotype was used in all experiments in this study. The VHA-a3-GFP and VHA-a3R729N-GFP expressing lines was established by (Dettmer et al., 2006) and (Neubert, 2011) respectively. *vha-a2 , vha-a3 and vha-a2 vha-a3* double mutant lines were characterized by (Krebs et al., 2010).

Growth of *Arabidopsis* seedlings for confocal microscopy was performed on plates. The standard growth medium used contained 1/2 Murashige and Skoog (MS), 0.5% sucrose, 0.5% phyto agar, and 10mM MES, and the pH was set to 5.8 using KOH. Agar and MS basal salt mixture were purchased from Duchefa. Seeds were surface sterilized with ethanol and stratified for 48h at 4°C. Plants were grown in long day conditions (LD) (16 h light/8 h dark) for 6 days.

For the rosette phenotype assays, seeds were stratified for 48 h at 4°C and then placed on soil. Seedlings were transferred to individual pots at 7 days after germination (DAG). Plants were grown either in LD or short day conditions (SD) (10 h light/14 h dark) for the required time.

Cold acclimation was performed with three-week-old plants. Plants were placed at 4˚C for 4 days in LD conditions.

Etiolated seedlings were grown on vertical plates with medium containing 1/2 MS, 0.5% sucrose, 0.7% phyto agar, and 10mM MES, and the pH was set to 5.8 using KOH. After seed sterilization and stratification, plates were exposed to light for 4 h, wrapped in two layers of aluminum foil and then kept at 22°C for 4 days.

Growth assays to determine sensitivity to $ZnCl_2$ were performed with plates containing either 0, 50, 100 or 150 uM $ZnCl_2$ with 1/2 MS, 0.5% sucrose, 0.7% phyto agar, and 10mM MES, and the pH was set to 5.8 using KOH.

Construct preparation

VHA-a3SS-GFP

The conserved two cysteines in the N-terminus of VHA-a3 were exchanged by two PCR steps using overlapping primers. The first PCR exchanged C10 and C11 to serines. The template used was VHA-a3 cDNA (a3+pBluscript). The second PCR step used the PCR product of step 1 and introduced an *ApaI* site at the 5' end and a *SpeI* site at the 3' end. Primers are listed in **Table 1**.The second PCR product was blunt end cloned into the pJET1.2 vector. The sequence was verified by sequencing which was performed by Eurofins. A Verified clone was then digested to generate sticky ends. The digested fragment was purified using the Qiagen kit. A double ligation was performed using the purified fragment and the destination vector; pUGT1Kan that had been cut with *ApaI* and *SpeI*.

VHA-a3NT-a1-GFP

Ten amino acids (aa) of the of VHA-a1 N terminus were replaced with 13 aa from VHA-a3 by three PCR steps using overlapping primers. The first PCR replaced the N-terminus of *VHA-a1* with that of *VHA-a3*. The template used was *VHA-a1* cDNA (pJET+a1). The second PCR step used the PCR product of step 1 and introduced an *ApaI* site at the 5' end and the reverse primer introduced a *BamHI* site at the 3' end (part 1). The last PCR amplified the remaining C-terminus of *VHA-a1* and introduced *BamHI* and *SpeI* sites at the 5' and 3' ends of this C-terminal fragment respectively (part 2). Primers are listed in **Table 1**. Part 1 and 2 were blunt end cloned into the pJET1.2 vector. The sequences were verified by sequencing which was performed by Eurofins. Verified clones were then digested to generate sticky ends. Digested fragments were purified using the Qiagen kit. A triple ligation was performed using part 1, part 2 and the destination vector; pUGT1Kan that had been cut with *ApaI* and *SpeI*.

Table 1. Primers used for cloning of VHA-a3SS-GFP and VHA-a3NT-a1-GFP

No.	PCR		Sequence 5' to 3'
1	VHA-a3SS-GFP PCR1	Forward	GGA AAG TGG CGG TGG CGG TGG CAG TAG TCC GCC GAT GGA TCT GAT GCG
		Reverse	ACT AGT GCT CTC GTC TTC GTT TGC CGT GA
	VHA-a3SS-GFP PCR2	Forward	TAT AGG GCC CAT GGC GGA AAG TGG CGG TGG CGG TGG CAG TAG TCC
		Reverse	ACT AGT GCT CTC GTC TTC GTT TGC CGT GA
2	VHA-a3NT-a1-GFP PCR1	Forward	GGT GGC GGT GGC TGT TGT CCG CCG ATG GAT CTG ATG CGT TCG GAG
		Reverse	GAT GTT GAA GGA TCC ATG ATT TC
	VHA-a3NT-a1-GFP PCR2	Forward	TAT AGG GCC CAT GGC GGA AAG TGG CGG TGG CGG TGG CTG TTG TCC
		Reverse	GAT GTT GAA GGA TCC ATG ATT TC
	VHA-a3NT-a1-GFP PCR3	Forward	GAA ATC ATG GAT CCT TCA ACA TC
		Reverse	ATA ACT AGT GAT TAA AGC GAA AGA GAA AGG

Arabidopsis transformation

5 µl of the ligation reactions were transformed into DH5α cells and plated on LB plates containing spectinomycin for selection of correct plasmids. Colony PCR was performed to pre-screen colonies. Overnight cultures of positive clones were made. Mini preps of cultured bacteria were done with the Qiagen kit. Preped plasmids were test digested and correct binary plasmids were transformed into *A. tumefaciens* strain GV3101 pMP90 and selected on 5 µg/ml rifampicin, 15 µg/ml gentamycin and 50 µg/ml kanamycin plates. *Arabidopsis* plants were transformed by the floral dip method as outlined by (Clough and Bent, 1998) and transgenic plants were selected on MS plates containing 50 µg/ml kanamycin.

Tonoplast vesicle preparation and enzyme assays

Preparation of tonoplast vesicles

Rosette leaf material (75 g) from plants grown under short day conditions was harvested. The leaf material was homogenized in homogenization buffer containing 0.4 M mannitol, 0.1 M Tris , 10% (vol/vol) glycerol, 3 mM Na2EDTA, 0.5% (wt/vol) BSA, 5% (vol/vol) PVP-10, 0.5 mM butylated hydroxytoluene, 0.3 mM dibucaine, 5 mM magnesium sulphate, 1 mM PMSF (phenylmethylsulphonyl fluoride), 1.3 mM benzamidine and 25 mM postassium metabisulfite. The homogenate was filtered through two layers of miracloth and centrifuged at 10,000 g for 20 min at 4°C. The supernatant was then centrifuged at 100,000 g for 45 min at 4°C. The microsomal membrane pellet was resuspended in resuspension buffer containing 0.4 M mannitol, 6 mM Tris-MES (pH 8) and 10% (vol/vol) glycerol. Tonoplast vesicles were obtained by performing a sucrose gradient with 22% sucrose. Centrifugation was performed at 97,000 g for 2 hours. Protein concentrations were determined as reported previously (Bradford, 1976).

ATP hydrolysis

ATP hydrolysis was measured at 28°C as described previously by (Krebs et al., 2010)

Proton translocation

The ATP-dependent proton transport activities were estimated from the initial rate of ATP-dependent fluorescence quenching in the presence of 3 mM ATP using the fluorescence dye ACMA (9-Amino-6-Chloro-2-Methoxyacridine). Excitation wavelength was 415 nm, and emission was measured at 485 nm in a microplate reader (Tecan Infinite M1000). Tonoplast vesicles were placed in a 96 well plate with a reaction buffer containing 0.25 M mannitol, 10 mM BTP-MES (pH 8), 100 mM tetramethylammonium chloride (TMA-Cl), 1 µM ACMA, 3 mM magnesium sulphate and 1 mM sodium vanadate. Measurements were started in the absence of ATP (1 measurement every 1 minute for 10 minutes). After 10 minutes, 6 µl of

100 mM ATP-BTP (pH 7.5) was added. Then 20 measurements were done every 25 seconds. The change in ACMA fluorescence over time after ATP addition was then calculated. Control measurements in the presence of 5 µm Concanamycin A were also performed.

SDS-PAGE and immunoblotting analysis

SDS-PAGE and immunoblotting were performed to determine protein levels in tonoplast membrane extracts. Before electrophoresis, protein samples were combined with the Smartalyzer dye and SMA-L calibrator from Dyeagnostics (http://www.dyeagnostics.com/site/en/products/spl/). After electrophoresis, proteins were transferred to a nitrocellulose membrane (Whatman). A GFP antibody (1:5000) was used. Antigen on the membrane was detected with fluorescent labelled anti-rabbit antibodies from Mobitec (#MFP-A1008). Excitation (488 nm) and fluorescence detection was carried out using a cooled CCD camera system (Intas *ADVANCED* Fluoreszenz u. ECL Imager). Total proteins in the samples were detected via excitation of the Smartlyzer dye at 550nm. Western blots were quantified with Fiji (based on ImageJ 1.47t).

pH measurements

Cell sap pH measurements were performed as previously described (Krebs et al., 2010).

Detection of S-acylation

Detection of S-acylation was carried out using two protocols. Namely the biotin switch assay outlined by (Hemsley, 2013) and the acyl resin-assisted capture (acyl-RAC) method (Forrester et al., 2011).

RNA Isolation and cDNA Synthesis

For the analysis of *VHA-a2* and *VHA-a3* transcript levels, RNA was isolated according to the manufacturer's instructions using the RNeasy Plant Mini Kit (Qiagen). cDNA was synthesized from 2 µg of total RNA using M-MuLV reverse transcriptase (Thermo) and an oligo (dT) primer.

Real-Time RT-PCR

Real-time PCR reactions were performed using the DNA Engine Opticon System (DNAEngine cycler and Chromo 4 detector; Bio-Rad) and Absolute qPCR SYBR Green Mix (Thermo Scientific). The real-time PCR reaction mixture with a final volume of 20 mL contained 0.5 µM of each forward and reverse primer, 10 mL of SYBR Green Mix, 4 mL of cDNA, and 4 mL of RNase-free water. The thermal cycling conditions were composed of an initial denaturation step at 95°C for 10 min followed by 40 cycles at 95°C for 15s ,58°C for 30s,and 72°C for 30s and ended with a melting curve. For the analysis of each sample, three analytical replicas were used. Target genes were normalized to the expression of *Actin2*. Primer sequences for *VHA-a2* and *VHA-a3*, and *Actin2* are reported in (Krebs, 2010).

Genotyping

The *vha-a2 vha-a3* double mutant background was confirmed by performing PCR using gene specific primer pairs. The primers were designed to check for the presence of *T-DNA* insertions and absence of the *vha-a2* and *vha-a3* genes. (Krebs, 2010) (Table 2).

Table 2. Primers used in genotyping the *vha-a2 vha-a3* double mutant

No.	PCR		Sequence 5' to 3'
1	Presence of *T-DNA*		
	LB of T-DNA in *vha-2* exon 3	Forward	TGCAACTTGTCGTTATTAGCATTG
		Reverse	CAATCAGCTGTTGCCCGTCTCAC
	LB of T-DNA in *vha-3* exon 1	Forward	CTGATGTTACTATTGTACCGAAC
		Reverse	CAATCAGCTGTTGCCCGTCTCAC
2	Absence of genes		
	vha-a2	Forward	TGCAACTTGTCGTTATTAGCATTG
		Reverse	CGAATACGAGATCGGAGAC
	vha-a3	Forward	CTGATGTTACTATTGTACCGAAC
		Reverse	TCGCGATATTCAAATAACAGCT

Confocal microscopy

Confocal laser scanning microscopy was performed using a Leica TCS SP5II microscope equipped with a Leica HCX PL APO lambda blue 63.0x 1.20 UV water immersion objective. GFP was excited at 488 nm with a VIS-argon laser and fluorescence emission was detected between 500 and 555 nm. The imaging parameters were as follows: image dimension: 512 X 512, pinhole: 1 airy unit, line average: 5. For image acquisition, the Leica Application Suite Advanced Fluorescence software was used. Processing of images was performed using Fiji (based on ImageJ 1.47t).

Imaging

Pictures of rosettes for the soil phenotype assays, plates for hypocotyl length measurements and plates for the $ZnCl_2$ root measurements were taken using a Nikon D60 digital camera. Images were processed using Adobe Photoshop (Cloud) and Fiji (based on ImageJ 1.47t).

Phylogenetic analysis

The online platform at http://www.Phylogeny.fr was utilized (Dereeper et al., 2008). Phylogenetic analysis was performed as described in (Li, Yanbang, Provenzano et al., 2016). Trees were constructed with Maximum likelihood (PHYML) using the WAG amino acid replacement matrix substitution model (Guindon et al., 2010). Branch support was calculated on the basis of 500 bootstraps.

Multiple sequence alignments

Multiple sequence alignments were performed using Clustal omega (Sievers et al., 2011). Aligned sequences were analyzed in Geneious 8.1.5.

List of Abbreviations

µg	Microgram
µM	Micromolar
mM	Milimolar
µm	Micrometer
cm	centimeter
°C	Degree Celsius
%	Percent
∆F	Change in fluorescence
aa	amino acid
acyl-RAC	Acyl resin-assisted capture
ADP	Adenosine diphosphate
ATP	Adenosine triphosphate
ARF	ADP-ribosylation factor
ARF-GEF	ARF-GEF ADP-ribosylation factor - guanine nucleotide exchange factor
A. tumefaciens	*Agrobacterium tumefaciens*
A. thaliana	*Arabidopsis thaliana*
A-ATPase	Archaeal ATPase
BFA	Brefeldin A
bp	base pair
cDNA	Complementary DNA
CO-IP	Coimmunoprecipitation
CLSM	Confocal laser scanning microscopy
Col-0	Columbia-0
COPII	coat protein complex II

DAG	Days after germination
DEX	Dexamethasone
DMSO	Dimethyl sulfoxide
DNA	Desoxyribonucleic acid
EE	Early endosome
ER	Endoplasmic reticulum
F-ATPase	F-type ATP synthase
g	Gram
g	relative centrifugal force
GFP	Green fluorescent protein
HYD	Hydroxylamine
kDa	Kilo dalton
LD	Long day
LV	Lytic vacuole
mass spec	Mass spectrometry
mGFP	Non dimerizing GFP
mRFP	Monomeric red fluorescent protein
min	Minute
MS	Murashige and Skoog
NEM	N-ethylmaleimide
P-ATPase	P-type H+- adenosintriphosphatase
Pi	Inorganic phosphate
qRT PCR	Quantitative real time polymerase chain reaction
RNA	Ribonucleic acid
SD	Standard deviation
SDS-PAGE	Sodium dodecylsulfate polyacrylamide gel electrophoresis

TGN	Trans-Golgi Network
T-DNA	Transfer-DNA
s	seconds
V-ATPase	Vacuolar H+-ATPase

References

Ahn, H.-K., Kang, Y.W., Lim, H.M., Hwang, I., and Pai, H.-S. (2015). Physiological Functions of the COPI Complex in Higher Plants. Mol. Cells **38**: 866–75.

Alconada, a, Bauer, U., and Hoflack, B. (1996). A tyrosine-based motif and a casein kinase II phosphorylation site regulate the intracellular trafficking of the varicella-zoster virus glycoprotein I, a protein localized in the trans-Golgi network. EMBO J. **15**: 6096–110.

Allan, A.K., Du, J., Davies, S. a, and Dow, J. a T. (2005). Genome-wide survey of V-ATPase genes in Drosophila reveals a conserved renal phenotype for lethal alleles. Physiol. Genomics **22**: 128–38.

Anders, N. and Jürgens, G. (2008). Large ARF guanine nucleotide exchange factors in membrane trafficking. Cell. Mol. Life Sci. **65**: 3433–3445.

Aniento F., Gu F., P.R.G. and G.J. (1996). An Endosomal BCOP is involved in the formation of Transport Vesicles Destined for Late Endosomes. Cell **133**: 29–41.

Annette M. Shewan, Ellen M. van Dam, Sally Martin, Tang Bor Luen, Wanjin Hong, Nia J. Bryant, and D.E.J. (2003). GLUT4 Recycles via a trans-Golgi Network (TGN) Subdomain Enriched in Syntaxins 6 and 16 But Not TGN38: Involvement of an Acidic Targeting Motif. Mol. Biol. Cell **14**: 973–986.

Barlowe, C. and Schekman, R. (1993). SEC12 encodes a guanine-nucleotide-exchange factor essential for transport vesicle budding from the ER. Nature **365**: 347–349.

Batistic, O. (2012). Genomics and Localization of the Arabidopsis DHHC-Cysteine-Rich Domain S-Acyltransferase Protein Family. Plant Physiol. **160**: 1597–1612.

Batistic, O., Sorek, N., Schültke, S., Yalovsky, S., and Kudla, J. (2008). Dual fatty acyl modification determines the localization and plasma membrane targeting of CBL/CIPK Ca2+ signaling complexes in Arabidopsis. Plant Cell **20**: 1346–1362.

Berken, A. and Wittinghofer, A. (2008). Structure and function of Rho-type molecular switches in plants. Plant Physiol. Biochem. **46**: 380–393.

Bielli, A., Haney, C.J., Gabreski, G., Watkins, S.C., Bannykh, S.I., and Aridor, M. (2005). Regulation of Sar1 NH2 terminus by GTP binding and hydrolysis promotes membrane deformation to control COPII vesicle fission. J. Cell Biol. **171**: 919–924.

Boehm, M. and Bonifacino, J.S. (2001). Adaptins: the final recount. Mol. Biol. Cell **12**: 2907–2920.

Bonifacino, J.S. and Glick, B.S. (2004). The Mechanisms of Vesicle Budding and Fusion. Cell **116**: 153–166.

Borner, G.H.H., Sherrier, D.J., Weimar, T., Michaelson, L. V, Hawkins, N.D., Macaskill, A., Napier, J.A., Beale, M.H., Lilley, K.S., and Dupree, P. (2005). Plant Physiol.-2005-Borner-104-16.pdf. **137**: 104–116.

Bos, K., Wraight, C., and Stanley, K.K. (1993). TGN38 is maintained in the trans-Golgi network by a tyrosine-containing motif in the cytoplasmic domain. EMBO J. **12**: 2219–2228.

Bottanelli, F., Foresti, O., Hanton, S., and Denecke, J. (2011). Vacuolar Transport in Tobacco Leaf Epidermis Cells Involves a Single Route for Soluble Cargo and Multiple Routes for Membrane Cargo. Plant Cell **23**: 3007–3025.

Bowers, K. and Stevens, T.H. (2005). Protein transport from the late Golgi to the vacuole in the yeast Saccharomyces cerevisiae. Biochim. Biophys. Acta **1744**: 438 – 454.

Bradford, M.M. (1976). A rapid and sensitive method for the quantitation of microgram quantities of protein utilizing the principle of protein-dye binding. Anal. Biochem. **72**: 248–254.

Bruce Alberts, Alexander Johnson, Julian Lewis, Martin Raff, Keith Roberts, and P.W. (2002). Molecular Biology of the Cell. 4th edition 4th ed. (Garland Science: New York).

Brückner, A., Polge, C., Lentze, N., Auerbach, D., and Schlattner, U. (2009). Yeast two-hybrid, a powerful tool for systems biology. Int. J. Mol. Sci. **10**:

2763–2788.

Bryant, N.J. and Stevens, T.H. (1997). Two separate signals act independently to localize a yeast late Golgi membrane protein through a combination of retrieval and retention. J. Cell Biol. **136**: 287–297.

Cereghino, J.L., Marcusson, E.G., and Emr, S.D. (1995). The cytoplasmic tail domain of the vacuolar protein sorting receptor Vps10p and a subset of VPS gene products regulate receptor stability, function, and localization. Mol. Biol. Cell **6**: 1089–102.

Chan, L.N., Hart, C., Guo, L., Nyberg, T., Davies, B.S.J., Fong, G., Young, S.G., Agnew, B.J., and Tamanoi, F. (2010). NIH Public Access. Young **30**: 3598–3606.

Chung, K.P., Zeng, Y., and Jiang, L. (2016). COPII Paralogs in Plants: Functional Redundancy or Diversity? Trends Plant Sci. **xx**: 1–12.

Clough, S.J. and Bent, A.F. (1998). Floral dip: A simplified method for Agrobacterium-mediated transformation of Arabidopsis thaliana. Plant J. **16**: 735–743.

Cooper, A.A. and Stevens, T.H. (1996). Vps10p cycles between the late-Golgi and prevacuolar compartments in its function as the sorting receptor for multiple yeast vacuolar hydrolases. J. Cell Biol. **133**: 529–541.

Cox, J., Hein, M.Y., Luber, C. a, and Paron, I. (2014). Accurate proteome-wide label-free quantification by delayed normalization and maximal peptide ratio extraction, termed MaxLFQ. Mol. Cell. … **13**: 2513–2526.

daSilva, L.L.P., Snapp, E.L., Denecke, J., Lippincott-Schwartz, J., Hawes, C., and Brandizzi, F. (2004). Endoplasmic reticulum export sites and Golgi bodies behave as single mobile secretory units in plant cells. Plant Cell **16**: 1753–1771.

Davis-Kaplan, S.R., Compton, M. a., Flannery, A.R., Ward, D.M., Kaplan, J., Stevens, T.H., and Graham, L. a. (2006). PKR1 encodes an assembly factor for the yeast V-type ATPase. J. Biol. Chem. **281**: 32025–32035.

Dereeper, A., Guignon, V., Blanc, G., Audic, S., Buffet, S., Chevenet, F., Dufayard, J.F., Guindon, S., Lefort, V., Lescot, M., Claverie, J.M., and

Gascuel, O. (2008). Phylogeny.fr: robust phylogenetic analysis for the non-specialist. Nucleic Acids Res. **36**: 465–469.

Dettmer, J., Hong-Hermesdorf, A., Stierhof, Y.-D., and Schumacher, K. (2006). Vacuolar H+-ATPase Activity Is Required for Endocytic and Secretory Traf cking in Arabidopsis. Plant Cell **18**: 715–730.

Fillingame, R.H., Jiang, W., and Dmitriev, O.Y. (2000). Coupling H(+) transport to rotary catalysis in F-type ATP synthases: structure and organization of the transmembrane rotary motor. J. Exp. Biol. **203**: 9–17.

Fink, F. (2012). The V-ATPase in Arabidopsis thaliana: A closer look to targeting, new interaction partners and its role for ER acidification.

Finnigan, G.C., Cronan, G.E., Park, H.J., Srinivasan, S., Quiocho, F. a., and Stevens, T.H. (2012a). Sorting of the Yeast Vacuolar-type, Proton-translocating ATPase Enzyme Complex (V-ATPase): IDENTIFICATION OF A NECESSARY AND SUFFICIENT GOLGI/ENDOSOMAL RETENTION SIGNAL IN Stv1p. J. Biol. Chem. **287**: 19487–19500.

Finnigan, G.C., Hanson-Smith, V., Houser, B.D., Park, H.J., and Stevens, T.H. (2011). The reconstructed ancestral subunit a functions as both V-ATPase isoforms Vph1p and Stv1p in Saccharomyces cerevisiae. Mol. Biol. Cell **22**: 3176–3191.

Finnigan, G.C., Hanson-Smith, V., Stevens, T.H., and Thornton, J.W. (2012b). Evolution of increased complexity in a molecular machine. Nature **481**: 360–4.

Forgac, M. (2007). Vacuolar ATPases: rotary proton pumps in physiology and pathophysiology. Nat. Rev. Mol. Cell Biol. **8**: 917–929.

Forrester, M.T., Hess, D.T., Thompson, J.W., Hultman, R.C., Moseley, M.A., Stamler, J.S., and Casey, P.J. (2011). Site-specific analysis of protein S-acylation by resin-assisted capture (Acyl-RAC). J Lipid Res **52**: 393–398.

Forrester, M.T., Thompson, J.W., Foster, M.W., Nogueira, L., Moseley, M.A., and Stamler, J.S. (2009). Proteomic analysis of S-nitrosylation and denitrosylation by resin-assisted capture. Nat. Biotechnol. **27**: 557–559.

Furt, F., Lemoi, K., Tüzel, E., and Vidali, L. (2012). Quantitative analysis of

organelle distribution and dynamics in Physcomitrella patens protonemal cells. BMC Plant Biol. **12**: 70.

Futai, E., Hamamoto, S., Orci, L., and Schekman, R. (2004). GTP/GDP exchange by Sec12p enables COPII vesicle bud formation on synthetic liposomes. EMBO J. **23**: 4286–4296.

Galichet, A., Hoyerová, K., Kamínek, M., and Gruissem, W. (2008). Farnesylation directs AtIPT3 subcellular localization and modulates cytokinin biosynthesis in Arabidopsis. Plant Physiol. **146**: 1155–1164.

Geldner, N., Anders, N., Wolters, H., Keicher, J., Kornberger, W., Muller, P., Delbarre, A., Ueda, T., Nakano, A., and Jürgens, G. (2003). The Arabidopsis GNOM ARF-GEF mediates endosomal recycling, auxin transport, and auxin-dependent plant growth. Cell **112**: 219–230.

Gendreau, E., Traas, J., Desnos, T., Grandjean, O., Caboche, M., and Hofte, H. (1997). Cellular basis of hypocotyl growth in Arabidopsis thaliana. Plant Physiol **114**: 295–305.

Gillon, A.D., Latham, C.F., and Miller, E. a. (2012). Vesicle-mediated ER export of proteins and lipids. Biochim. Biophys. Acta - Mol. Cell Biol. Lipids **1821**: 1040–1049.

Graham, L. a., Hill, K.J., and Stevens, T.H. (1998). Assembly of the yeast vacuolar H+-ATPase occurs in the endoplasmic reticulum and requires a Vma12p/Vma22p assembly complex. J. Cell Biol. **142**: 39–49.

Greaves, J. and Chamberlain, L.H. (2010). S-acylation by the DHHC protein family. Biochem. Soc. Trans. **38**: 522–524.

Gu, F., Crump, C.M., and Thomas, G. (2001). Trans-Golgi network sorting. Cell. Mol. Life Sci. **58**: 1067–1084.

Guindon, S., Dufayard, J.F., Lefort, V., Anisimova, M., Hordijk, W., and Gascuel, O. (2010). New algorithms and methods to estimate maximum-likelihood phylogenies: Assessing the performance of PhyML 3.0. Syst. Biol. **59**: 307–321.

Gürkan, C., Stagg, S.M., Lapointe, P., and Balch, W.E. (2006). The COPII cage: unifying principles of vesicle coat assembly. Nat. Rev. Mol. Cell Biol. **7**:

727–38.

Hanton, S.L., Chatre, L., Matheson, L.A., Rossi, M., Held, M.A., and Brandizzi, F. (2008). Plant Sar1 isoforms with near-identical protein sequences exhibit different localisations and effects on secretion. Plant Mol. Biol. **67**: 283–294.

Hemsley, P.A. (2013). Assaying protein S-acylation in plants. Methods Mol. Biol. **1043**: 141–146.

Hemsley, P.A. (2015). The importance of lipid modified proteins in plants. New Phytol. **205**: 476–489.

Hemsley, P.A., Kemp, A.C., and Grierson, C.S. (2005). The TIP GROWTH DEFECTIVE1 S -Acyl Transferase Regulates Plant Cell Growth in Arabidopsis. **17**: 2554–2563.

Hemsley, P.A., Weimar, T., Lilley, K.S., Dupree, P., and Grierson, C.S. (2013). A proteomic approach identifies many novel palmitoylated proteins in Arabidopsis. New Phytol. **197**: 805–814.

Hori, K. et al. (2014). Klebsormidium flaccidum genome reveals primary factors for plant terrestrial adaptation. Nat. Commun. **5**: 3978.

Hornemann, T. (2014). Palmitoylation and depalmitoylation defects. J. Inherit. Metab. Dis. **38**: 179–186.

Huaiyu Mi*, Xiaosong Huang, Anushya Muruganujan, Haiming Tang, Caitlin Mills, D.K. and P.D.T. (2016). PANTHER version 11: expanded annotation data from Gene Ontology and Reactome pathways, and data analysis tool enhancements. Nucleic Acids Res.: 1–15.

Hurtado-Lorenzo, A., Skinner, M., El Annan, J., Futai, M., Sun-Wada, G.-H., Bourgoin, S., Casanova, J., Wildeman, A., Bechoua, S., Ausiello, D. a, Brown, D., and Marshansky, V. (2006). V-ATPase interacts with ARNO and Arf6 in early endosomes and regulates the protein degradative pathway. Nat. Cell Biol. **8**: 124–136.

Jackson, L.P. (2014). Structure and mechanism of COPI vesicle biogenesis. Curr. Opin. Cell Biol. **29**: 67–73.

Jauh, G.-Y., Fischer, A.M., Grimes, H.D., JR, C.A.R., and Rogers, J.C. (1998).

-Tonoplast intrinsic protein defines unique plant vacuole functions. Proc. Natl. Acad. Sci. U. S. A. **95**: 12995–12999.

Jones, B.G., Thomas, L., Molloy, S.S., Thulin, C.D., Fry, M.D., Walsh, K. a, and Thomas, G. (1995). Intracellular trafficking of furin is modulated by the phosphorylation state of a casein kinase II site in its cytoplasmic tail. EMBO J. **14**: 5869–83.

Kanazawa, T. et al. (2016). SNARE molecules in Marchantia polymorpha: Unique and conserved features of the membrane fusion machinery. Plant Cell Physiol. **57**: 307–324.

Kane, P.M., Tarsio, M., and Jianzhong, L. (1999). Early steps in assembly of the yeast vacuolar H+-ATPase. J. Biol. Chem. **274**: 17275–17283.

Karpievitch, Y. V, Dabney, A.R., and Smith, R.D. (2012). Normalization and missing value imputation for label-free LC-MS analysis. BMC Bioinformatics **13 Suppl 1**: S5.

Kawasaki-Nishi, S., Bowers, K., Nishi, T., Forgac, M., and Stevens, T.H. (2001). The Amino-terminal Domain of the Vacuolar Proton-translocating ATPase a Subunit Controls Targeting and in Vivo Dissociation, and the Carboxyl-terminal Domain Affects Coupling of Proton Transport and ATP Hydrolysis. J. Biol. Chem. **276**: 47411–47420.

Kerppola, T.K. (2008). Bimolecular fluorescence complementation (BiFC) analysis as a probe of protein interactions in living cells. Annu Rev Biophys **37**: 465–87.

Kirchhausen, T. (2000). Three ways to make a vesicle. Nat. Rev. Mol. Cell Biol. **1**: 187–198.

Klemens, P.A.W., Patzke, K., Deitmer, J., Spinner, L., Hir, R. Le, Bellini, C., Bedu, M., Chardon, F., Krapp, A., and Neuhaus, H.E. (2013). Overexpression of the Vacuolar Sugar Carrier AtSWEET16 Modi fi es Germination , Growth , and Stress Tolerance. **163**: 1338–1352.

Kostova, Z. and Wolf, D.H. (2003). For whom the bell tolls: Protein quality control of the endoplasmic reticulum and the ubiquitin-proteasome connection. EMBO J. **22**: 2309–2317.

Krämer, U., Talke, I.N., and Hanikenne, M. (2007). Transition metal transport. FEBS Lett. **581**: 2263–2272.

Krebs, M. (2010). Multiple functions for a complex proton pump : The tonoplast V-ATPase from Arabidopsis.

Krebs, M., Beyhl, D., Gorlich, E., Al-Rasheid, K. a. S., Marten, I., Stierhof, Y.-D., Hedrich, R., and Schumacher, K. (2010). Arabidopsis V-ATPase activity at the tonoplast is required for efficient nutrient storage but not for sodium accumulation. Proc. Natl. Acad. Sci. **107**: 3251–3256.

Kriegel, A. et al. (2015). Job Sharing in the Endomembrane System: Vacuolar Acidification Requires the Combined Activity of V-ATPase and V-PPase. Plant Cell **27**: tpc.15.00733.

Kriegel, A. (2015). Vacuolar acidification relies on the combined activity of endomembrane proton pumps.

Kumar, M., Wightman, R., Atanassov, I., Gupta, A., Hurst, C.H., Hemsley, P.A., and Turner, S. (2016). S-Acylation of the cellulose synthase complex is essential for its plasma membrane localization. Science (80-.). **353**: 166–169.

Kurkdjian, A. and Guern, J. (1981). Vacuolar pH Measurement in Higher Plant Cells : I. EVALUATION OF THE METHYLAMINE METHOD. Plant Physiol. **67**: 953–7.

Lampropoulos, A., Sutikovic, Z., Wenzl, C., Maegele, I., Lohmann, J.U., and Forner, J. (2013). GreenGate - A novel, versatile, and efficient cloning system for plant transgenesis. PLoS One **8**.

Langhans, M., Förster, S., Helmchen, G., and Robinson, D.G. (2011). Differential effects of the brefeldin A analogue (6R)-hydroxy-BFA in tobacco and Arabidopsis. J. Exp. Bot. **62**: 2949–2957.

Lavy, M. and Yalovsky, S. (2006). Association of Arabidopsis type-II ROPs with the plasma membrane requires a conserved C-terminal sequence motif and a proximal polybasic domain. Plant J. **46**: 934–947.

Lee, D.H. (1998). Proteasome inhibitors: Valuable new tools for cell biologists. Trends Cell Biol. **8**: 397–403.

Lee, M.C.S., Orci, L., Hamamoto, S., Futai, E., Ravazzola, M., and Schekman, R. (2005). Sar1p N-terminal helix initiates membrane curvature and completes the fission of a COPII vesicle. Cell **122**: 605–617.

Lee, S.K., Li, W., Ryu, S.E., Rhim, T., and Ahnn, J. (2010). Vacuolar (H+)-ATPases in Caenorhabditis elegans: What can we learn about giant H+ pumps from tiny worms? Biochim. Biophys. Acta - Bioenerg. **1797**: 1687–1695.

Leng, X.H., Manolson, M.F., and Forgac, M. (1998). Function of the COOH-terminal domain of Vph1p in activity and assembly of the yeast V-ATPase. J. Biol. Chem. **273**: 6717–6723.

Li, Yanbang, Provenzano, S., Bliek, M., and Spelt, C. (2016). Evolution of tonoplast P-ATPase transporters involved in vacuolar hyperacidification. New Phytol.

Li, R., Jia, X., and Mao, X. (2005). Ethanol-inducible gene expression system and its applications in plant functional genomics. Plant Sci. **169**: 463–469.

Li, Y., Scott, R., Doughty, J., Grant, M., and Qi, B. (2016). Protein *S* -Acyltransferase 14: A Specific Role for Palmitoylation in Leaf Senescence in Arabidopsis. Plant Physiol. **170**: 415–428.

Liberman, R., Cotter, K., Baleja, J.D., and Forgac, M. (2013). Structural analysis of the N-terminal domain of subunit a of the yeast vacuolar ATPase (V-ATPase) using accessibility of single cysteine substitutions to chemical modification. J. Biol. Chem. **288**: 22798–22808.

Liu, D.Y.T., Smith, P.M.C., Barton, D.A., Day, D.A., and Overall, R.L. (2015). Characterisation of Arabidopsis calnexin 1 and calnexin 2 in the endoplasmic reticulum and at plasmodesmata. Protoplasma: 1–12.

Liu, T.-Y. (2008). Functional studies of V-ATPase subunit isoforms in Arabidopsis.

Luo, Y. et al. (2015). V-ATPase activity in the TGN/EE is required for exocytosis and recycling in Arabidopsis. Nat. Plants **1**: 15094.

Machamer, C.E. (1993). Targeting and retention of Golgi membrane proteins. Curr. Opin. Cell Biol. **5**: 606–612.

Maranda, B., Brown, D., Bourgoin, S., Casanova, J.E., Vinay, P., Ausiello, D.A., and Marshansky, V. (2001). Intra-endosomal pH-sensitive Recruitment of the Arf-nucleotide Exchange Factor ARNO and Arf6 from Cytoplasm to Proximal Tubule Endosomes. J. Biol. Chem. **276**: 18540–18550.

Margret Ryan, Laurie A. Graham, and T.H.S.I. (2008). Voa1p Functions in V-ATPase Assembly in the Yeast Endoplasmic Reticulum. Mol. Biol. Cell **19**: 5131–5142.

Marsh, J.A., Hern??ndez, H., Hall, Z., Ahnert, S.E., Perica, T., Robinson, C. V., and Teichmann, S.A. (2013). Protein complexes are under evolutionary selection to assemble via ordered pathways. Cell **153**: 461–470.

Marshansky, V. (2007). The V-ATPase a2-subunit as a putative endosomal pH-sensor. Biochem. Soc. Trans. **35**: 1092–1099.

Marshansky, V. and Futai, M. (2008). The V-type H+-ATPase in vesicular trafficking: targeting, regulation and function. Curr. Opin. Cell Biol. **20**: 415–426.

Marti, L., Fornaciari, S., Renna, L., Stefano, G., and Brandizzi, F. (2010). COPII-mediated traffic in plants. Trends Plant Sci. **15**: 522–528.

Mazhab-Jafari, M.T., Rohou, A., Schmidt, C., Bueler, S.A., Benlekbir, S., Robinson, C. V., and Rubinstein, J.L. (2016). Atomic model for the membrane-embedded VO motor of a eukaryotic V-ATPase. Nature **539**: 1–5.

Miller, E.A., Beilharz, T.H., Malkus, P.N., Lee, M.C.S., Hamamoto, S., Orci, L., and Schekman, R. (2003). Multiple cargo binding sites on the COPII subunit Sec24p ensure capture of diverse membrane proteins into transport vesicles. Cell **114**: 497–509.

Molendijk, A.J., Ruperti, B., and Palme, K. (2004). Small GTPases in vesicle trafficking. Curr. Opin. Plant Biol. **7**: 694–700.

Moore, I., Gälweiler, L., Grosskopf, D., Schell, J., and Palme, K. (1998). A transcription activation system for regulated gene expression in transgenic plants. Proc. Natl. Acad. Sci. U. S. A. **95**: 376–381.

Neubert, C. (2011). Assembly and quality control of the V- ATPase in

Arabidopsis. PhD thesis Unpubl.

Neubert, C., Graham, L. a., Black-Maier, E.W., Coonrod, E.M., Liu, T.Y., Stierhof, Y.D., Seidel, T., Stevens, T.H., and Schumacher, K. (2008). Arabidopsis has two functional orthologs of the yeast V-ATPase assembly factor Vma21p. Traffic **9**: 1618–1628.

Nielsen, E., Cheung, A.Y., and Ueda, T. (2008). The regulatory RAB and ARF GTPases for vesicular trafficking. Plant Physiol. **147**: 1516–1526.

Nishi, T. and Forgac, M. (2002). the Vacuolar (H+)-Atpases — Nature'S Most Versatile Proton Pumps. Nat. Rev. Mol. Cell Biol. **3**: 94–103.

Owen, D.J. and Evans, P.R. (1998). A structural explanation for the recognition of tyrosine-based endocytotic signals. Science **282**: 1327–1332.

Pagant, S., Wu, A., Edwards, S., Diehl, F., and Miller, E.A. (2015). Sec24 is a coincidence detector that simultaneously binds two signals to drive ER export. Curr. Biol. **25**: 403–12.

Paul, M.J. and Frigerio, L. (2007). Coated vesicles in plant cells. Semin. Cell Dev. Biol. **18**: 471–478.

Pedrazzini, E., Komarova, N.Y., Rentsch, D., and Vitale, A. (2013). Traffic Routes and Signals for the Tonoplast. Traffic **14**: 622–628.

Per Malkus, Laurie A. Graham, Tom H. Stevens, and R.S. (2004). Role of Vma21p in Assembly and Transport of the Yeast Vacuolar ATPase. Mol. Biol. Cell **15**: 5075–5091.

Peri, F. and Nüsslein-Volhard, C. (2008). Live Imaging of Neuronal Degradation by Microglia Reveals a Role for v0-ATPase a1 in Phagosomal Fusion In Vivo. Cell **133**: 916–927.

Perica, T., Marsh, J.A., Sousa, F.L., Natan, E., Colwell, L.J., Ahnert, S.E., and Teichmann, S.A. (2012). The emergence of protein complexes: quaternary structure, dynamics and allostery. Colworth Medal Lecture. Biochem. Soc. Trans. **40**: 475–91.

Phillipson, B. a, Pimpl, P., daSilva, L.L., Crofts, a J., Taylor, J.P., Movafeghi, a, Robinson, D.G., and Denecke, J. (2001). Secretory bulk flow of soluble proteins is efficient and COPII dependent. Plant Cell **13**: 2005–2020.

Qi, B., Doughty, J., and Hooley, R. (2013). A Golgi and tonoplast localized S-acyl transferase is involved in cell expansion, cell division, vascular patterning and fertility in Arabidopsis. New Phytol. **200**: 444–456.

Qi, J. and Forgac, M. (2007). Cellular environment is important in controlling V-ATPase dissociation and its dependence on activity. J. Biol. Chem. **282**: 24743–24751.

Reid, D.W. and Nicchitta, C. V (2015). Diversity and selectivity in mRNA translation on the endoplasmic reticulum. Nat Rev Mol Cell Biol **16**: 221–231.

Ren, J., Wen, L., Gao, X., Jin, C., Xue, Y., and Yao, X. (2008). CSS-Palm 2.0: An updated software for palmitoylation sites prediction. Protein Eng. Des. Sel. **21**: 639–644.

Resh, M.D. (2016). Fatty Acylation of Proteins: The Long and the Short of it. Prog. Lipid Res. **63**: 120–131.

Reyes, F.C., Buono, R., and Otegui, M.S. (2011). Plant endosomal trafficking pathways. Curr. Opin. Plant Biol. **14**: 666–673.

Richter, S., Geldner, N., Schrader, J., Wolters, H., Stierhof, Y.-D., Rios, G., Koncz, C., Robinson, D.G., and Jürgens, G. (2007). Functional diversification of closely related ARF-GEFs in protein secretion and recycling. Nature **448**: 488–492.

Rienmüller, F., Dreyer, I., Schönknecht, G., Schulz, A., Schumacher, K., Nagy, R., Martinoia, E., Marten, I., and Hedrich, R. (2012). Luminal and cytosolic pH feedback on proton pump activity and ATP affinity of V-type ATPase from Arabidopsis. J. Biol. Chem. **287**: 8986–8993.

Ristic, Z. and Ashworth, E.N. (1993). Changes in leaf ultrastructure and carbohydrates inArabidopsis thaliana L.(Heyn) cv. Columbia during rapid cold acclimation. Protoplasma: 111–123.

Ritzenthaler, C. and Robinson, D.G. (2002). Update on Brefeldin A Brefeldin A : Deciphering an Enigmatic Inhibitor of Secretion. **130**: 1102–1108.

Robinson, D.G., Jiang, L., and Schumacher, K. (2008). The Endosomal System of Plants: Charting New and Familiar Territories. Plant Physiol. **147**: 1482–1492.

Rojo, E. and Denecke, J. (2008). What Is Moving in the Secretory Pathway of Plants? Plant Physiol. **147**: 1493–1503.

Römisch, K. (2005). Endoplasmic reticulum-associated degradation. Annu. Rev. Cell Dev. Biol. **21**: 435–456.

Ron, D. and Walter, P. (2007). Signal integration in the endoplasmic reticulum unfolded protein response. **8**: 519–529.

Roy, A., Kucukural, A., and Zhang, Y. (2010). I-TASSER: a unified platform for automated protein structure and function prediction. Nat. Protoc. **5**: 725–738.

Samalova, M., Brzobohaty, B., and Moore, I. (2005). pOp6/LhGR: A stringently regulated and highly responsive dexamethasone-inducible gene expression system for tobacco. Plant J. **41**: 919–935.

Sankaranarayanan Srinivasan, Nand K. Vyas, Matthew L. Baker, and F.A. and Quiocho (2011). Crystal structure of the cytoplasmic N-terminal domain of subunit I, a homolog of subunit a, of V-ATPase. J Mol Biol . **412**: 14–21.

Sato, K. and Nakano, A. (2007). Mechanisms of COPII vesicle formation and protein sorting. FEBS Lett. **581**: 2076–2082.

Schäfer, W., Stroh, A., Berghöfer, S., Seiler, J., Vey, M., Kruse, M.L., Kern, H.F., Klenk, H.D., and Garten, W. (1995). Two independent targeting signals in the cytoplasmic domain determine trans-Golgi network localization and endosomal trafficking of the proprotein convertase furin. EMBO J. **14**: 2424–35.

Schep, D.G., Zhao, J., and Rubinstein, J.L. (2016). Models for the a subunits of the Thermus thermophilus V / A-ATPase and Saccharomyces cerevisiae V-ATPase enzymes by cryo-EM and evolutionary covariance.: 6–11.

Schulze, W.X., Schneider, T., Starck, S., Martinoia, E., and Trentmann, O. (2012). Cold acclimation induces changes in Arabidopsis tonoplast protein abundance and activity and alters phosphorylation of tonoplast monosaccharide transporters. Plant J. **69**: 529–541.

Segami, S., Makino, S., Miyake, A., Asaoka, M., and Maeshima, M. (2014). Dynamics of vacuoles and H+-pyrophosphatase visualized by monomeric green fluorescent protein in Arabidopsis: artifactual bulbs and native

intravacuolar spherical structures. Plant Cell **26**: 3416–34.

Shahinian, S. and Silvius, J.R. (1995). Doubly-lipid-modified protein sequence motifs exhibit long-lived anchorage to lipid bilayer membranes. Biochemistry **34**: 3813–3822.

Sievers, F., Wilm, A., Dineen, D., Gibson, T.J., Karplus, K., Li, W., Lopez, R., McWilliam, H., Remmert, M., Söding, J., Thompson, J.D., and Higgins, D.G. (2011). Fast, scalable generation of high-quality protein multiple sequence alignments using Clustal Omega. Mol. Syst. Biol. **7**: 539.

Simpson, C., Thomas, C., Findlay, K., Bayer, E., and Maule, A.J. (2009). An Arabidopsis GPI-anchor plasmodesmal neck protein with callose binding activity and potential to regulate cell-to-cell trafficking. Plant Cell **21**: 581–594.

Sorek, N., Gutman, O., Bar, E., Abu-Abied, M., Feng, X., Running, M.P., Lewinsohn, E., Ori, N., Sadot, E., Henis, Y.I., and Yalovsky, S. (2011). Differential Effects of Prenylation and S-Acylation on Type I and II ROPS Membrane Interaction and Function. Plant Physiol. **155**: 706–720.

Sorek, N., Poraty, L., Sternberg, H., Bar, E., Lewinsohn, E., and Yalovsky, S. (2007). Activation status-coupled transient S acylation determines membrane partitioning of a plant Rho-related GTPase. Mol. Cell. Biol. **27**: 2144–2154.

Springer, S. and Schekman, R. (1998). Nucleation of COPII vesicular coat complex by endoplasmic reticulum to Golgi vesicle SNAREs. Science (80-.). **281**: 698–700.

Srivastava, J., Barber, D.L., and Jacobson, M.P. (2007). Intracellular pH sensors: design principles and functional significance. Physiology (Bethesda). **22**: 30–9.

Stevens, T.H. and Forgac, M. (1997). Structure, function and regulation of the vacuolar (H+)-ATPase. Annu. Rev. Cell Dev. Biol. **13**: 779–808.

Sze, H., Schumacher, K., Müller, M.L., Padmanaban, S., and Taiz, L. (2002). A simple nomenclature for a complex proton pump: VHA genes encode the vacuolar H+-ATPase. Trends Plant Sci. **7**: 157–161.

Takeuchi, M., Ueda, T., Sato, K., Abe, H., Nagata, T., and Nakano, A. (2000). A dominant negative mutant of Sar1 GTPase inhibits protein transport from the endoplasmic reticulum to the Golgi apparatus in tobacco and Arabidopsis cultured cells. Plant J. **23**: 517–525.

Törnroth-Horsefield, S., Wang, Y., Hedfalk, K., Johanson, U., Karlsson, M., Tajkhorshid, E., Neutze, R., and Kjellbom, P. (2006). Structural mechanism of plant aquaporin gating. Nature **439**: 688–694.

Tournaire-Roux, C., Sutka, M., Javot, H., Gout, E., Gerbeau, P., Luu, D.-T., Bligny, R., and Maurel, C. (2003). Cytosolic pH regulates root water transport during anoxic stress through gating of aquaporins. Nature **425**: 393–397.

Trombetta, E.S. and Parodi, A.J. (2003). Quality control and protein folding in the secretory pathway. Annu. Rev. Cell Dev. Biol. **19**: 649–676.

Tyanova, S., Temu, T., Sinitcyn, P., Carlson, A., Hein, M.Y., Geiger, T., Mann, M., and Cox, J. (2016). The Perseus computational platform for comprehensive analysis of (prote)omics data. Nat. Methods **13**: 731–40.

Viotti, C. et al. (2010). Endocytic and secretory traffic in Arabidopsis merge in the trans-Golgi network/early endosome, an independent and highly dynamic organelle. Plant Cell **22**: 1344–1357.

Viotti, C. et al. (2013). The endoplasmic reticulum is the main membrane source for biogenesis of the lytic vacuole in Arabidopsis. Plant Cell **25**: 3434–49.

Wilcox, C.A., Redding, K., Wright, R., and Fuller, R.S. (1992). Mutation of a tyrosine localization signal in the cytosolic tail of yeast Kex2 protease disrupts Golgi retention and results in default transport to the vacuole. Mol. Biol. Cell **3**: 1353–71.

Wolfenstetter, S., Wirsching, P., Dotzauer, D., Schneider, S., and Sauer, N. (2012). Routes to the Tonoplast: The Sorting of Tonoplast Transporters in Arabidopsis Mesophyll Protoplasts. Plant Cell **24**: 215–232.

Woollard, A.A. and Moore, I. (2008). The functions of Rab GTPases in plant membrane traffic. Curr. Opin. Plant Biol. **11**: 610–619.

Xiang, Y., Molloy, S.S., Thomas, L., and Thomas, G. (2000). The PC6B

cytoplasmic domain contains two acidic clusters that direct sorting to distinct trans-Golgi network/endosomal compartments. Mol. Biol. Cell **11**: 1257–73.

Xin, Z. and Browse, J. (2000). Cold comfort farm: The acclimation of plants to freezing temperatures. Plant, Cell Environ. **23**: 893–902.

Yorimitsu, T., Sato, K., and Takeuchi, M. (2014). Molecular mechanisms of Sar/Arf GTPases in vesicular trafficking in yeast and plants. Front. Plant Sci. **5**: 411.

Zeng, Y., Chung, K.P., Li, B., Lai, C.M., Lam, S.K., Wang, X., Cui, Y., Gao, C., Luo, M., Wong, K.-B., Schekman, R., and Jiang, L. (2015). Unique COPII component AtSar1a/AtSec23a pair is required for the distinct function of protein ER export in *Arabidopsis thaliana*. Proc. Natl. Acad. Sci. **112**: 201519333.

Zeuzem, S., Feick, P., Zimmermann, P., Haase, W., Kahn, R.A., and Schulz, I. (1992). Intravesicular acidification correlates with binding of ADP-ribosylation factor to microsomal membranes. Proc. Natl. Acad. Sci. U. S. A. **89**: 6619–6623.

Zhao, J., Benlekbir, S., and Rubinstein, J.L. (2015). Electron cryomicroscopy observation of rotational states in a eukaryotic V-ATPase. Nature **521**: 241–245.

Zhou, L.-Z., Li, S., Feng, Q.-N., Zhang, Y.Y.-L., Zhao, X., Zeng, Y., Wang, H., Jiang, L., and Zhang, Y.Y.-L. (2013). Protein S-ACYL TRANSFERASE10 is critical for development and salt tolerance in Arabidopsis. Plant Cell **25**: 1093–1107.

Zwiewka, M., Feraru, E., Möller, B., Hwang, I., Feraru, M.I., Kleine-Vehn, J., Weijers, D., and Friml, J. (2011). The AP-3 adaptor complex is required for vacuolar function in Arabidopsis. Cell Res. **21**: 1711–1722.

Acknowledgements

"Everything is going to be fine in the end.
If it's not fine it's not the end."
- Oscar Wilde

First and foremost, I would like to thank my supervisor, Prof. Dr. Karin Schumacher. I thank her for giving me this opportunity to do my doctoral thesis in her lab and her faith in my abilities. She has been a fountain of encouragement and support that has steered this thesis to what it is today.

I would like to thank my family. My father who worked hard to give us a good education. My mother who treats her children like gold and her unwavering push for me to study further. My siblings for their encouragement and support. My daughter; Theresa, for being the best baby a mother pursing her PhD could have!

I would also like to thank my fellow lab and floor members, some of whom I have been with for almost a decade! I would like to give special thanks to:

Gorkem Patir Nebioglu, for being with me through all my big and small crises, all her help with my project and above all for being a friend.

Melanie, for her approachable and fun demeanor as well as her useful advice.

Falco, for his useful advice in and outside the lab and also help with my project.

Fabian, for all his help with my project and life and his deadly jokes!

Zaida for all her useful discussions and funny conversations.

All other Schumacher lab members, Stefan, Simon, Jana, Raina, Beata and Barbara for their support and encouragement.

I would also like to thank other floor members from the Maizel and Wolf labs as well as the entire COS for providing a fun environment to work in.

I would like to thank Angelica Wünderlich who first welcomed me to Heidelberg and has been a friend over the years. I would like to thank all my former neighbours at the family student house in the Altstadt for helping me with my

daughter through the years. I would also like to thank former lab members; Christoph Neubert, Nana Keinath and Esther Jawurek for all their support.

Lastly, I would like to thank, my other two TAC members, Prof. Dr. Jan Lohman Prof.Dr.Irmgard Sinning for guiding me through the years.